ISSN 1173-5996

Assessing the Feasibility of Reducing the Grid Resolution in FDS Field Modelling

by
Nathaniel Mead Patterson

Supervised by:
Dr Charley Fleischmann

Fire Engineering Research Report 02/12

May 2002

This report was presented as a project report as part of the ME (Fire) Degree at the University of Canterbury

School of Engineering
University of Canterbury
Private Bag 4800
Christchurch, New Zealand

Phone 643 364-2250
Fax 643 364-2758
www.civil.canterbury.ac.nz

Abstract

Field modelling is increasingly becoming the main form of fire modelling for design purposes. To reduce the computational running time of field models designers are sacrificing fine grid resolution without considering the consequences this could incur on the results. This report aims to provide some validation on the extent to which grid size can be increased in the field model Fire Dynamics Simulator (FDS) before the results are compromised and to determine whether there is a point at which zone model predictions become more reliable.

FDS model predictions using a range of grid sizes were compared against two separate sets of experiments:

1. The University of Canterbury McLeans Island tests. These tests were performed using two isorooms, each measuring 2.4 x 3.6 x 2.4 metres. 55kW and 110kW tests were simulated in FDS.
2. The US Navy Hanger tests in Hawaii. The hanger measured 98 x 74 metres x 15 metres high at its apex. Two tests were simulated in FDS. These had Heat Release Rates (HRRs) of 5580kW and 6670kW respectively. The second test had a draft curtain situated centrally around the fire. This was modelled in two different FDS constructions; one simulated the entire hanger, the other only the area of the draft curtain.

Simulations using the zone model CFAST were also performed for all the tests outlined above.

The comparisons with the McLeans Island Tests showed that FDS models with grids of 150mm (H/16) made temperature predictions as accurate as 100mm (H/24) grid models, generally falling well within +/-15% of the experimental temperature measurements. The 300mm (H/8) grid models made much poorer predictions and it was shown that the zone model, although vastly limited in the data it provided was more reliable.

The simulations of the Hawaii hanger tests gave very unreliable temperature predictions in the fire plume; the model with 600mm (H/25) grids over-predicted the temperatures by about 150°C. Over-predictions of as much as 60°C were also observed in the temperature predictions within the confines of the draft curtain. These large discrepancies were due to the poor modelling of the high degree of turbulence that occurred in these areas. Locations away from the fire plume or outside the draft curtain gave much better predictions because turbulence was less. In these regions grid sizes of up to 1800mm (H/8) still gave similar accuracy to the 600mm (H/24) grid models. The model using 3600mm (H/4) grids began to display some inaccuracy in the temperature gradients it predicted. The zone models made much better predictions for the temperatures within the draft curtain. This was due to the relatively steady state nature and uniform temperatures that existed there. It was difficult to compare the zone models to the main hanger space because of the limited experimental data that was provided.

Generally, the comparisons showed that the extent to which gird size could be increased not only depended on fire diameter but also on the size and geometry of the enclosure. FDS models were reliable for far field temperature predictions when grid sizes of up to half the fire diameter were used. However, for near field predictions the models could not be relied upon unless very fine grid resolution could be prescribed. The study also showed that in certain cases zone models are a better option than FDS models, especially in turbulent well-mixed scenarios where a steady state period is observed and FDS grids size is limited by computational time.

Acknowledgments

I would like to thank the following people for their assistance and support in helping me to complete this project:

- My supervisor, Dr Charley Fleischmann.
- The New Zealand Fire Service Commission for their financial help and continued support of the M.E. Fire program.
- Mike Spearpoint for his advise and patience with my problems in spite of the fact that he was not my supervisor.
- Tom and Donna, who each read various sections of the report when required and Dad, who waded through the final draft.
- Mr Peter Coursey and Mr Joost Stenfert-Kroese for providing prompt computer services and the facilities with which to work with.
- Clayton, for listening to my complaints all summer.

Table of Contents

List of Figures

List of Tables

Glossary of terms

Acronyms:

BRANZ	Building and Research Association of New Zealand
CFAST	Fire And Smoke Transport; the zone model used in this research
CFD	Computational Fluid Dynamics
DNS	Direct Numerical Simulation
FDS	Fire Dynamic Simulator; the CFD model used in this research
HRR	Heat Release Rate
HRRPUA	Heat Release Rate Per Unit Area
LES	Large Eddy Simulation
NIST	National Institute of Standards and Technology
RAM	Random Access Memory
RTE	Radiative Transport Equation

FDS input calls:

ALPHA	thermal diffusivity
C_DELTA_RHO	product of specific heat, thickness and density
DELTA	obstruction thickness
KS	thermal conductivity
TMPA	ambient temperature

Nomenclature:

C	Empirically derived constant
C_p	constant pressure specific heat
D	diffusion coefficient, fire diameter
D*	characteristic fire diameter

ΔH_o	HRR per unit mass of oxygen consumed
ΔT_o	centreline plume temperature above ambient
$\mathbf{f}$	external force vector (sprinkler droplet drag)
g	acceleration of gravity
H	enclosure height
h	enthalpy; heat transfer coefficient
h_i	enthalpy of ith species
I	radiation intensity
I_b	radiation blackbody intensity
k	thermal conductivity, turbulent kinetic energy
L	Flame height
M_i	molecular weight of ith gas species
m_o'''	oxygen consumption rate
p	pressure
$\mathbf{q}_r$	radiative heat flux vector
q'''	heat release rate per unit volume
Q*	Dimensionless HRR
Q	total heat release rate
Q_c	convective heat release rate
T	temperature
t	time
$\mathbf{u} = (u, v, w)$	velocity vector
W_i'''	production rate of ith species per unit volume
Y_F	mass fraction of fuel
Y_F^1	mass fraction of fuel in the fuel stream
Y_i	mass fraction of ith species
Y_O	mass fraction of oxygen
Y_O^{inf}	mass fraction of oxygen in ambient
z	height above fire base
z_o	virtual origin of fire
Z	mixture fraction
Z_f	mixture fraction at flame surface
$Z_{f,eff}$	effective flame mixture fraction

∇	$\frac{\partial}{\partial x}+\frac{\partial}{\partial y}+\frac{\partial}{\partial z}$
δx	nominal grid size
ε	viscous dissipation energy
κ	absorption coefficient
μ	dynamic viscosity
ρ	density
σ	Stefan-Boltzmann constant
τ	viscous stress tensor
ν_i	stoichiometric coefficient
χ_r	local radiative loss fraction
∞	subscript, at ambient conditions

1 Introduction

1.1 Overview

Fire Engineering is a continually expanding and complex multi disciplinary field. As this field expands and awareness of the role of fire engineering develops there is an increasing need for more case specific design solutions (Buchanan (Ed.), 2001). Fire engineering therefore is increasingly moving towards performance-based codes and away from the more restrictive prescriptive codes. A performance-based code is a much more rational and effective approach, giving scope to designers to use specific fire engineering design to arrive at a solution to a problem. New Zealand was the first to introduce a performance based code for fire engineering in 1992 and has been closely followed by Sweden (1994) and Australia (1996), with the USA currently in the process of introducing it (Buchanan (Ed.), 2001).

With the need for case specific design solutions the use of fire modelling techniques has become widely used in industry. This has fuelled the development of more and more complex fire models. It began with the introduction of zone models and progressed onto the development of the more complex field models over the last ten years (Collier, 1997). However, the use of fire modelling as a quantitative solution cannot be achieved without some sort of validation of the model that shows that it can perform satisfactorily in a wide range of scenarios. This is the main drive of this research.

1.2 Fire modelling

The idea that fires could be studied numerically was probably first conceived at the start of the computer age and indeed the fundamental equations of fluid dynamics, heat transfer and combustion that are used in the more complex models today were first described over a century ago (McGrattan et al, 2001). However, due to the innate complexity of fires and the large number of possible scenarios coupled with a limited amount of fire data and computer

power, actual computer modelling of fires has only just come to fruition in the last 20 years (Mawhinney et al, 1994).

The two approaches to fire modelling are: 1) probabilistic and 2) deterministic (Stroup, 1995). Probabilistic models make a risk based assessment of what could happen in a particular scenario based on experience and past occurrences of fires. Deterministic models on the other hand provide a more rigorous mathematical approach to modelling based on physical laws (Kanury, 1987). Many phenomena in classical physics are explained using deterministic models. For example, Newton's laws of motion are deterministic models. The modelling of fire behaviour, although vastly more complicated, naturally leads on from some of the classical physics equations such as those for fluid dynamics.

Deterministic fire models can range from quite simple correlations that utilise only a few equations to highly complex models requiring hours of computer time (Stroup, 1995). These models are generally divided into two types, zone models and field models. Both models are deterministic models of varying complexities (Kanury, 1987).

The zone model is the simpler of the two and has been widely used as a design tool in fire engineering for many years. The model simply represents the enclosure as two distinct homogenous zones: a hot upper layer and a relatively cool lower layer. These layers have resulted from thermal stratification due to buoyancy differences (Quintiere, 1995). A combination of empirically derived correlations and conservation equations derived from first principles are utilised to model the various transport and combustion processes that apply.

The field model is the second type of deterministic fire model. In a field model the domain of interest is divided into a three dimensional grid of control volumes. Computation Fluid Dynamics (CFD) are applied to each control volume and the conservation equations of mass, momentum, energy and species are solved. The most widely used field model in fire engineering at the moment is the Fire Dynamics Simulator (FDS) model developed by the National Institute of Standards and Technology (NIST) in the United States. This is the model that was used in this research.

1.3 Impetus for research

The use of CFD models is becoming more common in fire-engineering practise. Instead of being used solely as a research tool it is now beginning to replace the more familiar zone models as a design tool in industry. However, although CFD models provide much more insight into fire behaviour the simulation time is much longer than it is for zone models. Therefore, to reduce the computational time of CFD models designers are sacrificing fine grid resolution. To what extent decreasing grid resolution has on the final model predictions is unknown. Designers usually assign an arbitrary safety factor or assume it to be negligible.

There seems to be very limited data in literature that indicates to what extent grid size can be increased. Obviously some form of validation is needed. This research will concentrate on the effects of increased grid size in the CFD model FDS. It is envisaged that it will provide comparisons for the ongoing validation of the FDS model.

1.4 Research objectives

The objective of this research is to determine to what extent grid resolution can be sacrificed in the FDS field model before results are compromised. This will be achieved by:

1. Simulating fires in two different enclosures, a double isoroom and a high bay hanger.

2. Assessing the effect that different grid sizes have on the model predictions for each of these enclosures.

3. Comparing the model results with the experimental measurements to see if or when the accuracy of the predictions breaks down.

4. Comparing the results with zone model results to see if there comes a point when the zone models provide a better method of prediction.

1.5 Report outline

Section 2, which follows this introduction, provides a brief literature survey on the historical and current developments in field and zone modelling as well as the experimental work that has been carried out. Section 3 outlines the mathematical background and underlying principles of the field model used in this study. Sections 4 and 5 are concerned with the McLeans Island tests, while Sections 6 and 7 detail the Hawaii hanger tests. These sections provide descriptions of the experimental set-up as well as the simulation mythologies, followed by model results and discussions. Section 8 provides the overall conclusions of the research.

1.6 Limitations

The main limitations encountered in the modelling and analysis of results during this research are listed here:

- It was very difficult to obtain accurate output Heat Release Rates (HRRs) using FDS due to the trial and error procedure that had to be adopted. This became very time consuming.
- Restriction on grid size due to the fire diameter made it difficult to accurately model other areas.
- The experimental data recorded during the Hawaii hanger tests turned out to be very limited, making it difficult to compare model results confidently.
- There was limited data on the thermal properties and thickness of a number of the boundary materials used in the FDS models.
- The height of the fire pan in the Hawaii tests could not be simulated for larger grid sizes.
- Some surfaces could not be modelled as flat surfaces. They had to be stepped according to the grid size in order to correctly model slopes and the total volume of the Hawaii hanger.
- The limited data produced by zone models made it difficult to directly compare the results with the FDS models.

2 Literature Review

This section will serve to outline the work that has previously been done on field modelling. The history of field modelling will be introduced and the validation of models that have been performed to date will be given. Finally, current fire modelling techniques in industry will be outlined. A summary is also given which outlines how this literature review applies to this research project.

2.1 Field Modelling History

The use of mathematical models for the simulation of fires in compartments dates back nearly 40 years. These early models, which were developed before the advent of modern computers, were the precursor to the now well-known zone models (Mawhinney et al, 1994). The zone models, due to their speed and simplicity, became commercially available well before any Computational Fluid Dynamic (CFD) based field models. However, many field models were under development or being validated as early as the 1970s but remained for many years purely as research tools. Even after 20 or 30 years of development CFD field models are not totally integrated into the fire engineering community. This is essentially due to the lack of field model validation. Most experimental work is not performed for model validation purposes, or often only designed for comparisons with the less demanding zone models. It is much more difficult to perform a comprehensive validation with field models because of their complexity and the flexibility in the scenarios that they can simulate.

The 1970s and 1980s saw the introduction of many general-purpose CFD codes that had been developed for use in industry. These CFD models evolved into very important design tools with many industrial applications in aerodynamics, piping design, pump and turbine design and even environmental flow (Bilger, 1994). Some of these codes made claim to having fire modelling capabilities but were never validated for this application. However, by the late 1980s a variety of CFD models for fire simulation had emerged, including: JASMINE, KAMELEON, FLUENT and SOFIE. These field models utilised the general CFD equations

but incorporated a simple combustion model that simulated a lumped HRR. They also accounted for the dominant buoyancy forces that occur in fire plumes by modifications to the Navier-Stokes equations for fluid flow (Floyd et al, 2001) (see Section 3.1).

JASMINE, which stands for Analysis of Smoke Movement In Enclosures was developed as a fire specific code by the Fire Research Station in the United Kingdom in the early 1980s (Cox et al, 1985). It evolved from the 2-dimensional steady state CFD code called MOSIE, which had been developed in the 1970s for general purpose industrial applications (Lovatt, 1998). The equation solver in JASMINE is based on what is known as the PHONETICS code.

PHONETICS was developed by Spalding at the Imperial College, United Kingdom. It is a general purpose code which utilises a simple combustion model and the k-ε turbulence model for fire simulations. The k-ε turbulence model was developed as early as 1972 by Jones and Launder (Lovatt, 1998). It is a two equation model that has had very widespread application with reasonable success despite its known weaknesses (McGrattan et al, 2001). The two equations are solved to obtain a solution for the turbulent kinetic energy (k) and the viscous dissipation of this energy (ε) into internal fluid energy. It ultimately calculates an eddy viscosity based on the degree of turbulence in the flow rather than as a property of the fluid itself (Cox, 1995). In an enclosure, this translates to unstable stratification in the plume and stable stratification in the hot upper layer (Kumar et al, 1991).

SOFIE is also a fire specific CFD field model that was developed though collaboration between a number of countries. It also uses the k-ε turbulence model but has a more sophisticated eddy break-up model for combustion, which makes some attempt at simulating the combustion resulting from the turbulent mixing of oxygen and fuel (Lovatt, 1998).

The early 1990s saw the introduction of FLOW 3D, which is a general purpose model developed by Harwell Laboratories in the United Kingdom. More recently NIST-LES, which ultimately evolved into FDS (the model used in this research project) has been developed and made freely available on the internet by the National Institute of Standards and Technology (NIST) in the USA.

Many of the models mentioned above have had various validation studies performed and these are outlined below in Section 2.2. An overview of the FDS model equations is provided in Section 3.

2.2 Model Validation

2.2.1 Domestic sized enclosure fires

A large body of work has emerged on the validation of model predictions of domestic sized enclosure fires. The most commonly used experiments for these validations are those performed by Steckler, Quintiere and Rinkenin in the early 1980s (Mawhinney et al, 1994). These are subsequently referred to as the 'Steckler et al experiments'. A series of 45 experiments in an enclosure measuring 2.8 x 2.8 metres x 2.18 metres high were conducted. The experiments varied the fire size, fire location and door size, recording velocities and temperatures through the opening as well an array of temperatures within the enclosure. A 0.3 metre square methane burner was used as the fire source, the heat output ranged between 32 and 158kW.

Mawhinney et al (1994) compared results from the PHOENICS model with the experiments by Steckler et al. Several scenarios were modelled: three fire locations, 3 door widths and two fire sizes. The comparisons were based on the upper layer temperatures, mass fluxes across the door and doorway vertical velocity and temperature profiles. The k-ε model for turbulence (briefly explained in Section 2.1) was incorporated into the PHOENICS model, combustion and radiation were ignored and the walls were assumed adiabatic. The heat loss via conduction and radiation out of the opening were accounted for by reducing the input HRR. The numerical grid consisted of 23 x 20 x 18 (8280) cells. The average upper layer temperatures were found to be in good agreement with experimental results. Mass fluxes fell within 15% of those observed and neutral plane height in the opening fell within 10%. However, problems occurred when the fire location was near a wall or in the corner of the enclosure, with differences of up to 50%. The horizontal velocity distribution in the doorway curved the opposite way than that observed in the experiments. Further simulations found that this was due to the wall being modelled as a thin plate rather than a thick wall.

Kerrison et al (1994) also used the experiments by Steckler et al to compare with simulations using the FLOW3D field model. Various fire locations, door width and fire sizes were modelled. Essentially the same assumptions, boundary conditions and grid size as the simulations performed by Mawhinney et al (1994) were used, except that additional simulations with isothermal walls and one with a finer grid size were performed. It was found that the predictions using isothermal walls agreed more accurately than those with adiabatic walls. Again it was shown that simulations of fires near walls yielded poorer predictions and it was concluded that this was due to not having a full treatment of the thermal boundary conditions. Kerrison et al (1994) also performed one simulation with a finer mesh consisting of about 62,000 cells (the other simulations had 8280 cells). This refinement improved the overall level of agreement but still under-predicted the velocities through the door. However, it was mentioned that the experimental measurements in this region were questionable.

Other validation studies for JASMINE also used the Steckler et al experiments; Markatos and Cox in the early 1980s (Lovatt, 1998) and Kumar et al (1991) and Hadjisophocleous and Cacambouras in the early 1990s (Kerrison et al, 1994). All these comparisons gave similar results to Kerrison et al (1994) and Mawhinney et al (1994), described above. Kumar et al (1991) concentrated on the effects of radiation in compartment fires, concluding that the inclusion of radiation is important for realistic modelling of the fluid dynamics inside enclosures and in openings, where it was found that mass fluxes and lower layer temperatures increase due to radiation.

The CFD model SOFIE was also used to compare with the Steckler et al experiments. The simulations concentrated on incorporating a discrete thermal radiation model and the eddy break-up combustion model mentioned in Section 2.1. It was found that an improvement was made from the simply prescribed heat source of the JASMINE and PHONETICS models (Lovatt, 1991; Lewis et al, 1997).

Cox et al (1985) performed a series of experiments in a closed fire cell measuring 6 x 4 metres x 4.5 metres high and compared the collected data with JASMINE simulation predictions. These comparisons found that there was good agreement in the temperature predictions, except in areas close to the fire and fire plume. This was thought to be due to the following reasons: the radiation from the fire was not modelled, course grids were used and

the combustion model was poor. Gas composition measurements were also compared to predictions but the agreement was poorer than the temperature comparisons.

Cox et al (1985) also compared the JASMINE model against tests performed in a six-bed hospital ward. This ward had a 7.33 x 7.85 metre plan and was 2.7 metres high. Six 1 kW radiators were also used in the test and were modelled as one 6 kW radiator. The simulation was a challenging problem because the enclosure was sealed which meant the fire was under-ventilated. JASMINE did not have a combustion subroutine to account for this. Also the model did not account for the fire spread that occurred. As a result the predictions were unreliable (Cox et al, 1985).

All of the above model validations were usually performed alongside comparisons with various zone models, which were considered to be still at the forefront of fire safety design. All comparisons compared favourably in the direction of the field models.

2.2.2 Large scale enclosure fires

A number of large-scale enclosures have been used to test the CFD models more rigorously in less ideal situations. These enclosures include larger spaces with high ceilings and a number of comparisons with tunnel fires. The larger enclosures are intended to represent areas such as atriums, auditoriums, factories or hangers.

The Building and Research Association of New Zealand (BRANZ) performed experiments in an enclosure measuring 41 x 11 metres by 11 metres high. Theses experiments were solely for the validation of the zone models in high roofed enclosures, but have been extended to compare with field models (Collier, 1997). These comparisons showed that the capabilities of zone models were challenged but field model predictions were promising.

Cox et al (1985) details a series of experiments in the Zwenberg tunnel and the comparisons of the results of these tests with predictions from the field model JASMINE. These comparisons were in conjunction with the comparisons of the fire test cell and the hospital ward that are outlined in Section 2.2.1. The Zwenberg tunnel had a 2.2% gradient and was 390 metres long, 5 metres wide with a 4 metre high false ceiling. The field model was divided

into a total of 1566 grid nodes; these were stretched so that the area around the fire was resolved in more detail. The tunnel was sealed at one end and a fan installed to create forced ventilation of known velocities. The JASMINE model predictions were in good agreement to the experimental results except in areas close to the fire. This was reported to be due to too coarse a grid resolution and the poor combustion model used in JASMINE. Also radiation was not included in the model calculations, which would have produced the discrepancies for areas immediately above the fire (Cox et al, 1985).

Notarianni and Davis (1993) used a series of experiments performed in a hanger measuring 115 x 389 metres, which contained seven separate bays. The ceiling was 30.4 metres high. The test results of an 8250kW isopropyl pool fire were compared against predictions of a number of zone models and the FLOW3D field model. In these models it was assumed that all the heat was released by the 16 grids directly above the fire. FLOW3D displayed the best agreement for most of the comparisons except that the centreline plume temperature predictions were poor. The zone models tended to under-predict the temperatures. Several grid sizes were used in the model to assess the effect on model predictions. The finer grid models displayed more accurate predictions in the fire plume.

Notarianni and Davis (1993) also made comparisons of the FLOW3D model with experiments performed in a NASA clean room that was 27.4 metres high with forced horizontal laminar flow. The analysis was conducted for fires ranging from 40kW to 32,000kW. These comparisons were predominantly concerned with the detector activation times predicted by zone models. There were no direct conclusions drawn on the performance of the field model except to say that an advantage was gained over the zone models because the plume and associated lean due to the forced air flow in the enclosure were predicted.

The high bay hanger experiments in Hawaii that are used in this research have been used previously to compare against predictions made by various field models. Gott et al (1997) explains how NIST-LES was used prior to the tests at the facility being performed, to obtain an idea of the size of fires that were needed in order to activate sprinklers of different activation temperatures. A quantitative comparison of the experimental data was not performed.

Davis et al (1996) used the CFD models CFX and NIST-LES as well as a number of zone models to predict temperatures in the Hawaii hanger. The geometry and dimensions of this hanger are explained in more detail in Section 6.1. Davis et al (1997) concluded that the performance of the CFD models were better than the zone models in some comparisons but very poor in others. The NIST-LES results over predicted the experimental results of the tests considered. The reason for this was thought to be due to the poor grid resolution. It was observed that the model was in good agreement with the plume temperature correlations when the grids were in the order of one tenth of the characteristic fire diameter. The NIST-LES model worked best when the fire was large enough so that the entrainment processes could be modelled directly without resorting to an empirical turbulence model. For the fire sizes used there was still some relevant mixing that was not resolved which led to the higher temperatures that were observed in the plume (Davis et al, 1996).

2.3 Fire modelling for design

The validation studies outlined in Section 2.2, all make comparisons with results from relatively controlled experiments. The purpose of these comparisons is to obtain an idea of the performance and uncertainties associated with the field models so that they can be used confidently and appropriately as a design tool. However, because the experiments are in controlled environments the validation is very limited. Field modelling in industry is beginning to become more diverse in the range and complexity of the scenarios that are simulated. Large outdoor fires in the order of 1000kW/m^2 resulting from a large oil spill is one example that is outlined by Baum (2000). Simulations such as this are difficult to validate because of the large computational domain that is used, in this case a cube with 768 metre sides. Qualitative comparisons based on visual observations of similar fires are the only way of assessing the results. For this reason the results should be treated as strictly qualitative.

The simulation of different suppression mechanisms in fire scenarios is also beginning to be used. NIST have recently incorporated a sub-routine in FDS that simulates the effect of sprinklers on fires. This predicts the activation time of the sprinklers as well as the containment effect that the sprinklers have on the fire. Validation studies have been performed to compare this sprinkler simulation with experimental results. The comparisons

indicated that the activation times and gas temperatures after the sprinkler activation fell within 20% of the experimental results (Baum, 2000).

Using field modelling for design purposes is fast becoming the norm in industry. However, care must be taken to evaluate the nature of the particular scenario and assess the ability of the field model to accurately simulate it.

2.4 Summary

Section 2.2 outlined a range of studies that have been performed to compare various field models with experimental results. Generally these models gave good far field predictions but poor predictions for areas close to the fire and in the fire plume. This was due to the grids not being small enough to adequately resolve the mixing processes in these areas. It was also apparent that most of the combustion models used in the simulations were inadequate in modelling the actual fire behaviour and fire temperatures.

Limited studies have been performed on the effect of changing grid size, which is the main topic of this research. The limited data available suggested that finer grids did produce much better predictions of centreline plume temperatures but the improvements were only small for areas further away from the fire. Davis et al (1996) observed that when the grids were in the order of one tenth of the characteristic fire diameter the model gave predictions that were in good agreement to experimental plume centreline temperatures.

The extent to which field models are being used in design is increasing, so the need for more validation is essential, not only for a better understanding of the limitations of current models but also for the ongoing development of CFD field models.

3 FDS model

This chapter outlines the various concepts and equations behind the FDS model. It is only designed to give a brief overview and broad understanding of the mathematics behind the field model, the aim being to develop a familiarity with FDS.

The main references sited and are the work of Hinze (1975), who describes the equations and in-depth theory behind turbulence; McGrattan et al (2001), who provides the actual equations used in FDS and Cox (1995), who provides the derivations and basic concepts for the conservation equations and turbulence modelling.

3.1 Hydrodynamic model

The general fluid dynamic equations describing the transport of mass, momentum and energy can be used to describe a large and varied array of physical processes, many of which have nothing to do with fire. This generality is not needed in fire models and would only serve to complicate what is already a complicated task. The simplified equations, developed by Rehm and Baum (McGrattan et al, 2001) use an approximate form of the Navier-Stokes equations for flow in a thermally expandable multi-component fluid. The original Navier-Stokes equations, as well as derivations from first principles, are given in Hinze (1975, Chapter 1). This simplified form is achieved by filtering out acoustic waves to obtain what is known as the "low Mach number" equations. They describe the low speed motion of gases, driven by a chemical heat release and buoyancy forces. These equations allow for large variations in density and temperature but only small changes in pressure, which are typical of fire scenarios (Floyd et al, 2001).

The four equations of conservation detailed below are central to this generalised form of the Navier-Stokes equation. In order to numerically solve the equations in FDS they are discretised in space using a 2^{nd} order central difference method and in time using a 2^{nd} order predictor-corrector scheme. Both these methods are detailed in McGrattan et al (2001) and Kreyszig (1993).

3.1.1 Conservation of Mass

Generally, the conservation of mass states that the rate of mass storage, due to density changes within a control volume is balanced by the net rate of inflow of mass by convection (Lovatt, 1998). If the density is constant then the equation simply states that what flows in must flow out (Cox, 1995). The equation is written as:

$$\frac{\partial \rho}{\partial t} + \nabla \cdot \rho \mathbf{u} = 0$$

Equation 3.1

The first term describes the density changes with time and the second defines the mass convection; **u** is the vector describing the velocity in the *u, v* and *w* directions.

3.1.2 Conservation of Momentum

The equation for the conservation of momentum is derived by applying Newton's second law of motion, which states that the rate of change of momentum of a fluid element is equal to the sum of the forces acting on it (Cox, 1995):

$$\rho\left(\frac{\partial \mathbf{u}}{\partial t} + (\mathbf{u} \cdot \nabla)\mathbf{u}\right) + \nabla p = \rho \mathbf{g} + \mathbf{f} + \nabla \cdot \tau$$

Equation 3.2

Here the left hand side represents the rate of change of momentum of a volume of fluid, while the right hand side comprises the forces acting on it. These forces include gravity (**g**), an external force vector (**f**) (which represents the drag associated with sprinkler droplets that penetrate the control volume) and a measure of the viscous stress (τ) acting on the fluid within the control volume. Of these three forces, gravity is the most important because it represents the influence of buoyancy on the flow.

The viscous stress tensor (τ) is given by the product between the viscosity and a measure of the velocities that the fluid volume is subjected to in a turbulent environment. This velocity term is derived from what is known as a deformation tensor, which accounts for the

turbulence in the control volume. The viscosity term is calculated depending on the mode of simulation in FDS, which in turn depends on the grid resolution. The two modes are Large Eddy Simulation (LES) and Direct Numerical Simulation (DNS) and are described in more detail in Section 3.2 below. For the LES approach to fire modelling, where the grid resolution is not fine enough to capture all the relevant mixing processes, the sub-grid analysis of Smagorinsky is used to model the viscosity (McGrattan et al, 2001). This also utilises the deformation tensor mentioned above to arrive at a value for the local turbulent viscosity based on the density, an empirical constant and a characteristic length (which is in the order of the grid size used in the model). This turbulent viscosity can then be used to calculate thermal conductivity and diffusivity for the LES model. The various equations used to define these tensors and variables can be found in McGrattan et al, (2001) and more rigorous derivations of the turbulence modelling in Hinze (1975) and Cox (1995). The FDS model uses a set of different equations to directly model the diffusion if the DNS mode is used. The equations for these are also described in McGrattan et al, (2001).

The equation for the conservation of momentum (Equation 3.2) is simplified by utilising various substitutions as well as assumptions concerning the sources of vorticity in the force terms to obtain a linear algebraic equation that can be solved quickly and directly in the model calculations using fast Fourier transforms. The exact equations associated with this simplification can be found in McGrattan et al (2001).

3.1.3 Conservation of Energy

The energy equation can come in a variety of forms and contain a large number of variables. In general it describes the balance of energy within the control volume (Lovatt, 1998). This accounts for the energy accumulation due to internal heat and kinetic energy, as well as the energy fluxes associated with convection, conduction, radiation, the interdiffusion of species and the work done on the gases by viscous stresses and body forces (Cox, 1995). The form that the FDS model uses is:

$$\frac{\partial}{\partial t}(\rho h)+\nabla\cdot\rho h\mathbf{u}-\frac{\partial p}{\partial t}+\mathbf{u}\cdot\nabla p=q'''-\nabla\cdot q_r+\nabla\cdot k\nabla T+\nabla\cdot\sum_l h_l(\rho D)_l\nabla Y_l \qquad \textbf{Equation 3.3}$$

The left side describes the net rate of accumulation, while the right side is comprised of the various energy gain or loss terms that contribute to this accumulation. These include the energy driving the system, represented as the HRR (q'''), the radiative flux ($\mathbf{q_r}$) and the convective term ($\nabla \kappa v T$). The last term represents the energy change associated with species interdiffusion.

3.1.4 Conservation of Species

The conservation of species also has to be preserved within the system. The following equation is used in FDS to achieve this:

$$\frac{\partial}{\partial t}(\rho Y_I) + \nabla \cdot \rho Y_I \mathbf{u} = \nabla \cdot (\rho D)_I \nabla Y_I + W_I'''$$

Equation 3.4

The first term on the left side represents the accumulation of species due to a change in density, the second term is the inflow and outflow of species. The right side gives the terms for the inflow or outflow of species from the control volume due to diffusion and the production rate of the particular species.

3.2 Combustion model

There are two types of combustion models used in FDS. The choice of model is dependent on the grid resolution of the particular simulation. DNS is used when the diffusion of fuel and oxygen can be modelled directly (McGrattan, 2001). This applies when the grid size is very fine. For larger grid sizes, more often used in commercial applications of FDS, a LES calculation is performed.

LES refers to the turbulent mixing of combustion gases with the surrounding atmosphere (McGrattan et al, 2001). It therefore assumes that the mixing controls combustion and all species of interest can be represented by a single variable known as the mixture fraction (Z).

The mixture fraction is a quantity representing the fraction of material at a given location that originated as fuel (McGrattan et al, 2001), and is defined as:

$$Z = \frac{sY_F - (Y_O - Y_O^{\infty})}{sY_F^I + Y_O^{\inf}} \quad ; \quad s = \frac{\nu_O M_O}{\nu_F M_F} \qquad \textbf{Equation 3.5}$$

This equation specifies that Z varies from one in the region containing only fuel, to zero where the oxygen mass fraction equals its ambient value, $Y_O^{\inf}$.

This mixture fraction combustion model approximates the combustion process in both space and time so that the fire can be simulated more efficiently (Floyd et al, 2001). It assumes that large-scale convection and radiative transport phenomena can be modelled directly while small scale mixing can be ignored (McGrattan et al, 2001). An infinite reaction rate can be assumed because the combustion processes are on a much shorter time scale than the convection processes. This means that the reaction occurs so rapidly that both fuel and oxygen cannot coexist (Ma & Quintiere, 2001). As a consequence, at a certain point both species instantaneously vanish, their mass fractions (Y_i) dropping to zero. Equation 3.5 can therefore be simplified to obtain the flame mixture fraction (Z_f) at which this occurs:

$$Z_f = \frac{Y_O^{\inf}}{sY_F^{Ii} + Y_O^{\inf}} \qquad \textbf{Equation 3.6}$$

This point (Z_f) defines the flame by prescribing a two-dimensional surface in the three-dimensional computational domain (Floyd et al, 2001) and is known as the flame sheet.

The assumption that fuel and oxygen cannot coexist can also be used to define the state relation between the oxygen mass fraction (Y_O) and the mixture fraction (Z):

$$Y_O(Z) = \begin{cases} Y_O^{\inf}\left(1 - Z/Z_f\right) & Z < Z_f \\ 0 & Z > Z_f \end{cases} \qquad \textbf{Equation 3.7}$$

The mass fractions of all the other species of interest can also be described by individual state relations based on the mixture fraction. These state relations are determined by analysis of the stoichiometric reaction of the particular fuel in question. This is explained in more detail in Floyd et al (2001). Figure 3.1 is an illustration of the relations between the mixture fraction and the mass fraction (state relations) of various species for propane. Where the Fuel and O_2 (oxygen) lines meet at a mass fraction of zero is where the flame sheet is defined, as explained above.

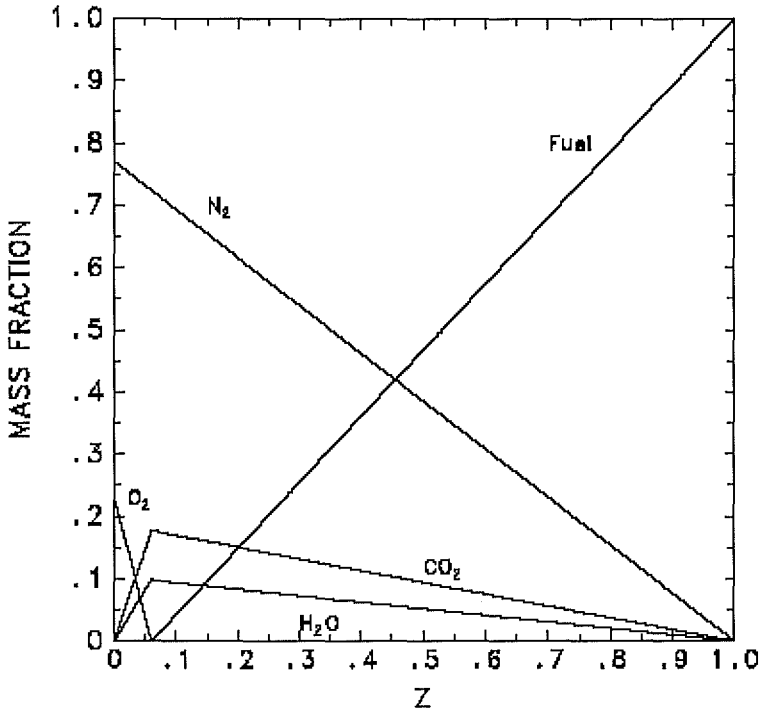

Figure 3.1: State relations for propane (McGrattan et al, 2001).

Since the local oxygen mass fraction has been defined (Equation 3.7), its derivative with time can be used as a means of determining the oxygen consumption rate (m_o'''). This is then used to calculate the local HRR by multiplying it with the HRR per unit mass of oxygen (ΔH_o). McGrattan et al (2001) and Floyd et al (2001) explain in more detail these calculations. They are not reproduced here because only a general understanding of the FDS calculations is required in order to grasp the overall method of the model.

One problem that occurs due to the local HRR calculation procedure (outlined above) is that if the fire is not adequately resolved the flame surface defined by the mixture fraction $Z = Z_f$ will tend to underestimate the observed flame height. An indication of whether the fire is adequately resolved is given by the ratio $D^*/\delta x$. Where D^* is the characteristic fire diameter defined as:

$$D^* = \left(\frac{Q}{\rho_\infty C_p T_\infty \sqrt{g}} \right)^{\frac{2}{5}}$$

Equation 3.8

and δx is the nominal grid size. It has been found that a better estimate of the flame height can be provided by using a different value for the mixture fraction (Z). The expression that is used to calculate this new mixture fraction ($Z_{f,eff}$) is:

$$\frac{Z_{f,eff}}{Z_f} = \min\left(1 \ , \ C\frac{D^*}{\delta x}\right)$$

Equation 3.9

C is an empirical constant that is independent of the scenario being simulated (McGrattan et al, 2001).

3.3 Thermal radiation model

Radiative fluxes are computed with the modified finite volume method, which is derived from the Radiative Transport Equation (RTE) for a non-scattering grey gas (Floyd et al, 2001). This equation relates radiation intensity to wavelength. A method similar to the finite volume method used in fluid flow is then used to solve this initial equation. This is explained in detail in McGrattan et al (2001)

One important change to the standard equations for the radiation intensity (I_b) needs to be made for the cells through which the flame sheet cuts (see Section 3.2). This is because the temperatures are averaged out across the cell and are therefore considerably lower than would

be expected for a particular point in a diffusion flame. Because radiation is dependent on the fourth power of temperature this can have a significant impact on the calculated radiation from those particular grids. Elsewhere the temperature is calculated with greater confidence so the source term can assume its ideal value (McGrattan et al, 2001). The radiation relations become:

$$\kappa I_b = \begin{cases} \kappa\sigma T^4 / \pi & \textit{Outside flame zone} \\ \chi_r q''' / 4\pi & \textit{Inside flame zone} \end{cases} \qquad \textbf{Equation 3.10}$$

q''' is the HRR per unit volume and χ_r is the local fraction of that HRR emitted as thermal radiation. This is not necessarily the same as the global radiative fraction due to re-absorption by smoke released from the fire. This is particularly the case for larger fires. κ is the local absorption coefficient and is dependent on the mixture fraction and temperature. It is determined by a sub-model implemented in FDS called RADCAL (McGrattan et al, 2001).

4 McLeans Island Tests

4.1 Experimental set-up

The McLeans Island isoroom tests were performed by the Civil Department at the University of Canterbury in November and December 2000. The tests consisted of two isorooms, which were the standard dimensions of 2.4 x 3.6 metres by 2.4 metres high. The separating wall between the two rooms was constructed of timber and was a total of 0.2 metres thick. A standard doorway connected the rooms; this was 0.8 metres wide by 2 metres high. Figure 4.1 provides an illustration of the layout and dimensions of the isorooms. One end of the second isoroom was entirely open to allow ventilation and the smoke and gases to flow freely out and into the natural draft exhaust hood above. The entire compartment including the ceiling, floor and all walls were lined with 12mm thick fire rated gypsum board overlaid with 25mm thick Fibreglass board (sold as "Intermediate service board") (Fleischmann, 2000).

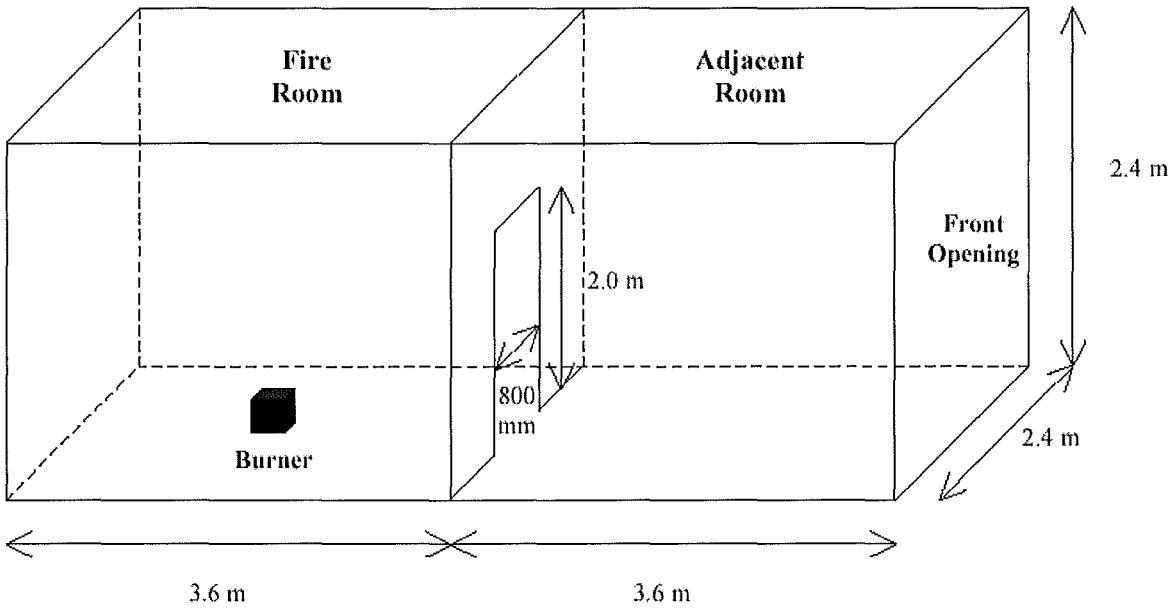

Figure 4.1: McLeans Island Isoroom illustration (reproduced from Nielsen (2000)).

The fire source was a LPG burner measuring 0.3 x 0.3 x 0.2 metres deep and sat 0.1 metres off the floor. The fuel flow could be controlled to generate a known HRR. A number of tests were performed using different heat outputs and burner placements. The HRRs ranged from 55 kW to 165 kW and all except one had the burner situated in the centre of the compartment (Fleischmann, 2000).

The tests used for comparisons in this report all had the burner at the centre of the first or rear isoroom, henceforth described as the fire room. Two experiments with HRRs of 110kW and 55kW were used for the model comparisons.

A series of nine thermocouple trees were used in the tests (see Figure 4.2). These were all placed along the centreline of the compartment. Trees #1 to #4 in the fire room were located at 0.15, 0.9, 1.8, and 2.7 metres from the rear wall. Trees #6 to #9 in the adjacent room were at 0.9, 1.8, 2.7 and 3.6 metres from the wall joining the two rooms (see Figure 4.2). On each of these trees were thirteen thermocouples at heights of 0.3, 0.6, 0.9, 1.1, 1.35, 1.6, 1.85, 2.1, 2.15, 2.2, 2.25, 2.3, 2.35 and 2.375 metres above the floor. The final tree (Doorway tree) was located in the centre of the doorway with thermocouples at 0.1, 0.25, 0.4, 0.55, 0.7, 0.85, 1.0, 1.15, 1.3, 1.45, 1.6, 1.75 and 1.9 metres above the floor. (Fleischmann, 2000).

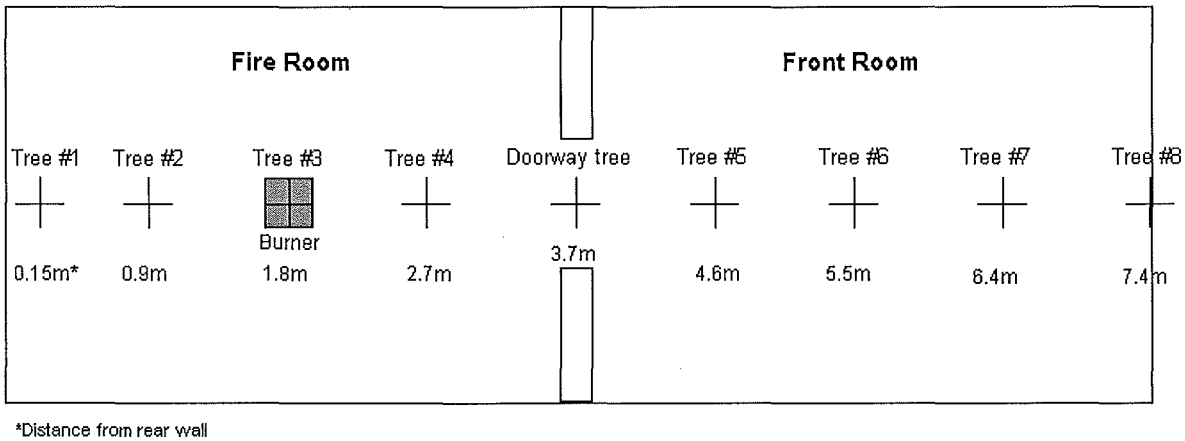

Figure 4.2: Location of the thermocouple trees for the McLeans Island isorooms.

16 species concentration probes were also placed along the centre of the compartments; a set of four in each of the locations corresponding to trees #2, #4 and #7 (see Figure 4.2) at heights of 0.3, 0.6, 1.95 and 2.25 metres, and a set of four in the doorway (Doorway tree) at heights of 0.4, 0.7, 1.6 and 1.9 metres (Fleischmann, 2000).

4.2 FDS modelling

An FDS model was constructed to resemble the experimental set up as outlined above; two rooms, open at one end, with a connecting wall and door. The computational domain was defined as 2.4 metres wide by 2.4 metres high by a length of 7.2 metres plus the width of the wall, which varied for different grid sizes. All the thermocouples and species concentration probes were placed in the locations described in Section 4.1. The burner was modelled as an obstruction 0.3 metres square by 0.3 metres high, located in the centre of the room. On top of this a vent was used to simulate the actual fire, this was assigned a constant Heat Release Rate Per Unit Area (HRRPUA). Figure 4.3 provides a Smoke view image of this FDS model, showing the burner at the centre of the Fire room, all the thermocouple trees and the connecting wall and door.

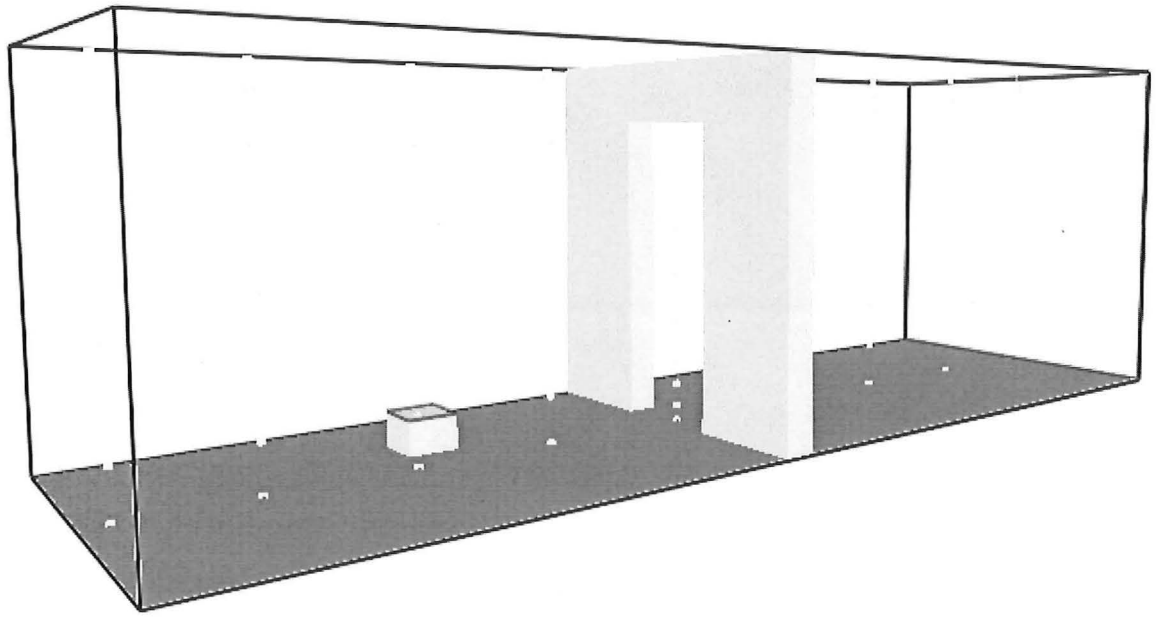

Figure 4.3: Smokeview picture of the FDS isorooms using a grid size of 100mm (H/24).

4.2.1 Grid sizes

Models with a grid size of 100mm, 150mm and 300mm were constructed. These correspond to enclosure height over grid size ratios of H/24, H/16 and H/8. These sizes were based on the physical dimensions of the burner. This meant that the burner or more specifically the HRR was being characterised more precisely.

For each grid size two fire sizes were modelled: 55kW and 110kW. The output from the FDS model is not exact in regards the HRR so in order to obtain the required HRR several runs had to be performed, each time changing the HRRPUA specified in the input FDS file until the required output HRR was obtained. Table 4.1 gives the final HRRPUA used for each model and the corresponding output HRR obtained.

Table 4.1: Input HRRPUA and output HRRs for the McLeans Island FDS models.

	110kW experiment			55kW experiment		
Grid size	**HRRPUA**	**HRR**	**Error**	**HRRPUA**	**HRR**	**Error**
100 mm (H/24)	1387	108	-1.8%	770	54	-1.8%
150 mm (H/16)	1305	111	0.9%	750	55	0%
300 mm (H/8)	1035	109	-0.9%	554	55	0%

4.2.2 Model discrepancies

As mentioned above the size of the fire was considered the most important variable and therefore dictated what size the grids could be. This restriction was at the expense of accuracy in other areas of the model. In particular the location of the burner in the experiments is at the centre of the first isoroom as shown in Figure 4.1 and Figure 4.2. However due to the fact that the obstructions in the model have to conform to the grids the actual burner location in the

FDS models sometimes could not be placed exactly in the centre of the room. This was the case for the models with the 100mm and 300mm grids. Also the thickness of the connecting wall could not be modelled exactly for the 150mm and 300mm grid size models because the actual thickness was 200mm. The dimensions of the door between the two rooms also became a problem, especially for the two larger grid sizes. Appendix A, Table A.1 gives a detailed list of the differences between the experiments and the FDS models used.

4.2.3 Input variables

All the surfaces in the isorooms were lined with a 12mm thick layer of fire rated gypsum board overlaid with a 25mm thick layer of Fibreglass board (Fleischmann, 2000). Because the FDS code only allows for one material in the heat transfer calculations (without a lot of added complexity) it was assumed that the top fibreglass layer was the dominant material contributing to the heat transfer out of the compartment. This fibreglass layer was the thicker of the two and had the greatest thermal resistance. The layer was modelled as thermally thick, which specifies the model to perform a one dimensional heat transfer calculation though the surfaces (McGrattan et al, 2001). The properties required for the thermally thick calculation were the thermal diffusivity (ALPHA), 8.6 x 10^{-8} m^2/s (Quintiere, 1998) and the thermal conductivity (KS), 0.036 W/m.K (Incropera & DeWitt, 1996). These are also tabulated in Appendix D. The terms in brackets (following the variable name) are the call names that are used in the actual FDS input files. These input files are given in Appendix B.1. The thermal properties were based on data for fibreglass board found in the various references cited. It is uncertain, due to lack of relevant documentation whether it is equivalent to what was used in the actual experiments. However, these values do not have to be exact as long as they provide a close approximation to the experiments. The nature of the comparisons between different grid sizes will be enough to deduce the required trends and establish relevant conclusions.

The isoroom models were run for 3600s of fire time. This is equivalent to the duration of the actual fire tests. The model was specified to record data in the spreadsheet every 2 seconds.

4.3 Zone modelling

The zone model CFAST was also used to give comparisons against the FDS models. The isorooms were simply modelled as two rooms of 2.4 x 3.6 metres by 2.4 metres high, connected by a vent or door measuring 0.8 by 2 metres. The front isoroom (Figure 4.2) was assigned an opening of 2.4 by 2.4 metres; this simulated the wall opening that was used in the experiments. The burner was located at the centre of the fire room and assigned a HRR depending on the test being simulated, either 110kW or 55kW. The walls, floor and roof were manually assigned thermal properties. These were equivalent to the thermal properties used in the FDS model as described in Section 4.2.3 for fibreglass board. All the properties are given in Appendix D, Table D.2. The zone model was set to simulate 3600 seconds of fire time.

4.4 Data analysis

As a result of the large amount of data that was obtained from the FDS models and the experiments, some form of data reduction had to be used so that it could be compacted and presented in a more manageable form. This section serves to outline the various techniques that were used to achieve this.

4.4.1 Temperature measurements

The average temperature of each thermocouple was calculated for the steady state period of the experiment. This was assumed to start at 1000 seconds and continue to the end of the test (3600 seconds). The initial 1000 seconds allowed to reach steady state was a conservative start up time based on observation of the time-temperature profiles of the experimental results. The FDS model temperature predictions were also averaged over the same time period.

"Difference" bars of -/+15% of the experimental values are shown on the comparisons to give an idea of the relative accuracy of the FDS predictions compared to the experimental results.

4.4.2 Layer height

In order to compare FDS and experimental results with predictions made by the zone model, CFAST, an indication of layer height was required. To do this the temperature gradients were calculated between each pair of adjacent thermocouples. The layer interface was assumed to occur half way between the two thermocouples which gave the greatest temperature gradient. This was assumed to be analogous to where the cool lower layer meets the hot upper layer in the more simplified zone model predictions. The layer height was calculated for each thermocouple tree and an average taken to obtain one layer height for each of the two isorooms. The tree above the burner (tree #3) was not used in this calculation because a marked temperature difference does not occur in the fire plume. The doorway tree was also excluded from the layer height calculations because it is not indicative of the room layer heights.

4.4.3 Upper and lower layer temperatures

Comparisons were also made between upper and lower layer temperatures. A weighted average of the thermocouple readings was calculated based on the distances between each thermocouple and the layer height (as calculated in Section 4.4.2). This was done for each thermocouple tree and averages taken for each isoroom. Tree #3 and the doorway tree were again not included in the layer temperature calculations.

4.4.4 Oxygen concentration data

The oxygen probe measurements and predictions were also averaged to obtain a single value for each probe. The same initial time of 1000 seconds until steady state was reached was used for the averages. The concentration averages from the fire room and the front room were separated and direct comparisons were made for each experimental point.

5 McLeans Island Results

This section presents the results from the FDS simulations of the McLeans Island isoroom tests. FDS models using three different grid cell sizes were used in the comparisons: 100mm (H/24), 150mm (H/16) and 300mm (H/8). Two sets of results are compared; the 55kW test and the 110kW test. Each set of comparisons include:

- Comparisons of thermocouple tree temperature profiles generated from the measurements taken in the experiments and those predicted by the FDS models.

- Comparisons of layer heights obtained from the experimental data, FDS model predictions and zone model results.

- Comparisons of upper and lower layer temperatures obtained from the experimental data, FDS model predictions and zone model results.

- Comparisons of experimental and FDS model oxygen concentrations at particular points in the isorooms.

- FDS model run times.

5.1 55kW test

5.1.1 Temperature tree profiles

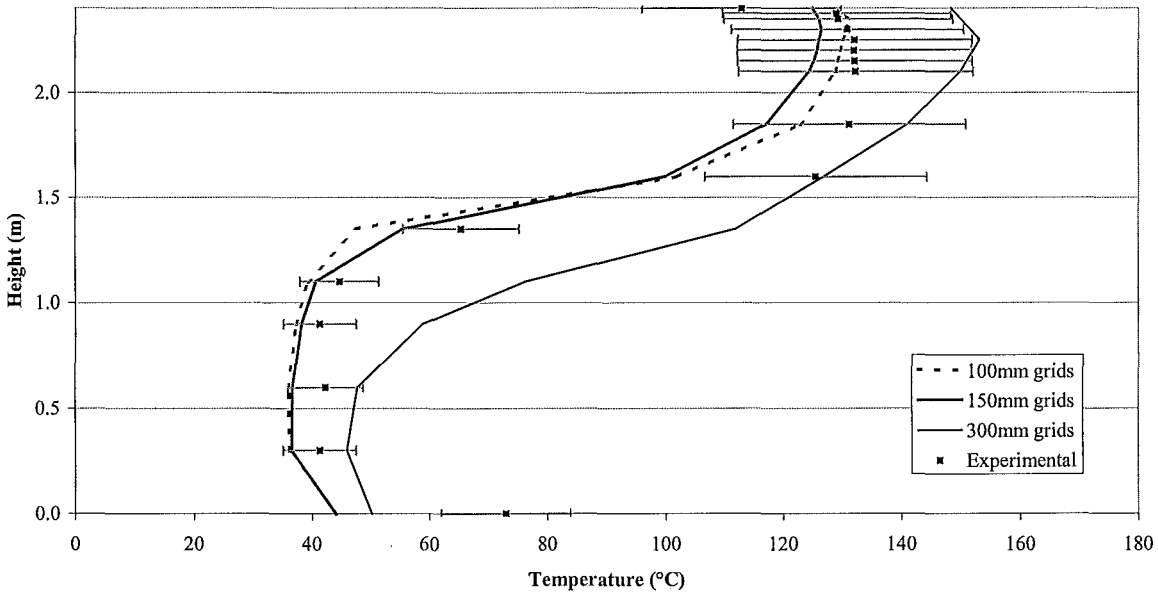

Figure 5.1: Temperature profiles for Tree 1 for the 55kW fire.

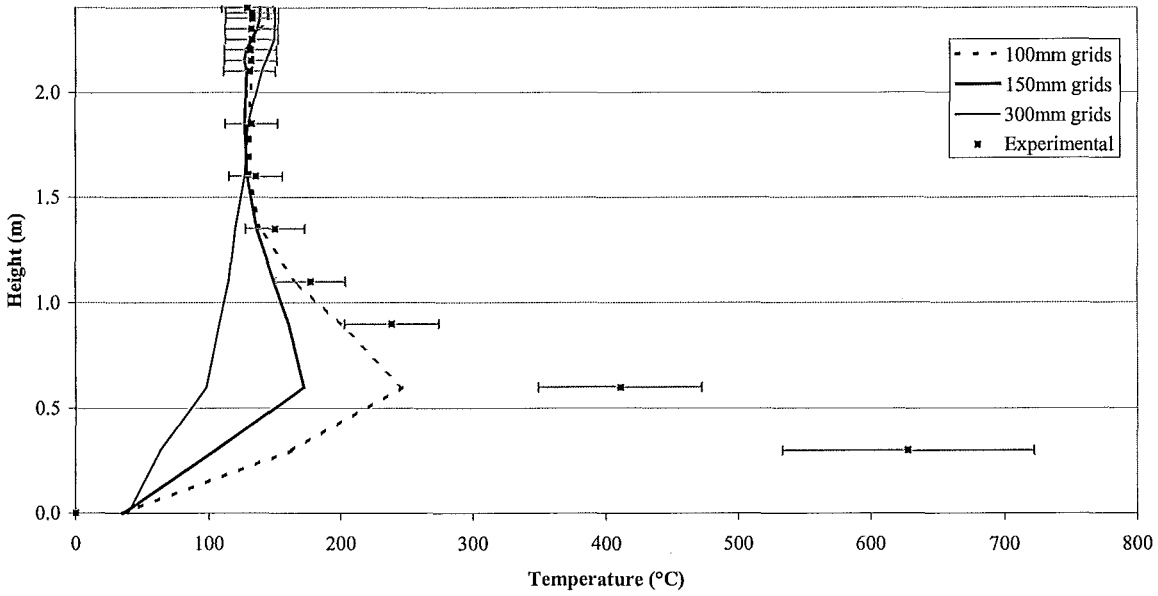

Figure 5.2: Temperature profile for Tree 3 (directly above the burner) for the 55kW fire.

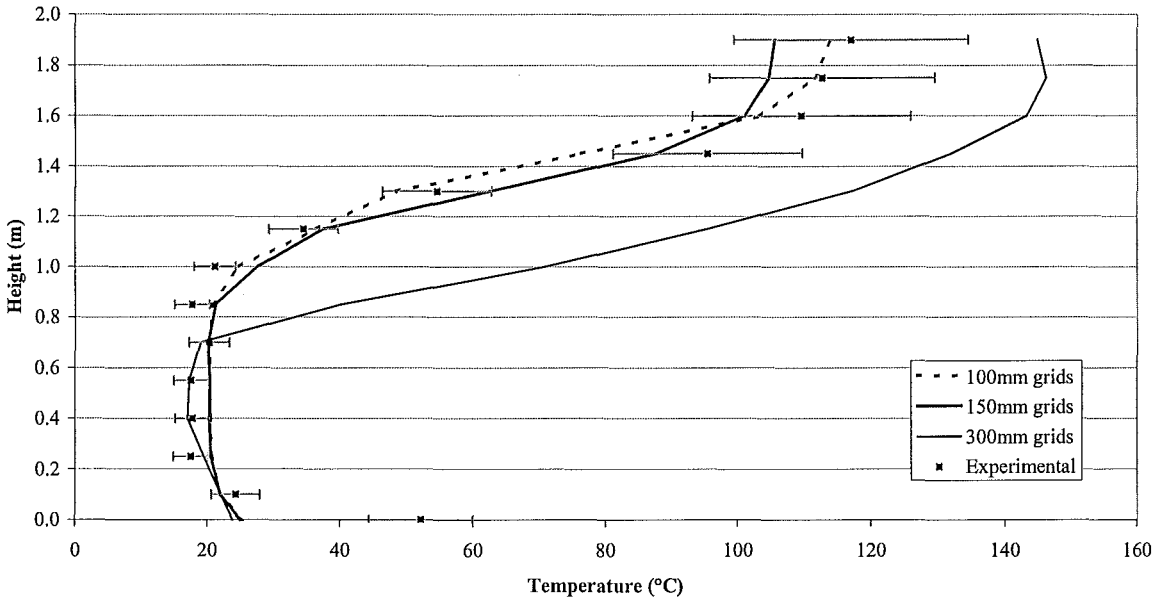

Figure 5.3: Temperature profile for the doorway tree for the 55kW fire.

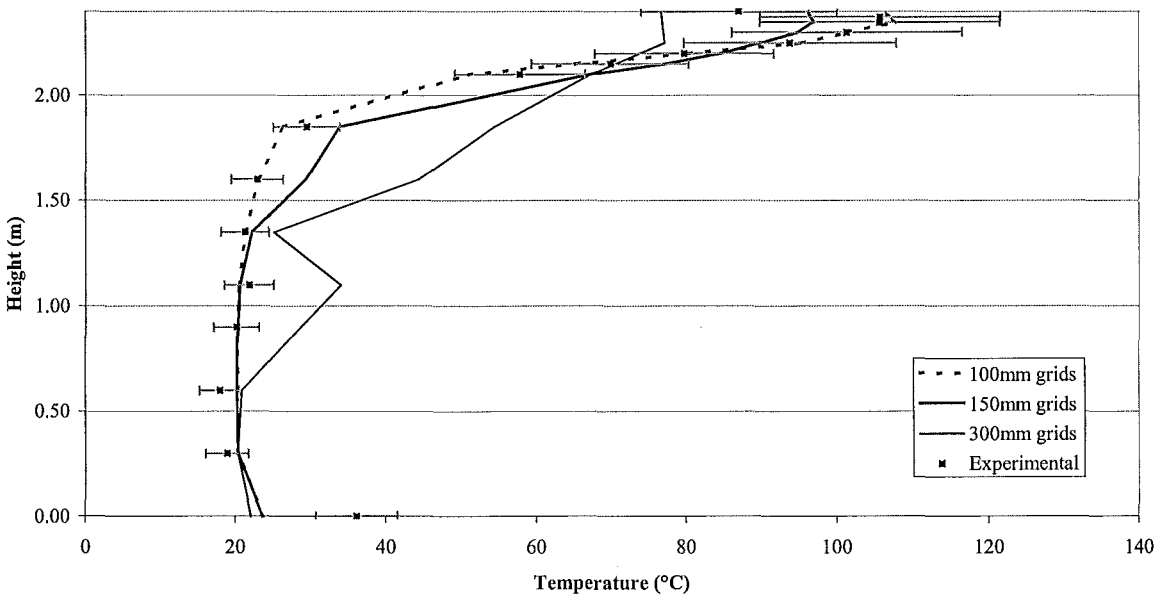

Figure 5.4: Temperature profiles for Tree 5 for the 55kW fire.

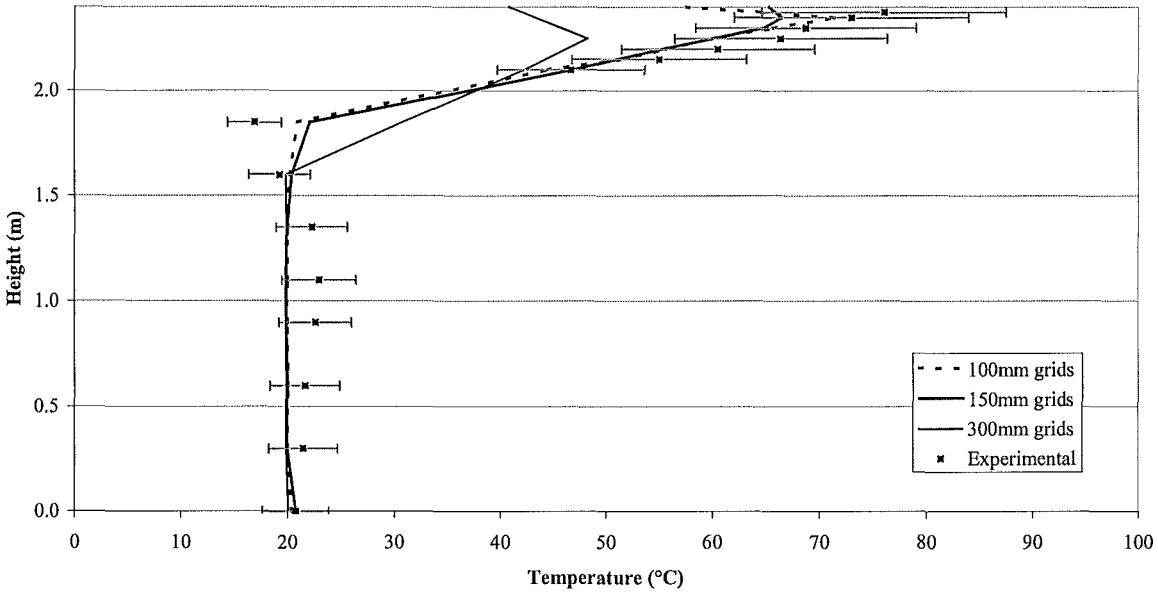

Figure 5.5: Temperature profile for Tree 8 for the 55kW fire.

Figure 5.1 to Figure 5.5 give comparisons of the FDS models with the experimental results. The experimental results are shown as discrete points while straight lines have been used to connect the FDS results. This is purely to aid in visualisation. Uncertainty bars of +/-15% have been added to the experimental points to indicate how good the FDS model predictions are.

To avoid repetition not all the thermocouple tree profiles have been shown here. Trees #2, #4, #6 and #7 are shown in Appendix C.1.

The profiles all show similar trends:

- The models using 100mm grids and 150mm grids both predict the temperature profiles in good agreement with the experimental results, with most predictions lying within +/-15%.

- The 300mm grid model has markedly poorer predictions for all five thermocouple trees.

- The comparisons suggest that for models with 300mm grid cells the greatest error is associated with the upper layer temperature predictions where they are over-predicted for the fire room (Figure 5.1) and under predicted for the front room (Figure 5.4 and Figure 5.5).

- Figure 5.2 shows that temperature predictions close to the burner are very poor for all the grid resolutions used in these comparisons; the larger the grid cells used the poorer the prediction.

- Most of the floor temperatures are being under predicted by the models while the ceiling temperatures are being over predicted. This is particularly obvious in Figure 5.1.

- Figure 5.4 indicates that that there is some sort of instability associated with the 300mm model.

5.1.2 Layer heights

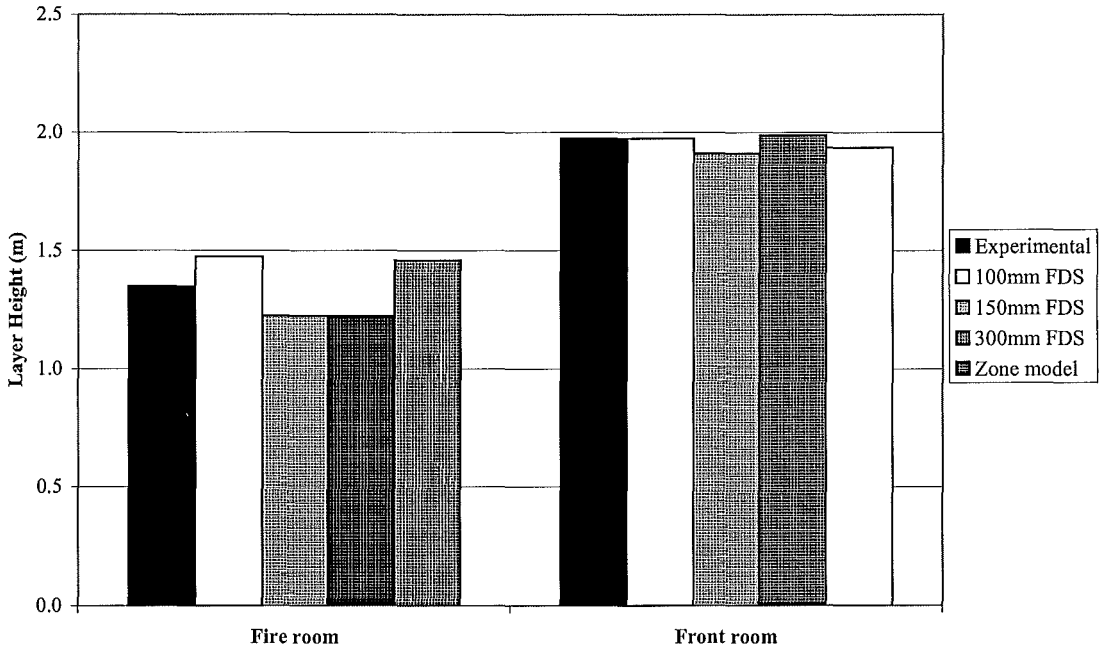

Figure 5.6: Layer height comparisons between FDS, CFAST and experimental results for the 55kW fire.

Figure 5.6 compares between the layer heights calculated from the experimental results and those calculated from the various models. These layer heights were calculated from temperature profiles as explained in Section 4.4. The comparison indicates that:

- There is only a small difference between all the layer height predictions. The predictions in the front room in particular are all very close at just under two metres.

- The 150mm and 300mm models under predict the layer height in the fire room, while the 100mm model and CFAST over predict it.

5.1.3 Upper and Lower Layer Temperatures

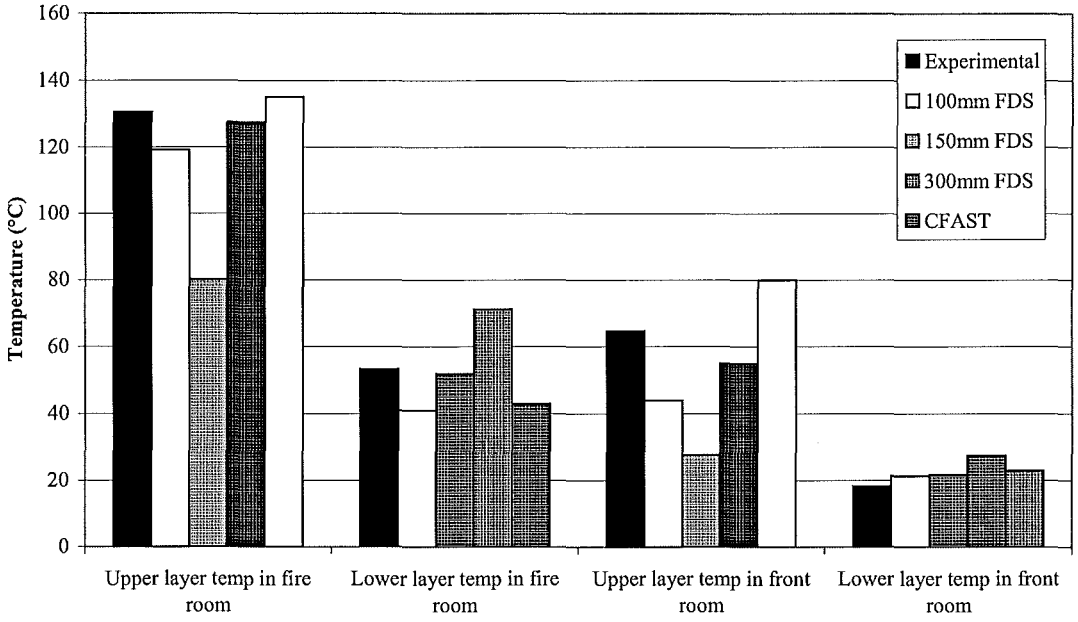

Figure 5.7: Upper and lower layer temperature comparisons between FDS, CFAST and experimental results for the 55kW fire.

Figure 5.7 shows that:

- The 100mm grid model under predicts the layer temperatures, except in the lower layer of the front room.

- The zone model over predicts for the upper layers of the two rooms but under predicts for the lower layers.

- There is a significant temperature increase in the 300mm grid FDS model. This corresponds to a large over prediction for the lower layer temperatures but a better prediction (compared to the other FDS models) for the upper layer temperatures.

5.1.4 Oxygen Concentration

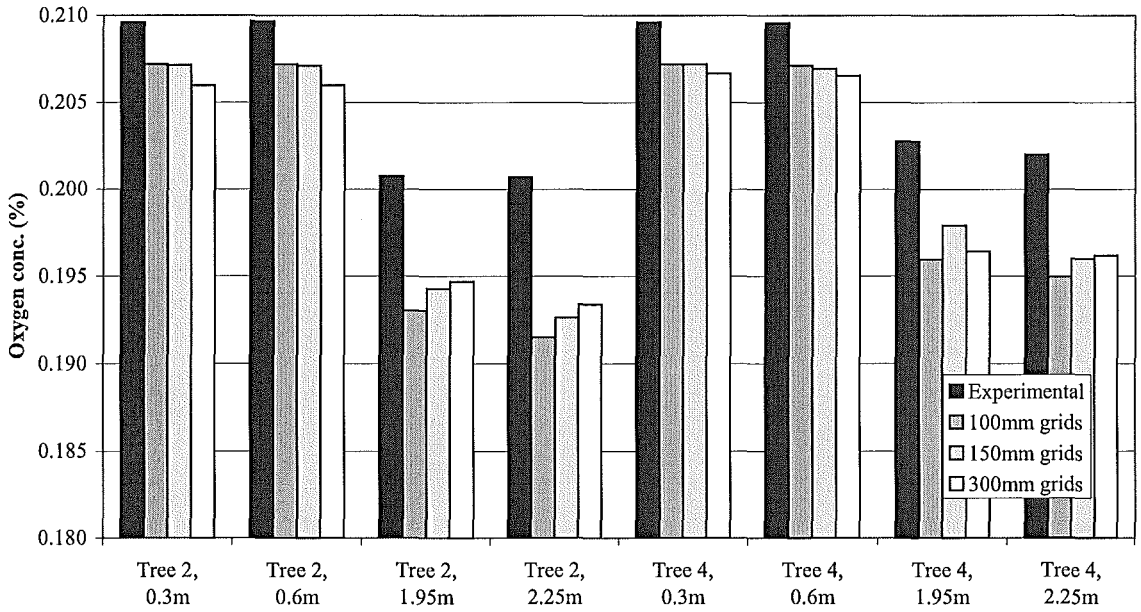

Figure 5.8: Oxygen concentration comparisons in the fire room between the FDS models and experimental results for the 55kW fire.

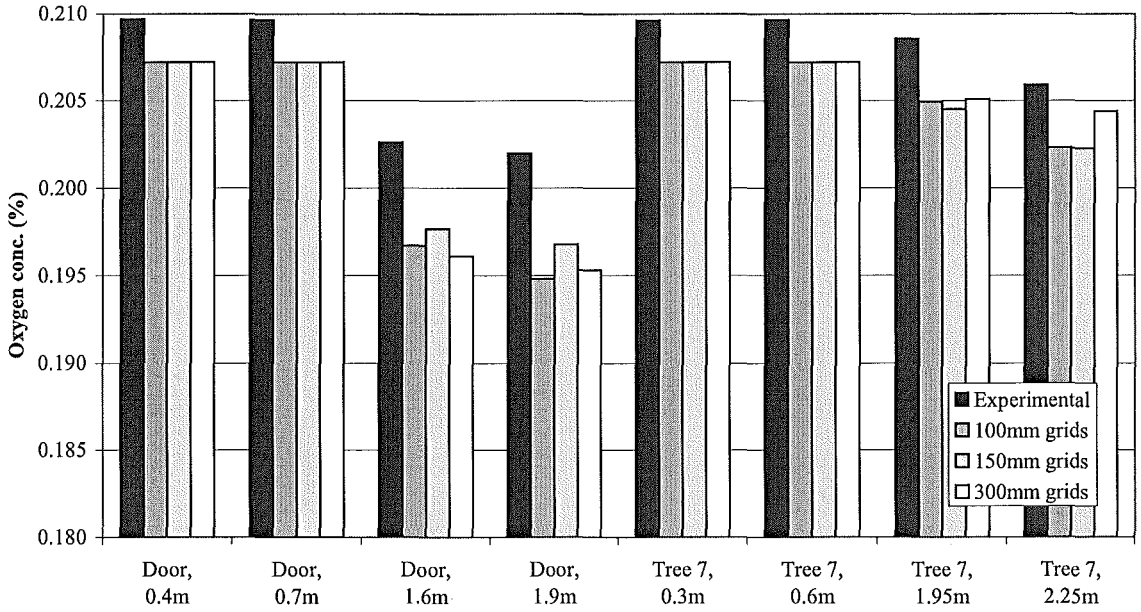

Figure 5.9: Oxygen concentration comparisons in the front room between the FDS models and experimental results for the 55kW fire.

Figure 5.8 and Figure 5.9 provide comparisons of experimental and predicted oxygen concentrations at discrete points.

- Although the difference is small the FDS models under predict the oxygen concentration at all points.

- In general, the predictions in the fire room as the grid size increases, decrease for the lower layer points and increase for the upper layer points (Figure 5.8).

5.2 110kW test

5.2.1 Temperature tree profiles

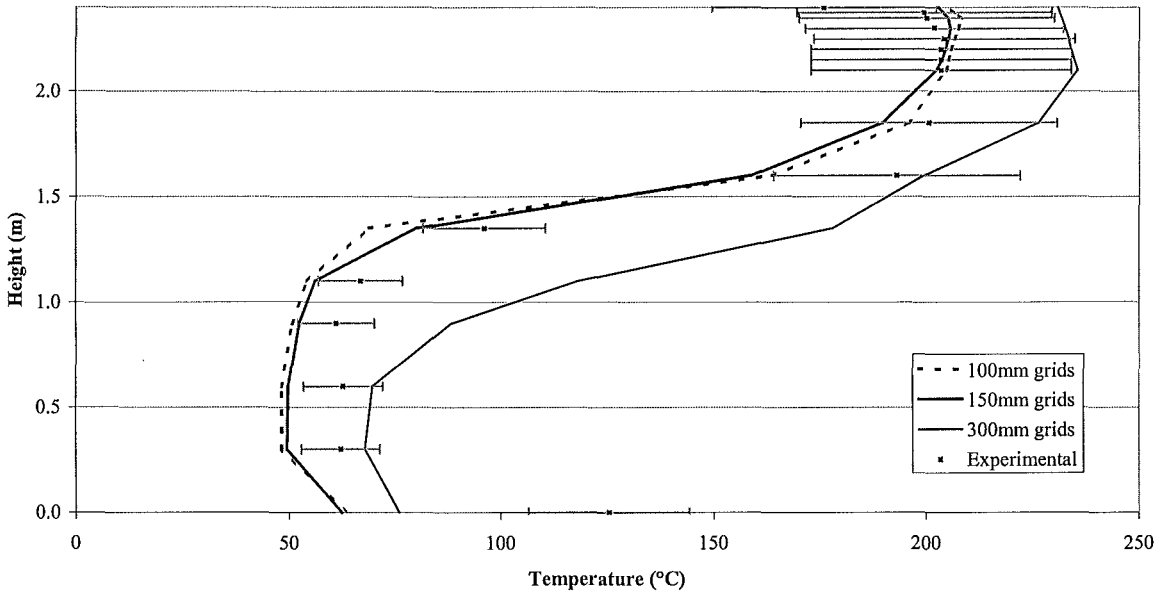

Figure 5.10: Temperature profiles for Tree 1 for the 110kW fire.

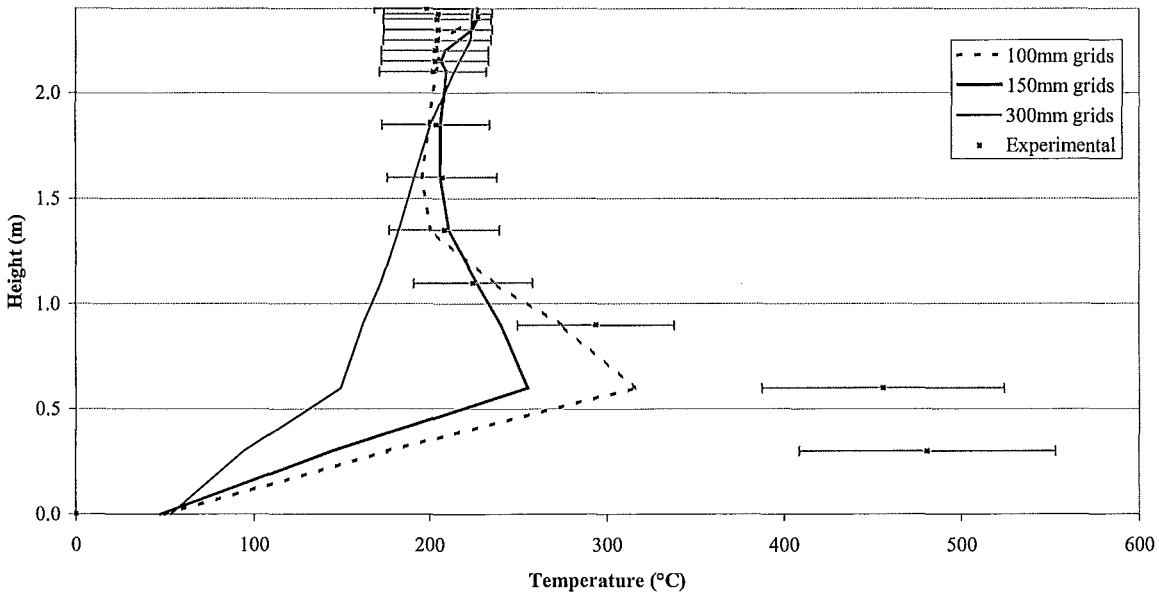

Figure 5.11: Temperature profile for Tree 3 (directly above the burner) for the 110kW fire.

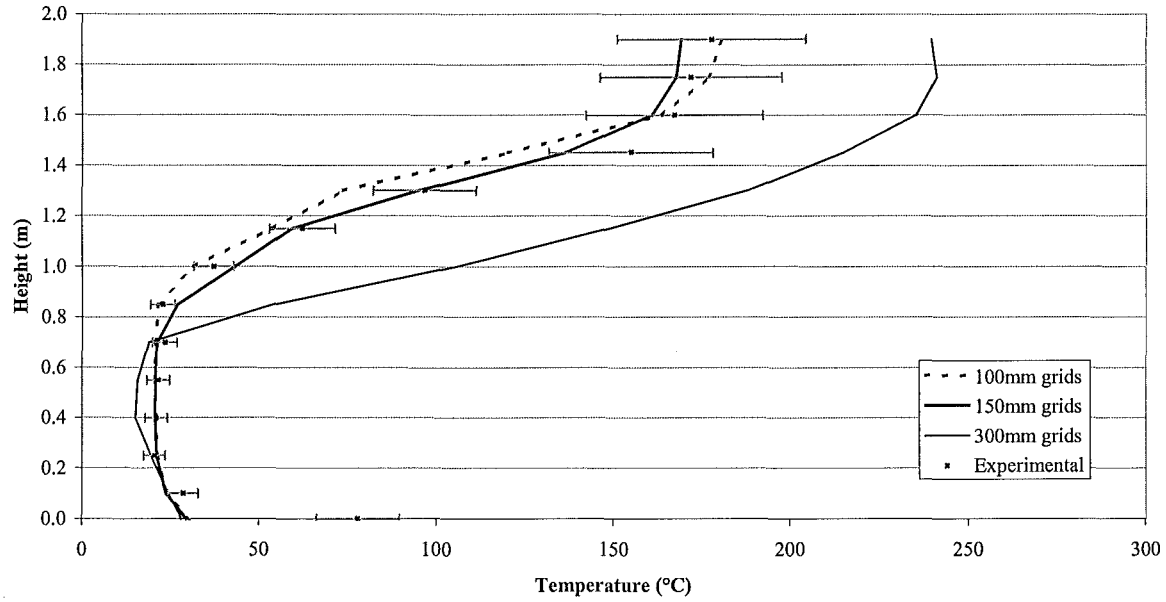

Figure 5.12: Temperature profiles for the doorway tree for the 110kW fire.

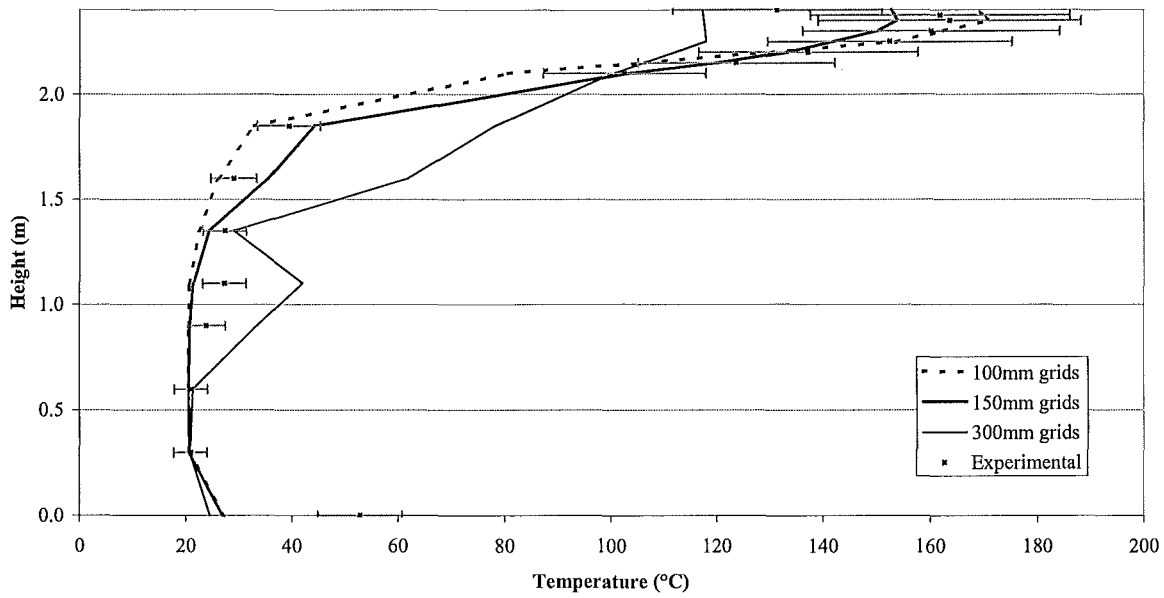

Figure 5.13: Temperature profiles for Tree 5 for the 110kW fire.

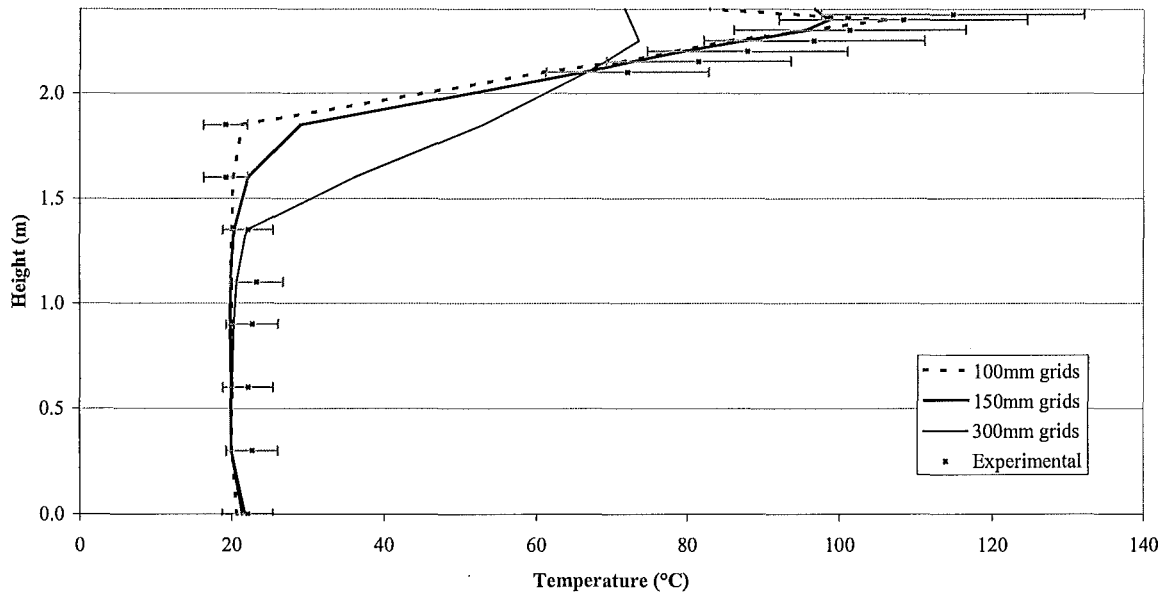

Figure 5.14: Temperature profiles for Tree 8 for the 110kW fire.

Figure 5.10 to Figure 5.14 give comparisons between the experimental results and the three FDS model predictions of the 110kW test, for the temperature profiles of five thermocouple trees. To avoid repetition the other four thermocouple tree profiles have been omitted but are shown in Appendix C.1.

All the profiles show similar trends when compared to the 55kW test comparisons in Section 5.1:

- Generally the 100mm grids and 150mm grid models predict within +/-15% of the experimental results.

- The 300mm grid model has markedly poorer predictions for all five thermocouple trees.

- Temperature predictions directly over the burner are excellent near the ceiling (especially for the 100mm grid model) but are well outside +/-15% of the experimental results close to the burner surface (Figure 5.11). In this region the larger the grid cells used the poorer the prediction.

- Figure 5.11, Figure 5.12 and Figure 5.13 suggest that for models with 300mm grid cells the greatest error is associated with the upper layer temperature predictions where they are over predicted for the fire room and under predicted for the front room.

- Most of the floor temperatures are being under predicted by the models while the ceiling temperatures are being over predicted (Figure 5.10, Figure 5.12 and Figure 5.13).

- Figure 5.13 indicates that there is some sort of instability associated with the 300mm model.

5.2.2 Layer Heights

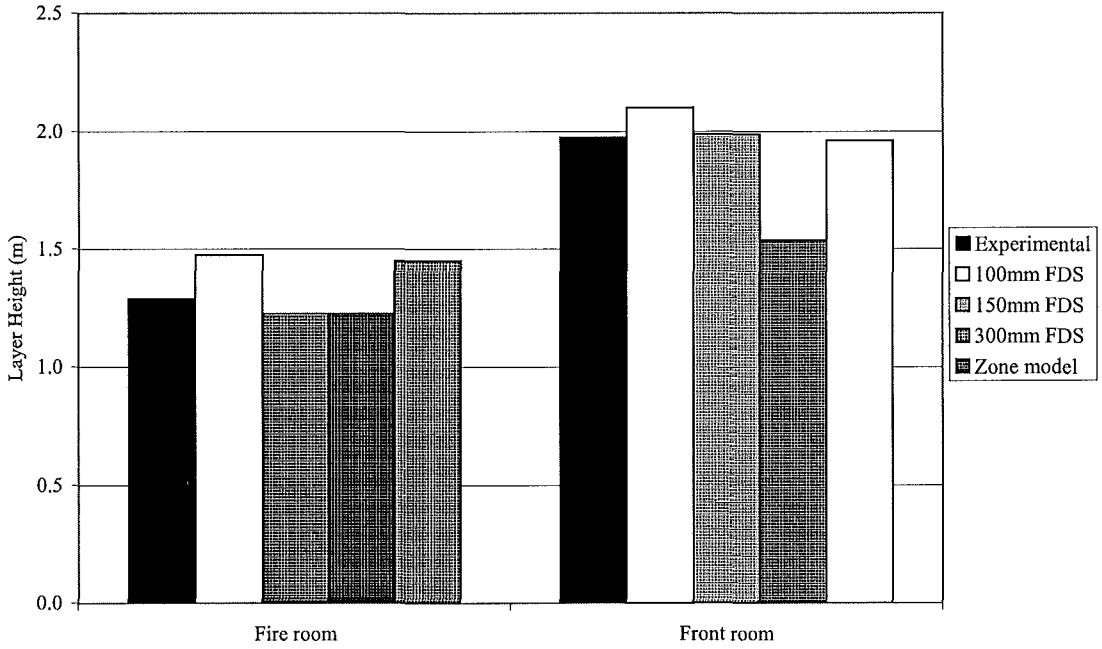

Figure 5.15: Layer height comparisons between FDS, CFAST and experimental results for the 110kW fire.

The following points can be summarised from Figure 5.15:

- The layer heights in the fire room are predicted reasonably well by all the models; the 100mm and the zone model over predict by about 0.2 metres.

- CFAST appears adequate in predicting the layer height in both isorooms, the prediction being closer to the experimental result than the 100mm FDS model.

- All the predictions of layer height in the front room are satisfactorily close to the experimental results except the 300mm model prediction. This is about 0.5 metres below the experimental value.

5.2.3 Upper and Lower Layer Temperatures

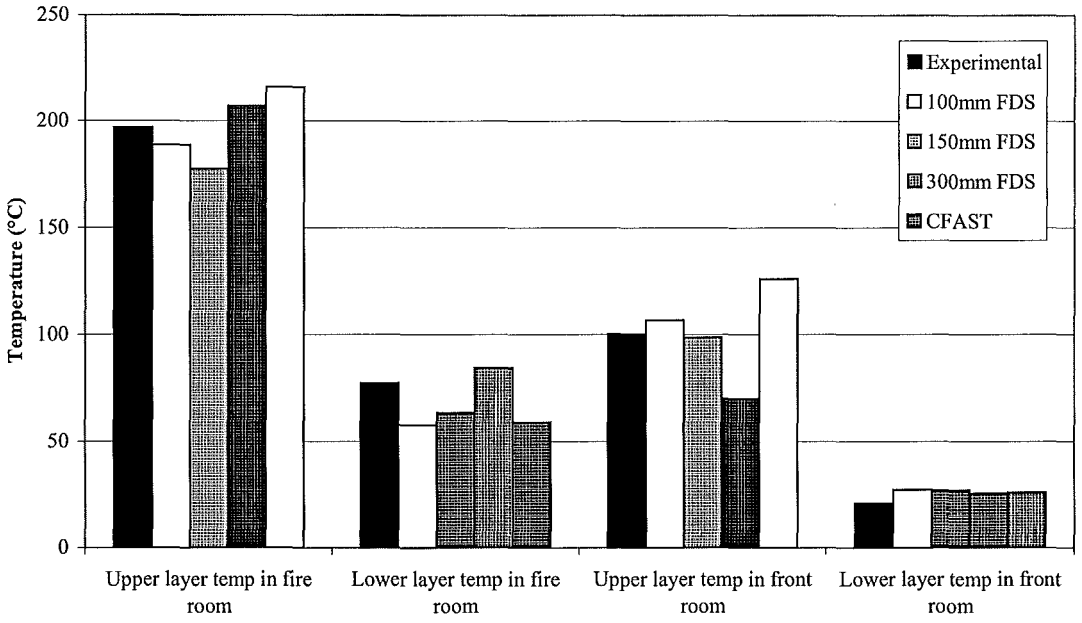

Figure 5.16: Upper and lower layer temperature comparisons between FDS, CFAST and experimental results for the 110kW fire

The temperature comparisons given in Figure 5.16 indicate the following:

- The FDS model predictions are in reasonable agreement to the experimental results, with the exception that the 300mm grid model provides a poor prediction for the upper layer temperature in the front room.

- The 100mm grid model under predicts temperatures in the fire room but slightly over predicts them in the front room.

- The zone model over predicts the upper layer temperatures in both rooms but provides a better prediction for the lower layer temperatures.

5.2.4 Oxygen Concentration

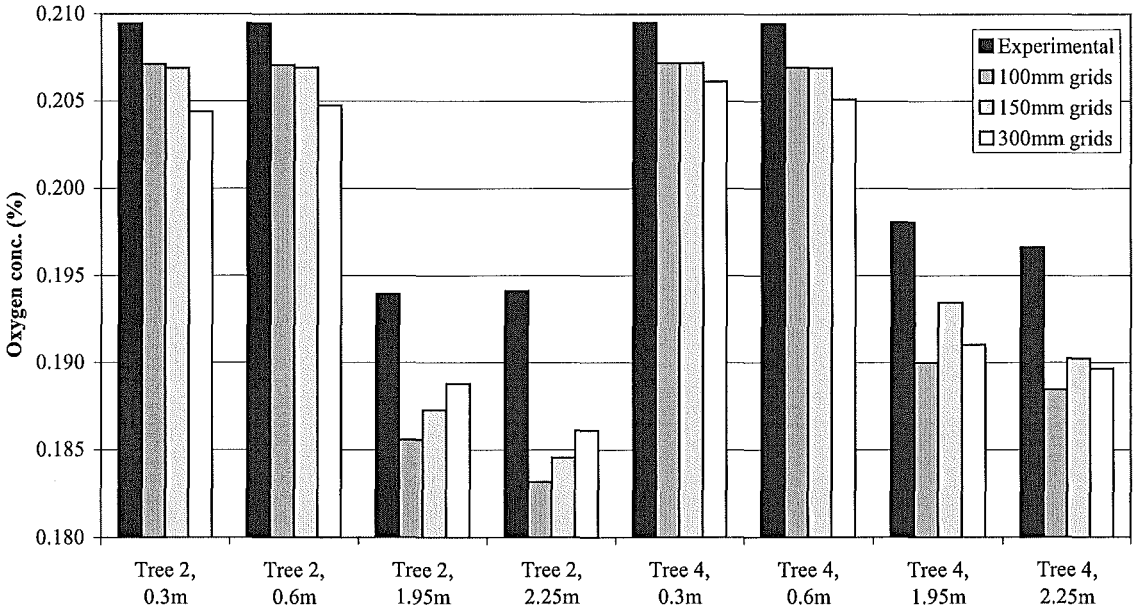

Figure 5.17: Oxygen concentration comparisons in the fire room between the FDS models and experimental results for the 110kW test.

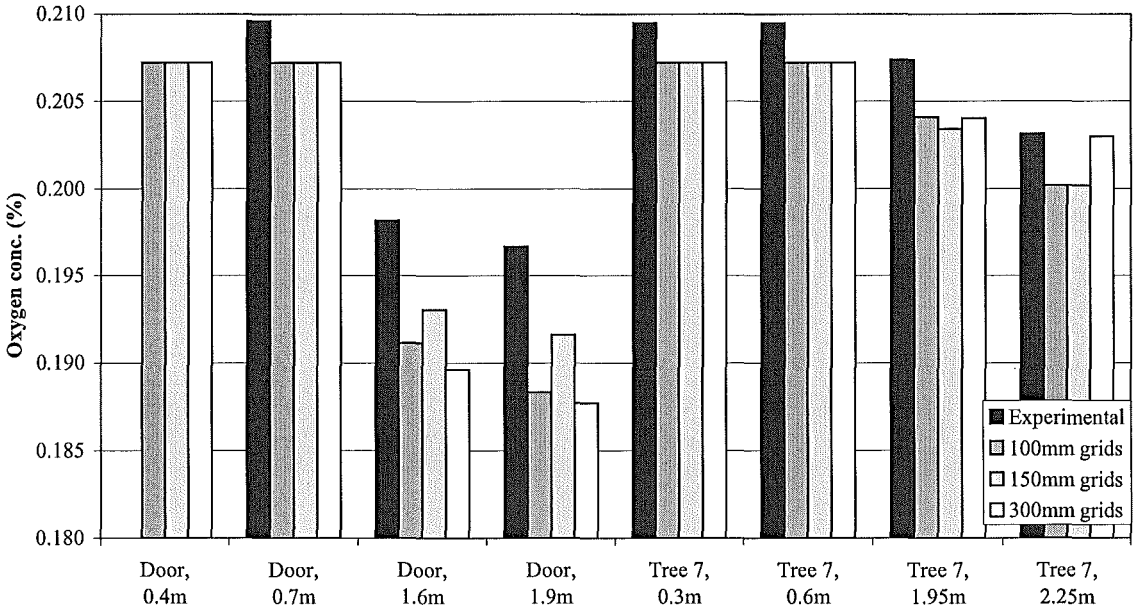

Figure 5.18: Oxygen concentration comparisons in the doorway and the front room between the FDS models and experimental results for the 110kW fire.

The following points are a summary of the oxygen concentration comparisons in Figure 5.17 and Figure 5.18:

- All the FDS models under predict the oxygen concentration.

- The greatest difference is at Tree #2, 2.25 metres above the floor, where the 100mm grid model displays a -6% error in relation to the experimental result (note the scale on the y-axes).

- The predictions of the lower two probes (at 0.3 and 0.6 metres above the floor) deteriorate as the grid resolution is decreased.

- Although there are trends associated with the different grid sizes there are no definite conclusions that can be drawn from them that applies to all of the locations compared.

5.3 Model run times.

The following table gives the times that each FDS model and the CFAST model took to run. The Random Access Memory (RAM) on each of the computers used for the modelling is also provided. There was no difference in the running time of the models for the two different fire sizes. The FDS model run times were obtained from the final data box displayed for the FDS model, this gave the total CPU time.

Table 5.1: FDS and CFAST model running times for the McLeans Island simulations.

Model	Run time	RAM
FDS models		
100mm grids (H/24)	52 hrs	256 Mb
150mm grids (H/16)	11.5 hrs	130 Mb
300mm grids (H/8)	0.8 hrs	130 Mb
CFAST	10 secs	130 Mb

5.4 Discussion and conclusions

5.4.1 Temperature prediction differences

The majority of the temperature predictions of the two FDS models using the smaller grid sizes of 100mm (H/24) and 150mm (H/16) fall within 15% of the experimental values. The 150mm grid models appear to make equally good or sometimes even better predictions than the 100mm grid models. This serves to illustrate that no advantage is gained (in this scenario) by using the smaller grid size of 100mm. Decreasing the grid resolution of the model to a 300mm (H/8) mesh displays a definite decrease in model accuracy. If the model run times are considered in Table 5.1, it is apparent that 150mm grids are the best modelling option with good predictive capabilities and an acceptable running time of 11.5 hours.

It should be noted at this point that there are errors associated with the experimental measurements. These errors will only be small and are due to inexact placement of the thermocouples and calibration errors in the data analysis equipment. The 'error bars' in the figures do not correspond to the actual error in the experimental measurements but are an indication of how good the FDS model predictions are (explained in Section 4.4).

Most of the gas temperatures predicted by FDS (for the 100mm and 150mm grid models) are slightly low (Figure 5.16). This is most noticeable for the temperatures in the fire room below about 2 metres (see Figure 5.10 and Figure 5.12). The reasons for this are most likely to be due to the input variables specified in FDS.

Firstly the specified thermal properties for the room insulation may have meant that there was more heat loss than in the experiments. This was made more likely by the fact that only one lining was modelled in FDS instead of the two that were used in the experiment. Also there was limited data on the lining, so an estimate had to be made for its thermal conductivity and diffusivity.

Secondly the radiation from the hot upper layer may have been less in the FDS models due to poor characterisation of the soot release from the burner. Because no soot yield was defined in the input files for these models the default value of 0.01 kg of soot per kg of fuel burned was

used. The actual soot yield of propane (the major component of LPG fuel) is closer to 0.024 kg/kg (Tewarson, 1995). This means that in the experiment there would be more soot in the upper layer, which would mean a greater emmisivity. This would correspond to more radiation being directed at the lower layer gases, producing the slightly higher temperatures that are observed when compared to the FDS models.

Another possible uncertainty that is introduced into these comparisons is due to the uncertainty of the HRR. The experimental HRR and the FDS output HRR are not exact. A mass flow meter monitors the flow of LPG to the burner in the experiments in order to obtain the correct HRR based on the heat of combustion of the fuel. This obviously has inherent uncertainty associated with it. Also, as explained in Section 4.2, a trial and error method had to be adopted in order to arrive at the desired output HRR. Table 4.1 gives the average HRRs for the FDS models. It shows that all HRRs fell within 2%. It is difficult to characterise these uncertainties but they could combine to give some of the differences observed in the temperature comparisons.

5.4.2 Floor and ceiling temperatures

There is a marked discrepancy between the experimental floor and ceiling temperatures and those predicted by the FDS model. It was thought that the reason for this was that the thermocouples specified to record the data at these points in FDS were not specified to be surface readings. This meant that the surface temperatures calculated by the FDS models were actually the temperatures of the gas right next to the surface, not the temperatures of the surface itself.

These differences in predicted temperatures can be explained by considering the various processes of radiation and convection involved in heat transfer to the floor and ceiling. The higher temperature of the floor is caused by radiation from the hot upper layer. The gas temperature is cooler, in spite of re-radiation and convection from the floor, because there is a continuous airflow across the floor from the door to the fire. This can be confirmed by noting that the predicted gas temperature next to the floor in the doorway (Figure 5.12) is about 30°C, whereas where the airflow across the floor is less on the other side of the fire (Tree #1, Figure 5.10) the surface gas temperature is predicted somewhat higher at 62°C. The ceiling is

cooler than the gas in the upper layer simply because of convective and radiative heat transfer losses; the ceiling can never be hotter than the gas in the upper layer.

To see if defining the thermocouples as surface readings did produce more accurate predictions, another simulation was run using 150mm grids. The problem with defining a surface temperature probe in FDS so that a surface temperature can be recorded is that it can only be done on a defined solid obstruction and not on the edge of the computational domain. As a consequence obstructions had to be added to represent the ceiling and the floor of the isorooms. The surface probes were then located on the surface of these obstructions. The ceiling and floor temperatures for this simulation are compared against the initial FDS simulation and the experimental results in Figure 5.19 and Figure 5.20.

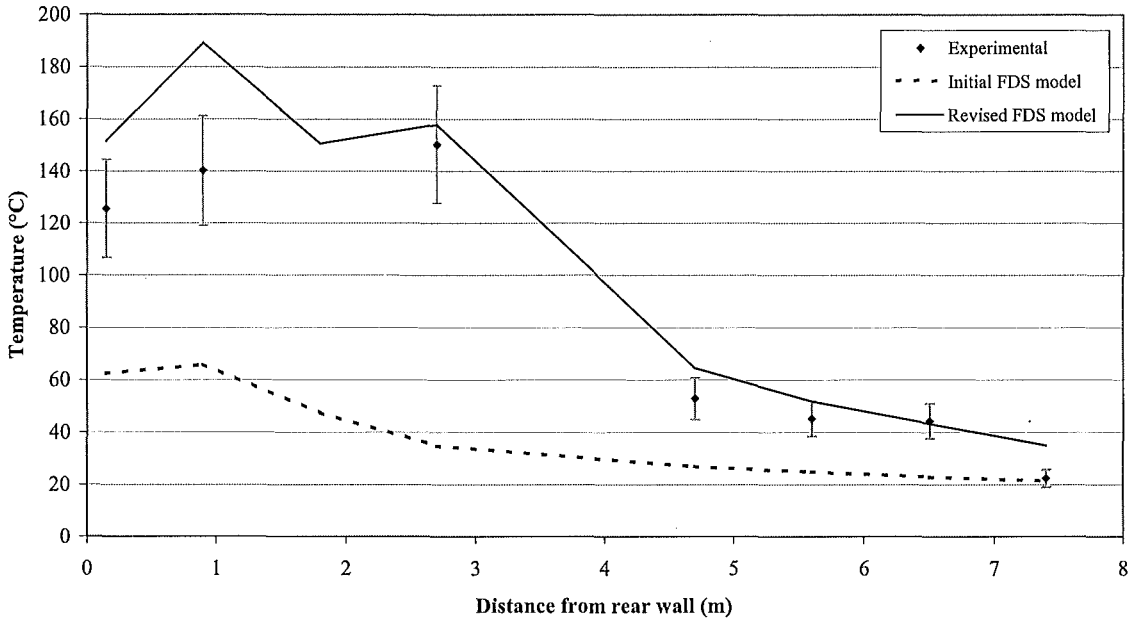

Figure 5.19: Floor temperature comparisons between initial and revised FDS model results and experimental values.

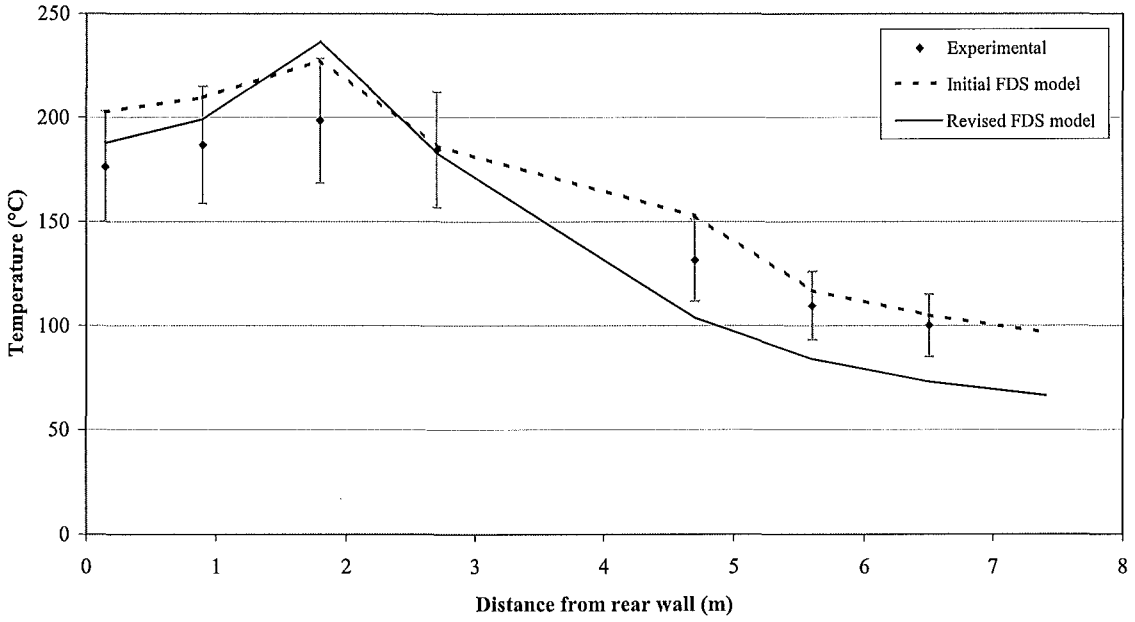

Figure 5.20: Ceiling temperature comparisons between initial and revised FDS model results and experimental values.

The comparisons show that the revised model provides much closer predictions of the floor temperatures than the initial model (Figure 5.19). The improvements are not as noticeable for the ceiling temperatures (Figure 5.20). However, these results do show that in order to adequately extract surface temperature data from the FDS models, obstructions need to be specified so that surface probes can be located on them.

5.4.3 Temperatures directly over the burner

The temperatures are all significantly under predicted for locations directly above the burner. In order to predict these flame temperatures all the local HRRs that are calculated by the flame sheet method (explained in Section 3.2) are smeared across all the grid cells that fall within the flame itself. The temperatures within the flame therefore become averages of a number of grids; this results in low temperatures being predicted. This is even more exaggerated when the grids are large because the HRR has to be 'smeared' to a greater extent over the limited number of cells that occupy the flaming region. As a result, the predicted temperatures above the burner, as illustrated in Figure 5.11 become poorer as the grid size is increased.

Another reason that contributes to this poor prediction of the temperatures above the burner is the fact that for larger grids the model provides a poorer prediction of the flame itself. The flame heights for each model are given in Table 5.2. These heights were obtained by analysing the simulated flame in Smokeview and estimating the point at which the flame occurred half of the time.

Table 5.2: Experimental and FDS model flame heights for McLeans Island isorooms.

	55kW test	100kW test
100mm grids (H/24)	0.45m	0.75m
150mm grids (H/16)	0.5m	0.75m
300mm grids (H/8)	0m	0.6m plus ½ the ceiling

The smaller grid models were similar in flame height but the 300mm grids predicted a mixture fraction that produces a flame sheet in Smokeview that either did not appear in the 55kW simulation or covered half the ceiling in the fire room, as in the 110kW simulation. The Smokeview image of this flame sheet for the 110kW simulation is shown in Figure 5.21 on the following page.

Both these extremes in flame height, observed for the 300mm grid model will under predict the temperatures above the fire. The 55kW simulation will not provide a flame sheet near the thermocouples so the necessary high temperatures will not be observed. The 110kW simulation has a large volume over which the HRR needs to be "smeared out" in order to predict the temperatures above the burner. This will also result in a low temperature being predicted.

The poor prediction of the flames in the FDS model when large grids are used has been observed by McGrattan et al (2001). A subroutine has been added to the combustion model in FDS to account for this and is based on the ratio between the grid size and the characteristic fire diameter. This is multiplied by an empirical constant to obtain an effective flame sheet mixture fraction (McGrattan et al, 2001) (this is explained in Section 3.2). This correction factor seemed to either work or was not needed for the two smaller grid models but is not effective for the 300mm grid model and means unreliable predictions were produced.

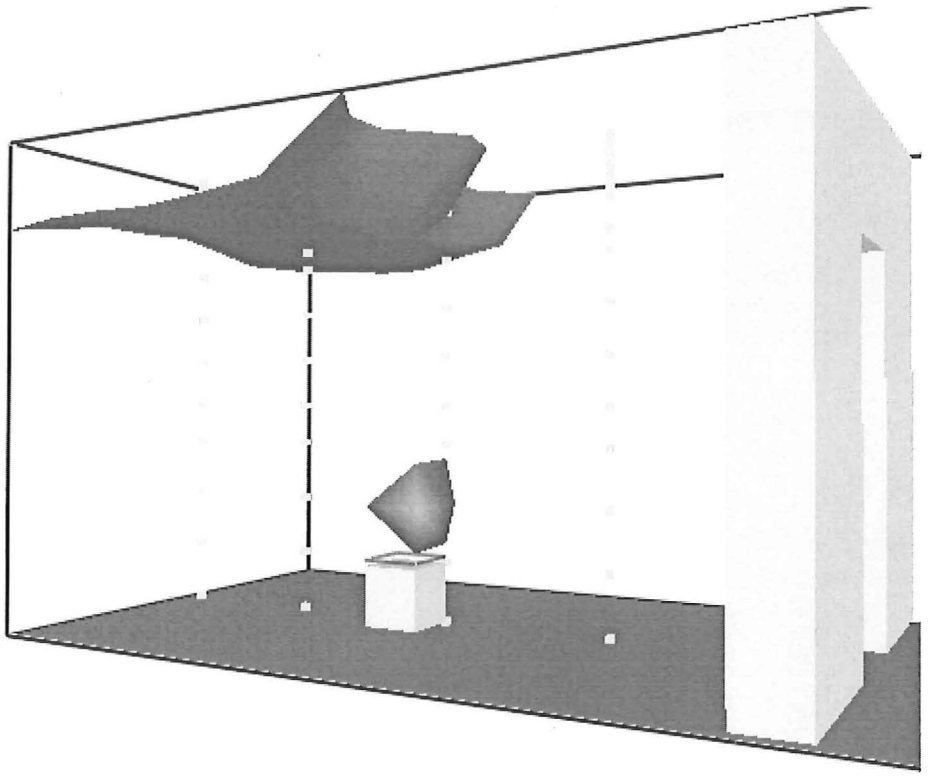

Figure 5.21: Illustration of the flame sheet predicted by the 300mm (H/8) grid model.

Figure 5.21 also shows that the burner in the 300mm grid model is offset from the centre of the room. This would course an additional reduction in the temperature predictions because the thermocouples are not situated directly above the centre of the fire. By assigning more thermocouples directly above the fire in another FDS model, the extent that this offset effected the predictions could have been tested. This was not done due to time restrictions. This serves to show that increasing the grid size does not only effect the capabilities of FDS to model the fire but also effects the physical geometry that it is modelling, which may cause even greater errors in the final predictions.

.

5.4.4 Temperature gradient instability

The instability in the temperature profile observed for the predictions of thermocouple tree #5, in Figure 5.13 for the 300mm grid model predictions may be related to the interaction of the flow through the door when calculated with such a large grid size. Figure 5.22 shows the

temperature profile at a time of 520 seconds for the region where the anomaly occurs. Thermocouple tree #5 is shown down the centre of the illustration and the thermocouple that displays the instability is circled.

Although the exact temperatures are not given in Figure 5.22 the 'hole' in the profile indicates a lower temperature than the immediate surroundings for the area near the thermocouple that displays the unexpected decrease in temperature. The temperature profile was extracted from an animated temperature slice of the isorooms. The animation showed that this 'hole' was not stationary but alternated between adjacent locations. This hole always occurs on the boundary of the fire plume that is exiting through the door. Obviously the calculations and interpolation required in such large grids of 300mm do not produce adequate predictions of the small scale mixing processes occurring in this plume boundary layer. This observation reiterates the fact that 300mm grids are too large to adequately model the temperature profiles and fire processes for this scenario.

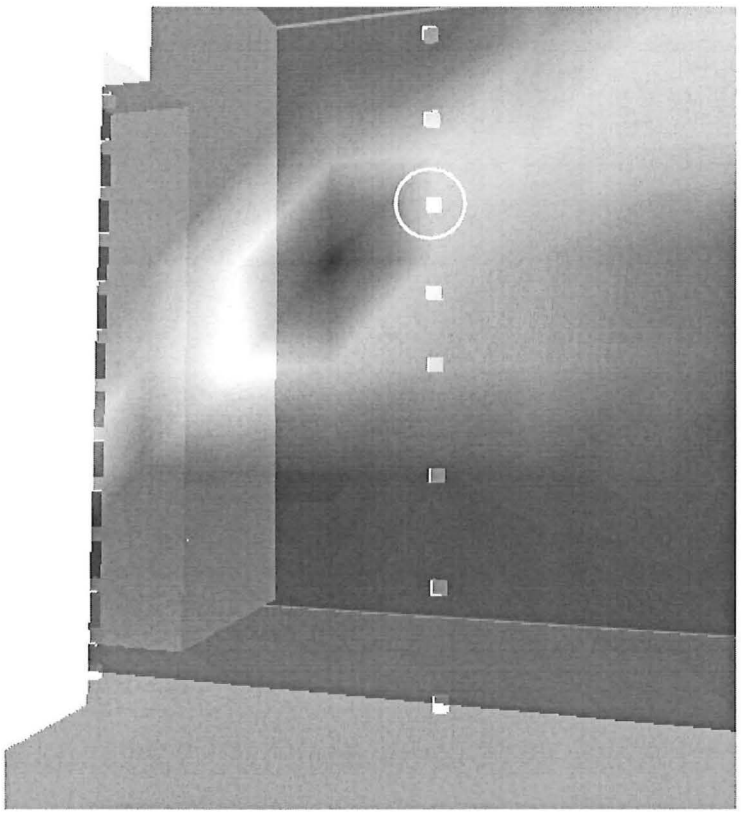

Figure 5.22: Smokeview image of the temperatures near the door at a fire time of 520 seconds, showing the thermocouple that displays the anomaly (circled).

5.4.5 Layer height comparisons

Figure 5.6 and Figure 5.15 give layer height comparisons between the zone model and those calculated from the experimental and FDS data. It is important to realise that these calculated layer heights have a large error associated with them. This is due to the method in which they are calculated. This method is outlined in Section 4.4 and seems a very crude indication of where the layer interface occurs. Because it relies on the compartment temperature profiles it is only accurate to the distance between the closest two thermocouples. For the fire room this means a vertical distance of 0.25 metres. Even the assumption that a distinct interphase exists is only a rough approximation to reality. This means that Figure 5.6 and Figure 5.15 should only be used as a qualitative indication of the relative accuracy of the zone model compared to experimental results and the FDS models. In light of this the only conclusions that can be made from the layer height analysis is that the zone model provides a much better prediction of the layer height in the front room than the 300mm grid FDS model does. All other model predictions are a fair representation of what was observed in the experiment.

It should also be noted that the FDS model should not be discarded in favour of the simpler and faster zone model just because the zone model provides similar or sometimes better predictive capabilities. The zone model is very limited in the data that can be extracted from it. FDS models on the other hand yield a vast amount of data that can be used to get an idea of the actual behaviour of the fire and associated compartment effects, not just approximations of layer heights and average temperatures.

5.4.6 Layer temperature comparisons

Figure 5.7 and Figure 5.16 give average layer temperatures for the two rooms. The accuracy of these temperatures is also questionable for the same reasons outlined above for the layer height calculations. Section 4.4 explains the averaging technique used to arrive at these temperatures. In actual room fires the interface is not a distinct boundary but more of a layer. This can be seen by looking at the temperature profile in Figure 5.10 where there is not a distinct temperature jump at a certain height but rather a gradual change. Therefore when the upper and lower layer temperatures are calculated some of these boundary temperatures are included in the calculation. This is particularly exaggerated in the front room temperature

profiles were it is difficult to distinguish by observation, a layer height at all (see Figure 5.13 and Figure 5.14). This results in the FDS models and experimental results having upper layer temperatures slightly lower and lower layer temperatures slightly higher than the zone model predictions. If this boundary layer were not included in the temperature averaging then the zone model would provide a better approximation to experimental and FDS model results. A direct comparison of the zone model predictions with FDS and experimental results for thermocouple trees #1 and #8 are made in Figure 5.23 and Figure 5.24. Other comparisons are provided in Appendix C.1.

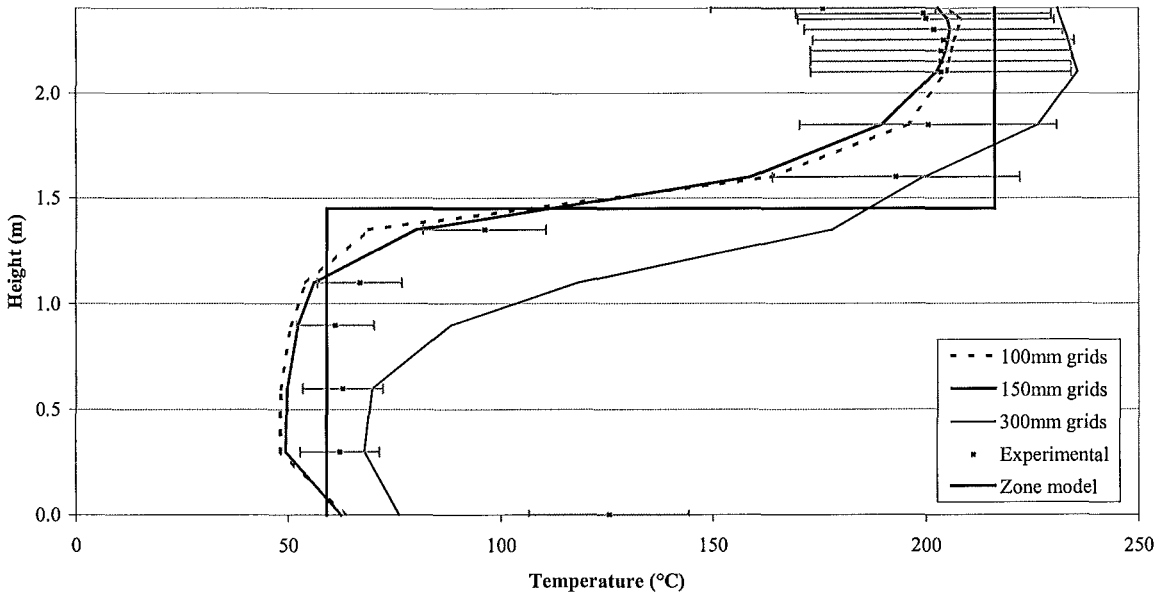

Figure 5.23: Comparison of the zone model temperature approximations with FDS and experimental results for Tree 1.

Figure 5.23 shows that the zone model prediction when compared against temperature profiles of tree #1, falls within 15% of all except one of the experimental results. The floor and ceiling temperatures are discounted here because they were not extracted from the zone model. This is a lot better than the 300mm grid FDS model predictions, which frequently fall outside +/-15% of the experimental data points and in most cases displays less accurate predictions than the zone model.

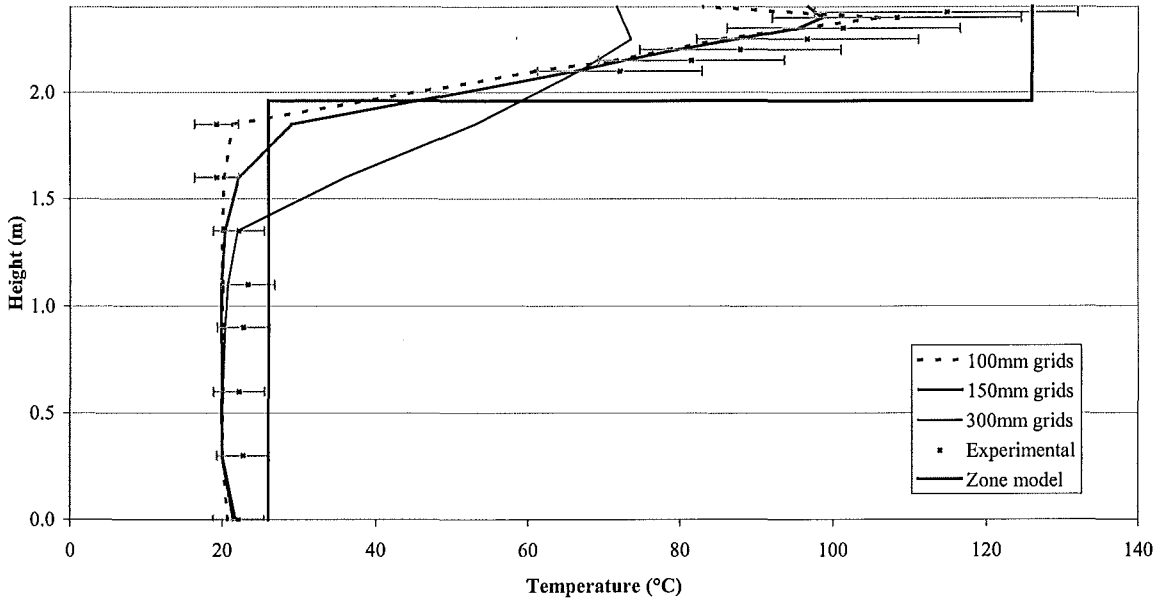

Figure 5.24: Comparison of the zone model temperature approximations with FDS and experimental results for Tree 8.

The comparisons of the zone model predictions for tree #8 in the front room (Figure 5.24) do not compare as well, especially for the upper layer temperatures. However the zone model still provides a conservative estimate unlike the 300mm grid FDS model.

Again it should be stressed that a comparison such as this does not provide an indication of the actual accuracy of zone models compared to the FDS models. However the analysis above serves to show that the most important variables, that is the upper and lower layer temperatures, can indeed be modelled using CFAST and provide a better representation of some of the data than FDS models with coarse grid resolutions.

5.4.7 Oxygen concentration comparisons

The last two figures in the results sections of each set of comparisons (55kW and 110kW) compare the experimental oxygen concentration with the predictions of the FDS models (Figure 5.8, Figure 5.9, Figure 5.17 and Figure 5.18). It was noted that in all of the locations the three FDS models under predicted the concentrations. However the differences were very small, with the largest being about 6%. Some of the difference observed was due to the

default oxygen concentration of air in FDS being 20.72%. The experiment gave a value of 20.95%. This value was taken from data recordings before the fire was ignited. With this difference taken into account the concentrations recorded by the lower two probes, at 0.3 and 0.6 metres were very close to the experimental results. The upper two probes situated at 1.95 and 2.25 metres were still lower than experimental but the difference was very small.

There seemed to be no definite trend associated with the different grid sizes that applied to all the locations. The only trend that was noted was that the lower probes predicted less accurate concentrations for the larger grid size of 300mm. The small differences may have been simply due to the need to interpolate over a relatively large distance compared to the smaller grids, which would result in errors being introduced.

5.4.8 Summary

The results and discussion for the McLeans Island isoroom tests are summarised in the following points:

- The 150mm (H/16) grid models were more than adequate in providing comparable predictions, most of the time falling well within 15% of the experimental results. By increasing the resolution to 100mm (H/24) grids the model run time increased from 11.5 hours to 52 hours with no significant gain in accuracy.

- The 300mm (H/8) grid models did not provide reliable comparisons with the experimental results. The accuracy being compromised by poor characterisation of the flaming region and limited resolution of the smaller scale eddies and turbulence that occurred as well as poor representation of the experimental set up. All of these were the direct consequence of too large a grid size.

- The zone model provided limited but reliable results for the specific variables that were compared. The temperature profiles produced by the zone model, although only defined by an upper and lower layer temperature gave better predictions than the FDS models using the 300mm grids and in a much shorter model run time.

6 US Navy Hanger Tests

6.1 Experimental set-up

The US Navy hanger tests were performed in two locations, Iceland and Hawaii (Gott et al, 1997). For the comparisons in this report the facility at Barbers point, Hawaii, was chosen over the Iceland tests. This was due to several reasons, The most important being that the Iceland hanger had a barrelled roof which would have made it extremely difficult to construct adequately in an FDS model, especially with large grid cells. Also the locations of the thermocouples were not detailed specifically enough to warrant a detailed comparison with an FDS model.

The dimensions of the Barbers point hanger were 97.8 metres long by 73.8 metres wide by 14.9 metres high at its apex. The roof angled down to 13.4 metres at the east and west ends of the hanger (see the elevation view in Figure 6.1). The hanger was built in 1942; its construction consisted of concrete masonry walls on the east and west sides of the building (with numerous windows); full height horizontal sliding metal and glass doors on the north and south sides (see Figure 6.1) and a concrete floor (Gott et al 1997; Davis et al, 1996). The roof was constructed of built up tar and gravel over a metal deck. This was directly supported by 0.25 metre I-beams, spaced at 4.1 metre centres running along the width of the hanger in the north-south direction. The I-beams were supported by open trusses spaced 6.1 metres apart running from east to west. The roof also contained two skylights, each measuring 73 by 6 metres, running parallel to the hanger doors (east to west).

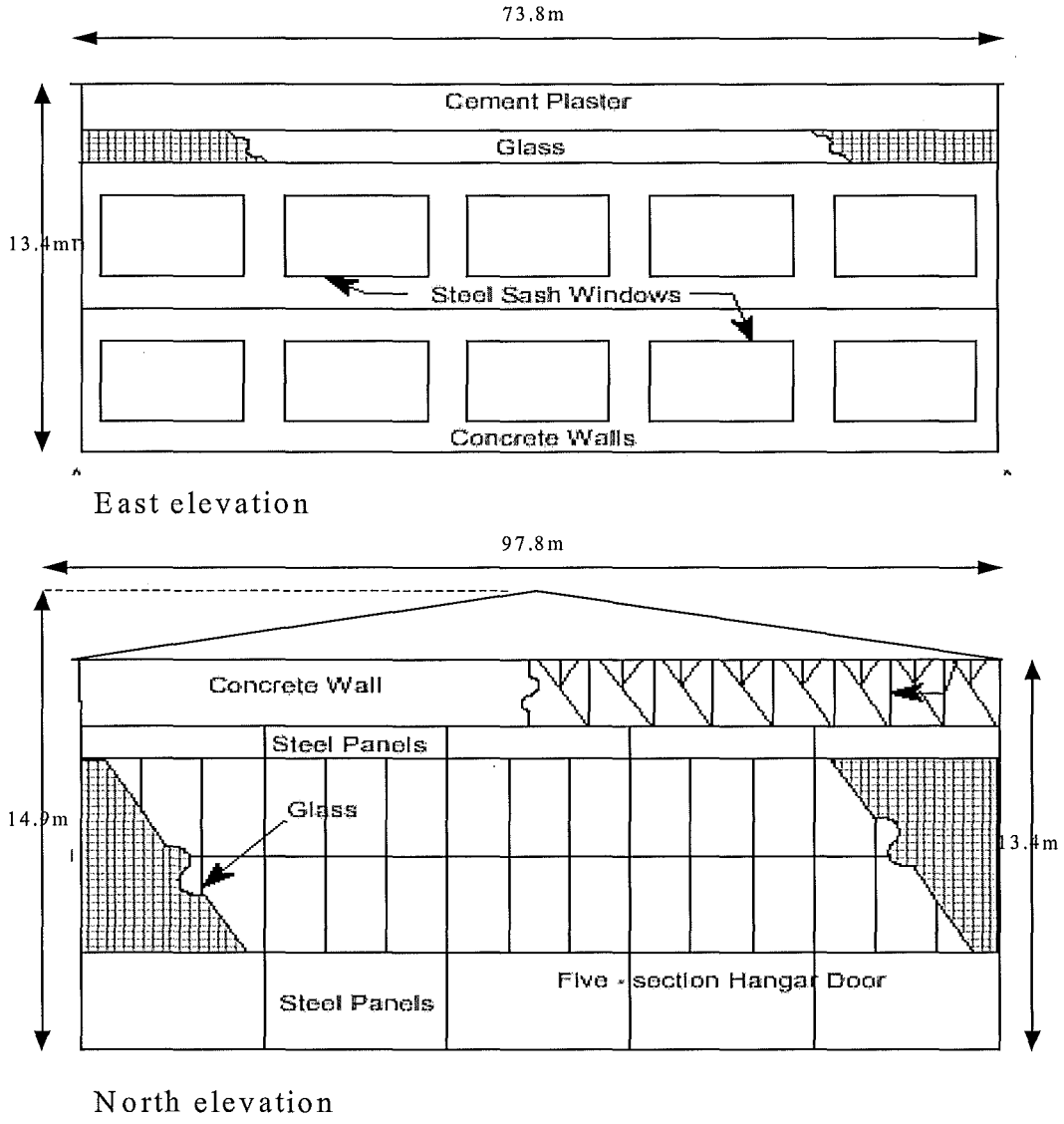

Figure 6.1: North and east elevations of the Hawaii hanger (not to scale) (modified from Gott et al (1997)).

Eleven test fires were conducted at the Hawaii facility. These ranged in size from 100kW up to about 8600kW. All the tests used JP-5 jet fuel in a pan of varying size depending on the fire size required. The pool fire was located in the northwest quadrant of the hanger, 3 metres north and 12.2 metres west of the building centre (see Figure 6.2). A draft curtain hanging from the ceiling, measuring 18.3 by 24.4 metres by 3.7 metres deep surrounded the fire centre. This can also be seen in Figure 6.2. This draft curtain was only used for some of the tests. A load cell underneath the fire pan recoded the mass loss rate of the fuel.

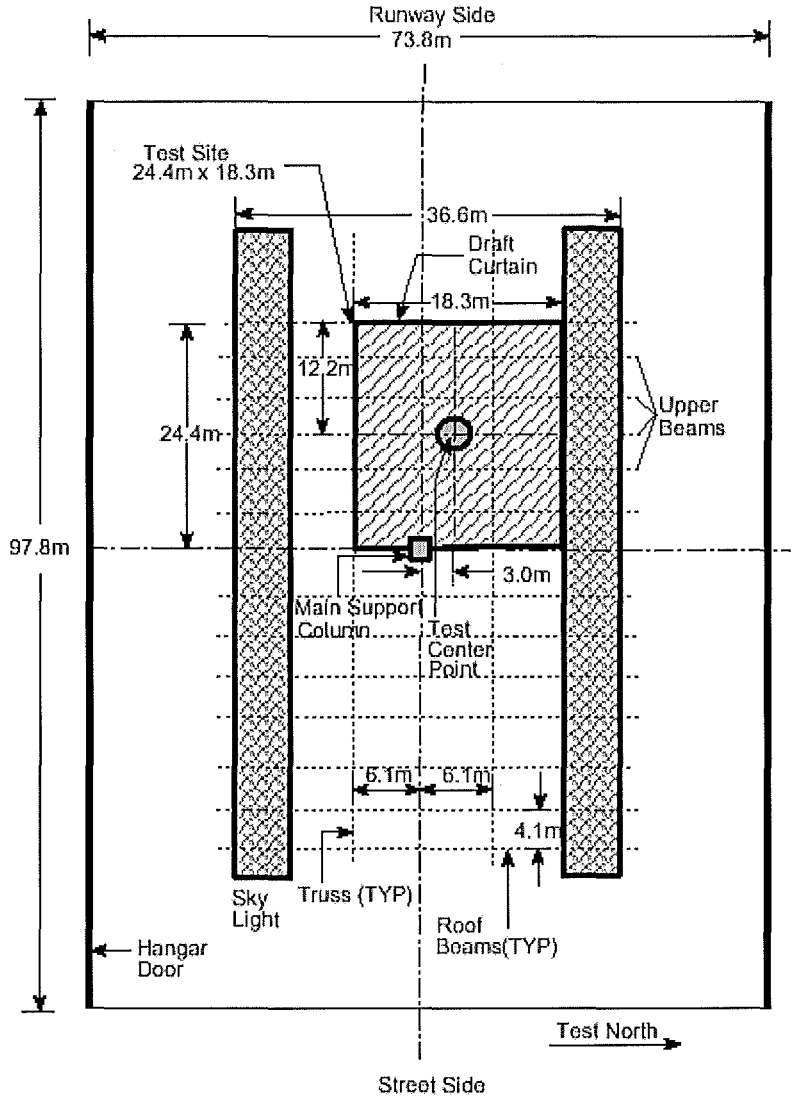

Figure 6.2: Plan view of the Hawaii hanger (Gott et al, 1997).

The tests were predominately concerned with sprinkler and detector activation and placement (Davis et al, (1996)). Numerous sprinklers, heat detectors, beam detectors, mass flow meters and radiometers were installed. Of interest to this study were the 60 thermocouples that were installed above the fire and along the ceiling. These thermocouples were placed radially out from the centre; north, south, east and west. The thermocouples directly above the fire for measuring the plume temperatures were situated at 0.3, 1.5, 3 and 6.1 metres below the ceiling. At 3 metres below the ceiling an additional array of eight thermocouples were placed at 0.9 and 2.1 metres radially out in the four directions. Single thermocouples at 0.3 metres below the ceiling were placed at 1.5, 3 and 11.6 metres north from the fires centre line; 1.5, 3, 8.5, 11.6 and 14.6 metres south and 1.5, 3, 11.6, 14.6, and 17.7 metres in the east and west

directions. At a 6.1 metre radius (in all four directions) there was a tree of five thermocouples spaced at 0.15, 0.3, 0.46, 0.61 and 0.76 metres below the ceiling. At 9.1 metres in the east direction there was an additional tree of five thermocouples; 0.3, 0.46, 0.76, 1.22 and 3 metres below the ceiling. In the north direction at 8.5 metres radius a tree of three probes at 0.15, 1.22 and 3 metres below the ceiling was installed (Gott et al, (1997)). All these thermocouple locations are shown in Figure 6.3.

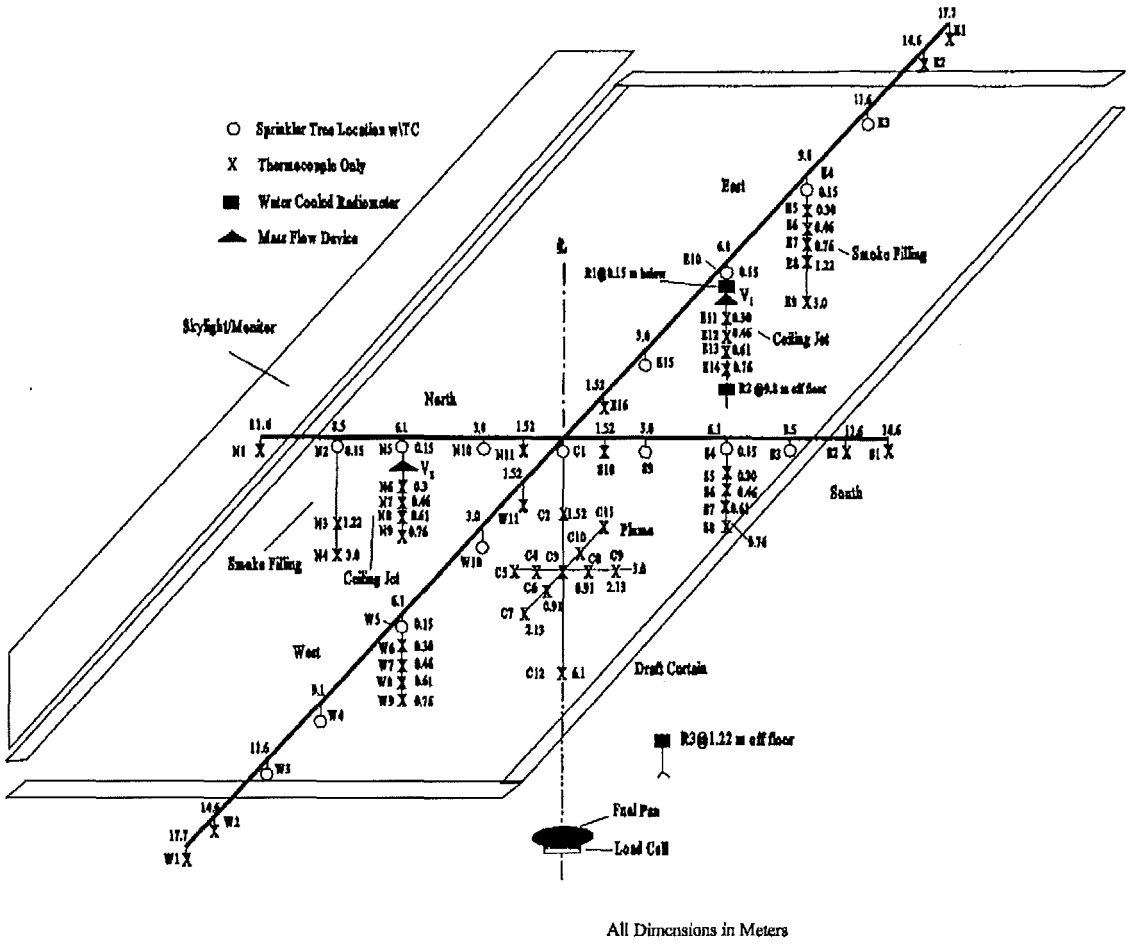

Figure 6.3: Thermocouple locations for the Hawaii hanger experiments (Gott et al, 1997).

6.2 FDS modelling

The FDS models were constructed to resemble as closely as possible the experimental set up described above in Section 6.1. The following section outlines the various methods used and the input data required to model the hanger and the problems that were encountered.

6.2.1 Test fires

Two test fires were used for the modelling comparisons, designated as Test fire 7 and Test fire 5. Both tests used a pan with a diameter of 2 metres by 0.3 metres deep which was filled with JP-5 jet fuel. An illustration of one of these fires is given in Figure 6.4.

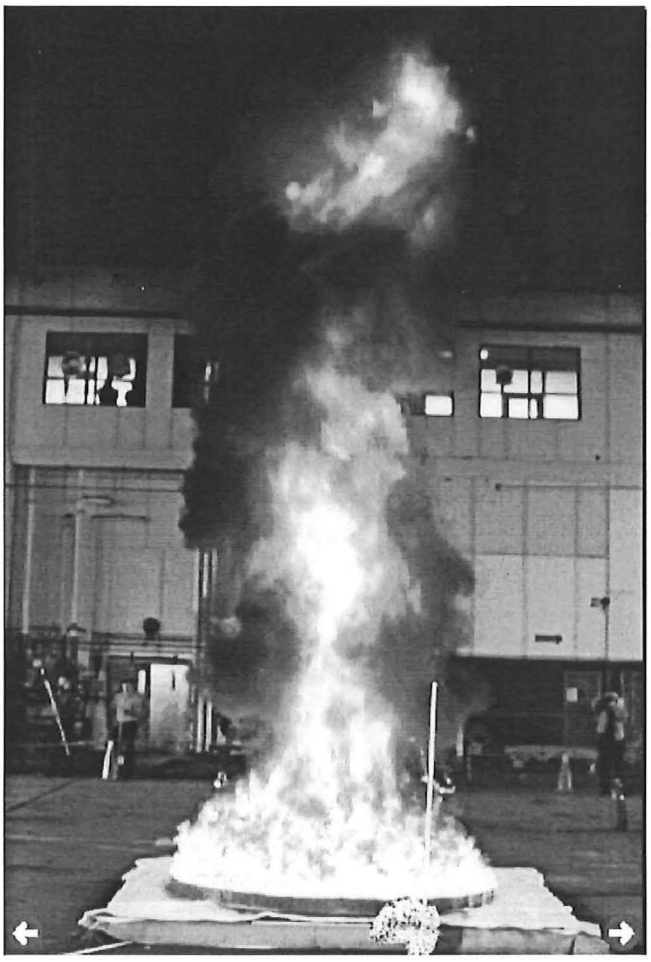

Figure 6.4: Hawaii hanger test fire using JP4 jet fuel in a 2 metre diameter pan (Gott et al, 1997).

Test 7 was chosen initially because it was a large fire and therefore displayed an appreciable temperature rise across all the thermocouples and was also performed without a draft curtain. It was initially thought that to model a thin draft curtain in a computational domain with relatively large grid sizes would be pointless because the minimum thickness of the curtain would be dictated by the size of the grids. The grid sizes used for the modelling are given in Section 6.2.2. However, the modelling of draft curtains was studied further in subsequent modelling comparisons, which are described below. The HRR of test 7, based on the total volume loss of the JP-5 fuel during the test was 5580 kW (Gott et al, 1997). The test had a duration of about 750 seconds. This model is referred to as **Test 7, entire hanger** for the remainder of this report. Figure 6.5 provides a Smokeview illustration of this FDS model using 600mm grids. The steeped ceiling and floor are explained in Section 6.2.3.

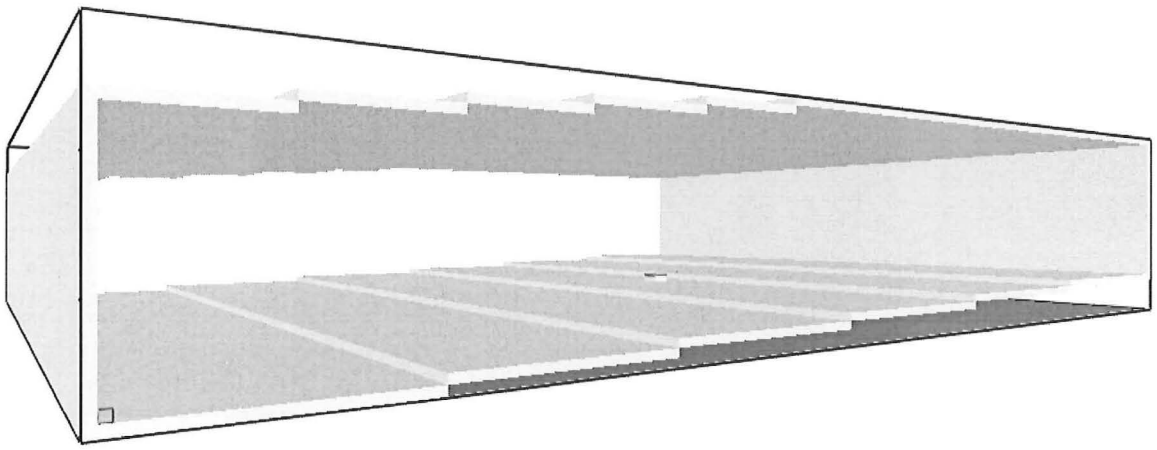

Figure 6.5: FDS model of Test 7, entire hanger using 600mm (H/25) grids.

Test 5 was used because it was performed with a draft curtain in place. The draft curtain was made of fire retardant canvas and was located centrally around the fire. Its dimensions were 24.4 metres long by 18.3 metres wide and it hung down 3.7 metres from the roof of the hanger. The HRR of Test 5, based on the mass loss as recorded by the load cells underneath the pan, was 6760kW (Gott et al, 1997). The duration of this test was about 600 seconds. Two separate FDS constructions were used for comparisons of this test: one modelled the entire hanger (referred to as **Test 5, entire hanger**), the other modelled just the area enclosed by the draft curtain (referred to as **Test 5, draft curtain**). Examples of these two FDS models, using a grid size of 600mm (H/25) are given in Figure 6.6.

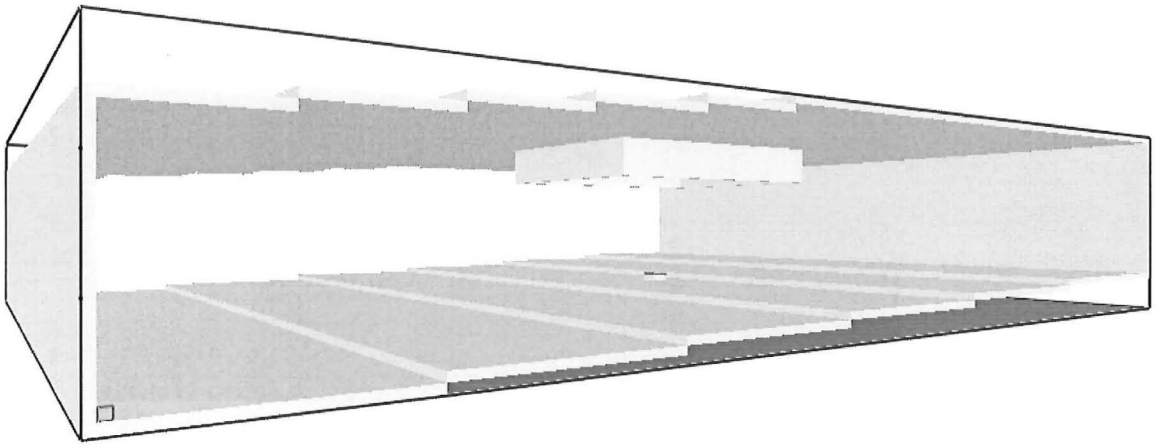

(a) Test 5, entire hanger

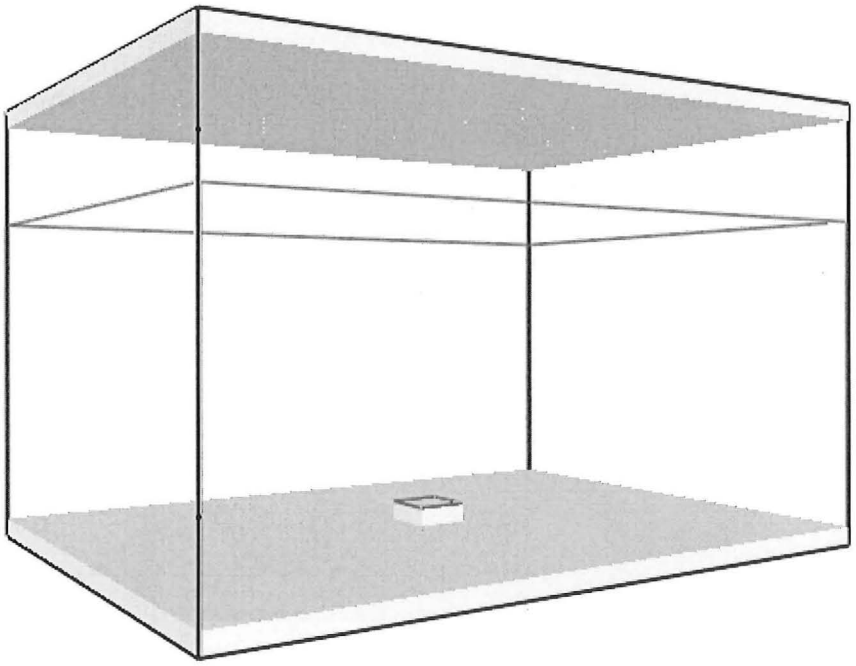

(b) Test 5, draft curtain

Figure 6.6: Smokeview images of the FDS models that were used for Test 5 using a 600mm (H/25) grid.

The fire pan in all the FDS simulations was modelled as square with 1.8 metre sides. This gave an equivalent area to the 2-metre diameter pan that was used in the actual experiments. The depth of the pan was modelled as one grid cell thick for models that had grids of up to 600mm, but no depth for models with grids larger than this.

The fire was characterised by modelling a vent on top of the fire pan which was assigned a specific HRRPUA. Due to a shortfall in the FDS model, this value had to be determined by trial and error. Successive simulations were performed, each time changing the HRRPUA until the required output HRR for the particular model was obtained. As a consequence the final outputs were not exactly equal to the test fire size. The HRRPUA used, the output HRRs obtained and associated differences to the experimental value are given in Table 6.1 below. The grid sizes are explained in Section 6.2.2.

Table 6.1: Input HRRPUA and output HRRs for the Hawaii hanger tests

	Test 7, entire hanger			Test 5, entire hanger		
Grid size	**HRRPUA**	**HRR**	**Diff.**	**HRRPUA**	**HRR**	**Diff.**
	kW/m^2	kW		kW/m^2	kW	
600mm (H/25)	1625	5645	1.2%	1940	6758	0.0%
900mm (H/17)	1250	5570	-0.2%	1461	6773	0.2%
1800 mm (H/8)	1210	5587	0.1%	1447	6740	-0.3%
3600mm (H/4)	1285	5680	0.8%	-	-	-
Test fire		5580			6760	

	Test 5, draft curtain		
Grid size	**HRRPUA**	**HRR**	**Diff.**
	KW/m^2	kW	
300 mm (H/48)	2140	6730	-0.4%
450 mm (H/32)	2090	6743	-0.3%
600 mm (H/25)	1940	6758	0.0%
900 mm (H/17)	1485	6730	-0.4%
1800 mm (H/8)	1492	6772	0.2%
Test fire		6760	

6.2.2 Grid sizing

The grid resolutions used were 300mm (H/48), 450mm (H/32), 600mm (H/25), 900mm (H17) and 1800 mm (H/8). The ratios in parenthesises are the ratios between the enclosure height (H) used in the FDS models and the grid size. These grid sizes all divide evenly into the pool fire dimensions of 1.8 by 1.8 metres. The grid sizing was based on the pan size so that the fire, which is the most important variable in the model, could be simulated as accurately as possible. One of the simulations performed for the entire hanger without a draft curtain used 3600mm grids. This corresponds to an enclosure height ratio of H/4. For this model the grids around the fire pan were linearly stretched so that the grid that defined the fire pan itself had a 1800 by 1800mm base. This is illustrated in Figure 6.7. The vertical grid length or z dimension of the grids was kept at 3600mm.

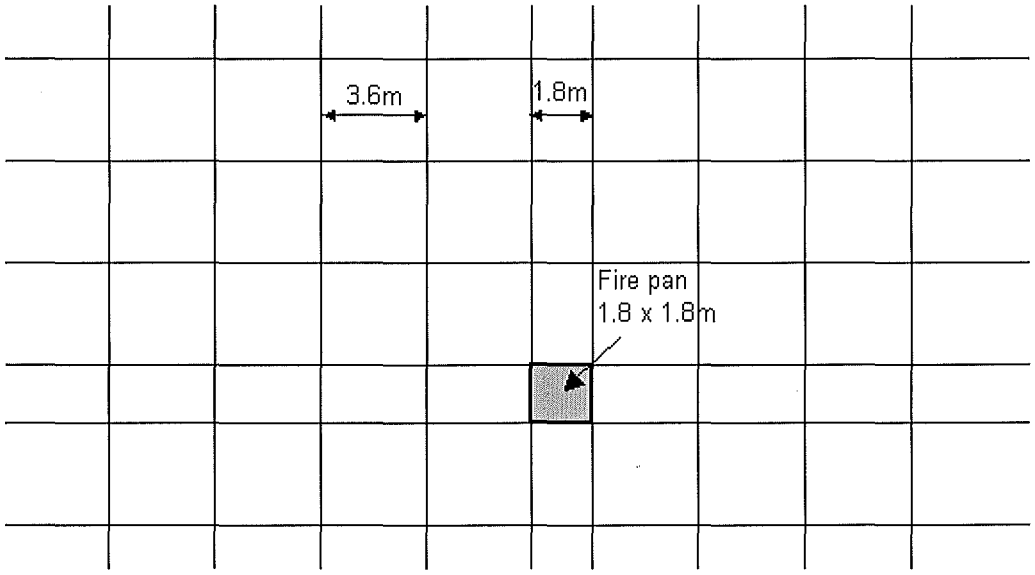

Figure 6.7: Illustration showing the stretched grids for the 3600mm (H/4) FDS model.

Only models with grid sizes larger than 600mm could be run when modelling the entire hanger; smaller grids resulted in a stack overload error message being displayed in the FDS window. This was due to the enormous number of grid cells (in the order of millions) that needed to be resolved. The smaller grid sizes, 300mm and 450mm, were used when only the draft curtain area was modelled.

6.2.3 Inclined roof

The sloped roof of the Hawaii hanger had an angle of incline of about 1.5 degrees. It was initially thought that this incline could be ignored. However, due to the large size of the hanger this assumption significantly changed the volume and therefore the smoke filling characteristics of the enclosure. The next obvious solution was to step the roof using obstructions to simulate a slope of equal angle. However due to the large grid sizes of up to 3600mm, it became apparent that this also did not provide a realistic representation of the sloping roof. The thermocouples were essentially still located below a horizontal surface because the first "step" in the roof often didn't occur until well after the thermocouple located furthest from the fire. Alternatively an inclined flat roof was modelled by altering the gravity vector. By default the gravity vector in the FDS model points down, as would be expected. By altering the vector so that it is directed downwards but on an angle equal to the roof angle (still with the same magnitude) a sloping roof could be simulated. This is illustrated in Figure 6.8.

6.2.4 Problems with gravity vector.

Although changing the gravity vector solves one problem it creates several more. Note that by changing this gravity vector the walls and floor also become sloped by the same angle (Figure 6.8 (b)). It was assumed that because the sloping walls are only at an angle of 1.7 degrees they provide negligible difference to the modelling results. This can be justified because the walls provide only a small contribution to the overall modelling calculations; the heat loss calculation through the walls is only very weakly dependent on orientation at such small angles from the vertical and the ceiling jet would not be altered significantly by a wall sloping at 1.7 degrees. The horizontal distance between the bottom of the wall and where it meets the roof is about 0.35 metres, remembering that the wall is 13.4 metres high. When this is compared to the overall size of the hanger it can be assumed to provide negligible difference to the simulation results.

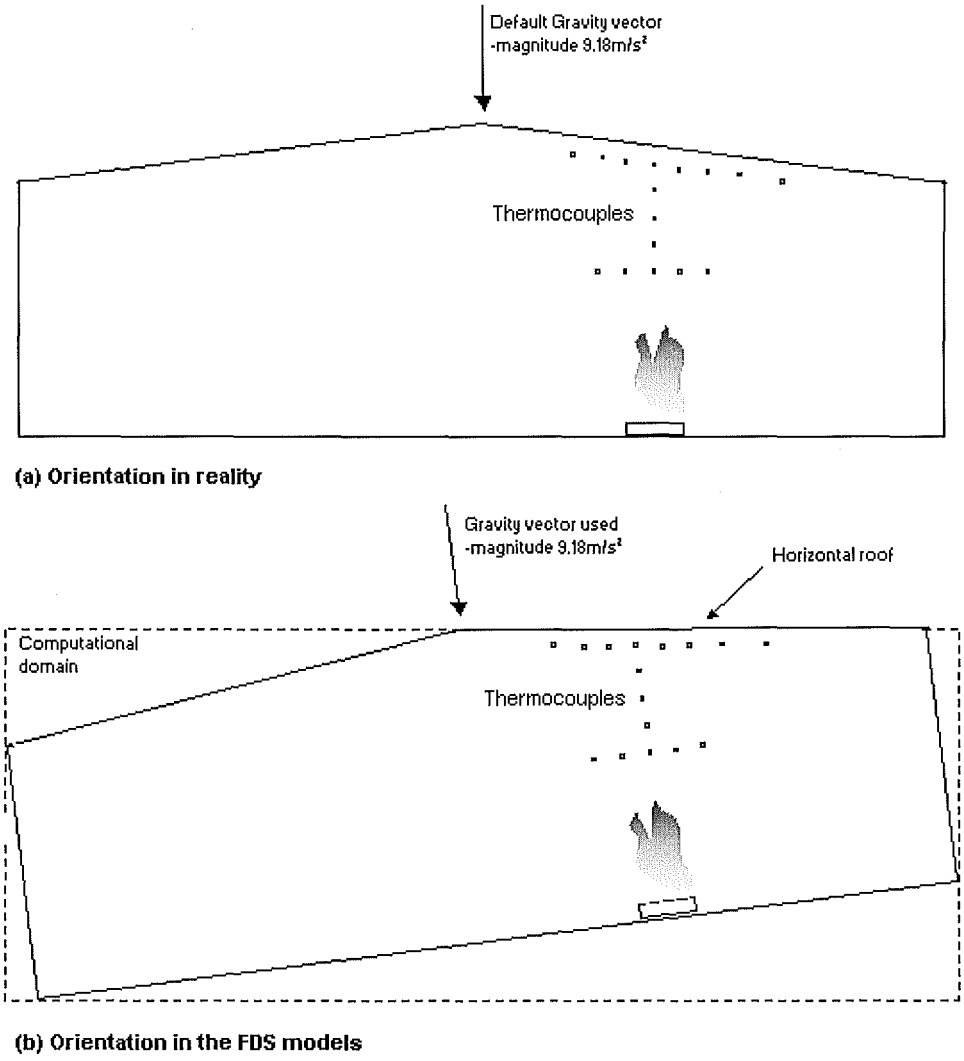

Figure 6.8: Illustration of how the hanger orientation was specified in the FDS models

Due to this, the floor and the east side of the roof needed to be stepped in order for the volume and smoke filling characteristics to be equivalent to the actual experiments. The number and size of the "steps" or blocks depended on the size of the computational grids. These steps can be seen in the Smokeview images of the hanger in Figure 6.9.

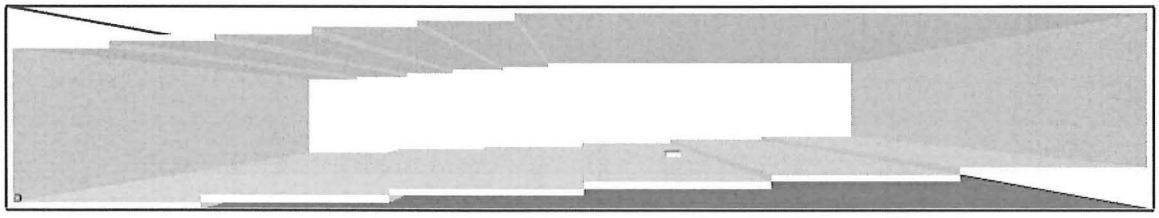

(a) 600mm grids (H/25)

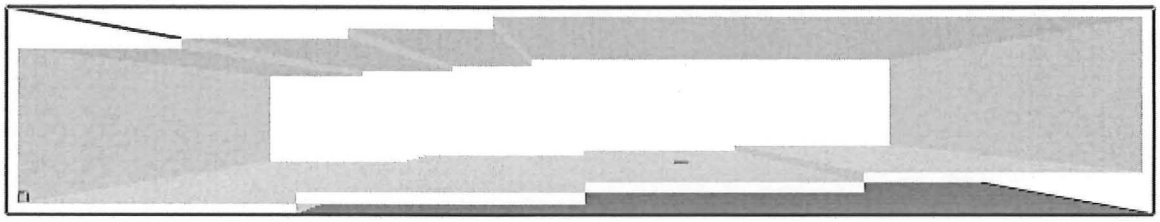

(b) 900mm grids (H/17)

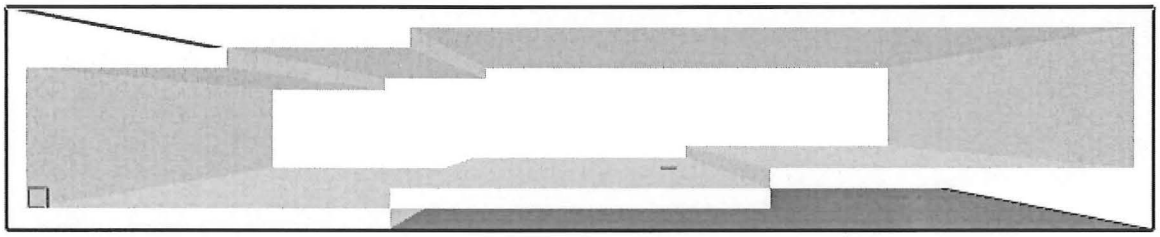

(c.) 1800mm grids (H/8)

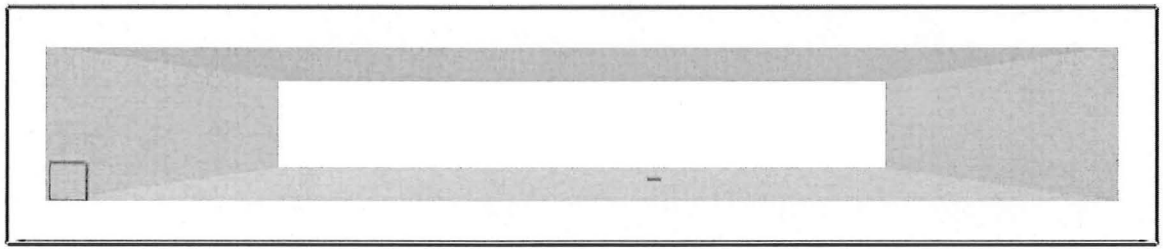

(d) 3600mm grids (H/4)

Figure 6.9: Smokeview images of the FDS models of the Hawaii Hanger, without a draft curtain.

Each step in the floor and ceiling are equal to the height of one grid. This encounters the same problem as when the entire roof was stepped because the areas that are stepped are now less important surfaces for model comparisons and so it was deemed to be a better modelling option. The main roof area under which most of the thermocouples are situated is a uniform,

flat roof. This area is the right half of the rooves shown in Figure 6.9. The 3600mm grids (Figure 6.9 (d)) were too large to be able to model the incline required in the roof or floor of the hanger, the volume was modelled more accurately by not having any steps (the gravity vector was still defined on an angle).

6.2.5 Thermocouples

All the thermocouples that were installed in the Hawaii hanger (see Section 6.1) were used in the FDS models. The angled gravity vector was accounted for when defining the co-ordinates for the thermocouple locations. This meant that the thermocouples above the fire had to slope with the gravity vector. This can be seen in Figure 6.8 (b) (Orientation in the FDS models) where the thermocouples are on an angle rather than in a vertical line as shown in Figure 6.8 (a) (Orientation in reality).

The thermocouple locations also accounted for the varying position of the fire pan. This variation was due to the different grid sizes and is explained in Section 6.2.7. The FDS fire centre for each model and the experimental fire centre are given in Appendix A. The thermocouples were always located directly over the centre of the FDS fire pan.

6.2.6 Ventilation

In order for FDS to run without pressure build-up and to simulate ventilation in the hanger, a vent was inserted into the model at ground level on the northeast corner. This vent was defined as one grid square therefore the exact vent size varied depending on the model being run. This vent can be seen in the bottom left corner of each of the images in Figure 6.9. It was assumed that this varying vent size, because it is so small in relation to the rest of the hanger, would have negligible effect on the model predictions.

6.2.7 Model discrepancies

Due to the restriction imposed by the FDS grids some of the model dimensions and geometry were not exactly the same as the actual hanger. As described in Section 6.2.2, the grids were restricted in size to divisions of the fire pan size of 1.8 metres. This restriction was at the expense of other dimensions in the model. The most notable being the location of the fire centre and the dimensions of the hanger itself. The draft curtain also had slightly varied dimensions for different grid sizes. The effect that these variances had on the FDS model results are discussed in Section 7.5. All the differences in the model as well as the corresponding experimental values are tabulated in Appendix A.

6.2.8 Input variables

The various input variables described below for the FDS models were based on the descriptions given in the two reports on the hanger tests by Gott et al (1997) and Davis et al (1996). The inputs are described and references to the values cited, are given. In brackets after each variable is the call name for the variable in the FDS input file, these input files can be viewed in Appendix B.2.

The main component for heat transfer through the hanger roof was considered to be the built up tar and gravel layer. This layer was modelled as thermally thick and was assumed to be similar in thermal properties to asphalt; this gives a thermal diffusivity (ALPHA) of 3.6×10^{-7} m^2/s and a thermal conductivity (KS) of 0.7 W/m.K (DiNenno (Ed.), 1995). These values compared satisfactorily with other asphalt data (Incropera & DeWitt, 1996) and current but limited data on built up gravel rooves (ww1). The thickness (DELTA) was not given in the reports but was estimated to be 0.01 metres, based on modern accounts of built up rooves (ww1) and observation of the rooves of old buildings. Modelling the roof as thermally thin may have been a simpler and less computationally expensive option but there was essentially no data on the specific heat of the roof material, which is required for thermally thin calculations.

The concrete walls at the east and west ends of the hanger were also modelled as thermally thick with a thermal diffusivity (ALPHA) of 5.7×10^{-7} m^2/s and a thermal conductivity (KS)

of 0.7 W/m.K (DiNenno (Ed), 1995). The wall thickness was estimated to be 0.2 metres. This was based on the fact that the building is of old construction and is tall, requiring reasonably thick walls (C.J. Wastney, pers. comm.). The entire wall was assumed to be concrete even though numerous windows existed (especially on the north end). It was assumed that ignoring these windows would not affect the final results significantly.

The two large sliding doors on the north and south of the hanger were modelled as thermally thin. This means that the temperature through the steel is the same at any particular time and location. This is a reasonable assumption because the doors were assigned a thickness (DELTA) of only 1.5mm. This was estimated from the overall size of the doors (C.J. Wastney, pers. comm.). The product of the specific heat, density and thickness (C_DELTA_RHO) need also be prescribed for a thermally thin calculation. This was taken as 5.1 $kJ/m^2.K$ for plain carbon steel (extracted from data in Incropera & DeWitt, 1996).

Some of the FDS models needed the draft curtain to be defined. The curtain was assumed to be thermally thin in its heat transfer characteristics. It was assigned a C_DELTA_RHO of 0.5 $kJ/m^2.K$. This value was based on the assumption that it was similar to a felt or mineral fibre blanket with a density of $200kg/m^3$ and a specific heat of 0.8 kJ/kg.K, (DiNenno (Ed), 1995; Incropera & DeWitt, 1996). The thickness (DELTA) was assumed to be 3mm.

The concrete floor of the hanger was modelled as a cold inert surface. This means it has no heat transfer interaction with the surroundings.

The soot release rate was also specified in the input file. This is an important variable because the optical thickness of the smoke has an impact on the heat transfer calculations, particularly the radiation from the smoke layer. The soot release rate was assigned a value of 0.042 grams per gram of fuel burnt (DiNenno (Ed), 1995). This value was based on kerosene, which is the major component of JP5 fuel.

It is important to note that the accuracies of the model inputs described above are not entirely critical. As long as they are kept constant for every model that is run they will provide sufficient comparison amongst themselves to show the required trends.

The ambient temperatures (TMPA) were specified for each model. Test fires 5 and 7 were run with ambient temperatures of 27°C and 30°C respectively. These were calculated directly from the thermocouple measurements during the pre-fire period at the start of each experiment.

The hanger models were all run for 1000 seconds of fire time. This exceeded the duration of the tests. The models were specified so that data was recorded every 2 seconds of fire time.

6.3 Zone Modelling

The hanger tests were also simulated using the zone model CFAST. The results from these models were compared with the experimental and FDS model results to see if the simpler and quicker modelling procedure becomes more appropriate when large grid sizes were used in the FDS model.

6.3.1 Test 7, entire hanger

This test was simulated in the zone model using a single compartment measuring 97.8 metres long by 73.8 metres wide. CFAST could not simulate the inclined roof of the hanger so a constant height of 14.15 metres was given so that the total volume of the hanger was conserved. The fire was assigned a HRR of 5580kW and located at 61.1 metres in the x direction and 33.9 metres in the y direction. This corresponds to the position of the fire in the experiment. A "Roof" material was created in the zone model based on thermal properties for asphalt and other built up roof data as described for the FDS models in Section 6.2.8. These values along with other material properties used in the zone model are tabulated in Appendix D. Ventilation was prescribed as a 0.5 metre slit extending from the floor to a height of 13 metres. This represented the leakage that would occur through the large hanger doors on the north and south sides and was based on the area leakage ratio for loose construction as listed in Klote, (1995, Table 4-12.1).

6.3.2 Test 5, entire hanger

This test was simulated in the zone model by constructing two compartments: one to represent the hanger and the other to represent the draft curtain. The draft curtain "compartment" had a base of 24.4 by 18.3 metres and a height of 14.5 metres, which was the average height of the ceiling within the draft curtain. Vents were prescribed in all four walls of this compartment stretching the entire width of each wall and to a height of 10.8 metres and opening into the larger compartment that represented the hanger. In this way a 3.7 metre deep draft curtain was simulated. The walls of this compartment were assigned the properties of the draft curtain itself and are listed in Appendix D. The ceiling and floor were given the same properties as **Test 7, entire hanger** (described in the previous sub-section). To conserve volume in the rest of the hanger the volume of the draft curtain compartment was subtracted from the total hanger volume and a new length of 92 metres was assigned, the same width and height as the actual hanger of 73.8 metres and 14.15 metres were used. The roof, floor and walls also had the same properties as the simulation of **Test 7, entire hanger** described above (also refer to Appendix D for a list of the properties that were used for the models). The same ventilation of 0.5 metres by 13 metres high was also used.

6.3.3 Test 7, draft curtain only

This test was simulated as a single compartment with the same dimensions and properties as the draft curtain compartment described in Section 6.3.2 except the vents opened out to ambient.

6.4 Data analysis

The main form of data analysis for the comparisons of these hanger tests was to directly compare the temperature profiles from the models with those from the experiment at specific locations. This was done because it was difficult to reduce the data by averaging due to the unsteady nature of most of the temperature profiles; they continually increase during the experiment. Where averages could be taken, for example in the fire plume, an initial period of

200 seconds was taken as the time that the experiments and the FDS models took to reach steady state. This was based on observation of the temperature profiles. A period of 60 seconds at the end of the experimental results was also excluded from the averages because the temperature decreases due to the fire being extinguished.

In all the direct comparisons the experimental data was presented as discrete points at time steps of about four seconds and the model predictions as moving averages of 20 points. This was simply to aid in visualisation of the comparisons.

Because this moving average was used it is not clear how good the model predictions were at the beginning of the simulations. For this reason separate tables are presented, these detail the times that particular thermocouples experience a temperature rise. This gives a measure of the draft curtain smoke filling times. These initial times were simply extracted from the original temperature data files by observing the time at which the temperature had risen by more than 2°C above ambient.

The limited data that is obtained from the zone models made it difficult to compare with the experimental results and the FDS models. Especially since the thermocouples in the test were not well placed for zone model comparisons. To obtain an approximation of the upper layer temperature that is predicted by the zone model the temperatures at each time step were averaged for the five thermocouples E5, E6, E7, E8 and E9 (refer to Figure 6.3). These thermocouples make up the tree that is situated 9.1 metres east of the fire centre and are located at 0.3, 0.46, 0.76, 1.22 and 3 metres below the ceiling.

7 US Navy Hanger Results

This section presents the results for all the FDS models that were compared with the data from the high bay hanger tests in Hawaii. The results include:

- Time temperature profile comparisons for various locations directly above the fire. This was to show the accuracy of the predictions associated with the fire plume.

- Time temperature profile comparisons for various locations on the thermocouple tree 9.1 metres east of the fire, labelled Smoke Filling in Figure 6.3. These serve to illustrate the accuracy of the model predictions in the ceiling jet and upper layer of the hanger.

- Comparisons of the initial temperature delay displayed by relevant thermocouples. This provides an indication of the smoke filling times of the draft curtain.

- Zone model comparisons.

- FDS and CFAST model run times.

7.1 Test 7, entire hanger

7.1.1 Plume temperature comparisons

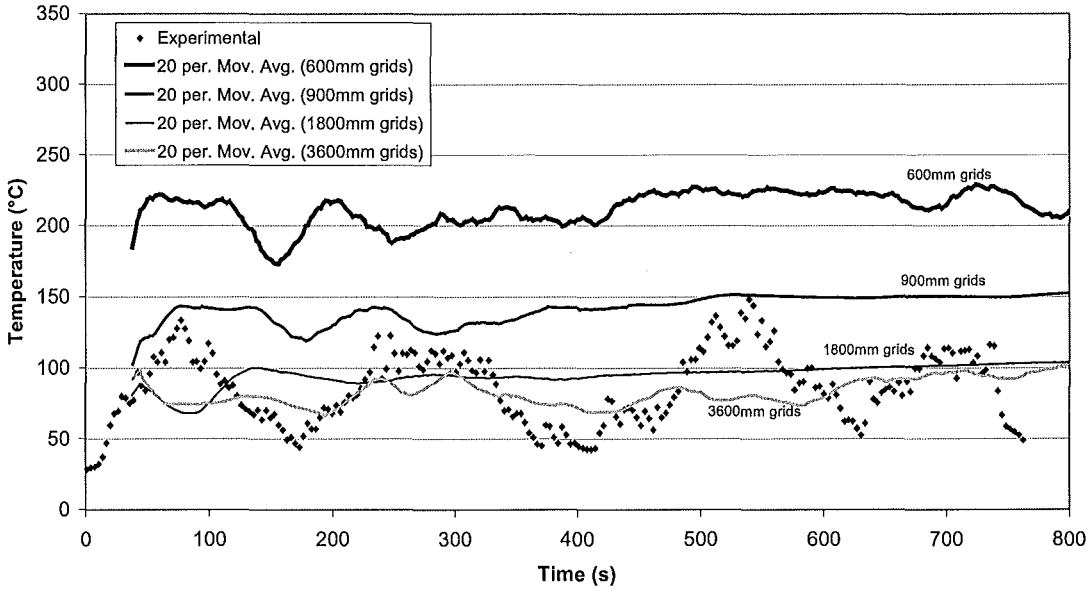

Figure 7.1: Test 7, entire hanger; predicted time-temperature profiles for thermocouple C1, directly above the fire, 0.3 metres below the ceiling.

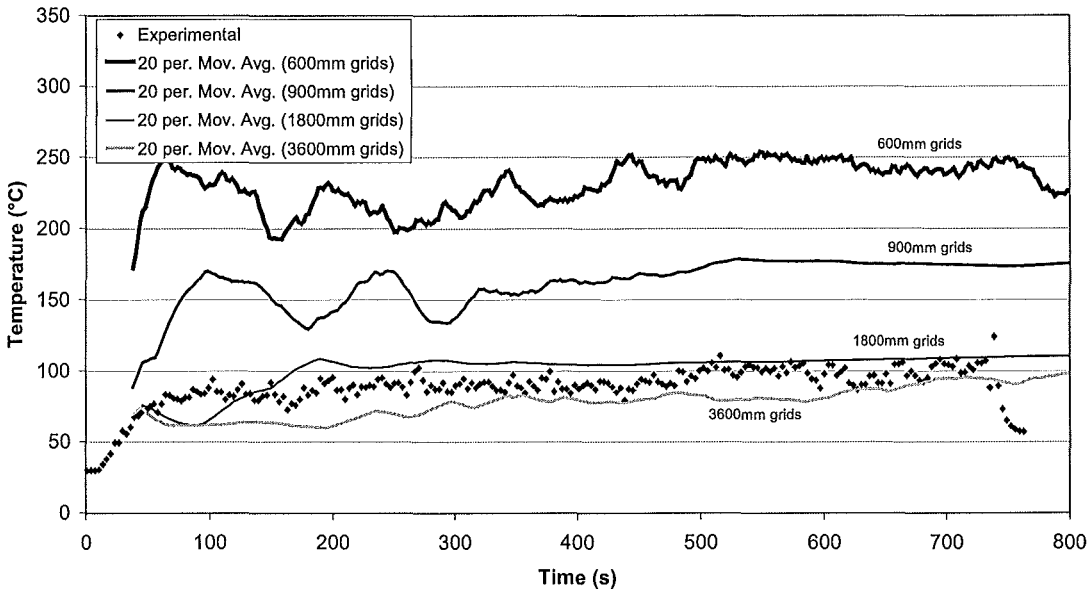

Figure 7.2: Test 7, entire hanger; predicted time-temperature profiles for thermocouple C12, directly above the fire, 6.1 metres below the ceiling.

This FDS simulation incorporated the entire hanger. Test fire 7 was performed with no draft curtain and had a HRR of 5580kW.

Figure 7.1 and Figure 7.2 are locations directly in the fire plume: 0.3 metres and 6.1 metres below the ceiling respectively. This corresponds to 14.2 metres and 8.4 metres above the fire. Comparisons at intermediate heights of 11.5 and 13 metres are given in Appendix C.2. The comparisons show:

- The smaller the FDS model grid size the greater the model over predicts the temperatures compared to those reported by the experiment. Towards the end of the test the 600mm grid model has a temperature of 150°C greater than experimental results. Both the 1800mm and 3600mm grid model seem to provide the closest prediction.

- There is very little difference in the temperatures at the two heights shown.

- The experimental results vary considerably with time at the lower thermocouple compared to relatively steady state up near the ceiling. The same trend is not displayed in the models.

7.1.2 East thermocouple tree comparisons

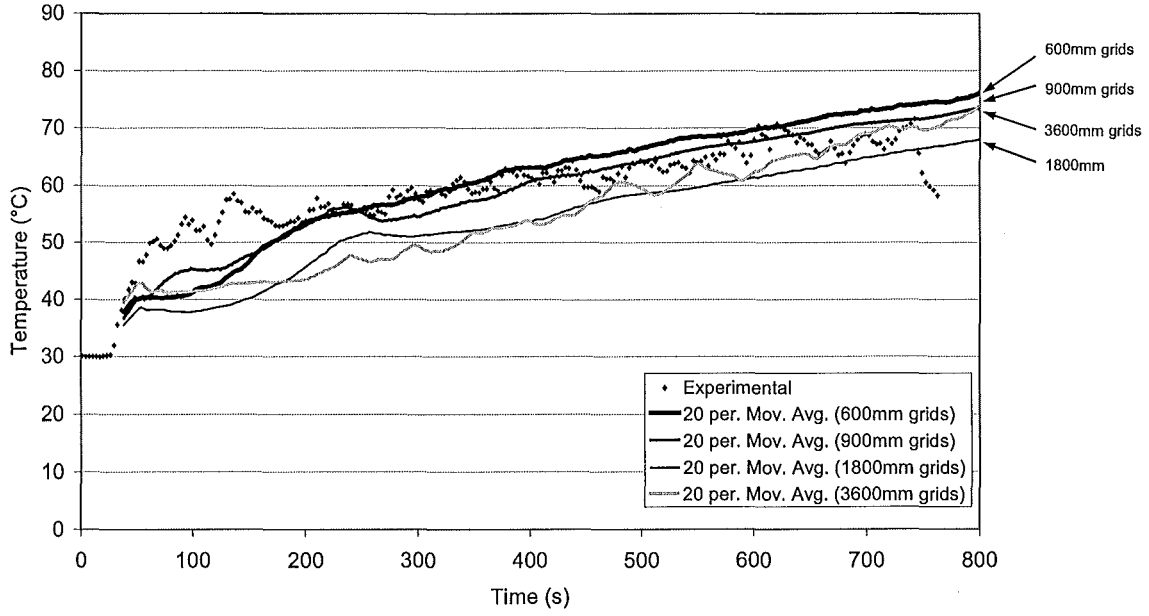

Figure 7.3: Test 7, entire hanger; predicted time-temperature profiles for thermocouple E5, 9.1 metres east of the fire, 0.3 metres below the ceiling.

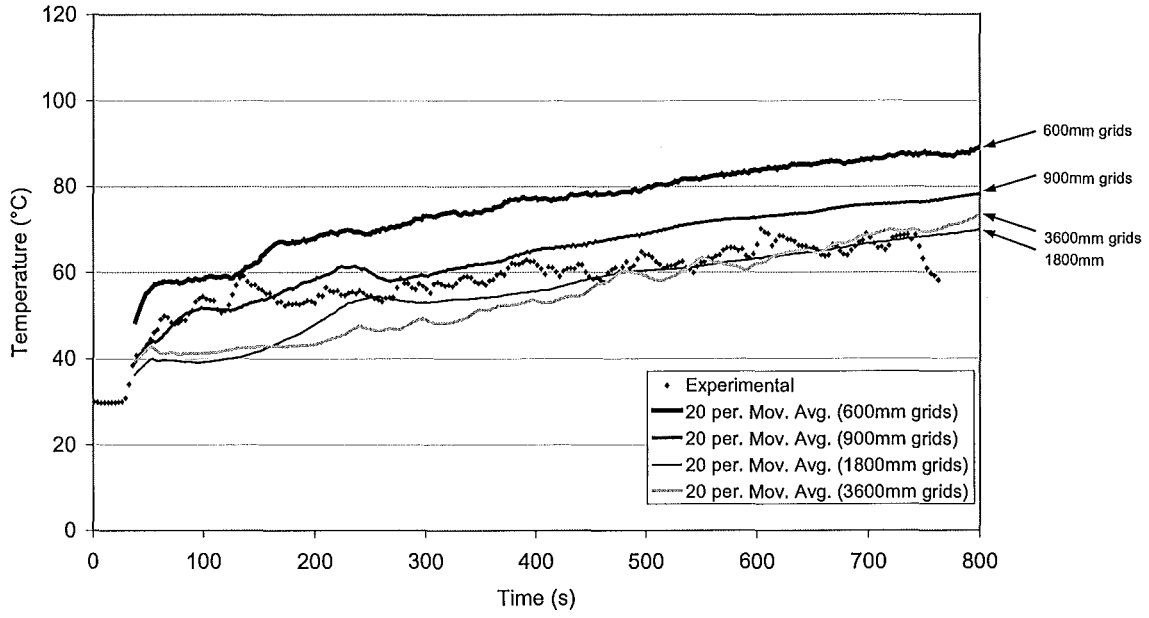

Figure 7.4: Test 7, entire hanger; predicted time-temperature profiles for thermocouple E7, 9.1 metres east of the fire, 0.76 metres below the ceiling.

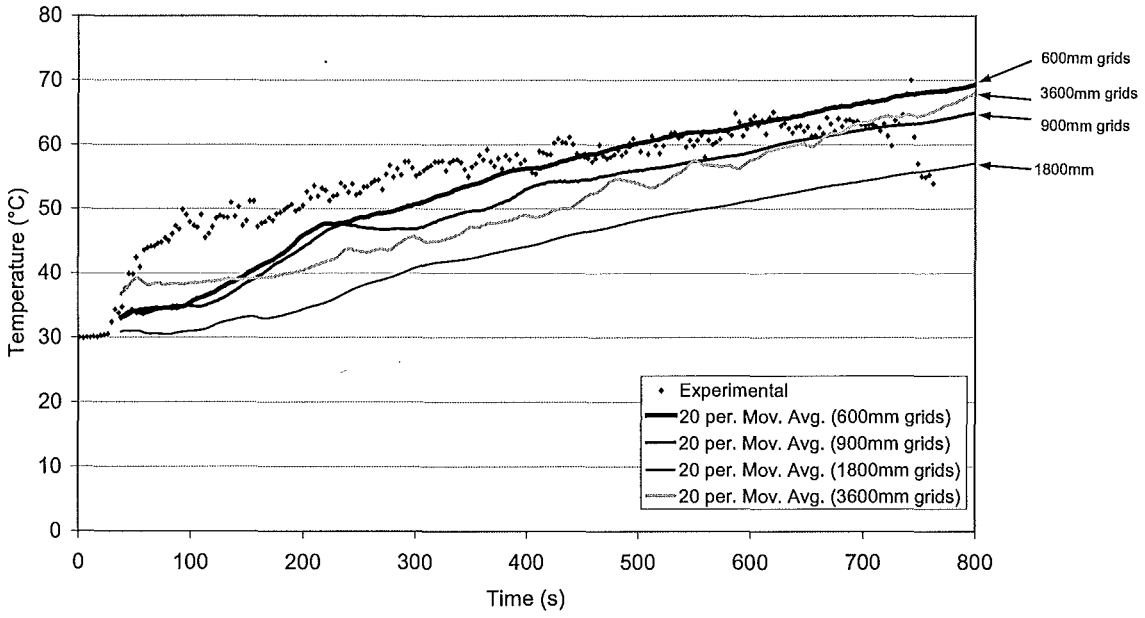

Figure 7.5: Test 7, entire hanger; predicted time-temperature profiles for thermocouple E8, 9.1 metres east of the fire, 1.22 metres below the ceiling.

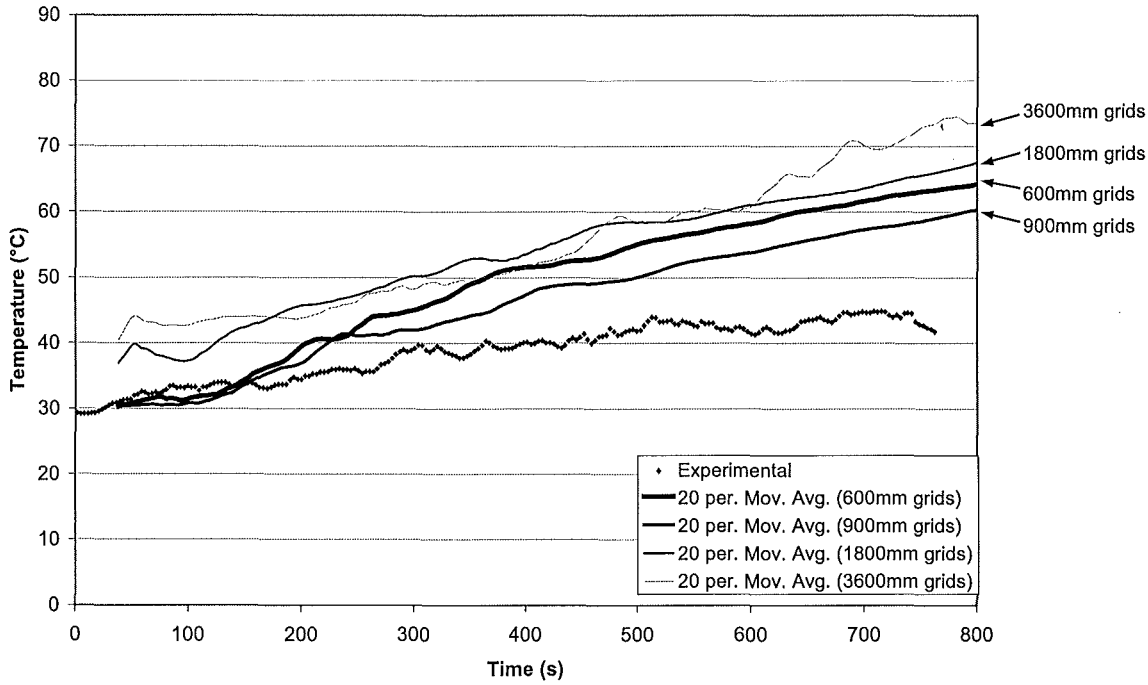

Figure 7.6: Test 7, entire hanger; predicted time-temperature profiles for thermocouple E9, 9.1 metres east of the fire, 3 metres below the ceiling.

Figure 7.3 to Figure 7.6 give the time temperature predictions of the FDS models for various locations on the thermocouple tree that is situated 9.1 metres east of the fire centre. To avoid repetition only the results at heights of 0.31 (E5), 0.76 (E7), 1.22 (E8) and 3 (E9) metres below the ceiling are given. This corresponds to heights of approximately 14.5, 14, 13.6 and 11.8 metres above the floor of the hanger. Comparisons for the remaining two thermocouples in this tree are provided in Appendix C.2. The four figures above indicate that:

- Although the gradients are the same there is a marked difference in the actual temperatures that the models predict. In general smaller grid sizes predict greater temperatures. This is best illustrated in Figure 7.4.

- The model predictions, when compared to the experimental results become less accurate at lower heights. This is most noticeable in Figure 7.6 where all the models considerably over predict both the temperatures and the gradient of the experimental results.

- The 600mm, 900mm and 1800mm grids all have roughly the same temperature profile gradients whereas the 3600mm model in all cases shows an increased gradient. This indicates an additional inaccuracy when using this large grid size. This trend is particularly noticeable in Figure 7.6.

7.1.3 Zone model comparisons

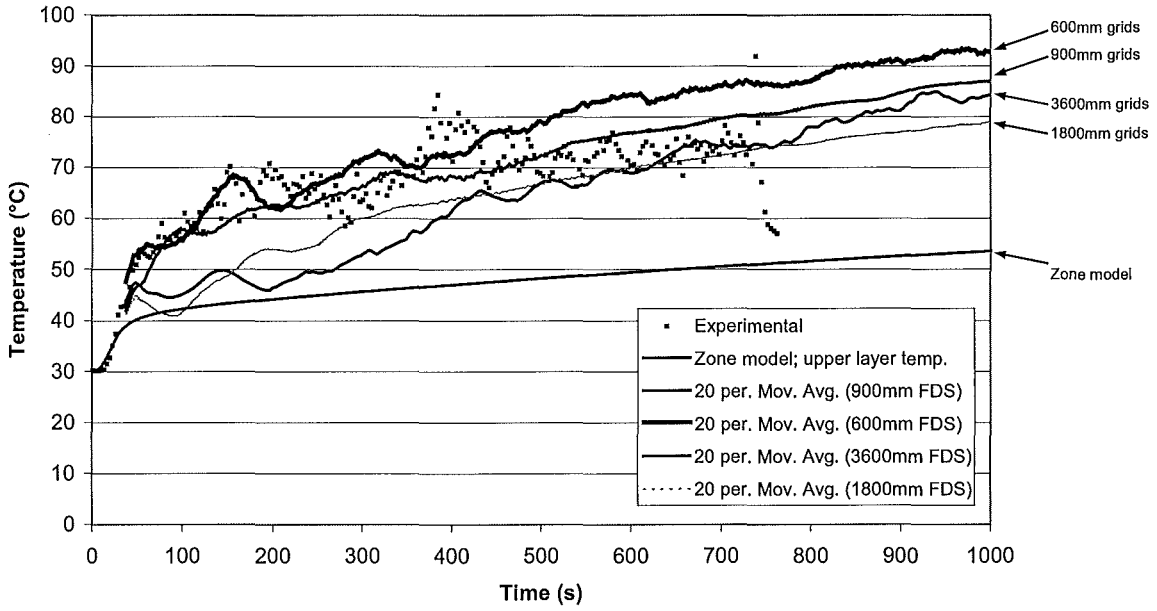

Figure 7.7: Test 7, entire hanger; comparison of the zone model upper layer temperature profile with profiles from FDS models and experimental averages.

Figure 7.7 provides a comparison between the temperature profile predicted by the zone model and those predicted by the FDS models. The temperature profiles given in Figure 7.7 provide an indication of the average temperature above the thermocouple E9, which is situated 3 metres below the ceiling. Section 6.4 explains how this average was calculated.

All the FDS models provide an average temperature that compares better to the experimental average than the zone model prediction does. The zone model under predicts the temperature and the temperature gradient significantly.

7.2 Test 5, entire hanger

7.2.1 Plume temperature comparisons

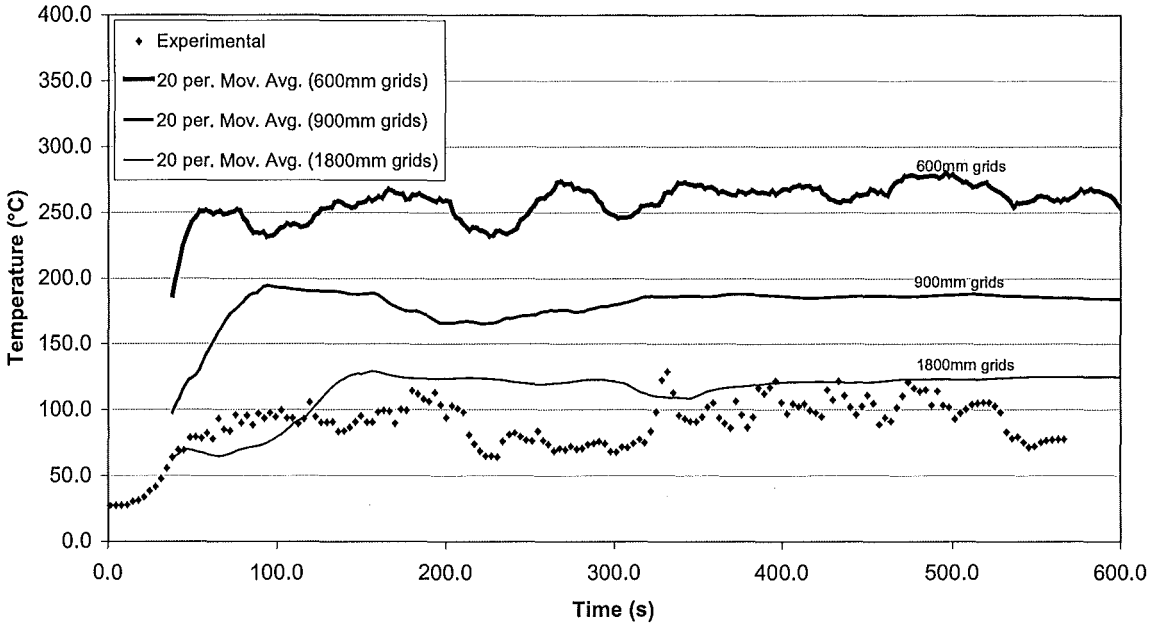

Figure 7.8: Test 5, entire hanger; predicted time-temperature profiles for thermocouple C1, directly above the fire, 0.3 metres below the ceiling.

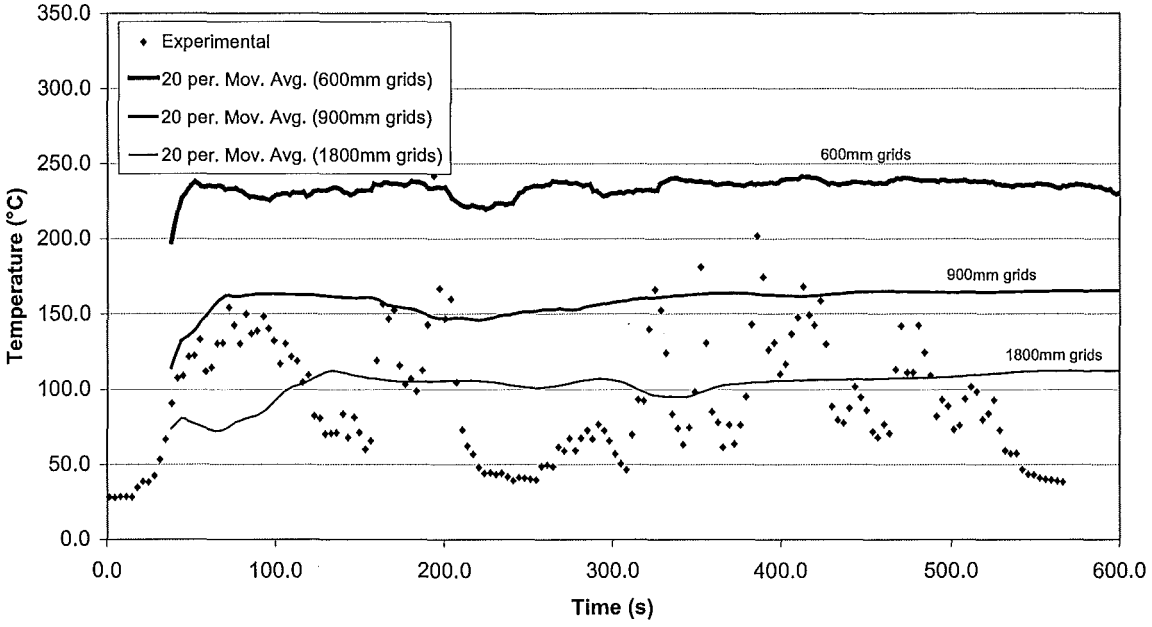

Figure 7.9: Test 5, entire hanger; predicted time-temperature profiles for thermocouple C12, directly above the fire, 6.1 metres below the ceiling.

Figure 7.8 and Figure 7.9 show similar trends as the comparisons at these locations for **Test 7, entire hanger** (Section 7.1). The difference in this test is that the HRR is greater (6760kW compared to 5580kW) and there is a draft curtain installed. The consequences of these differences and the comparisons with the experimental are listed below:

- As in the comparison of test 7 without the draft curtain (Figure 7.1 and Figure 7.2) the smaller grid models predict much greater temperatures than the larger grid models. Again, the 1800mm grid model provides predictions that fall closer to the experimental temperatures.

- The predictions and the experiment results both show a similar trend in that the temperatures near the ceiling (C1) are only slightly less than those at the lower point (C12), which is closer to the flame.

- The experimental results vary considerably with time at the lower thermocouple compared to relatively steady state up near the ceiling. The same trend is not displayed in the models.

- Compared to Figure 7.1 and Figure 7.2 (comparisons of **Test 7, entire hanger**) the temperatures are slightly hotter as expected. The addition of a draft curtain should not influence the plume temperatures considerably whereas the increased HRR should.

Appendix C.2 provides the temperature profile comparisons for the intermediate heights corresponding to locations C2 and C3.

7.2.2 East thermocouple tree comparisons

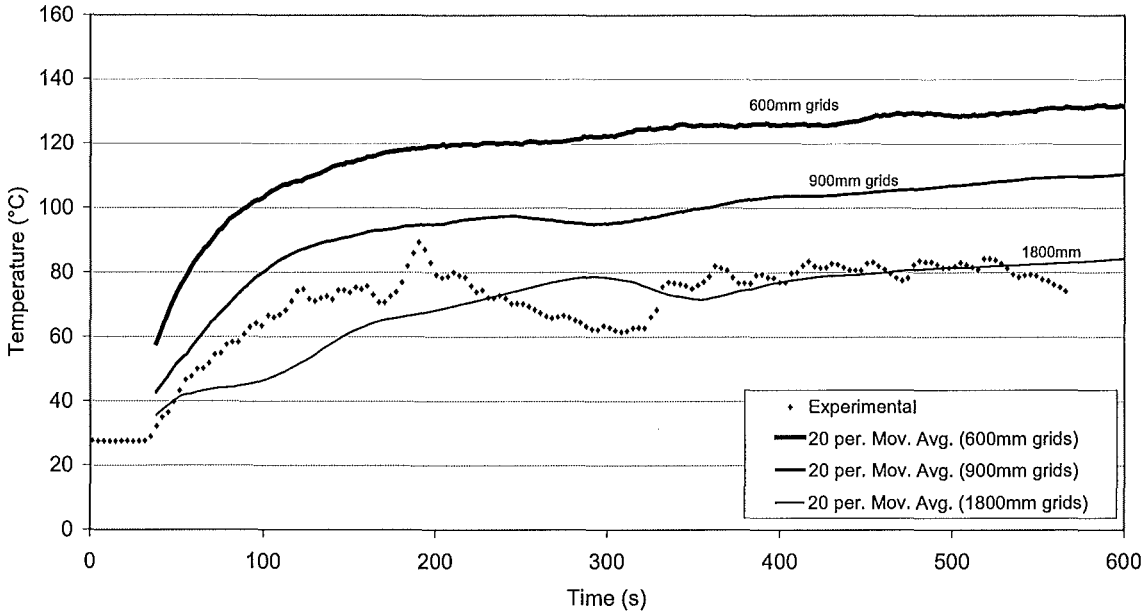

Figure 7.10: Test 5, entire hanger; predicted time-temperature profiles for thermocouple E5, 9.1 metres east of the fire, 0.3 metres below the ceiling.

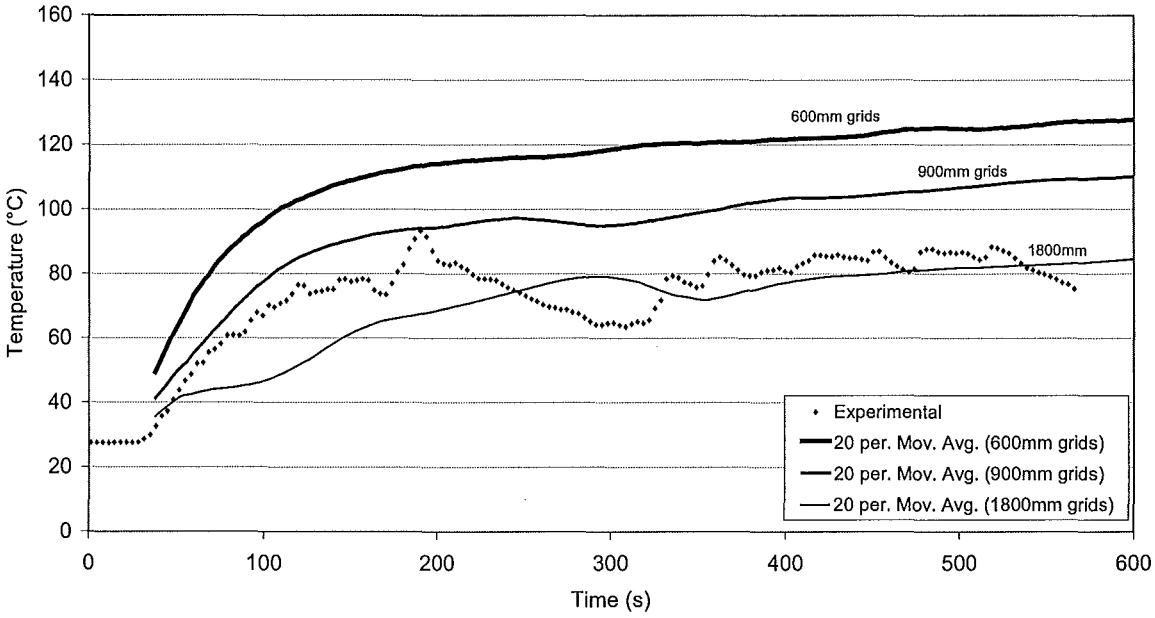

Figure 7.11: Test 5, entire hanger; predicted time-temperature profiles for thermocouple E7, 9.1 metres east of the fire, 0.76 metres below the ceiling.

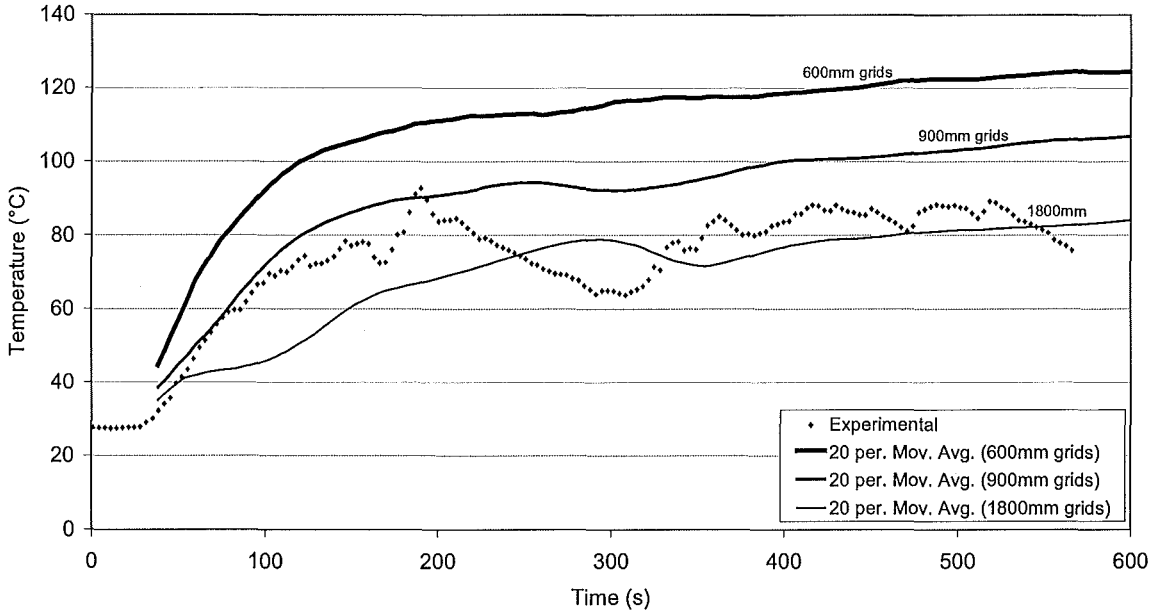

Figure 7.12: Test 5, entire hanger; predicted time-temperature profiles for thermocouple E8, 9.1 metres east of the fire, 1.22 metres below the ceiling.

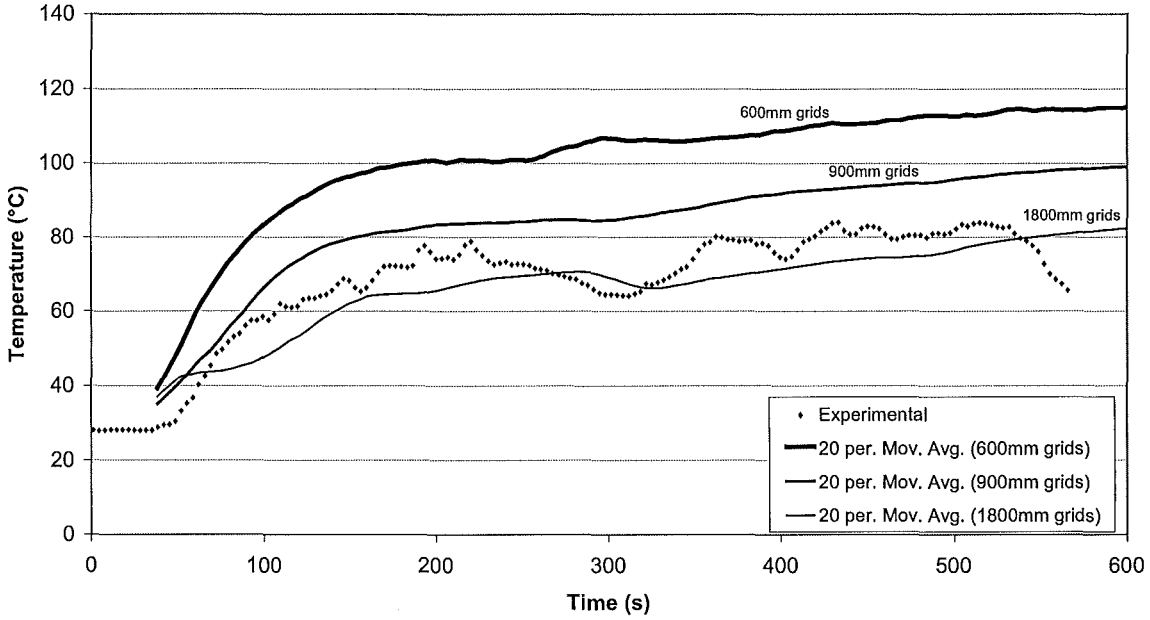

Figure 7.13: Test 5, entire hanger; predicted time-temperature profiles for thermocouple E9, 9.1 metres east of the fire, 3 metres below the ceiling.

Figure 7.10 to Figure 7.13 give the time temperature profile predictions for the thermocouple tree located 9.1 metres east of the fire. All these thermocouples lie within the draft curtain, which extends 3.7 metres down from the ceiling. The temperature profiles for the other two thermocouples in this tree (E4 and E5) are provided in Appendix C.2. The temperature profiles are all similar, as is expected in a relatively small draft curtain situated over the fire. To illustrate the trends in the draft curtain an average of 20 points around the time of 500 seconds has been taken and plotted in Figure 7.14. Error bars of +/-20% have also been shown on the experimental points.

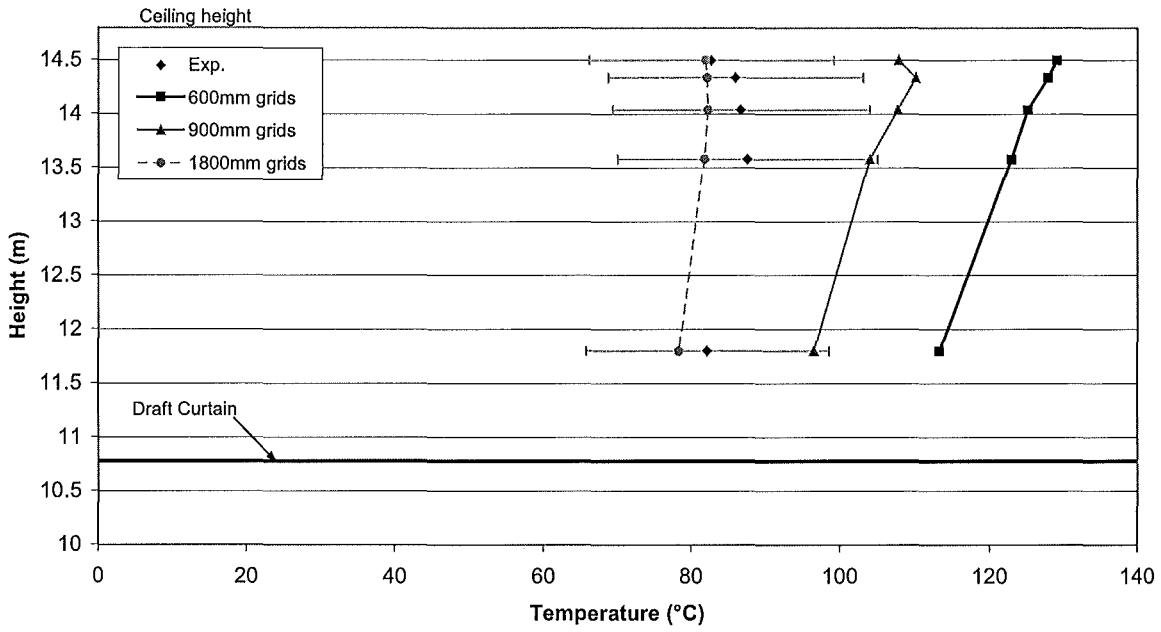

Figure 7.14: Test 5, entire hanger; temperature profiles in relation to height for the thermocouple tree 9.1 metres east of the fire at a time of 500 seconds.

Because Figure 7.14 only provides temperatures at a single time in the test the results should only be taken as qualitative. The 600mm grid model over predicts the temperature the most for all locations, falling well outside +/-20% of the experimental results. The 1800mm grid model provides the most accurate predictions of temperature at all the thermocouple locations.

The above comparisons only provide information about the capability of the FDS models to predict temperatures inside the confines of the draft curtain. Two thermocouples that lie outside the draft curtain are compared in Figure 7.15 and Figure 7.16 in the following section.

7.2.3 Draft curtain results

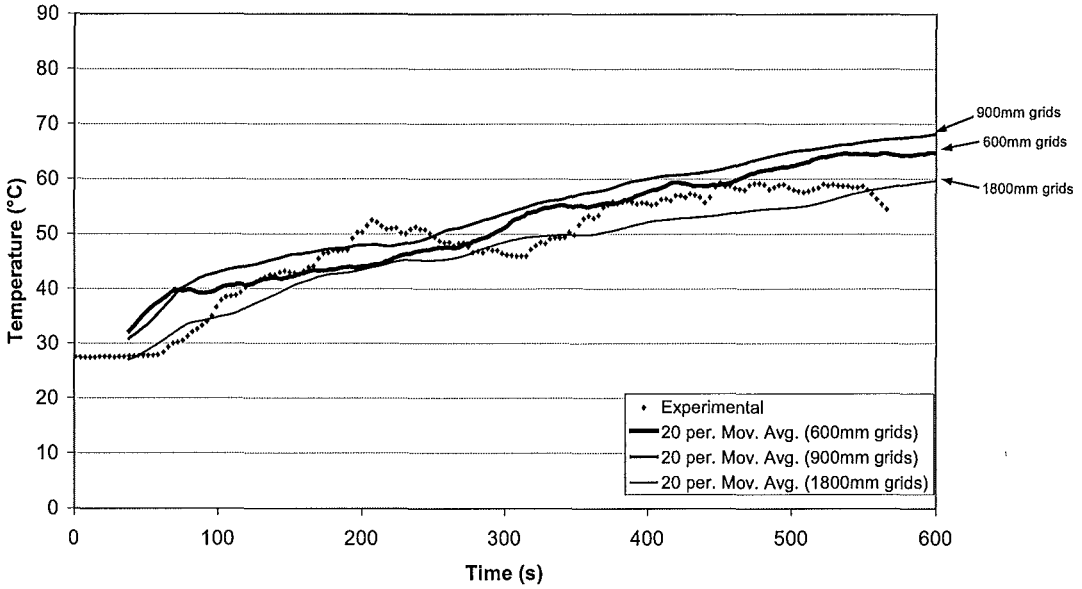

Figure 7.15: Test 5, entire hanger; predicted time-temperature profiles for thermocouple W1, 17.7 metres west of the fire, 0.3 metres below the ceiling, outside the draft curtain.

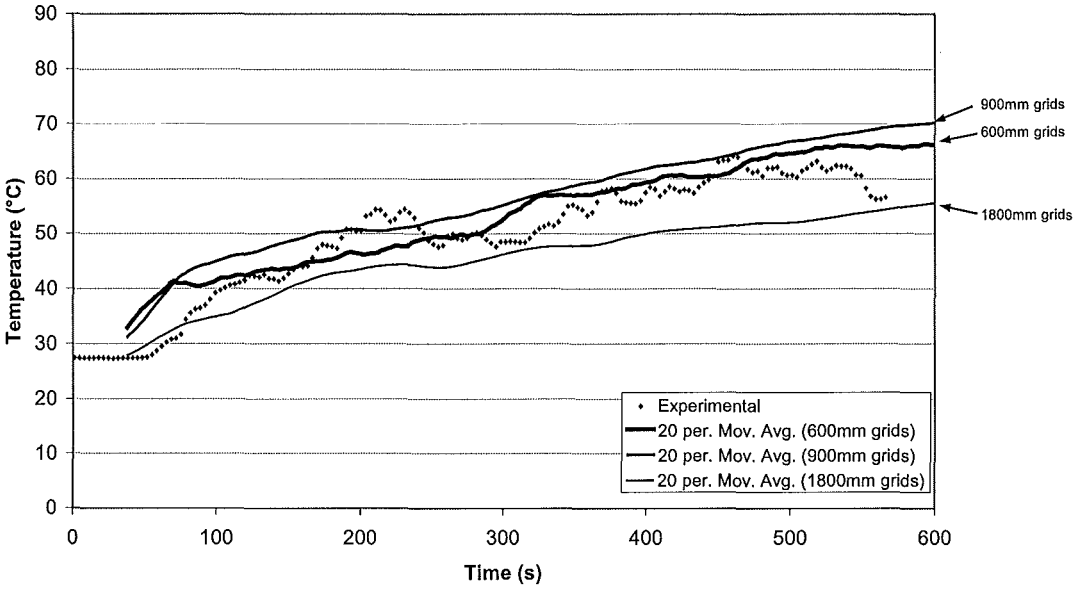

Figure 7.16: Test 5, entire hanger; predicted time-temperature profiles for thermocouple W2, 14.6 metres west of the fire, 0.3 metres below the ceiling, outside the draft curtain.

Figure 7.15 and Figure 7.16 are comparisons at locations outside the draft curtain and indicate the following:

- The FDS temperature predictions outside the curtain are much more accurate than those inside the curtain.

- All the FDS models provide reasonable predictions of the experimental results

- The initial delay in the temperature rise of the experimental results is due to the time the draft curtain takes to fill. This is also displayed in the FDS predictions. Table 7.1 provides comparisons of this time.

Table 7.1: Approximate draft curtain filling time based on the temperature rise of thermocouples immediately outside the draft curtain.

	Thermocouple	
	E2	**W2[1]**
Experiment	45 seconds	55 seconds
600mm grids	28 seconds	30 seconds
900mm grids	30 seconds	30 seconds
1800mm grids	34 seconds	35 seconds
CFAST	40 seconds	40 seconds

[1] The difference in the filling times predicted by these two thermocouples is due to the slope of the ceiling; the bottom of the draft curtain at the west end is lower than the bottom at the east end. The result is that the smoke spills from the east end first.

Table 7.1 shows that:

- The draft curtain filling time is under predicted by all the FDS models.

- The difference between the spill time of the east and west sides of the draft curtain are not as great as those observed in the experimental results.

- The zone model provides a closer approximation of curtain filling time but could not model the difference in times at different ends of the curtain.

The filing time for the zone model was taken directly from the plot of the draft curtain "compartment" layer height (see Section 6.3.2 for an explanation of how the hanger tests were simulated using the zone model). This plot is given in Appendix C.2, Figure C.17.

7.2.4 Zone model comparisons

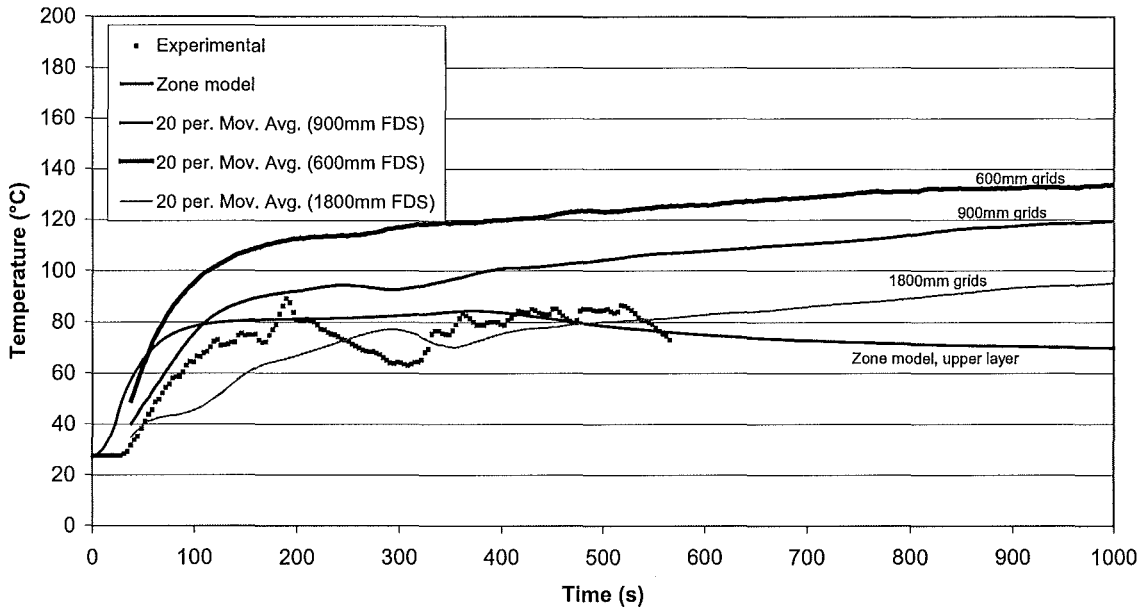

Figure 7.17: Test 5, entire hanger; comparison of the zone model upper layer temperature profile within the draft curtain with profiles from FDS model and experimental averages.

Figure 7.17 gives the comparisons of the zone model predictions for the upper layer temperature within the confines of the draft curtain. The zone model provides a good prediction of the experimental temperature profile, significantly better than either the 600mm or 900mm grid FDS models. The 1800mm model is comparable but under predicts the initial part of the test. The zone model also displays the steady state period after about 100 seconds of fire time whereas the FDS models do not.

No comparisons have been made with the zone model predictions outside the confines of the draft curtain because not enough temperature recordings were made to obtain an indication of the upper layer temperature in this region.

7.3 Test 5, draft curtain only.

7.3.1 Plume temperature comparisons

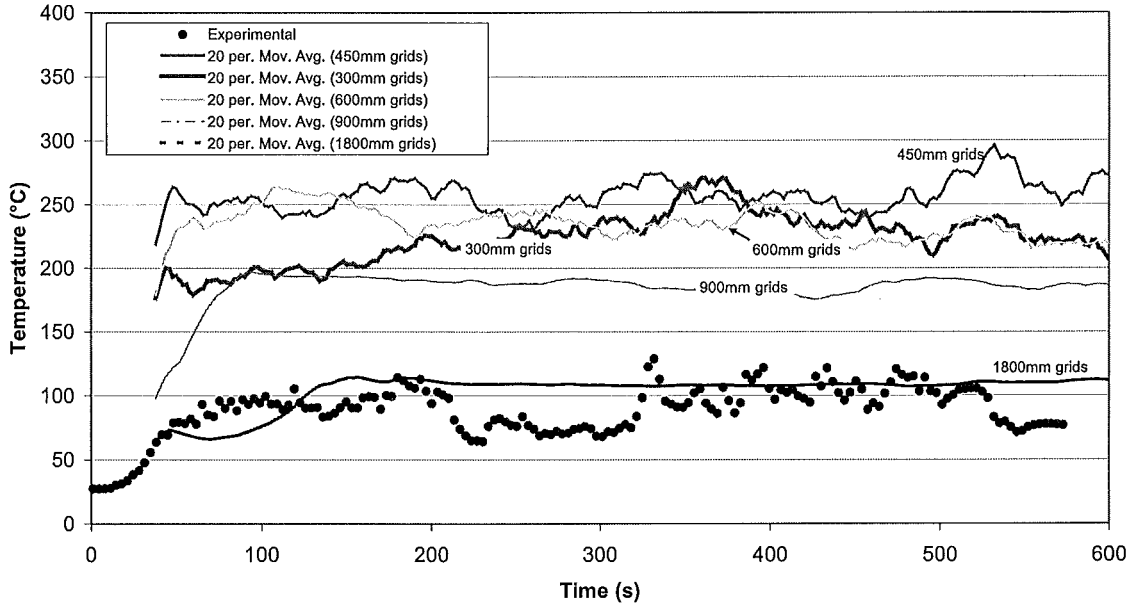

Figure 7.18: Test 5, draft curtain only; predicted time-temperature profiles for thermocouple C1, directly above the fire, 0.3 metres below the ceiling.

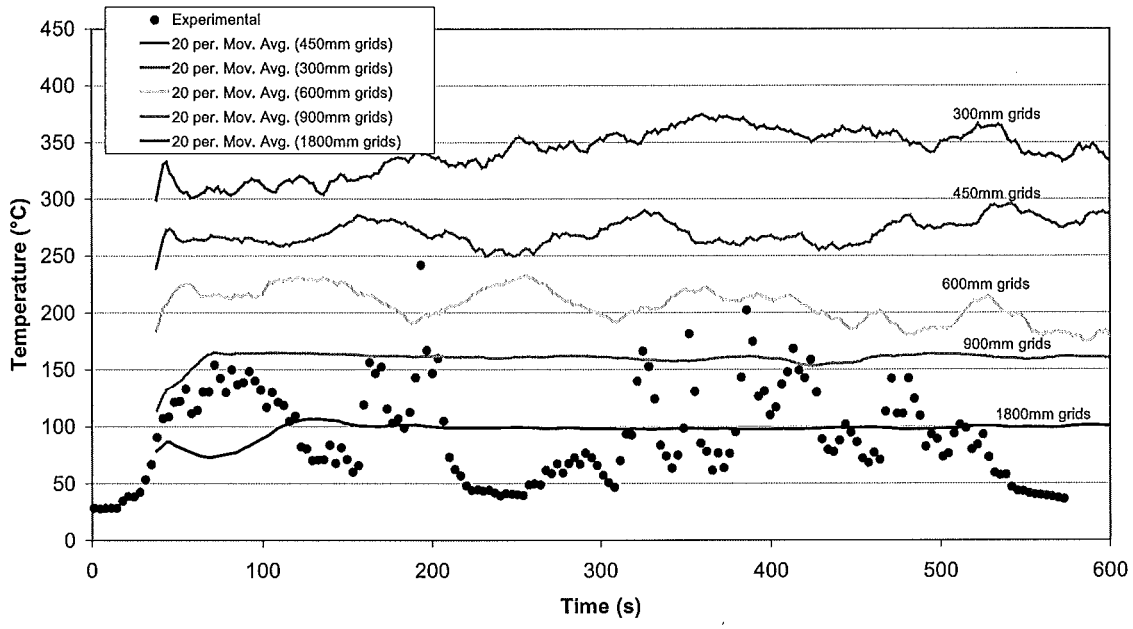

Figure 7.19: Test 5, draft curtain only; predicted time-temperature profiles for thermocouple C12, directly above the fire, 6.1 metres below the ceiling.

These simulations compare the same test as the previous section **Test 5, entire hanger**, except the FDS models only model the area of the draft curtain. This means that finer grids of 300 and 450mm can be used without overloading the FDS program.

Figure 7.18 and Figure 7.19 are time temperature profiles for thermocouples that are located directly above the fire centre corresponding to heights of 14.5 metres and 8.7 metres respectively. Profile comparisons at intermediate heights are provided in Appendix C.2.

- The same trends are shown as in the previous comparisons of the plume temperatures; the smallest grids display very poor predictions, the larger grids fall closer to the experimental results (Figure 7.19).

- The profiles are less variable for greater grid size (Figure 7.18 and Figure 7.19).

- The experimental results are a lot more erratic at the location closer to the fire (Figure 7.19). This phenomenon is not observed to the same extent in the models.

7.3.2 East thermocouple tree comparisons

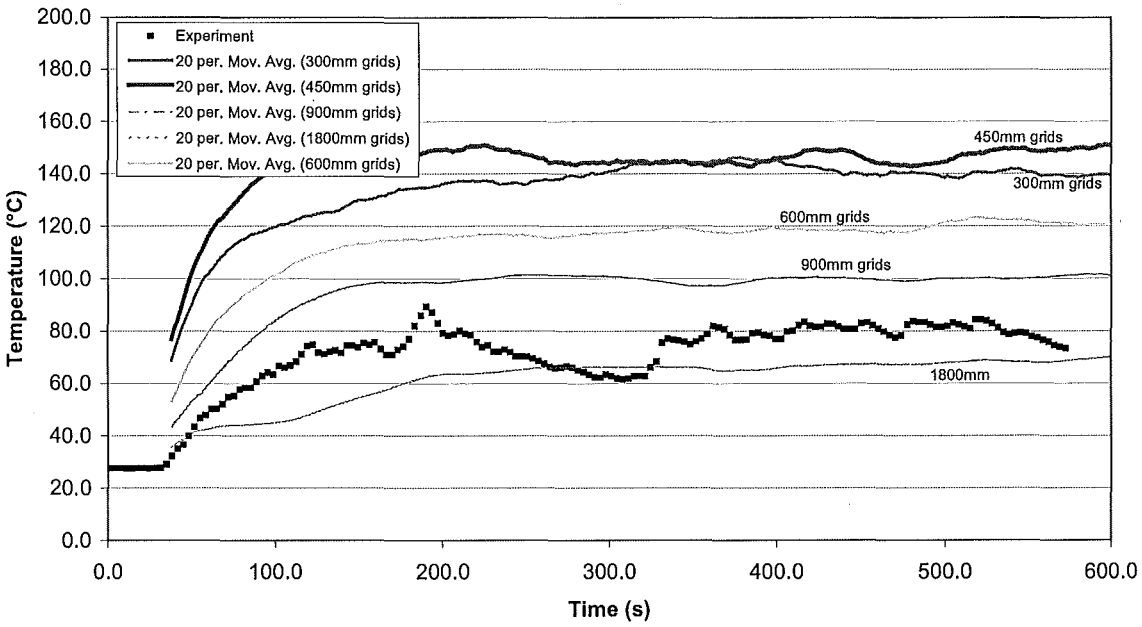

Figure 7.20: Test 5, draft curtain; predicted time-temperature profiles for thermocouple E5, 9.1 metres east of the fire, 0.3 metres below the ceiling.

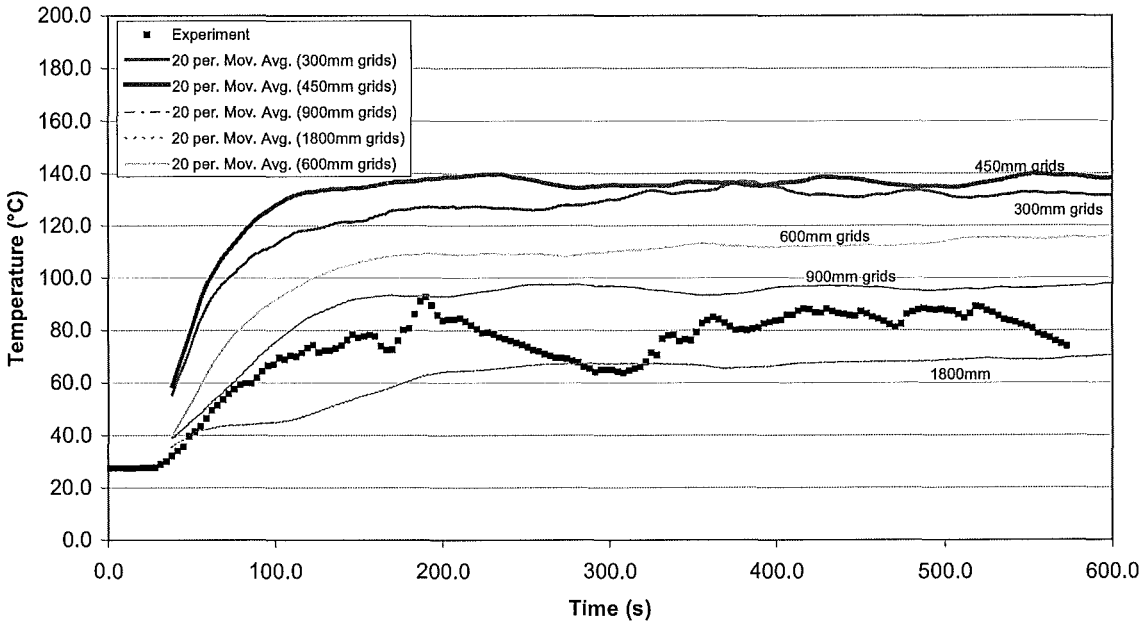

Figure 7.21: Test 5, draft curtain; predicted time-temperature profiles for thermocouple E8, 9.1 metres east of the fire, 1.22 metres below the ceiling.

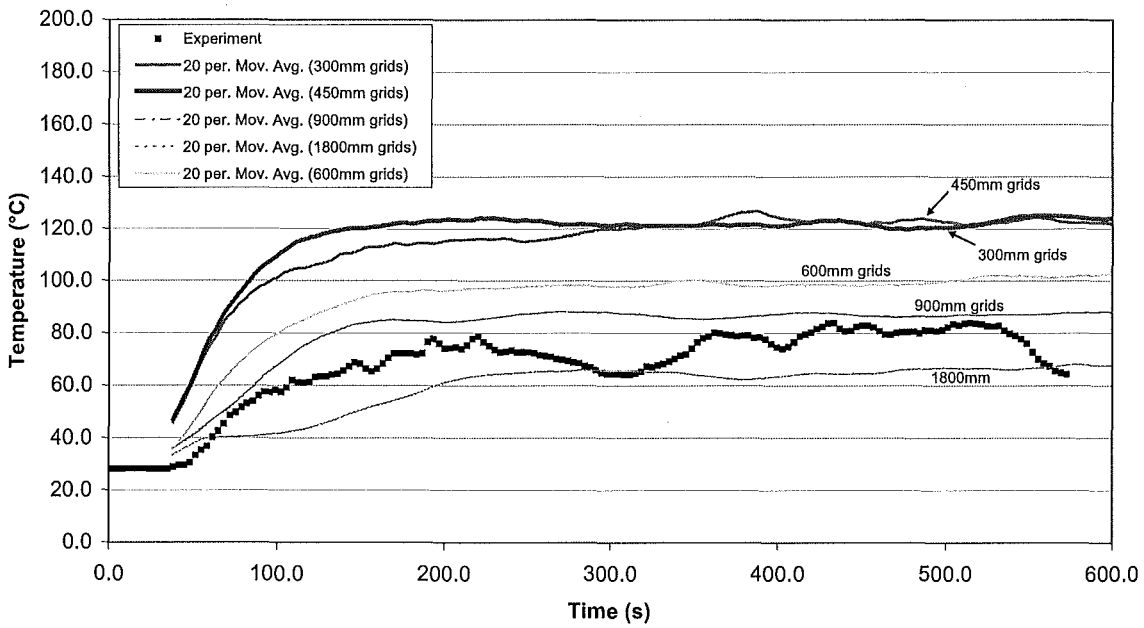

Figure 7.22: Test 5, draft curtain; predicted time-temperature profiles for thermocouple E9, 9.1 metres east of the fire, 3 metres below the ceiling.

Figure 7.20 to Figure 7.22 are temperature profile predictions for selected heights on the thermocouple tree located 9.1 metres east of the fire centre. This tree is located within the confines of the draft curtain. Only three locations have been given here to avoid repetition. Comparisons at other locations can be seen in Appendix C.2.

- The predictions become poorer the greater the grid size.

- The difference in temperatures predicted by the models at the various heights is very small; the experimental results also show this trend. This observation is shown better in Figure 7.23.

- The 300mm grid and 450mm grid models provide very similar temperature predictions.

- The models reach steady state after about 200 seconds. This steady state period does not occur in the results of the previous section when the entire hanger is modelled

(Section 7.2 **Test 5, entire hanger**). This is simply due to an upper layer forming when the entire hanger is modelled, which increases the temperature within the draft curtain. This upper layer does not form in the model of the above comparisons because the hanger is not modelled.

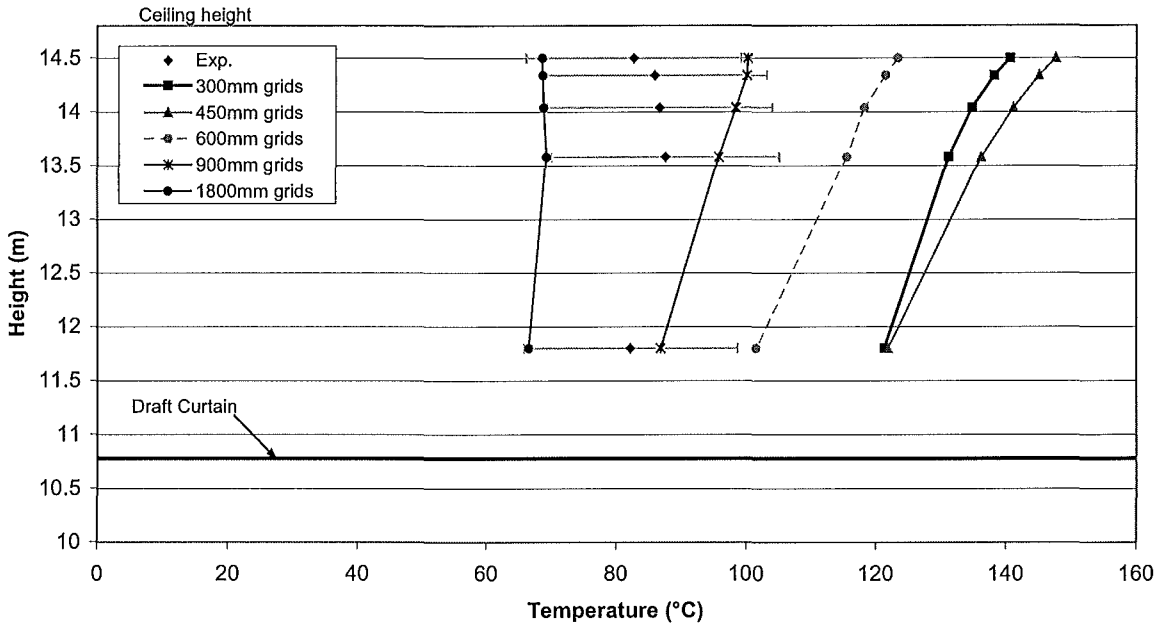

Figure 7.23: Test 5, draft curtain; temperature profiles in relation to height for the thermocouple tree 9.1 metres east of the fire at a time of 500 seconds.

Figure 7.23 shows the general trends in the temperature profiles predicted by the FDS model.

- The 300mm and 450mm grid models are very similar.

- The 900mm model predicts values that are the closest to the experimental results, falling within the 20% difference bars shown.

- The lower temperature at the highest thermocouple (14.5 metres) is not predicted by any of the models. This is most probably due to the low resolution of the grids.

7.3.3 Draft curtain results

Figure 7.20 to Figure 7.22 above, all indicate an initial delay in the temperature rise of the experimental results. Due to the moving average trendline this initial delay cannot be distinguished in the FDS model predictions. Table 7.2 serves to define these delays in temperature rise for two thermocouples. A zone model time is also given. This is the time that the layer height predicted by the zone model, reaches these thermocouples. The plot from which these times were taken is provided in Appendix C.2, Figure C.23.

Table 7.2: Test 5, draft curtain; initial temperature rise delays for thermocouples E5 and E9.

	Thermocouple	
	E5	**E9**
Experiment	35 seconds	48 seconds
300mm grids	6 seconds	16 seconds
450mm grids	6 seconds	16 seconds
600mm grids	6 seconds	20 seconds
900mm grids	8 seconds	10 seconds
1800mm grids	10 seconds	12 seconds
CFAST	3 seconds	21 seconds

- The FDS models all under predict the delay in temperature rise.

- The general trend shown by the experimental results of a longer delay for lower thermocouples is repeated in all the models.

- Larger grid models, when compared to smaller grid models, provide longer delays for the highest thermocouple (E5) but shorter delays for the lower thermocouple (E9).

- The times at which the layer height descends to the respective thermocouples compares better with the FDS model times. They are still considerably less than the experimental times, especially at the location of the thermocouple E5.

7.3.4 Zone model comparisons

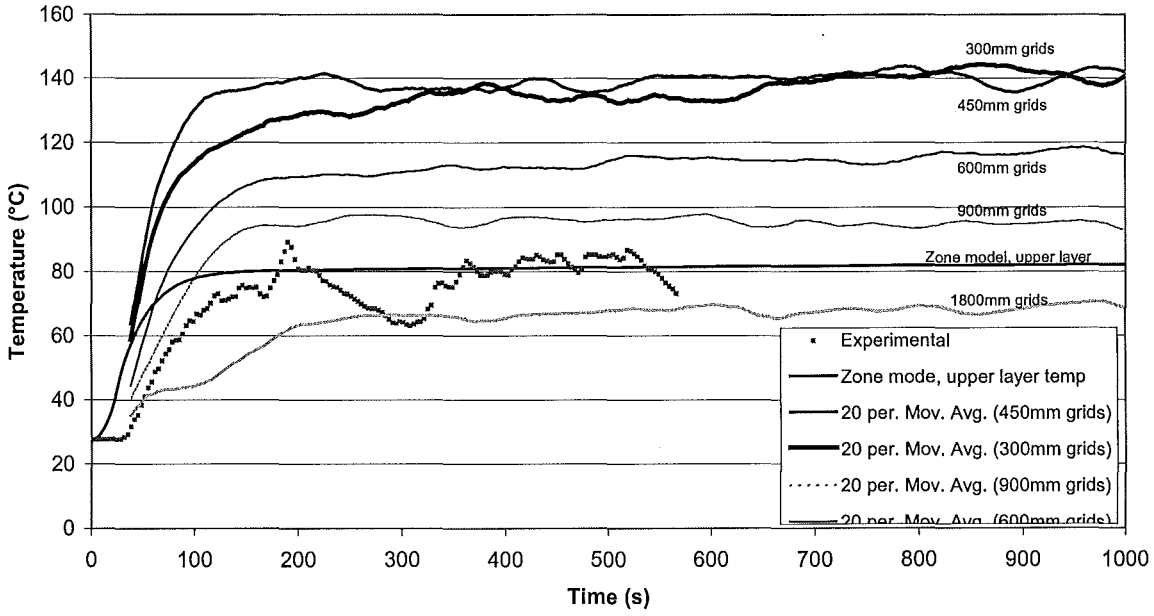

Figure 7.24: Test 5, draft curtain; comparison of the zone model upper layer temperature profile within the draft curtain with profiles from FDS model and experimental averages.

Figure 7.24 compares the temperature profile in the upper layer of the draft curtain area predicted by the zone model with the same profiles predicted by the FDS models.

The zone model provides a very good approximation to the experimental results, comparing much better than any of the FDS models.

7.4 Model Run times

Table 7.3 gives the running times for all the FDS and CFAST model simulations that were performed. The time to model the fire in the entire hanger was the same whether a draft curtain was simulated or not, therefore the columns labelled **Entire hanger** give the running times for **Test 7, entire hanger** and **Test 5, entire hanger**. The RAM of the computers used for each model is also provided.

Table 7.3: FDS and CFAST model running times for the Hawaii hanger simulations.

	Entire Hanger		Draft curtain only	
Grid size	**Run time**	**RAM**	**Run time**	**RAM**
300mm (H/48)	-	-	98.8 hrs	256 Mb
450mm (H/32)	-	-	16.5 hrs	256 Mb
600mm (H/25)	123.2 hrs	511 Mb	5.7 hrs	130 Mb
900mm (H/17)	13.6 hrs	256 Mb	51.6 mins	130 Mb
1800mm (H/8)	50 mins	130 Mb	3.5 mins	130 Mb
3600mm (H/4)	4.5 mins	130 Mb	-	-
CFAST	10 secs	130 Mb	10 seconds	130 Mb

7.5 Discussion and conclusions

This section outlines and discusses the main areas of the Hawaii hanger results, which need to be explained in more detail, and presents the conclusions drawn from them.

In order to judge if any particular sized model is better than another an understanding of the reasons why it is better is required. The reason for this is that the trend may only apply to this particular scenario. It can be concluded that one grid size is better than another for one particular scenario by direct comparisons but a more generic conclusion for other scenarios can be made if the reasons are established and they can be applied to the actual modelling procedure, be it the FDS model itself or the inputs and modelling requirements defined by the user.

7.5.1 Plume temperature comparisons

Most of the results presented above indicate that the models with the finer grid sizes of 300mm (H/48) to 600mm (H/25) do not predict temperatures as well as the models with larger grid sizes of 1800 (H/8) and 3600mm (H/4). One area where this trend is particularly exaggerated is for the temperature predictions in the fire plume. This can be seen directly in Figure 7.1 and Figure 7.8 where the 600mm model over predicts by as much as 150 to 200°C.

This is the opposite of what was expected. Finer grid resolution should, in all cases provide better predictions. In particular, in areas close to the fire the greater number of grids defining the fire surface should mean much better characterisation of the combustion processes and flame behaviour. Obviously this was not the case. The reasons may be due to several conflicting errors that serve to cancel each other out when large grid sizes are used so it then appears that good predictions are made.

The first problem that was analysed was not in the FDS models but in the actual experimental results. The thermocouple C12, which is located directly above the fire centre at a height of

8.4 metres, only yields an average experimental temperature of 90°C[1]. This is much too low for a fire plume temperature. An estimation of what the temperature should be at this height can be obtained using Heskestad's correlation for centreline plume temperatures:

$$\Delta T_0 = 25\left(\frac{\dot{Q}_c^{2/5}}{(z - z_0)}\right)^{5/3} \qquad \textbf{Equation 7.1}$$

Where z_0 is the virtual origin of the fire and is defined as:

$$z_0 = 0.083\dot{Q}^{2/5} - 1.02D \qquad \textbf{Equation 7.2}$$

This estimation is given in Table 7.4 along with the experimental value and the predictions from the FDS models.

Table 7.4: Average temperatures for Test 7, at thermocouple C12 (directly above the fire, 6.1 metres below the ceiling).

	Exp.	Heskestad	600mm grids (H/25)	900mm grids (H/17)	1800mm grids (H/8)
Test 7	90°C	219°C	218°C	147°C	102°C

The Heskestad correlation provides an estimation that is much closer to the 600mm model prediction than the experimental, indicating that the experimental temperature measurement is too low as initially thought and that the smaller grid model may in fact be predicting better than initially observed. The larger grid models become progressively worse when compared to the Heskestad correlation.

[1] The temperature profiles for the thermocouples in the fire plume have a steady state period after about 200 seconds. This can be seen in Figure 7.1 and Figure 7.2. For ease of analysis an average was taken of this period

One possible reason why the experimental temperatures are so low may be due to leaning and swaying of the fire plume due to drafts in the hanger during the experiment or asymmetric ignition of the fuel. From video footage of Test 7 it was observed that the plume leaned to the west by about 0.5 metres and to the south by up to 1.2 metres for the initial part of the test. A small fuel spill produced an even stronger westward lean after about 170 seconds. By the end of the test the lean had increased to 0.8 metres west and 2 metres south (Gott et al, 1997).

If this plume lean was the reason for these low plume temperatures then it would follow that nearer the ceiling the experimental temperatures would become more reliable due to the formation of the more stable ceiling jet. The fact that temperature predictions are closer to the experiment results at locations further out from the fire, as is observed in Figure 7.3 and Figure 7.4, may provide evidence for this. Also if experimental results are compared with the Heskestad correlation at a height of 14.2 metres (this corresponds to 0.3 metres below the ceiling, location C12) then the difference is only small. This is illustrated in Figure 7.25, which gives the profiles of temperature verse height directly above the fire.

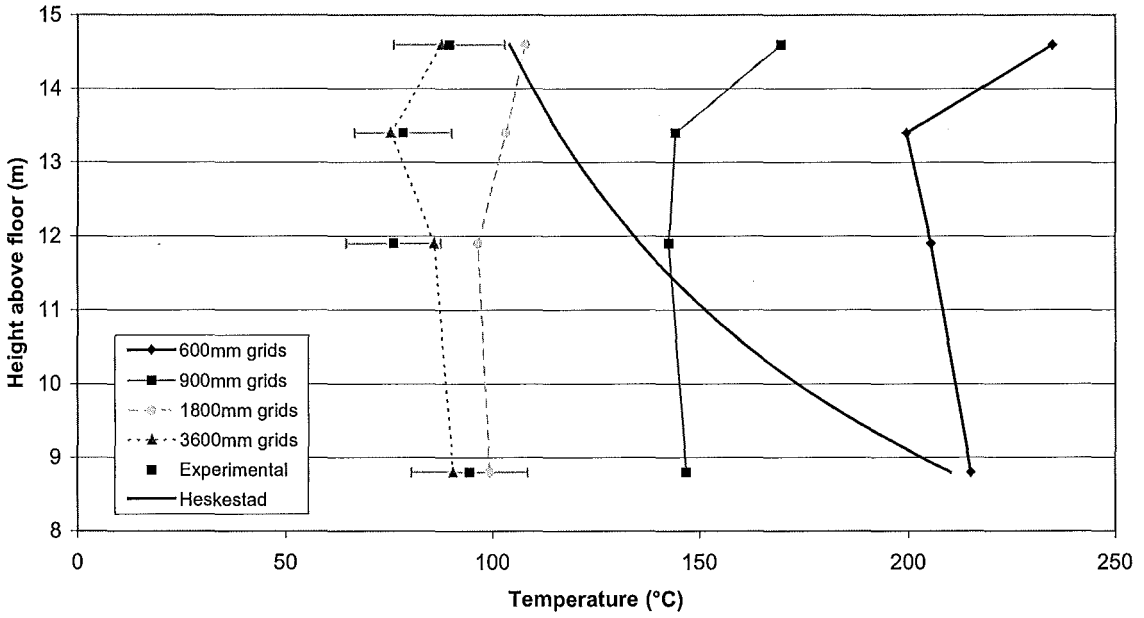

Figure 7.25: Comparisons of average temperatures at various heights in the fire plume for Test 7, entire hanger.

However, Figure 7.25 also shows that the trend produced by the Heskestad correlation is not predicted by any of the FDS models. Although the predictions at a height of 8.8 metres, as given in Table 7.4, were comparable to the Heskestad estimation, the predictions at locations near the ceiling are still grossly over predicted by the 600mm grid model. It was initially thought that the reason for this might be due to the Heskestad correlation not accounting for the increased temperature due to a hot upper layer forming. However this would also be observed in the experimental profile.

An obvious explanation for this large difference in temperatures is that the grid size is still too large to resolve adequately all the small scale eddies and turbulence phenomena that occur in the fire plume itself. These would cause added mixing with the surrounding air and therefore a reduction in temperature, especially higher up in the plume were the problem occurs. Some evidence to support this hypothesis is that at locations immediately adjacent to the plume the temperatures compare more favourably between the models and the experiment. An example of this is shown in Figure 7.26, which are the results for the thermocouple C11, located at a height of 3 metres below the ceiling (11.5 metres off the floor) and only 2.13 metres to the east of the fire centre.

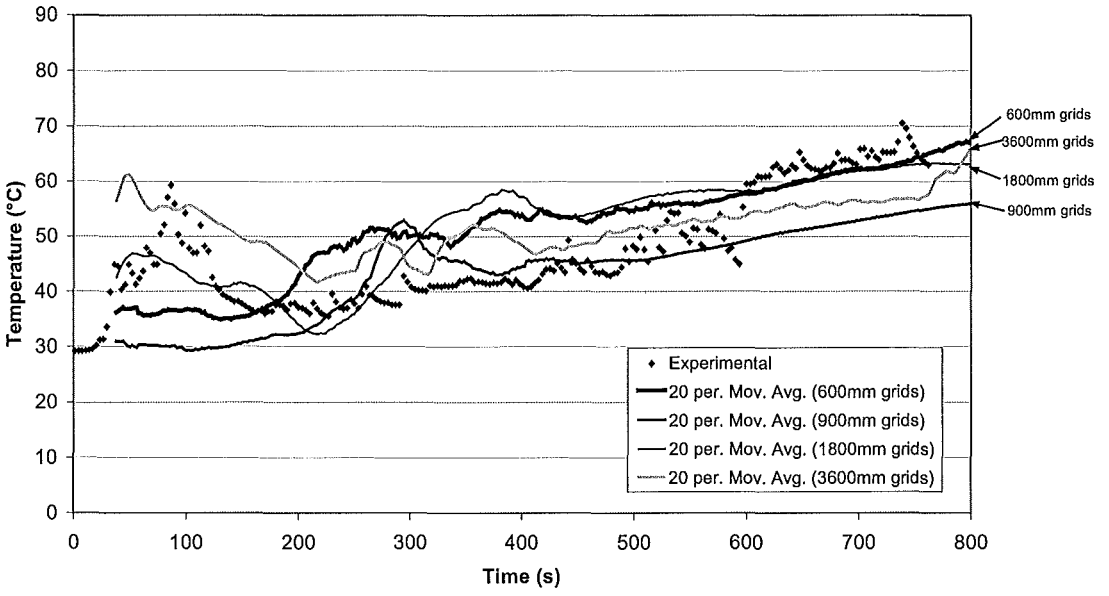

Figure 7.26: Test 7, entire hanger; predicted time-temperature profiles for thermocouple C11, 2.13 metres east of the fire, 3 metres below the ceiling.

This thermocouple can be assumed to be out of the plume because it does not have a steady state period that is characteristic of the thermocouples directly over the fire centre. It is apparent that all the models provide a much better prediction of the experimental temperature profiles in this location were there is less turbulence.

7.5.2 Stretched grid FDS model

An attempt was made to define the fire surface and plume better by stretching the grids so that the grid mesh provided a high resolution on the pool surface and in the plume but a coarse resolution further away from the fire. The plume temperatures could then be modelled accurately without compromising the model run time. This was achieved by utilising the grid transformation capabilities in FDS. A polynomial transformation was used. This provides a gradual change in grid dimensions based on a polynomial equation with user-defined constraints. The actual equations for this transformation are defined in McGrattan et al (2001) and the input file defining the constraints used is given in Appendix B.2.

The transformation can only be applied to two out of three dimensions so because the hanger is large it was difficult to stretch the grids without exceeding the recommended maximum grid aspect ratio of 1:3 (McGrattan et al, 2001). It could be done with more grid cells but this would mean too long a running time. In this case the grids in the z direction remained constant at 400mm and the other two dimensions were transformed. A plan view of the grids in the vicinity of the fire pan for this model is shown in Figure 7.27.

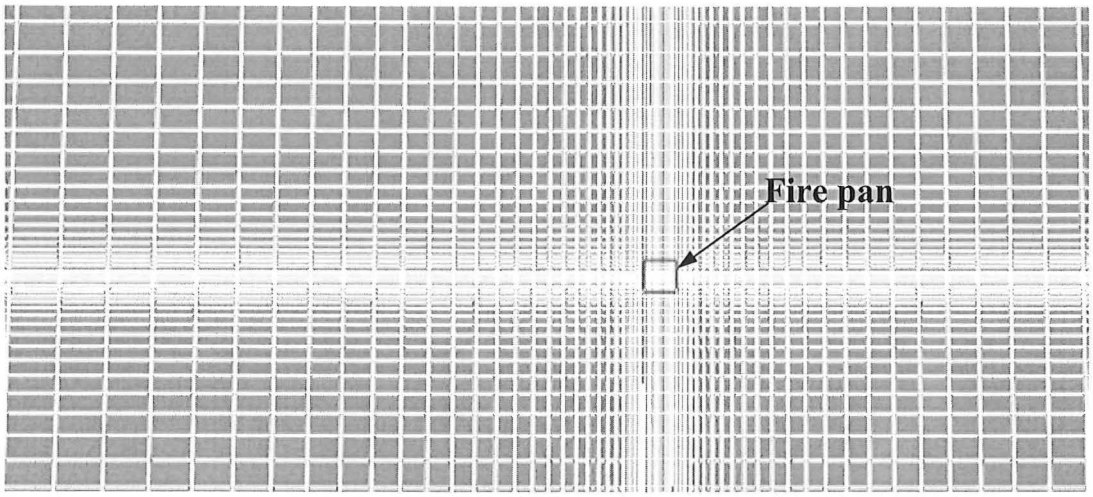

Figure 7.27: Plan view of a portion of the Hawaii hanger floor showing the fine grids over the fire and plume area.

The aspect ratio of the grids close to the fire was about 1:5 but decreased rapidly to less than 1:3. The aspect ratios of the grids far away from the fire became very large but it was considered that this was not an important area for accurate modelling and would only have a small effect on the results close to the fire.

The results from this FDS model showed that all the temperature profile comparisons of the thermocouples out of the fire plume were similar to the results obtained from the 600mm model (see Figure 7.3 to Figure 7.6); some of these comparisons are shown in Appendix C.2.

Examples of the temperature profiles observed in the fire plume itself are shown in Figure 7.28. This indicates that the temperature predictions for the stretched grid model fall close to the 1800mm model. This is for the thermocouple located directly above the fire and 6.1 metres below the ceiling. This trend is indicative of all the results of this model directly above the fire. Based on the arguments presented above this would indicate that stretching the grids to this extent produces much worse results than uniform grids of larger size (i.e. 600mm) and still does not predict the expected trend of the Heskestad correlation (Figure 7.25). This can probably be attributed to the aspect ratios of the grids being too large.

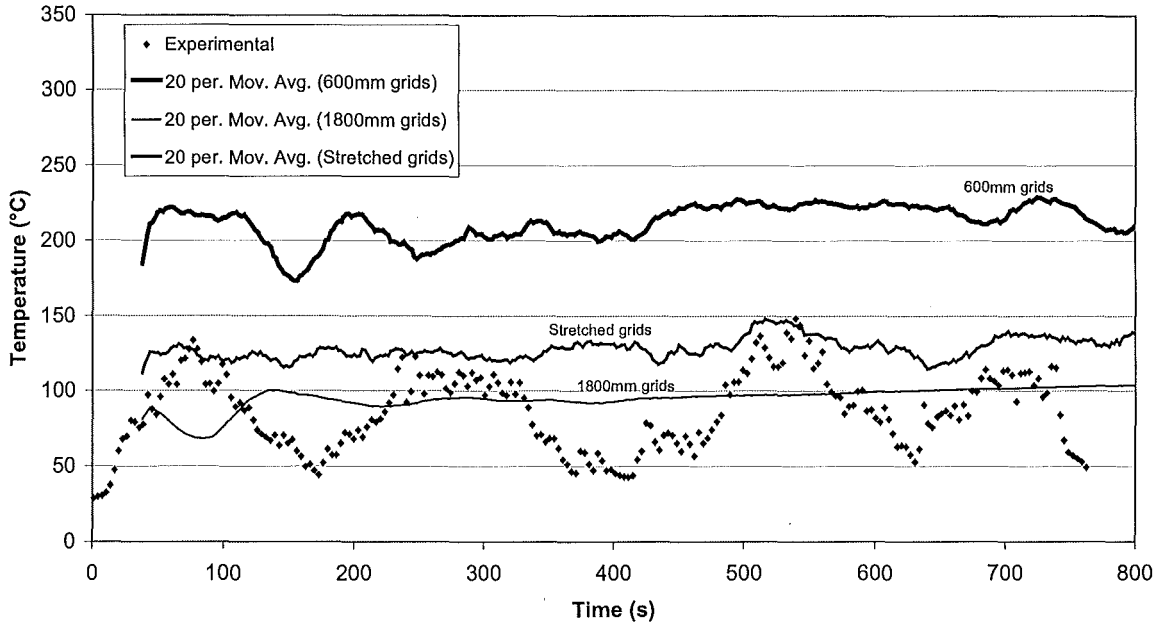

Figure 7.28: Comparison of the results from the model with stretched grids for the thermocouple at location C12 (directly above the fire 6.1 metres below the ceiling).

7.5.3 Flame heights

Another possible cause that was explored to try and explain the unexpected trends in the fire plume temperatures predicted by the FDS models was the difference in predicted flame heights. Even though this line of reasoning proved to be all but redundant it still revealed some important variables that were associated with changing grid size.

It was initially suspected that the high plume temperatures associated with the smaller grid models was due to the inadequate modelling of the fire itself. The HRRs for each model are all within 2% of experimental results (see Table 6.1) so should not produce the large discrepancies observed. The other variable that would influence the temperatures in the plume is the flame height itself.

By analysing each simulation in Smokeview a rough estimation of the flame height could be obtained by counting the number of grids in the vertical direction that the simulated flame

occupied half of the time. The flame height was also calculated by hand using Heskestad's correlation, which is reproduced here from Karlsson and Quintiere, (2001, pp 51):

$$\frac{L}{D} = 3.7\,\dot{Q}^{*2/5} - 1.02$$

Equation 7.3

Where Q* is defined by:

$$\dot{Q}^{*} = \frac{\dot{Q}}{\rho_{\infty} C_p T_{\infty} \sqrt{gD} D^2}$$

Equation 7.4

This prediction along with the FDS models and experimental flame heights are presented in Table 7.5.

Table 7.5: Flame height comparisons.

	Test 7, entire hanger	**Test 5, entire hanger**	**Test 5, draft curtain**
Experiment[1]	8.2m	8.2	8.2
Heskestad	5m	5.5m	5.5m
100mm grids (H/145)[2]	5m	-	-
300mm grids (H/48)	-	-	9.6m
450mm grids (H/32)	-	-	
600mm grids (H/25)	10.2m	9m	9m
900mm grids H/17)	9.9m	9.5m	9.5m
1800mm grids (H/8)	6.3m	5.4m	5.4
3600mm grids (H/4)	Up to ceiling	-	-

[1] Reported by Gott et al (1997), pp 62

[2] This model only simulated the area close to the fire, not the entire hanger. This is explained below in Section 7.5.4.

Table 7.5 shows a significant difference between Heskestad's correlation for flame height and the experimental flame height. Heskestad's correlation is based on data from a range of separate investigations and is valid for this fire based on the value of the dimensionless HRR (Q*), defined in Equation 7.4 (Karlsson and Quintiere, 2001). The experimental flame height however is not defined quite as well. Gott et al (1997) simply states that the heights are obtained through visual accounts and video footage. No information is given for exactly how the height was defined. Observations may have reported closer to the maximum flame height instead of a height at which the flame occurred 50% of the time. For this reason the experimental heights given in Table 7.5 are not necessarily reliable and further comparisons will only be made with Heskestad's correlation.

Table 7.5 also shows that the FDS models do not all show good approximations of flame height when compared to Heskestad's prediction. The smaller grid sized models of 300mm, 450mm, 600mm and 900mm all over predict the height by 4 or 5 metres. The 1800mm grid model however provides a much closer prediction to Heskestad's correlation (see Figure 7.29 below).

7.5.4 Mixture fraction

The mixture fraction is the variable used to define where the flame occurs in the computation domain of the FDS model and therefore dictates to a certain degree the height of the predicted flame. Its calculation and definition are defined in more detail in Section 3.2. In the simulations of the hanger test fires the only variables that were defined for the fuel were the soot and carbon monoxide release rates. By default the FDS model uses the properties of propane to define all the other variables (McGrattan et al, 2001). Because it is a fuel specific constant the flame mixture fraction of propane would have been used in the models instead of JP4 jet fuel. Values for the stoichiometric coefficients for the combustion process of JP4 fuel could not be found so the influence this modelling error had on the final results could not be quantified. However it would only produce the differences that are associated with the Heskestad and experimental flame heights and not the large variations observed amongst the FDS models.

To find out the reason why this large difference in predicted flame height occurs another model was constructed. This model used 100mm grids but only modelled the area in the vicinity of the fire. Using a much smaller mesh such as this means that the fire surface is defined by a lot more grids; 324 grids compared to 9 grids for the 600mm models. The computation domain had a base of 2.8 metres by 2.8 metres and a height of 10 metres. A thermocouple was defined at a height of 8.4 metres. This corresponds to thermocouple C12 of the experiments, which is located 6.1 metres below the hanger ceiling (refer to Figure 6.3). A HRRPUA of 1722 kW/m^2 was used which gave an output HRR of 5920kW. This is about 6% higher than the experiment. This simulation gave a flame height of about 5 metres (as indicated in Table 7.5), which is in much better agreement to Heskestad's correlation and the 1800mm grid flame height.

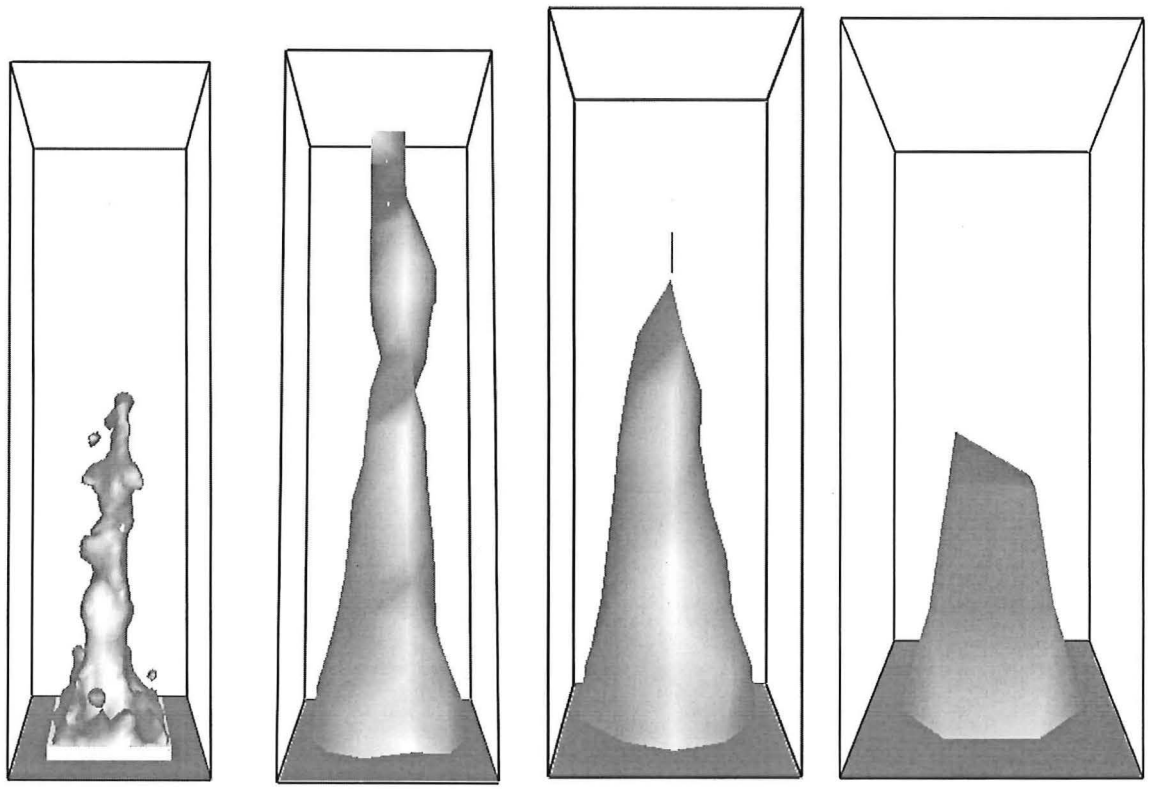

(a) 100mm grids **(b) 600mm grids** **(c.) 900mm grids** **(d) 1800mm grids**

Figure 7.29: Smokeview images of the flames as predicted by the FDS model showing the variation in height.

Additional models using 600mm, 900mm and 1800mm grids, were also constructed that only modelled the area in close vicinity to the fire. This was to provide direct comparisons with the 100mm grid model. Figure 7.29 gives an illustration of these modelled flames and clearly shows a difference in the flame height between models of different sized grids.

This suggests that the grid size is affecting the flame height considerably. The simulated flame that is observed in Smokeview is the two-dimensional sheet which is defined by a fuel specific mixture fraction at which combustion occurs. This is explained in Section 3.2. McGrattan et al (2001) recognised that the flame heights calculated by FDS when coarse grids were used can be under predicted. To remedy this problem the mixture fraction is redefined based on grid size and characteristic fire diameter. This is also explained in Section 3.2, the equation is repeated here for convenience:

$$\frac{Z_{f,eff}}{Z_f} = \min\left(1 \ , \ C\frac{D^*}{\delta x}\right) \qquad \textbf{Equation 3.9}$$

Based on the above analysis of flame height, presented in Figure 7.29 and Table 7.5, it seems that a likely explanation for the range of heights observed is due to the calculation of this mixture fraction. McGrattan et al (2001) does not specify the value of the empirical constant C that is used in Equation 3.9 so it is not known at what grid size a correction is made to the mixture fraction. The trends observed in Table 7.5 suggest that the 100mm model is adequately resolved so as not to require this adjustment while the 1800mm grid model has a correction made and the resulting flame height is reasonably comparable to the 100mm grid model. However models with intermediate grid sizes (300mm to 900mm) over correct the mixture fraction and hence over predict flame height. The 3600mm grids become too large for the correction to work properly. Table 7.5 shows that the flame in this model extends to the roof and the animation of this model in Smokeview revealed that the flame sheet extended several metres across the ceiling as well.

To test if the mixture fraction was producing these increased flame heights another two models were run. Both models used grids of 600mm and a computational domain with a base

of 3 by 3 metre and a height of 10.2 metres. The fire was defined as 1.8 by 1.8 metres and had a HRRPUA of 1722kW/m^2. The second model utilised the inbuilt command of FDS that turns the mixture fraction correction off; this command is AUTOMATIC_Z=.FALSE. (McGrattan et al, 2001).

Table 7.6: Comparison between FDS models when the mixture fraction correction is turned off and on.

	Correction off	Correction on
Flame height	0m	8.5m
Average HRR	1640kW	5250kW
Temp. at C12	117°C	119°C

Table 7.6 shows that there is a significant difference between the two models. The flame sheet for the model with no correction does not appear at all in Smokeview and its HRR is considerably lower than the corrected model. This shows that the mixture fraction is altered when 600mm grids are used and therefore must be the reason for the over estimation of flame height.

7.5.5 Unstable flame

Running these two models also revealed another anomaly in FDS. Table 7.6 also gives the average temperatures predicted for thermocouple location C12, situated 8.5 metres above the fire. Obviously the difference in these temperatures is not as great as would be expected when the large difference in the HRR is considered. The low temperature in the model with the **Correction on** is due to a very unstable flame being produced. Figure 7.30 gives snap shots of the flame at successive times over a 30 second period. This shows the extent of the lean as well as the unstable nature of the simulated flame. This behaviour is not observed when the entire hanger is modelled with 600mm grids or in any of the other models. Exactly why it occurs for this model was not resolved because it was out of the scope of this research. Interestingly the low temperature predicted by this model is much closer to the temperature measured in the experiment at the same location (see Table 7.4); the leaning flame being common to this model and the experiment.

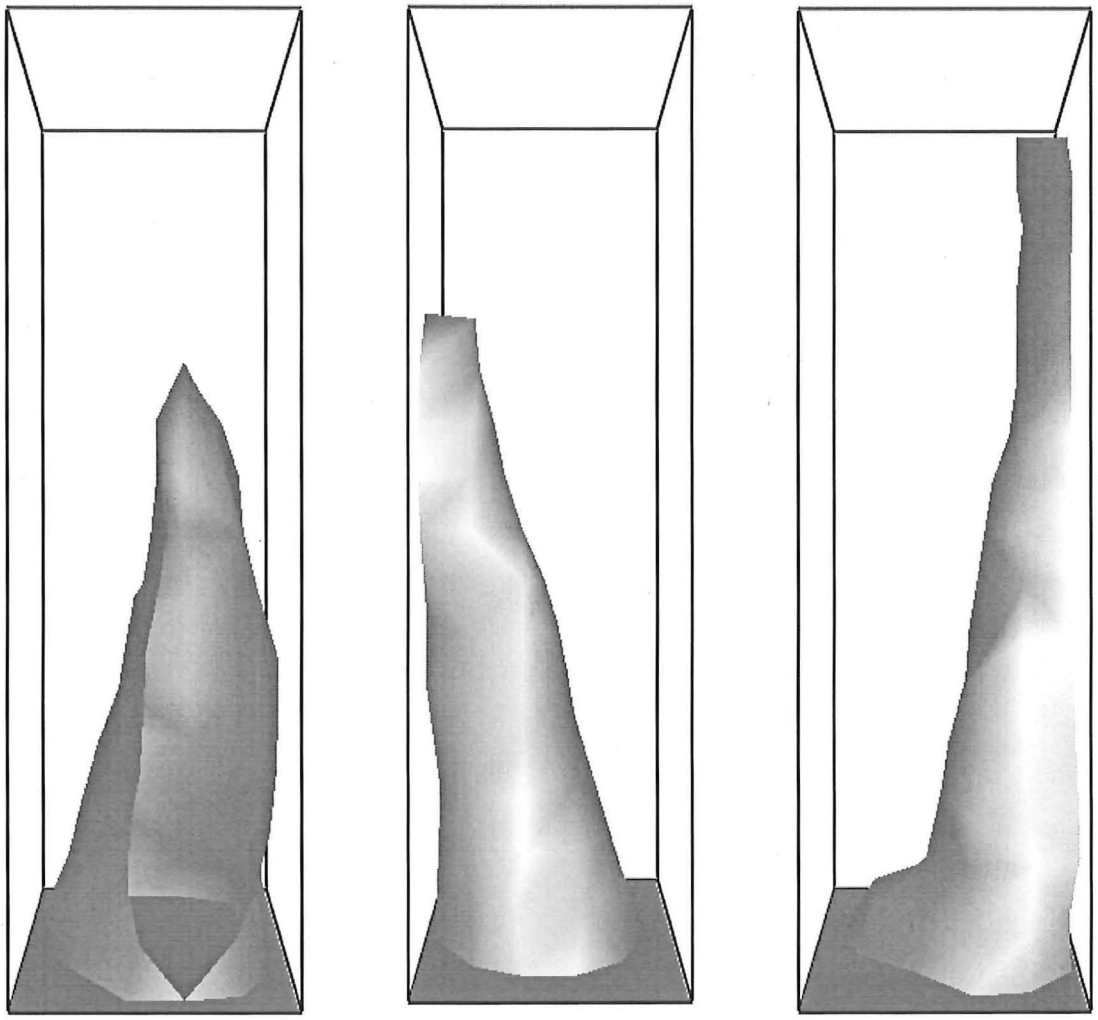

(a) 656 seconds **(b) 673 seconds** **(c.) 685 seconds**

Figure 7.30: Smokeview image of the 600mm grid model showing the extent of leaning and instability in the simulated flame over a short time span.

7.5.6 Draft curtain trends

Section 7.2 and 7.3 present results for the FDS models that simulated the hanger with the draft curtain in place. In these simulations the temperatures within the confines of the draft curtain displayed the same trends as the temperature profiles in the plume region; the models with finer grids provide the worst predictions while the 900mm and 1800mm grid models fall much closer to the experimental values. The 600mm grid model over predicts the

temperatures by about 40°C for the comparisons of **Test 5, entire hanger** (Figure 7.14), while the 300mm grid model in the comparisons of **Test 5, draft curtain** exceeds a difference of 60°C (Figure 5.23).

These are large differences and indicate that the modelling is very unreliable. There seems to be a fundamental error in the basic modelling of the area within the draft curtain. This could be due to the grid size still being too large to accurately resolve the eddies and mixing processes that occur in the draft curtain. It is worth noting that the 300mm grid model produces results that are slightly better than the 450mm grid model, especially in the initial stage of the fire. Possibly, this indicates that with smaller grids the models would begin to become progressively more accurate. However this is not practical because the model run time of the 300mm model is already about 100 hours (given in Table 7.3).

It was also initially thought that defining the draft curtain as one grid cell thick may be the cause of the problem due to poor heat transfer or fluid flow calculations. However, this cannot be the case because the same trends are observed in the comparisons of **Test 5, draft curtain**, where the curtain is modelled as the correct thickness of 3mm. Also comparisons at locations just outside the draft curtain (given in Figure 7.15 and Figure 7.16) show that even with grids of 1800mm, which means a 1800mm thick draft curtain, the accuracy of the predictions is not significantly compromised. Obviously predictions very close to the curtain would be unreliable but the simulations show that all other areas are unaffected when the curtain is defined as one grid cell thick.

The reason for such unreliable results for areas inside the draft curtain is therefore still unresolved and the problem requires ongoing analysis, which is outside the scope of this report.

Indications of the filling times of the draft curtain are compared in Table 7.1 and Table 7.2. Numerous errors are associated with these times. The thermocouples used are still 2.4 metres away from the draft curtain; this would mean an extra delay after the curtain had filled before the smoke reached them. Also the curtain is much thicker in the models, up to 1800mm instead of 3mm. This might cause a delay in the temperature rise of the thermocouples in the models because the smoke would travel slower across the base of the thick draft curtain than it would if it was added by buoyancy after it had rounded the bottom of the curtain. Also, due

to grid restrictions the depth of the curtain is less than in the experiment (see Appendix A), this would correspond to a shorter curtain filling time. However, these uncertainties do not account for the observed trends. The under predicted times in Table 7.1 and Table 7.2 may be due to the course grids over predicting the speed that the ceiling jet travels at due to having large volumes (each grid cell) of uniform velocity and temperature.

7.5.7 Other differences

The comparisons of the temperature profiles for thermocouples situated away from the fire plume are generally much better than those that are directly in the plume; all the models display this trend. It seems that the size of the grids are not as important for far field predictions in FDS as they are for the near field predictions close to the fire. The slight differences that occur in relation to the experimental results are probably due to the way in which the scenario has been modelled and not in the FDS calculation technique. This section serves to briefly outline some possible modelling limitations and uncertainties that may contribute to these differences.

The heat transfer properties of the roof were only estimated. The overestimation of the ceiling jet temperatures may be due to an underestimate in the thermal conductivity. This would correspond to less heat loss through the roof. Extra heat loss due to the windows in the concrete walls, which are not modelled in FDS, may also provide an increase in temperature of the FDS predictions compared to experimental results. Leakage out the doors on either side of the hanger as well as general building leakage may also serve to produce a slightly lower temperature in the hot upper layer. This leakage is not modelled in the FDS simulations.

Extra mixing may also occur due to the beams and trusses present in the building. These were not modelled in the FDS simulations because they were too small to define accurately. This extra mixing would have resulted in a lower temperature in the experiments compared to the FDS models.

The small discrepancies in dimensions and geometry, due to the limitations on the grid size in FDS may also have produced some differences in the temperature predictions. These model

discrepancies are defined in Appendix A. These discrepancies however are only small in relation to the hanger as a whole and would have negligible influence on the temperature calculations.

7.5.8 Zone models

As mentioned previously it was difficult to compare the zone models with the FDS models and experimental results because of the limited amount of data that was obtained. The placement of the thermocouples did not give a good indication of the floor to ceiling temperature profiles that occur in the hanger during the tests. The eventual method that was used to make the comparisons was to average the temperatures of each of the thermocouples located on the tree situated 9.1 metres east of the fire. However, the problem with this is that the lowest thermocouple on this tree is only 3 metres below the ceiling; this is equivalent to 11.6 metres above the floor. This essentially means that the temperature obtained is the average temperature of a 3 metre deep ceiling layer. When the zone model layer becomes greater than 3 metres deep, the upper layer temperatures calculated from the FDS and experimental values will be over predicted because of the cooler area below the lowest thermocouple that is not included in the average.

This is most noticeable in the comparisons of the test without a draft curtain (**Test 7, entire hanger,** see Figure 7.7). For this model the layer height predicted by the zone model reaches 11.6 metres after about 190 seconds. After this time the predicted layer height is below the lowest thermocouple used in the FDS averages. To refine the method a weighted average was used so that each thermocouple represented only the area down and up to a point half way to the next thermocouple. The area that the lower thermocouple represented was varied according to the layer height predicted by the zone model so increased with time. Figure 7.31 gives the results for this refined weighted average method for the 600mm FDS model and the experimental results. The initial average that was used in Figure 7.7 is also shown as a comparison. This method produces a vast improvement and indicates that the zone model is in fact in reasonable agreement with the experiment and better than the 600mm FDS model. The method could be refined more by only averaging the temperatures of the thermocouples that are in the upper layer as it descends. This would create better averages for times before 190 seconds when the layer is above the bottom thermocouple.

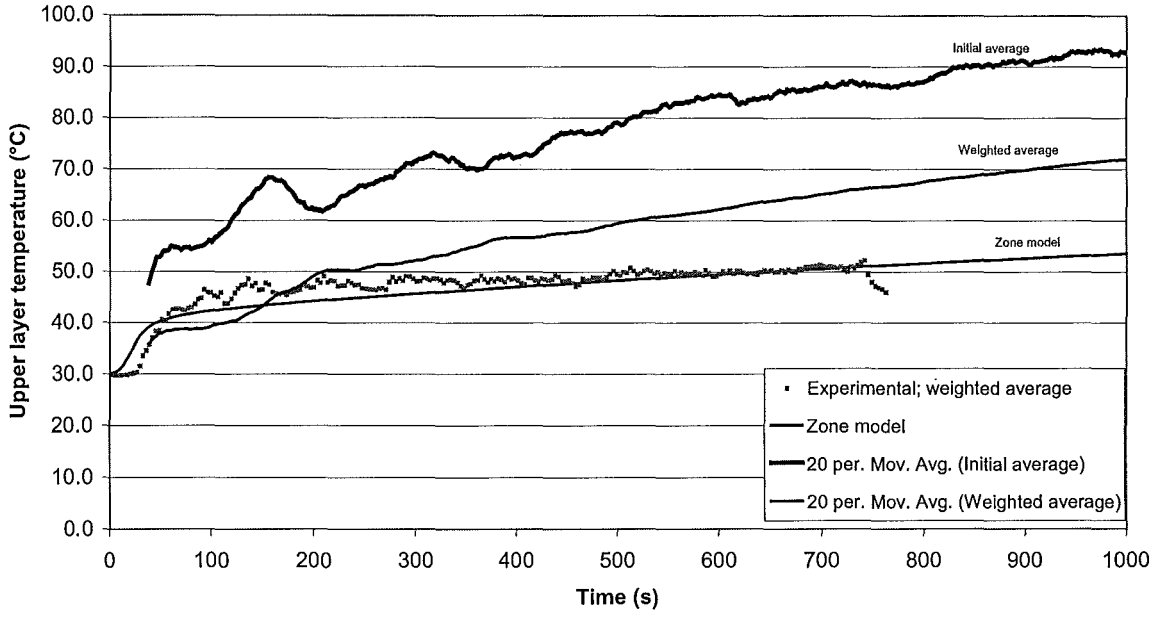

Figure 7.31: Test 7, entire hanger; upper layer temperature comparisons using a revised weighted average for the 600mm FDS model and experimental temperatures.

The problem in predicting the upper layer temperature is not as great in the two FDS constructions that incorporated a draft curtain. The temperatures inside the curtain are much more uniform and the layer height remains constant as smoke spills from the curtain to fill the rest of the hanger. The thermocouple tree used is situated within the draft curtain and the lowest thermocouple is only 0.6 metres above the base of it. This all aids in a much better prediction of the average temperature within the draft curtain meaning that a refined analysis was not required.

However all the refinements to the averages explained above assume the layer height predicted by the zone model to be correct. Another FDS model was constructed using 900mm grids with an array of thermocouples placed in the centre of each grid in the vertical direction at a distance of 9.1 metres east of the fire. This attempted to use FDS to obtain an indication of the layer height in the hanger. 900mm grids were used due to limited time.

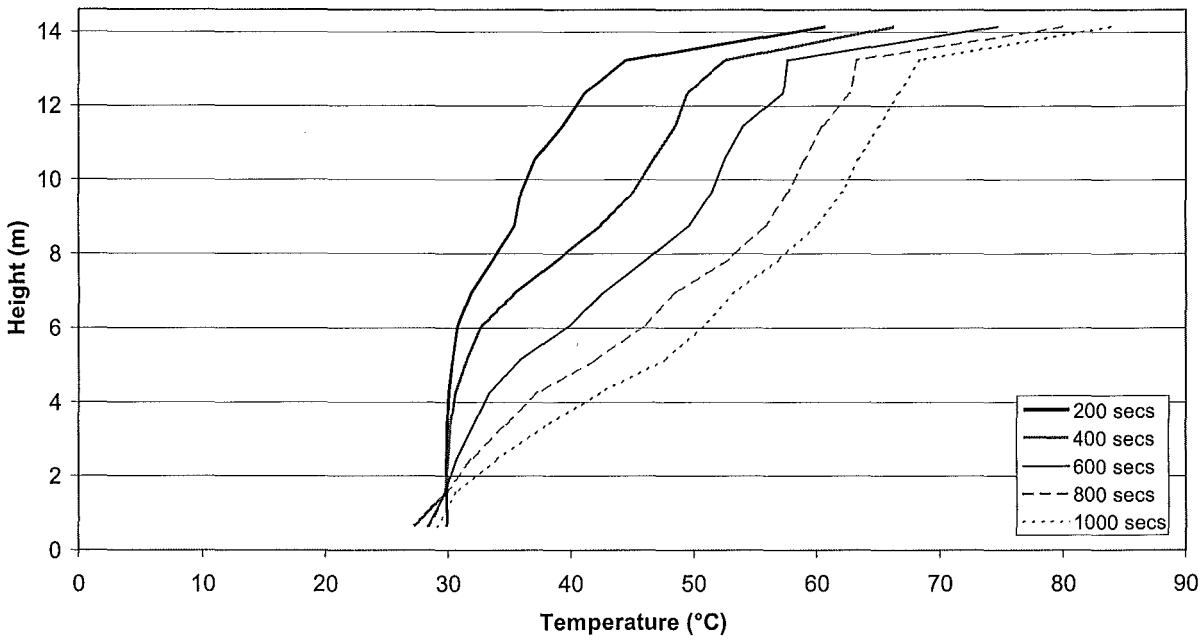

Figure 7.32: Temperature profiles in the hanger at a location 9.1 metres east of the fire using a 900mm grid.

Figure 7.32 illustrates the results from this model showing the temperature profiles at various times throughout the run. This shows there is large boundary layer between the hot upper layer and the cooler lower layer that could not be realistically compressed into a finite interface as is assumed in the zone model.

Figure 7.32 only gives temperature height profiles for the 900mm grid FDS model. Experimental results could not be compared at this range of heights because no thermocouples were located below 11.6 metres. The temperatures above this height are reasonable when compared with experimental values as was shown in Figure 7.3 to Figure 7.6. It therefore was assumed that the FDS model provides a reasonable estimation of the general profile that occurs between the floor and ceiling in the hanger.

7.5.9 Summary

The following provides a summary of the conclusions drawn from the discussions presented in Section 7.5 for the Hawaii hanger tests:

- The temperature predictions near the flame and fire plume were very unreliable for all the grid sizes used. Further away from the plume the predictions became much more accurate and are relatively independent of grid size.

- It is assumed that the experimental temperatures near the ceiling and away from the fire plume were correct, whereas those lower down in the fire plume were too low due to flame lean. This conclusion was reiterated by the Heskestad correlation for plume centreline temperatures.

- A possible cause for the temperature predictions being too high for the 600mm (H/25) models was due to the flame height being over predicted. This over prediction appeared to be due to the way in which the mixture fraction is corrected for "intermediate" grid sizes. The 1800mm (H/8) grid model had grids that were coarse enough for the correction to work and the flame height and therefore temperatures near the ceiling were predicted reasonably well.

- Heskestad's correlation compared well with the temperature predictions of the 600mm grid model at lower heights but not with the larger grid models because of the way in which the HRR was averaged over the grids in areas within the flame. This produced lower temperatures for larger grids because the volume that the HRR was averaged over was much greater.

- The FDS temperature predictions for areas within the draft curtain were unreliable. This may have been due to inadequate simulation of the turbulence in this region resulting from poor grid resolution. However the exact reason was not resolved.

- The analysis showed that the zone models, although giving good predictions of the average temperatures in the upper layer, oversimplified the temperature profiles in the hanger because of the well-defined layer interface that is assumed.

- The zone model predictions of the temperatures within the draft curtain were much more reliable because of the steady state nature that was provided by the confinement of the curtain. The predictions are also in better agreement with the experimental results than any of the FDS models.

8 Conclusions

8.1 McLeans Island test

The McLeans Island isoroom tests were simulated in FDS using 100mm (H/24), 150mm (H/16) and 300mm (H/8) grids. Models were compared against two tests, one with a 110kW fire and the other a 55kW fire. The size of the burner was 300mm by 300mm. Zone models for each test were also compared. The conclusions that were drawn from these comparisons are presented below:

- The 100 and 150mm grid models both provided temperature predictions that generally fell well within 15% of the experimental results. The 150mm grid model was deemed the better option because it only took 11.5 hours to run compared to 52 hours for the 100mm grid model, with no significant loss in accuracy.

- The 300mm grid model was significantly less accurate. In particular the upper layer temperatures in the fire room were over predicted by more than 15% and severely under predicted in the front room.

- The temperature predictions above the burner were under predicted for all the FDS models, becoming less accurate with greater grid size. This was due to inadequate grid resolution of the burner surface and the flaming region.

- The zone models compared well with the layer heights and the average upper layer temperatures that were calculated from the experimental results. However the limited information provided by the zone models was a fundamental limitation.

- The zone model gave temperature profiles that were more accurate than the 300mm grid FDS model profiles. The zone model predictions fell within +/-15% of the experimental results for most thermocouples in the fire room. The front room predictions were conservative, unlike the under predicted temperatures of the 300mm grid models.

8.2 US Navy Hanger tests

Two US Navy hanger tests were simulated in FDS using grid sizes ranging from 300mm (H/48) to 3600mm (H/4). The fire sizes of the two tests were 5580 and 6760kW and had a pool diameter of 2 metres. The second test that was compared had a draft curtain around the fire that extended 3.7 metres down from the ceiling. Zone models were also compared against the experimental results and the FDS predictions. The conclusions are presented below:

The temperatures in the fire plume predicted by the FDS models were very unreliable.

- The 600mm grid model over predicted by as much as 200°C, this difference become less for larger grids.
- A number of conflicting problems contributed to this result. The most obvious were the unreliable experimental results and too large a grid size to adequately model the flame or the turbulence in the plume.

The predicted temperatures in regions away from the fire plume were much better.

- The general trend was that the 600mm grid model provided predictions slightly greater than the experimental and decreased with greater grid size.
- The predictions close to the ceiling were more accurate than those further down from the ceiling.
- The 1800mm grid models still gave reasonable comparisons showing the same trends as the 600mm grid models.
- The 3600mm grid model began to yield unreliable results.

The FDS temperature predictions within the confines of the draft curtain were also very unreliable.

- The 600mm grid models over predicted the temperature by as much as 40°C when the entire hanger was modelled. The 300mm grid model that was used when only the draft curtain area was modelled over predicted by 60°C. This difference decreased for larger grid sizes.

- For thermocouples outside the draft curtain the predictions were extremely good for all the FDS models.
- Defining the draft curtain as one grid cell thick did not significantly influence the results except in areas very close to the curtain.
- The exact reason for unreliable predictions within the draft curtain was not resolved. The problem was considered to be similar to the problem associated with the fire plume temperature predictions. The high degree of turbulence in these areas meaning that the exact mixing processes were poorly modelled.

The zone model comparisons gave mixed results:

- The upper layer temperatures in the draft curtain were predicted with much more accuracy by the zone models than any of the FDS models.
- For the model without the draft curtain the comparisons were not as good due to an absence of a well-defined layer height in the hanger. Also, there was limited experimental data to make conclusive comparisons against.

8.3 Overall conclusions

- The grid size had a significant influence on the results. The extent to which grid size could be increased to reduce computational time depended on the size of the fire as well as the geometry and size of the enclosure.

- Finer grid resolution did not necessarily mean better accuracy in the predictions. Sometimes a larger grid size produced insignificant change to the results but was associated with a large reduction in model run time.

- Temperature predictions in the fire and plume were generally unreliable unless a very fine grid was used. Far field predictions on the other hand were very good, even with large grids in the order of half the fire diameter. This corresponded to enclosure height to grid ratios of H/16, for large enclosures this could be reduced to H/8.

- The information that the zone model provided was vastly more limited than the FDS models but in some cases the zone model provided better temperature profile predictions than the FDS models. This depended not only on the size of the grids but also on the size and extent of turbulence in the enclosure and whether there was a steady state period during the test.

8.4 Recommendations

1. A more detailed study needs to be made of the reasons why such poor predictions of experimental results are obtained near the fire.

2. Further work on larger grid sizes in other enclosures with higher ceilings and more complicated geometry would be beneficial. This would help in determining a standard grid size with which to base future design or research on and may also give a better understanding of the limitations of field models when larger grids are used.

3. The effects of high degrees of turbulence on the predictive capabilities of FDS should also be studied.

9 References

Baum, R. H. (2000) Large Eddy Simulations of Fires – From Concepts to Computations, *Fire Protection Engineering,* Spring, **6**, pp 36-42.

Bilger, R.W. (1994) Computational Field Model in Fire Research and Engineering. *Proc. Fourth International Symp. Fire Safety Science,* June. pp 95-110.

Buchanan, A.H. (Ed) (2001) *Fire Engineering Design Guide (2nd Edition)*, CAE, University of Canterbury, Christchurch.

Collier, P. (1997). Modelling of Fires in Large Spaces. *Build,* August, 38-39.

Cox, G. (1995) 'Basic Considerations'. In: *Combustion Fundamentals of Fire.* Ed. G. Cox. Academic Press, London.

Cox, G., Kumar, S. and Markatos, N.C. (1985) Some Field Model Validation Studies, *Proc. First International Symp. Fire Safety Science, November*, pp 159-171.

Davis, W.D., Notarianni, K.A. and McGrattan, K.B. (1996) *Comparison of Fire Model Predictions with Experiments conducted in a Hanger with a 15 meter Ceiling*, NISTIR 5927, National Institute of Standards and Technology, Gaithersburg, Maryland, USA.

DiNenno, P.J. (Ed) (1995) Appendices to the SFPE Handbook of Fire Protection Engineering, Society of Fire Protection Engineering and the National Fire Protection Ass., Quincy, Massachusetts, USA.

Fleischmann, C. M. (2000), *Experimental Data for Model Comparison*, Lecture Handout, Advanced Fire Dynamics, University of Canterbury.

Floyd, J.E., Baum, H.R., McGrattan, K.B. (2001) A mixture fraction combustion model for fire simulation using CFD. *The International Conference on Engineered Fire Protection Design (San Francisco)*, June 11-15. pp 279-290

Gott, E.J., Lowe, D.L., Notarianni, K.A. and Davis, W. (1997), *Analysis of High Bay Hanger Facilities for Fire Detection Sensitivity and Placement,* NIST TN 1423, National Institute of Standards and Technology, Gaithersburg, Maryland, USA.

Hinze, J.O. (1975) *Turbulence.* 2nd Edition. McGraw-Hill, New York

Incropera, F.P. and DeWitt, D.P. (1996), *Fundamentals of Heat and Mass Transfer (4th Edition),* John Wiley & Sons, New York.

Karlsson B. & Quintiere J.G. (2000), *Enclosure Fire Dynamics*, CRC Press, London.

Kanury, A.M. (1987) On the Craft of Modelling in Engineering and Science, *Fire Safety J.*, **12**, 65-74.

Kerrison, L., Galea, E.R., Hoffmann, N. and Patel, M.K. (1994) A comparison of Two Field Models with Experimental Room Fire Data. *Proc. Fourth International Symp. Fire Safety Science,* June 1994, pp 161-172.

Kerrison, L., Mawhinney, N., Galea, E.R., Hoffmann, N. and Patel, M.K. (1994) A comparison of a FLOW3D Based Fire Field Model with Experimental Room Fire Data, *Fire Safety J.*, **23**, 387-411.

Klote, J. H. (1995) 'Smoke Control'. In: *The SFPE Handbook of Fire Protection Engineering,* 2nd Edition. Society of Fire Protection Engineering and National Fire Protection Ass., Quincy, Massachusetts, USA. Sec. 4, Ch. 12 pp 237.

Kreyszig, E. (1993), *Advanced Engineering Mathematics.* 7th Edition. John Wiley and Sons Inc., New York, pp 965.

Kumar, S. Gupta, A.K. and Cox, G. (1991) Effects of Thermal Radiation on the Fluid Dynamics of Compartment Fires. *Proc. Third International Symp. Fire Safety Science, July*, pp 345-354.

Lewis, M.J., Moss, M.B. and Rubini, P.A. (1997) CFD Modelling of Combustion and Heat Transfer in Compartment Fires. *Proc. Fifth International Symp. Fire Safety Science,* March, pp 463-474.

Lovatt, A. (1998) Comparison studies of zone and CFD fire simulations. Fire Engineering Research Report, University of Canterbury.

Ma, T. and Quintiere, J. (2001) Accuracy of 3D LES model with combustion for axi-symmetric fire plume. *The International Conference on Engineered Fire Protection Design (San Francisco)*, June 11-15. pp 291-303.

Mawhinney, N., Galea, E.R., Hoffmann, N. and Patel, M.K. (1994) A critical Comparison of a Phonetics Based Fire Field Model with Experimental Compartment Fire Data, *J. of Fire Protection Eng.,* **6**, 137-152.

McGrattan, K.B., Baum, H.R., Rehm, R.G., Hamins, A., Forney, G.P., Floyd, J.E., Hostikka, S. (2001) *Fire Dynamics Simulator (Version 2) – Technical Reference Guide,* NISTIR 6783 (Draft), National Institute of Standards and Technology, Gaithersburg, Maryland, USA.

McGrattan, K.B., Forney, G.P., Floyd, J.E., Hostikka, S. (2001) *Fire Dynamics Simulator (Version 2) – User's Guide,* NISTIR 6784 (Draft), National Institute of Standards and Technology, Gaithersburg, Maryland, USA.

Nielsen, C. (2000) An Analysis of Pre-flashover Fire Experiments with Field Model Comparisons. Fire Engineering Research Report, University of Canterbury.

Notarianni, K. and Davis, W. (1993) *The use of Computer Models to Predict Temperature and Smoke movement in High Bay Spaces,* NISTIR 5304, National Institute of Standards and Technology, Gaithersburg, Maryland, USA.

Stroup, D.W. (1995) 'Using Field Modelling to Simulate Enclosure Fires'. In: *The SFPE Handbook of Fire Protection Engineering,* 2nd Edition. Society of Fire Protection Engineering and National Fire Protection Ass., Quincy, Massachusetts, USA. Ch. 3 pp 152-159.

Tewarson, A. (1995) 'Generation of Heat and Chemical Compounds in Fires'. In: *The SFPE Handbook of Fire Protection Engineering,* 2nd Edition. Society of Fire Protection Engineering and National Fire Protection Ass., Quincy, Massachusetts, USA. Sec. 3, Ch. 4 pp 78.

Quintiere, J.G. (1998) *Principles of Fire Behaviour.* Delmar Publishers, Albany.

Quintiere, J.G. (1995) 'Compartment Fire Modelling'. In: *The SFPE Handbook of Fire Protection Engineering,* 2nd Edition. Society of Fire Protection Engineering and National Fire Protection Ass., Quincy, Massachusetts, USA. Sec. 3, Ch. 5 pp 125-133.

www1:
www.rooves.com

Models used:

Fire Dynamics Simulator (FDS), Version 2, 2001, National Institute of Standards and Technology, Gaithersburg, Maryland, USA.

Smokeview, Version 2.0, 2001, National Institute of Standards and Technology, Gaithersburg, Maryland, USA

CFAST, Version 3.1.6, 1999, National Institute of Standards and Technology, USA.

Appendix A: Differences between the FDS models and the experiments

This Appendix provides the dimensions and sizes of the obstructions and computational domains of all the FDS models that were used in this report. The experimental sizes are also given so comparisons can be made.

Table A 1: Discrepancies in the FDS model when modelling the McLeans isorooms.

	Experimental	100mm grids	150mm grids	300mm grids
Fire centre - x	1.8 m	1.85 m	1.8 m	1.65 m
- y	1.2 m	1.25 m	1.2 m	1.05 m
Wall thickness	0.2 m	0.2 m	0.15 m	0.3 m
Door width	0.8 m	0.8 m	0.9 m	0.6 m
Door height	2 m	2 m	1.95 m	2.1 m
Burner height	0.3 m	0.3 m	0.3 m	0.3 m
Burner depth	0.2 m	0.2 m	0.2 m	0.3 m

Table A 2: Discrepancies in the FDS model when modelling the entire hanger

	Exp.	600mm grids	900mm grids	1800mm grids	3600mm grids
Dimensions – Length	97.8 m	97.8 m	98.1 m	99 m	99 m
- Width	73.8 m	73.8 m	73.8 m	73.8 m	72 m
Roof height – Apex	14.9 m	15 m	15.3 m	14.4 m	14.4 m
- lower ends	13.4 m	13.2 m	13.5 m	12.6 m	14.4 m
Fire centre[1]	61.1 m	60.9 m	61.2 m	60.3 m	62.1 m
	33.9 m	33.9 m	34.2 m	33.3 m	33.3 m
Roof height above fire	14.5 m	14.4 m	14.4 m	14.4 m	14.4 m
Pool surface height	0.4 m	0.6 m	0 m	0 m	0 m
Draft curtain – Length	24.4 m	24.6 m	24.3 m	25.2 m	-
- Width	18.3 m	18.6 m	18 m	18 m	-
- Depth	3.7 m	3.6 m	3.6 m	3.6 m	-
- Thickness[2]	0.003 m	0.6 m	0.9 m	1.8 m	-
Ventilation	General leakage	0.6 x 0.6 m	0.9 x 0.9 m	1.8 x 1.8 m	3.6 x 3.6 m

[1] The fire centres given here are not the FDS input fire centres because in the input files the west wall (which is modelled as an obstruction one grid thick) is accounted for.

[2] The draft curtain thickness is assumed and is assigned to the surface properties in FDS but the physical thickness has to be at least one grid cell.

Table A 3: Discrepancies in the FDS model when modelling the draft curtain only.

	Exp.	300mm grids	450mm grids	600mm grids	900mm grids	1800mm grids
Length	24.4 m	24.6 m	24.3 m	24.6 m	24.3 m	25.2 m
Width	18.3 m	18.3 m	18.45 m	18 m	18 m	18 m
Height	14.5 m[1]	14.4 m	14.4 m	14.4 m	14.4 m	14.4 m
Curtain depth	3.7 m	3.6 m	3.6 m	3.6 m	3.6 m	3.6 m
Pool surface height	0.3 m	0.3 m	0.45 m	0.6 m	0 m	0 m

[1] This is the average ceiling height within the area of the draft curtain.

Appendix B: Model input data files

Appendix B provides the FDS and CFAST input files that were used in this research. Many of the FDS files used were very similar, so to avoid repetition the file describing the model with the smallest grids is given in its complete form, while for subsequent input files, only the parts that are considerably different are provided.

B.1 McLeans Island input files.

FDS models.

100mm grids:

```
&HEAD CHID='Iso(100mmgrids)', TITLE='McLeans Is. Isorooms, 100mm grids' /
```

Defining the file title and file name

```
&GRID IBAR=74, JBAR=24, KBAR=24 /
```

Defining the number of grids

```
&PDIM XBAR=7.4, YBAR=2.4, ZBAR=2.4 /
```

Defining the size of the computational domain

```
&TIME TWFIN=3600 /
```

Simulated fire time

```
&MISC SURF_DEFAULT='FIBREGLASS'/
```

Setting the default surface

```
&SURF ID ='BURNER',  HRRPUA =1375./
```

Defining the HRRPUA

```
&SURF ID  ='FIBREGLASS'
    FYI ='Thermally-thick material'
    KS    = 0.036
    ALPHA  = 8.6E-8
    DELTA  = 0.025 /
```

Surface properties of the fibreglass lining

```
&VENT XB=1.65,1.95,1.05,1.35,0.3,0.3,SURF_ID='BURNER'/
```
Defining and naming a vent for the fire

```
&VENT CB='XBAR',SURF_ID='OPEN'/
```
Wall opening

```
&OBST XB=1.65,1.95,1.05,1.35,0.1,0.3 /
```
Burner

```
&OBST XB=3.6,3.8,0,0.8,0,2.4 /
```
Doorside#1

```
&OBST XB=3.6,3.8,1.6,2.4,0,2.4 /
```
Doorside#2

```
&OBST XB=3.6,3.8,0.8,1.6,2.0,2.4 /
```
Doortop

```
&SLCF PBY=1.2, QUANTITY='TEMPERATURE'/
&SLCF PBX=0.1, QUANTITY='TEMPERATURE'/
&SLCF PBX=1.8, QUANTITY='TEMPERATURE'/
&SLCF PBX=3.7, QUANTITY='TEMPERATURE'/
&SLCF PBX=5.5, QUANTITY='TEMPERATURE'/
&SLCF PBX=3.7, QUANTITY='VELOCITY'/
&SLCF PBY=1.2, QUANTITY='VELOCITY'/
&SLCF PBY=1.2, QUANTITY='oxygen'/
```
Prescribing slices files for various variables

```
&THCP XYZ=0.15,1.2,0,QUANTITY='TEMPERATURE', LABEL='T1 Floor'/
&THCP XYZ=0.15,1.2,0.3,QUANTITY='TEMPERATURE', LABEL='T1 0.3m' /
&THCP XYZ=0.15,1.2,0.6,QUANTITY='TEMPERATURE', LABEL='T1 0.6m' /
&THCP XYZ=0.15,1.2,0.9,QUANTITY='TEMPERATURE', LABEL='T1 0.15m' /
&THCP XYZ=0.15,1.2,1.1,QUANTITY='TEMPERATURE', LABEL='T1 1.1m' /
&THCP XYZ=0.15,1.2,1.35,QUANTITY='TEMPERATURE', LABEL='T1 1.35m' /
&THCP XYZ=0.15,1.2,1.6,QUANTITY='TEMPERATURE', LABEL='T1 1.6m'/
&THCP XYZ=0.15,1.2,1.85,QUANTITY='TEMPERATURE', LABEL='T1 1.85m' /
&THCP XYZ=0.15,1.2,2.1,QUANTITY='TEMPERATURE', LABEL='T1 2.1m' /
&THCP XYZ=0.15,1.2,2.15,QUANTITY='TEMPERATURE', LABEL='T1 2.2m' /
&THCP XYZ=0.15,1.2,2.2,QUANTITY='TEMPERATURE', LABEL='T1 2.25m'/
&THCP XYZ=0.15,1.2,2.25,QUANTITY='TEMPERATURE', LABEL='T1 2.3m' /
&THCP XYZ=0.15,1.2,2.3,QUANTITY='TEMPERATURE', LABEL='T1 2.35m' /
```

&THCP XYZ=0.15,1.2,2.35,QUANTITY='TEMPERATURE', LABEL='T1 2.375m'/
&THCP XYZ=0.15,1.2,2.375,QUANTITY='TEMPERATURE', LABEL='T1 0.3m' /
&THCP XYZ=0.15,1.2,2.4,QUANTITY='TEMPERATURE', LABEL='T1 ROOF'/

The above commands define the thermocouples on Tree 1, which is located 0.15 metres from the back of the fire room. &THCP calls were repeated and the thermocouples and oxygen probes on all the trees in the isorooms were prescribed in the same way as above. An example of how the Oxygen probe were prescribed follows:

&THCP XYZ=0.9,1.2,0.3,QUANTITY='oxygen', LABEL='O2 T2 0.3'/

The FDS input files for larger grid sizes were identical to the one given above except the &GRID line was changed to obtain the required grid size. These changes are given below. The &PDIM line was also adjusted slightly to account for the change in wall thickness due to the change in cell size.

150mm grids:

&GRID IBAR=50,JBAR=16,KBAR=16 /
&PDIM XBAR=7.5,YBAR=2.4, ZBAR=2.4 /

300mm grids:

&GRID IBAR=25,JBAR=8,KBAR=8 /
&PDIM XBAR=7.5,YBAR=2.4,ZBAR=2.4 /

150mm grids with surface probes defined.

This input file was essentially the same as the initial 150mm grid model except for the following changes to the &GRID and &PDIM lines:

&GRID IBAR=50,JBAR=16,KBAR=18 /
&PDIM XBAR=7.5,YBAR=2.4,ZBAR0=-0.15,ZBAR=2.55 /

Where probes need to be defined to record surface temperatures the following commands were used:

```
&THCP XYZ=0.15,1.2,0,QUANTITY='WALL_TEMPERATURE', IOR=3 ,LABEL='T1
                Floor'/
```

The IOR subcommand in the line above designates the orientation of the probe, in this case the 3 represents in the z direction or upwards.

CFAST input file for the McLeans Island isorooms

```
#VERSN 3 Two Compartment Base Case
TIMES  3610    0    10    20    0
ADUMP C:/TEMP/ZONE110.CSV NS
TAMB  293       101300. 0.000000
EAMB  293       101300. 0.000000
HI/F  0.000000 0.000000
WIDTH  2.40000  2.40000
DEPTH  3.60000  3.60000
HEIGH  2.40000  2.40000
CEILI ISOLINE  ISOLINE[1]
WALLS ISOLINE  ISOLINE
FLOOR ISOLINE  ISOLINE
#CEILI ISOLINE  ISOLINE
#WALLS ISOLINE  ISOLINE
#FLOOR ISOLINE  ISOLINE
HVENT  1  2  1 0.800000  2.00000 0.000000 0.000000 0.000000 0.000000
CVENT  1  2  1     1.00000     1.00000     1.00000     1.00000     1.00000     1.00000
       1.00000     1.00000     1.00000     1.00000     1.00000     1.00000     1.00000
       1.00000     1.00000     1.00000     1.00000     1.00000     1.00000     1.00000
```

[1] ISOLINE was the name given to the material used in the isoroom experiments. The prperties were defined in CFAST, these properties can be found in **Error! Reference source not found.**.

HVENT 2 3 1 2.40000 2.40000 0.000000 0.000000 0.000000 0.000000

CVENT 2 3 1 1.00000 1.00000 1.00000 1.00000 1.00000 1.00000
1.00000 1.00000 1.00000 1.00000 1.00000 1.00000 1.00000
1.00000 1.00000 1.00000 1.00000 1.00000 1.00000 1.00000

CHEMI 16.0000 50.0000 10.0000 4.60000E+007 293.150 493.150 0.300000

LFBO 1

LFBT 2

CJET ALL

FPOS -1.00000 -1.00000 0.300000

FTIME 1.00000 2.00000 3.00000 4.00000 5.00000 6.00000
7.00000 8.00000 10.0000 3600.00 3601.00 3602.00 3603.00
3604.00 3605.00 3606.00 3607.00 3608.00 3610.00

FMASS 0.000000 4.07826E-006 1.63130E-005 3.67043E-005 6.52522E-005
0.000101957 0.000146817 0.000199835 0.000261009 0.00239130 0.00239130
0.000330339 0.000261009 0.000199835 0.000146817 0.000101957 6.52522E-
005 3.67043E-005 1.63130E-005 0.000000

FQDOT 0.000000 187.600 750.400 1688.40 3001.60 4690.00
6753.60 9192.40 12006.4 110000. 110000. 15195.6 12006.4
9192.40 6753.60 4690.00 3001.60 1688.40 750.400 0.000000

HCR 0.0800000 0.0800000 0.0800000 0.0800000 0.0800000 0.0800000
0.0800000 0.0800000 0.0800000 0.0800000 0.0800000 0.0800000
0.0800000 0.0800000 0.0800000 0.0800000 0.0800000 0.0800000
0.0800000 0.0800000

OD 0.0300000 0.0300000 0.0300000 0.0300000 0.0300000 0.0300000
0.0300000 0.0300000 0.0300000 0.0300000 0.0300000 0.0300000
0.0300000 0.0300000 0.0300000 0.0300000 0.0300000 0.0300000
0.0300000 0.0300000

CO 0.0300000 0.0300000 0.0300000 0.0300000 0.0300000 0.0300000
0.0300000 0.0300000 0.0300000 0.0300000 0.0300000 0.0300000
0.0300000 0.0300000 0.0300000 0.0300000 0.0300000 0.0300000
0.0300000 0.0300000

SELECT 1 2 0

#GRAPHICS ON

DEVICE 1

```
WINDOW   0.   0. -100. 1280. 1024. 1100.
LABEL  1  970.  960.   0. 1231. 1005.  10. 15 00:00:00 0.00  0.00
GRAPH  1  100.  50.   0.  600.  475.  10. 3 TIME HEIGHT
GRAPH  2  100.  550.   0.  600.  940.  10. 3 TIME CELSIUS
GRAPH  3  720.  50.   0. 1250.  475.  10. 3 TIME FIRE_SIZE(kW)
GRAPH  4  720.  550.   0. 1250.  940.  10. 3 TIME O|D2|O()
HEAT  0 0 0 0 3  1 U
HEAT  0 0 0 0 3  2 U
TEMPE 0 0 0 0 2  1 U
TEMPE 0 0 0 0 2  2 U
INTER 0 0 0 0 1  1 U
INTER 0 0 0 0 1  2 U
O2    0 0 0 0 4  1 U
O2    0 0 0 0 4  2 U
```

The only difference in 55kW test input files was the HRR value. The FDS models had a different HRRPUA while the CFAST model had a slightly different FQDOT input line.

B.2 Hawaii Hanger tests

Test 7, entire hanger

FDS models.

600mm grids:

```
&HEAD CHID='15m(600mm)', TITLE='Test fire 7, entire hanger, 600mm grids'/
```
Defining the file title and file name

```
&GRID IBAR=165, JBAR=123, KBAR=29 /
```
Defining the number of grids along each dimension

```
&PDIM XBAR=99.2, YBAR=74, ZBAR=17.6 /
```
Defining the size of the computational domain

```
&TIME TWFIN=1000 /
```
Length of simulation

```
&MISC GVEC=0.3008,0.0,-9.8054
```
Defining the gravity vector

```
    TMPA = 30
```
Ambient temperature

```
    NFRAMES=500
```
Number of datum recorded

```
    SURF_DEFAULT='STEEL'/
```
Setting default surface

```
&REAC ID='JP5 Fuel'
    SOOT_YIELD=0.042
    CO_YIELD=0.012
```
Defining the soot and CO release of the burning fuel

```
&SURF ID='POOLFIRE', HRRPUA=1630./
```
Characterising the fire

```
&SURF ID='ROOF'
    FYI='Tar/gravel over corrugated deck'
    ALPHA = 3.6E-7
    KS = 0.7
    DELTA = 0.01 /
&SURF ID='CONCRETE'
```

```
    FYI='Thermally-thick material'
    ALPHA = 5.7E-7
    KS    = 1.0
    DELTA = 0.3 /
&SURF ID='STEEL'
    FYI='Thermally-thin material'
    C_DELTA_RHO= 5.1
    DELTA = 0.0015 /
```

Defining the properties of the surfaces

```
&VENT XB=60.7,62.5,33.1,34.9,3,3, SURF_ID='POOLFIRE'/
```

Defining and naming a vent for the fire

```
&OBST XB=60.7,62.5,33.1,34.9,2.4,3 /
```

Defining the fire pan as an obstruction

```
&VENT XB=0.6,1.2,0,0,0.6,1.2, SURF_ID='OPEN' /
```

Prescribing a vent to ambient for ventilation

```
&OBST XB=82.2,98.6,0,74,3,3.6, SAWTOOTH=.FALSE., SURF_ID='INERT' /
&OBST XB=65.9,82.2,0,74,2.4,3, SAWTOOTH=.FALSE., SURF_ID='INERT' /
&OBST XB=49.6,65.9,0,74,1.8,2.4, SAWTOOTH=.FALSE., SURF_ID='INERT' /
&OBST XB=33.3,49.6,0,74,1.2,1.8, SAWTOOTH=.FALSE., SURF_ID='INERT' /
&OBST XB=17,33.3,0,74,0.6,1.2, SAWTOOTH=.FALSE., SURF_ID='INERT' /
&OBST XB=0.6,17,0,74,0,0.6, SAWTOOTH=.FALSE., SURF_ID='INERT' /
```

Defining the floor

```
&OBST XB=43.8,99.2,0,74,17,17.6, SAWTOOTH=.FALSE. , SURF_ID='ROOF'/
```

West side of roof

```
&OBST XB=35.2,43.8,0,74,16.4,17, SAWTOOTH=.FALSE., SURF_ID='ROOF'/
&OBST XB=26.5,35.2,0,74,15.8,16.4, SAWTOOTH=.FALSE., SURF_ID='ROOF' /
&OBST XB=17.9,26.5,0,74,15.2,15.8, SAWTOOTH=.FALSE., SURF_ID='ROOF'/
&OBST XB=9.2,17.9,0,74,14.6,15.2, SAWTOOTH=.FALSE., SURF_ID='ROOF'/
&OBST XB=0.6,9.2,0,74,14,14.6, SAWTOOTH=.FALSE., SURF_ID='ROOF'/
```

East side of roof

```
&OBST XB=0,0.6,0,74,0,14.6,SURF_ID='CONCRETE' /
&OBST XB=98.6,99.2,0,74,3,17.6,SURF_ID='CONCRETE' /
```

East & West walls

```
&SLCF PBX=61.6, QUANTITY='TEMPERATURE'/
&SLCF PBY=34, QUANTITY='TEMPERATURE'/
&SLCF PBX=61.6, QUANTITY='VELOCITY'/
&SLCF PBY=34, QUANTITY='VELOCITY'/
&SLCF PBX=61.6, QUANTITY='oxygen'/
```

Prescribing slices files for various variables

```
&THCP XYZ=61.2,33.99,16.7, QUANTITY='TEMPERATURE',LABEL='C1' /
&THCP XYZ=59.7,33.99,16.7, QUANTITY='TEMPERATURE',LABEL='E16' /
&THCP XYZ=62.7,33.99,16.7, QUANTITY='TEMPERATURE',LABEL='W11' /
&THCP XYZ=61.2,32.5,16.7, QUANTITY='TEMPERATURE',LABEL='S10' /
&THCP XYZ=61.2,35.5,16.7, QUANTITY='TEMPERATURE',LABEL='N11' /
```

TCs 0.31m below ceiling, 1.5m radially

```
&THCP XYZ=61.24,33.99,15.59, QUANTITY='TEMPERATURE',LABEL='C2' /
```

TC above fire, 1.5m below

```
&THCP XYZ=61.28,33.99,14, QUANTITY='TEMPERATURE',LABEL='C3'
&THCP XYZ=62.19,33.99,14.02, QUANTITY='TEMPERATURE',LABEL='C6' /
&THCP XYZ=63.68,33.99,14.07, QUANTITY='TEMPERATURE',LABEL='C7' /
&THCP XYZ=60.37,33.99,13.97, QUANTITY='TEMPERATURE',LABEL='C10'/
&THCP XYZ=58.89,33.99,13.92, QUANTITY='TEMPERATURE',LABEL='C11'/
&THCP XYZ=61.28,34.9,14, QUANTITY='TEMPERATURE',LABEL='C8' /
&THCP XYZ=61.28,36.1,14, QUANTITY='TEMPERATURE',LABEL='C9'/
&THCP XYZ=61.28,33.08,14, QUANTITY='TEMPERATURE',LABEL='C4'/
&THCP XYZ=61.28,31.89,14, QUANTITY='TEMPERATURE',LABEL='C5'//
```

TC's above the fire, 3m below

```
&THCP XYZ=61.38,33.99,10.9, QUANTITY='TEMPERATURE',LABEL='C12' /
```

TC above fire, 6.1m below ceiling

&THCP XYZ=58.2,33.99,16.7, QUANTITY='TEMPERATURE',LABEL='E15' /
&THCP XYZ=55.1,33.99,16.84, QUANTITY='TEMPERATURE',LABEL='E10' /
&THCP XYZ=52.1,33.99,16.84, QUANTITY='TEMPERATURE',LABEL='E4' /
&THCP XYZ=49.6,33.99,16.7, QUANTITY='TEMPERATURE',LABEL='E3' /
&THCP XYZ=46.6,33.99,16.6, QUANTITY='TEMPERATURE',LABEL='E2' /
&THCP XYZ=43.5,33.99,16.4, QUANTITY='TEMPERATURE',LABEL='E1' /

TC's 0.31m below ceiling, East

&THCP XYZ=64.2,33.99,16.7, QUANTITY='TEMPERATURE',LABEL='W10' /
&THCP XYZ=67.29,33.99,16.84, QUANTITY='TEMPERATURE',LABEL='W5' /
&THCP XYZ=70.3,33.99,16.7, QUANTITY='TEMPERATURE',LABEL='W4' /
&THCP XYZ=72.8,33.99,16.7, QUANTITY='TEMPERATURE',LABEL='W3' /
&THCP XYZ=75.8,33.99,16.7, QUANTITY='TEMPERATURE',LABEL='W2' /
&THCP XYZ=78.9,33.99,16.7, QUANTITY='TEMPERATURE',LABEL='W1' /

TCs in the west direction

&THCP XYZ=61.2,36.99,16.7, QUANTITY='TEMPERATURE',LABEL='S9' /
&THCP XYZ=61.2,40.09,16.84, QUANTITY='TEMPERATURE',LABEL='S4' /
&THCP XYZ=61.2,42.49,16.7, QUANTITY='TEMPERATURE',LABEL='S3' /
&THCP XYZ=61.2,45.59,16.7, QUANTITY='TEMPERATURE',LABEL='S2' /
&THCP XYZ=61.2,48.59,16.7, QUANTITY='TEMPERATURE',LABEL='S1' /

TCs in the south direction

&THCP XYZ=61.2,30.99,16.7, QUANTITY='TEMPERATURE',LABEL='N10'/
&THCP XYZ=61.2,27.85,16.84, QUANTITY='TEMPERATURE',LABEL='N5' /
&THCP XYZ=61.2,25.49,16.84, QUANTITY='TEMPERATURE',LABEL='N2' /
&THCP XYZ=61.2,22.39,16.7, QUANTITY='TEMPERATURE',LABEL='N1'/

TCs in the north direction

&THCP XYZ=55.1,33.99,16.7, QUANTITY='TEMPERATURE',LABEL='E11' /
&THCP XYZ=55.1,33.99,16.53, QUANTITY='TEMPERATURE',LABEL='E12' /
&THCP XYZ=55.11,33.99,16.38, QUANTITY='TEMPERATURE',LABEL='E13' /
&THCP XYZ=55.11,33.99,16.23, QUANTITY='TEMPERATURE',LABEL='E14' /

Vertical TC's at 6.1m radial, east

&THCP XYZ=67.3,33.99,16.7, QUANTITY='TEMPERATURE',LABEL='W6' /
&THCP XYZ=67.3,33.99,16.53, QUANTITY='TEMPERATURE',LABEL='W7' /
&THCP XYZ=67.31,33.99,16.38, QUANTITY='TEMPERATURE',LABEL='W8' /
&THCP XYZ=67.31,33.99,16.23, QUANTITY='TEMPERATURE',LABEL='W9' /

Vertical TC's at 6.1m radial, east

&THCP XYZ=61.2,40.09,16.7, QUANTITY='TEMPERATURE',LABEL='S5' /
&THCP XYZ=61.2,40.09,16.53, QUANTITY='TEMPERATURE',LABEL='S6' /
&THCP XYZ=61.2,40.09,16.38, QUANTITY='TEMPERATURE',LABEL='S7' /
&THCP XYZ=61.2,40.09,16.23, QUANTITY='TEMPERATURE',LABEL='S8' /

Vertical TC's at 6.1m radial, south

&THCP XYZ=61.2,27.89,16.7, QUANTITY='TEMPERATURE',LABEL='N6' /
&THCP XYZ=61.2,27.89,16.53, QUANTITY='TEMPERATURE',LABEL='N7' /
&THCP XYZ=61.2,27.89,16.38, QUANTITY='TEMPERATURE',LABEL='N8' /
&THCP XYZ=61.2,27.89,16.23, QUANTITY='TEMPERATURE',LABEL='N9' /

Vertical TC's at 6.1m radial, north

&THCP XYZ=52.1,33.99,16.7, QUANTITY='TEMPERATURE',LABEL='E5' /
&THCP XYZ=52.1,33.99,16.53, QUANTITY='TEMPERATURE',LABEL='E6' /
&THCP XYZ=52.11,33.99,16.23, QUANTITY='TEMPERATURE',LABEL='E7' /
&THCP XYZ=52.13,33.99,15.77, QUANTITY='TEMPERATURE',LABEL='E8' /
&THCP XYZ=52.18,33.99,14, QUANTITY='TEMPERATURE',LABEL='E9' /

Vertical TC's at 9.1m radial, East

&THCP XYZ=61.23,25.49,15.77, QUANTITY='TEMPERATURE',LABEL='N3' /
&THCP XYZ=61.28,25.49,14, QUANTITY='TEMPERATURE',LABEL='N4' /

Vertical TC's at 8.5m radial, North

900mm grids

&HEAD CHID='15m(900mm)',TITLE=' Test fire 7, entire hanger, 900mm grid' /
&GRID IBAR=111, JBAR=82, KBAR=20 /
&PDIM XBAR=99.9, YBAR=74, ZBAR=18 /

&SURF ID='POOLFIRE', HRRPUA=1234./

&VENT XB=61.2,63,33.3,35.1,2.7,2.7, SURF_ID='POOLFIRE'/

&VENT XB=0.9,1.8,0,0,0.9,1.8, SURF_ID='OPEN' /

&OBST XB=74.5,99,0,74,2.7,3.6, SAWTOOTH=.FALSE., SURF_ID='INERT' /
&OBST XB=50,74.5,0,74,1.8,2.7, SAWTOOTH=.FALSE., SURF_ID='INERT' /
&OBST XB=25.4,50,0,74,0.9,1.8, SAWTOOTH=.FALSE., SURF_ID='INERT' /
&OBST XB=0.9,25.4,0,74,0,0.9, SAWTOOTH=.FALSE., SURF_ID='INERT' /

Floor

&OBST XB=42.5,99,0,74,17.1,18, SAWTOOTH=.FALSE., SURF_ID='ROOF'/
&OBST XB=29.3,42.5,0,74,16.2,17.1, SAWTOOTH=.FALSE., SURF_ID='ROOF'/
&OBST XB=15.1,29.3,0,74,15.3,16.2, SAWTOOTH=.FALSE., SURF_ID='ROOF' /
&OBST XB=0.9,15.1,0,74,14.4,15.3, SAWTOOTH=.FALSE., SURF_ID='ROOF'/

Roof

&OBST XB=0,0.9,0,74,0,15.3,SURF_ID='CONCRETE' /
&OBST XB=99,99.9,0,74,2.7,18,SURF_ID='CONCRETE' /

East & West walls

All the thermocouple locations were the same as the 600mm model except for slight changes due to the hanger geometry and fire location having to conform to the grid mesh.

1800mm grids

&HEAD CHID='15m(1800mm)',TITLE='Test fire 7, entire hanger, 1800mm grids' /
&GRID IBAR=57, JBAR=41, KBAR=11 /
&PDIM XBAR=102.6, YBAR=74, ZBAR=19.8 /

&SURF ID='POOLFIRE', HRRPUA=1210./
&VENT XB=61.2,63,32.4,34.2,3.6,3.6, SURF_ID='POOLFIRE'/

```
&VENT XB=1.8,3.6,0,0,1.8,3.6, SURF_ID='OPEN' /

&OBST XB=67.8,100.8,0,74,3.6,5.4, SAWTOOTH=.FALSE., SURF_ID='INERT' /
&OBST XB=34.8,67.8,0,74,1.8,3.6, SAWTOOTH=.FALSE., SURF_ID='INERT' /
&OBST XB=1.8,34.8,0,74,0,1.8, SAWTOOTH=.FALSE., SURF_ID='INERT' /
```

Floor

```
&OBST XB=36.1,100.8,0,74,18,19.8, SAWTOOTH=.FALSE., SURF_ID='ROOF'/
&OBST XB=18.9,36.1,0,74,16.2,18, SAWTOOTH=.FALSE., SURF_ID='ROOF'/
&OBST XB=1.8,18.9,0,74,14.4,16.2, SAWTOOTH=.FALSE., SURF_ID='ROOF' /
```

Roof

```
&OBST XB=0,1.8,0,74,0,16.2,SURF_ID='CONCRETE' /
&OBST XB=100.8,102.6,0,74,3.6,19.8,SURF_ID='CONCRETE' /
```

Concrete walls

All the thermocouple locations were the same as the 600mm model except for slight changes due to the hanger geometry and fire location having to conform to the grid mesh.

3600mm grids:

```
&HEAD CHID='15m(3600mm)',TITLE='Test fire 7, entire hanger, 3600mm grids' /
&GRID IBAR=30, JBAR=20, KBAR=6 /
&PDIM XBAR=106.2, YBAR=73.8, ZBAR=21.6 /
&TIME TWFIN=1000 /

&TRNX CC=60.18,PC=61.2/
&TRNX CC=63.72,PC=63/
&TRNY CC=33.21,PC=32.4/
&TRNY CC=36.9,PC=34.2/
```

Linear stretching

```
&SURF ID='POOLFIRE', HRRPUA=1689./
&VENT XB=61.2,63,32.4,34.2,3.6,3.6, SURF_ID='POOLFIRE'/
```

```
&VENT XB=3.6,7.2,0,0,3.6,7.2, SURF_ID='OPEN' /

&OBST XB=0,106.2,0,73.8,0,3.6, SAWTOOTH=.FALSE., SURF_ID='INERT' /
```
Floor
```
&OBST XB=0,106.2,0,73.8,18,21.6, SAWTOOTH=.FALSE., SURF_ID='ROOF'/
```
Roof
```
&OBST XB=0,3.6,0,73.8,3.6,18,SURF_ID='CONCRETE' /
&OBST XB=102.6,106.2,0,73.8,3.6,18,SURF_ID='CONCRETE' /
```
Concrete walls

All the thermocouple locations were the same as the 600mm model except for slight changes due to the hanger geometry and fire location having to conform to the grid mesh.

Stretched grid, polynomial transformation

```
&HEAD CHID='15m(stretched)',TITLE='Test fire 7, entire hanger, stretched grids' /
&GRID IBAR=78, JBAR=59, KBAR=42 /
&PDIM XBAR=98, YBAR=74, ZBAR=16.8 /

&TRNX IDERIV=0, CC=62.2, PC=62.2/
&TRNX IDERIV=1, CC=62.2, PC=0.15/
&TRNY IDERIV=0, CC=33.7, PC=33.7/
&TRNY IDERIV=1, CC=33.7, PC=0.09/
```
Polynomial transformation
```
&SURF ID='POOLFIRE', HRRPUA=1500./
&VENT XB=60.6,62.4,33,34.8,2,2, SURF_ID='POOLFIRE'/

&VENT XB=0,2.5,0,0,0.4,1.2, SURF_ID='OPEN' /

&OBST XB=86,98,0,74,2.4,2.8, SAWTOOTH=.FALSE., SURF_ID='INERT' /
&OBST XB=72,86,0,74,2,2.4, SAWTOOTH=.FALSE., SURF_ID='INERT' /
&OBST XB=57,72,0,74,1.6,2, SAWTOOTH=.FALSE., SURF_ID='INERT' /
```

&OBST XB=43,57,0,74,1.2,1.6, SAWTOOTH=.FALSE., SURF_ID='INERT' /
&OBST XB=28,43,0,74,0.8,1.2, SAWTOOTH=.FALSE., SURF_ID='INERT' /
&OBST XB=14,28,0,74,0.4,0.8, SAWTOOTH=.FALSE., SURF_ID='INERT' /
&OBST XB=0,14,0,74,0,0.4, SAWTOOTH=.FALSE., SURF_ID='INERT' /

Floor

&OBST XB=46.5,98,0,74,16.4,16.8, SAWTOOTH=.FALSE., SURF_ID='ROOF'/
&OBST XB=39.5,46.5,0,74,16,16.4, SAWTOOTH=.FALSE., SURF_ID='ROOF'/
&OBST XB=32.5,39.5,0,74,15.6,16, SAWTOOTH=.FALSE., SURF_ID='ROOF' /
&OBST XB=25.5,32.5,0,74,15.2,15.6, SAWTOOTH=.FALSE., SURF_ID='ROOF'/
&OBST XB=18.5,25.5,0,74,14.8,15.2, SAWTOOTH=.FALSE., SURF_ID='ROOF'/

&OBST XB=10.5,18.5,0,74,14.4,14.8, SAWTOOTH=.FALSE., SURF_ID='ROOF'/
&OBST XB=0,10.5,0,74,14,14.4, SAWTOOTH=.FALSE., SURF_ID='ROOF'/

Roof

All the thermocouple locations were the same as the 600mm model except for slight changes due to the hanger geometry and fire location having to conform to the grid mesh.

CFAST input file for Test 7, entire hanger

#VERSN 3 One Compartment Base Case
TIMES 1010 0 10 20 0
ADUMP C:/TEMP/15MT5B.CSV NS
TAMB 303 101300. 0.000000
EAMB 303 101300. 0.000000
HI/F 0.000000 0.000000
WIDTH 74.0000 18.3000
DEPTH 92.0000 24.4000
HEIGH 14.1500 14.5000
CEILI ROOF ROOF [1]

[1] ROOF and CURTAIN were defined in the CFAST model, the properties used are given in Appendix D.

WALLS STEEL1/8 CURTAIN

FLOOR CONCRETE CONCRETE

#CEILI ROOF ROOF

#WALLS STEEL1/8 CURTAIN

#FLOOR CONCRETE CONCRETE

HVENT 1 2 1 24.4000 10.8000 0.000000 0.000000 0.000000 0.000000

CVENT 1 2 1 1.00000 1.00000 1.00000 1.00000 1.00000 1.00000
1.00000 1.00000 1.00000 1.00000 1.00000 1.00000 1.00000
1.00000 1.00000 1.00000 1.00000 1.00000 1.00000 1.00000

HVENT 1 2 2 24.4000 10.8000 0.000000 0.000000 0.000000 0.000000

CVENT 1 2 2 1.00000 1.00000 1.00000 1.00000 1.00000 1.00000
1.00000 1.00000 1.00000 1.00000 1.00000 1.00000 1.00000
1.00000 1.00000 1.00000 1.00000 1.00000 1.00000 1.00000

HVENT 1 2 3 18.3000 10.8000 0.000000 0.000000 0.000000 0.000000

CVENT 1 2 3 1.00000 1.00000 1.00000 1.00000 1.00000 1.00000
1.00000 1.00000 1.00000 1.00000 1.00000 1.00000 1.00000
1.00000 1.00000 1.00000 1.00000 1.00000 1.00000 1.00000

HVENT 1 2 4 18.3000 10.8000 0.000000 0.000000 0.000000 0.000000

CVENT 1 2 4 1.00000 1.00000 1.00000 1.00000 1.00000 1.00000
1.00000 1.00000 1.00000 1.00000 1.00000 1.00000 1.00000
1.00000 1.00000 1.00000 1.00000 1.00000 1.00000 1.00000

HVENT 1 3 1 0.0300000 13.0000 0.000000 0.000000 0.000000 0.000000

CVENT 1 3 1 1.00000 1.00000 1.00000 1.00000 1.00000 1.00000
1.00000 1.00000 1.00000 1.00000 1.00000 1.00000 1.00000
1.00000 1.00000 1.00000 1.00000 1.00000 1.00000 1.00000

CHEMI 16.0000 50.0000 10.0000 4.30000E+007 302.000 493.150 0.350000

LFBO 2

LFBT 2

CJET CEILING

FPOS -1.00000 -1.00000 0.300000

FTIME 2.00000 4.00000 6.00000 8.00000 10.0000 12.0000
14.0000 16.0000 20.0000 1000.00 1001.00 1002.00 1003.00
1004.00 1005.00 1006.00 1007.00 1008.00 1010.00

FMASS 0.000000 0.00136894 0.00547577 0.0123205 0.0219031 0.0342235

0.0492819 0.0670781 0.0876123 0.157209 0.157209 0.110884
0.0876123 0.0670781 0.0492819 0.0342235 0.0219031 0.0123205
0.00547577 0.000000

FQDOT 0.000000 58864.5 235458. 529780. 941832. 1.47161E+006
2.11912E+006 2.88436E+006 3.76733E+006 6.76000E+006 6.76000E+006
4.76802E+006 3.76733E+006 2.88436E+006 2.11912E+006 1.47161E+006
941832. 529780. 235458. 0.000000

HCR 0.0800000 0.0800000 0.0800000 0.0800000 0.0800000 0.0800000
0.0800000 0.0800000 0.0800000 0.0800000 0.0800000 0.0800000
0.0800000 0.0800000 0.0800000 0.0800000 0.0800000 0.0800000
0.0800000 0.0800000

OD 0.0300000 0.0300000 0.0300000 0.0300000 0.0300000 0.0300000
0.0300000 0.0300000 0.0300000 0.0300000 0.0300000 0.0300000
0.0300000 0.0300000 0.0300000 0.0300000 0.0300000 0.0300000
0.0300000 0.0300000

CO 0.0300000 0.0300000 0.0300000 0.0300000 0.0300000 0.0300000
0.0300000 0.0300000 0.0300000 0.0300000 0.0300000 0.0300000
0.0300000 0.0300000 0.0300000 0.0300000 0.0300000 0.0300000
0.0300000 0.0300000

SELECT 1 2 0

#GRAPHICS ON

DEVICE 1

WINDOW 0. 0. -100. 1280. 1024. 1100.

LABEL 1 970. 960. 0. 1231. 1005. 10. 15 00:00:00 0.00 0.00

GRAPH 1 100. 50. 0. 600. 475. 10. 3 TIME HEIGHT

GRAPH 2 100. 550. 0. 600. 940. 10. 3 TIME CELSIUS

GRAPH 3 720. 50. 0. 1250. 475. 10. 3 TIME FIRE_SIZE(kW)

GRAPH 4 720. 550. 0. 1250. 940. 10. 3 TIME O|D2|O()

HEAT 0 0 0 0 3 1 U

TEMPE 0 0 0 0 2 1 U

INTER 0 0 0 0 1 1 U

O2 0 0 0 0 4 1 U

Test 5, entire hanger

The geometry and fire locations were the same for the modelling of this test as they were for **Test 7, entire hanger**. The only difference is extra obstructions were defined to model the draft curtain. The draft curtain was also assigned relevant material properties. These additions are given below for each grid size.

FDS model

600mm grids:

```
&SURF ID='CURTAIN'
    FYI='THERMALLY THIN'
    C_DELTA_RHO= 0.5
    DELTA = 0.003 /                                    Draft curtain properties
&OBST XB=48.6,49.2,24,43.2,13.4,17, SURF_ID='CURTAIN' /
&OBST XB=73.8,74.4,24,43.2,13.4,17, SURF_ID='CURTAIN' /
&OBST XB=49.2,73.8,24,24.6,13.4,17, SURF_ID='CURTAIN' /
&OBST XB=49.2,73.8,42.6,43.2,13.4,17, SURF_ID='CURTAIN' /
                                                       Draft curtain
```

900mm grids:

```
&OBST XB=48.6,49.5,24.3,43.2,13.5,17.1, SURF_ID='CURTAIN' /
&OBST XB=74.7,75.6,24.3,43,13.5,17.1, SURF_ID='CURTAIN' /
&OBST XB=49.5,74.7,24.3,25.2,13.5,17.1, SURF_ID='CURTAIN' /
&OBST XB=49.5,74.7,42.3,43.2,13.5,17.1, SURF_ID='CURTAIN' /
                                                       Draft curtain
```

1800mm grids:

```
&OBST XB=48.6,50.4,23.4,45,14.4,18, SURF_ID='CURTAIN' /
&OBST XB=75.6,77.4,23.4,45,14.4,18, SURF_ID='CURTAIN' /
&OBST XB=50.4,75.6,23.4,25.2,14.4,18, SURF_ID='CURTAIN' /
&OBST XB=50.4,75.6,43.2,45,14.4,18, SURF_ID='CURTAIN' /
```

Draft curtain

All the thermocouple locations were the same as the 600mm model in **Test 7, entire hanger** except for slight changes due to the hanger geometry and fire location having to conform to the grid mesh.

CFAST input file for Test 5, entire hanger

```
#VERSN 3 One Compartment Base Case
TIMES  1010    0    10    20    0
ADUMP C:/TEMP/15MT5B.CSV NS
TAMB  300      101300. 0.000000
EAMB  300      101300. 0.000000
HI/F  0.000000 0.000000
WIDTH  74.0000  18.3000
DEPTH  92.0000  24.4000
HEIGH  14.1500  14.5000
CEILI ROOF    ROOF
WALLS STEEL1/8 CURTAIN
FLOOR CONCRETE CONCRETE
#CEILI ROOF    ROOF
#WALLS STEEL1/8 CURTAIN
#FLOOR CONCRETE CONCRETE
HVENT  1  2  1  24.4000  10.8000 0.000000 0.000000 0.000000 0.000000
CVENT  1  2  1     1.00000     1.00000     1.00000     1.00000     1.00000     1.00000
       1.00000     1.00000     1.00000     1.00000     1.00000     1.00000     1.00000
       1.00000     1.00000     1.00000     1.00000     1.00000     1.00000     1.00000
HVENT  1  2  2  24.4000  10.8000 0.000000 0.000000 0.000000 0.000000
```

CVENT 1 2 2 1.00000 1.00000 1.00000 1.00000 1.00000 1.00000
1.00000 1.00000 1.00000 1.00000 1.00000 1.00000 1.00000
1.00000 1.00000 1.00000 1.00000 1.00000 1.00000 1.00000
HVENT 1 2 3 18.3000 10.8000 0.000000 0.000000 0.000000 0.000000
CVENT 1 2 3 1.00000 1.00000 1.00000 1.00000 1.00000 1.00000
1.00000 1.00000 1.00000 1.00000 1.00000 1.00000 1.00000
1.00000 1.00000 1.00000 1.00000 1.00000 1.00000 1.00000
HVENT 1 2 4 18.3000 10.8000 0.000000 0.000000 0.000000 0.000000
CVENT 1 2 4 1.00000 1.00000 1.00000 1.00000 1.00000 1.00000
1.00000 1.00000 1.00000 1.00000 1.00000 1.00000 1.00000
1.00000 1.00000 1.00000 1.00000 1.00000 1.00000 1.00000
HVENT 1 3 1 0.0300000 13.0000 0.000000 0.000000 0.000000 0.000000
CVENT 1 3 1 1.00000 1.00000 1.00000 1.00000 1.00000 1.00000
1.00000 1.00000 1.00000 1.00000 1.00000 1.00000 1.00000
1.00000 1.00000 1.00000 1.00000 1.00000 1.00000 1.00000
CHEMI 16.0000 50.0000 10.0000 4.30000E+007 302.000 493.150 0.350000
LFBO 2
LFBT 2
CJET CEILING
FPOS -1.00000 -1.00000 0.300000
FTIME 2.00000 4.00000 6.00000 8.00000 10.0000 12.0000
14.0000 16.0000 20.0000 1000.00 1001.00 1002.00 1003.00
1004.00 1005.00 1006.00 1007.00 1008.00 1010.00
FMASS 0.000000 0.00136894 0.00547577 0.0123205 0.0219031 0.0342235
0.0492819 0.0670781 0.0876123 0.157209 0.157209 0.110884
0.0876123 0.0670781 0.0492819 0.0342235 0.0219031 0.0123205
0.00547577 0.000000
FQDOT 0.000000 58864.5 235458. 529780. 941832. 1.47161E+006
2.11912E+006 2.88436E+006 3.76733E+006 6.76000E+006 6.76000E+006
4.76802E+006 3.76733E+006 2.88436E+006 2.11912E+006 1.47161E+006
941832. 529780. 235458. 0.000000
HCR 0.0800000 0.0800000 0.0800000 0.0800000 0.0800000 0.0800000
0.0800000 0.0800000 0.0800000 0.0800000 0.0800000 0.0800000
0.0800000 0.0800000 0.0800000 0.0800000 0.0800000 0.0800000

```
        0.0800000   0.0800000
OD      0.0300000   0.0300000   0.0300000   0.0300000   0.0300000   0.0300000
        0.0300000   0.0300000   0.0300000   0.0300000   0.0300000   0.0300000
        0.0300000   0.0300000   0.0300000   0.0300000   0.0300000   0.0300000
        0.0300000   0.0300000
CO      0.0300000   0.0300000   0.0300000   0.0300000   0.0300000   0.0300000
        0.0300000   0.0300000   0.0300000   0.0300000   0.0300000   0.0300000
        0.0300000   0.0300000   0.0300000   0.0300000   0.0300000   0.0300000
        0.0300000   0.0300000
SELECT 1 2 0
#GRAPHICS ON
DEVICE 1
WINDOW   0.   0. -100. 1280. 1024. 1100.
LABEL  1  970.  960.   0. 1231. 1005.  10. 15 00:00:00 0.00  0.00
GRAPH  1  100.   50.   0.  600.  475.  10. 3 TIME HEIGHT
GRAPH  2  100.  550.   0.  600.  940.  10. 3 TIME CELSIUS
GRAPH  3  720.   50.   0. 1250.  475.  10. 3 TIME FIRE_SIZE(kW)
GRAPH  4  720.  550.   0. 1250.  940.  10. 3 TIME O|D2|O()
HEAT   0 0 0 0 3   1 U
TEMPE  0 0 0 0 2   1 U
INTER  0 0 0 0 1   1 U
O2     0 0 0 0 4   1 U
```

Test 5, draft curtain

FDS models

300mm grids:

```
&HEAD CHID='draft(300mm)', TITLE='Test fire 5, with draft curtain, 300mm grids' /
&GRID IBAR=82, JBAR=61, KBAR=50 /
&PDIM XBAR=24.6, YBAR=18.3, ZBAR=15 /
&TIME TWFIN=1000 /
&MISC GVEC=0.3008,0.0,-9.8054
    TMPA = 30
    NFRAMES=500
    SURF_DEFAULT='CURTAIN'
    SET_UP=.TRUE. /

&REAC ID='JP5 Fuel'
    SOOT_YIELD=0.042
    CO_YIELD=0.012

&SURF ID='POOLFIRE', HRRPUA=2144./

&VENT XB=11.4,13.2,8.1,9.9,0.6,0.6, SURF_ID='POOLFIRE'/
&OBST XB=11.4,13.2,8.1,9.9,0.3,0.6, /                    Fire and fire pan

&VENT XB=0,24.6,0,0,0.3,11.1, SURF_ID='OPEN' /
&VENT XB=0,24.6,18.3,18.3,0.3,11.1, SURF_ID='OPEN'/
&VENT XB=0,0,0,18.3,0.3,11.1, SURF_ID='OPEN'/
&VENT XB=24.6,24.6,0,18.3,0.3,11.1, SURF_ID='OPEN'/
                                                         Defining the draft curtain
&OBST XB=0,24.6,0,18.3,0,0.3, SURF_ID='INERT' /          Floor
&OBST XB=0,24.6,0,18.3,14.7,15, SURF_ID='ROOF'/          Roof
```

450mm model.

```
&HEAD CHID='draft(450mm)', TITLE=Test fire 5, draft curtain only, 450mm  grids' /
&GRID IBAR=54, JBAR=41, KBAR=35 /
&PDIM XBAR0=49.45, XBAR=73.75, YBAR0=24.39, YBAR=42.84, ZBAR0=2.25,
                                        ZBAR=17.55 /

&SURF ID='POOLFIRE', HRRPUA=1720./
&VENT XB=60.7,62.5,32.94,34.74,3.15,3.15, SURF_ID='POOLFIRE'/
&OBST XB=60.7,62.5,32.94,34.74,2.7,3.15 /
```

Defining the fire

```
&VENT XB=49.45,73.75,24.39,24.39,2.25,13.5, SURF_ID='OPEN' /
&VENT XB=49.45,73.75,42.84,42.84,2.25,13.5, SURF_ID='OPEN'/
&VENT XB=73.75,73.75,24.39,42.84,2.25,13.5, SURF_ID='OPEN'/
&VENT XB=49.45,49.45,24.39,42.84,2.25,13.5, SURF_ID='OPEN'/
```

Defining the draft curtain

```
&OBST XB=49.45,73.75,24.39,42.84,2.25,2.7, SURF_ID='INERT' /
&OBST XB=49.45,73.75,24.39,42.84,17.1,17.55, SURF_ID='ROOF'/
```

Floor

Roof

600mm model

```
&HEAD CHID='draft(600mm)',TITLE='Test fire 5, draft curtain only, 600mm grids' /
&GRID IBAR=41, JBAR=30, KBAR=26 /
&PDIM XBAR0=49, XBAR=73.6, YBAR0=25, YBAR=43, ZBAR0=2,  ZBAR=17.6 /

&SURF ID='POOLFIRE', HRRPUA=1825./
&VENT XB=60.7,62.5,33.1,34.9,3.2,3.2, SURF_ID='POOLFIRE'/
&OBST XB=60.7,62.5,33.1,34.9,2.6,3.2 /
```

Defining the fire

```
&VENT XB=49,73.6,25,25,2,13.3, SURF_ID='OPEN' /
&VENT XB=49,73.6,43,43,2,13.3, SURF_ID='OPEN'/
&VENT XB=73.6,73.6,25,43,2,13.3, SURF_ID='OPEN'/
```

&VENT XB=49,49,25,43,2,13.3, SURF_ID='OPEN'/

Defining the draft curtain

&OBST XB=49,73.6,25,43,2,2.6, SURF_ID='INERT' / **Floor**

&OBST XB=49,73.6,25,43,17,17.6, SURF_ID='ROOF'/ **Roof**

900mm model

&HEAD CHID='draft(900mm)',TITLE='Test fire 5, draft curtain, 900mm grids' /

&GRID IBAR=27, JBAR=20, KBAR=18 /

&PDIM XBAR0=50.4, XBAR=74.7, YBAR0=25.2, YBAR=43.2, ZBAR0=1.8, ZBAR=18 /

&SURF ID='POOLFIRE', HRRPUA=1470./

&VENT XB=61.2,63,33.3,35.1,2.7,2.7, SURF_ID='POOLFIRE'/ **Pool Fire and pan**

&OBST XB=50.4,74.7,25.2,43.2,1.8,2.7, SURF_ID='INERT' / **Floor**

&OBST XB=50.4,74.7,25.2,43.2,17.1,18, SURF_ID='ROOF'/ **Roof**

&VENT XB=50.4,74.7,25.2,25.2,2.7,13.5, SURF_ID='OPEN' /

&VENT XB=50.4,74.7,43.2,43.2,2.7,13.5, SURF_ID='OPEN'/

&VENT XB=74.7,74.7,25.2,43.2,2.7,13.5, SURF_ID='OPEN'/

&VENT XB=50.4,50.4,25.2,43.2,2.7,13.5, SURF_ID='OPEN'/ **Defining the draft curtain**

1800mm grids

&HEAD CHID='draft(1800mm)',TITLE='Test fire 5, draft curtain, 1800mm grids' /

&GRID IBAR=14, JBAR=10, KBAR=10 /

&PDIM XBAR0=50.4,XBAR=75.6,YBAR0=25.2,YBAR=43.2,ZBAR0=1.8,ZBAR=19.8 /

&SURF ID='POOLFIRE', HRRPUA=1492./

&VENT XB=61.2,63,32.4,34.2,3.6,3.6, SURF_ID='POOLFIRE'/

&OBST XB=50.4,75.6,25.2,43.2,1.8,3.6, SURF_ID='INERT' / **Floor**

&OBST XB=50.4,75.6,25.2,43.2,18,19.8, SURF_ID='ROOF' / **Roof**

&VENT XB=50.4,75.6,25.2,25.2,3.6,14.4, SURF_ID='OPEN' /

&VENT XB=50.4,75.6,43.2,43.2,3.6,14.4, SURF_ID='OPEN'/

&VENT XB=75.6,75.6,25.2,43.2,3.6,14.4, SURF_ID='OPEN'/

&VENT XB=50.4,50.4,25.2,43.2,3.6,14.4, SURF_ID='OPEN'/

Most of the thermocouples that are defined in the input file for **Test 7, entire hanger** with 600mm grids were also defined in the files for the **Test 5, draft curtain** models given above. However, some thermocouples did not fall within the confines of the modelling domain so were not used.

CFAST input file for Test 5, draft curtain

#VERSN 3 One Compartment Base Case

TIMES 1010 0 10 20 0

ADUMP C:/TEMP/DRAFT.CSV NS

TAMB 300 101300. 0.000000

EAMB 300 101300. 0.000000

HI/F 0.000000

WIDTH 18.3000

DEPTH 24.4000

HEIGH 14.5000

CEILI ROOF

WALLS CURTAIN

FLOOR CONCRETE

#CEILI ROOF

#WALLS CURTAIN

#FLOOR CONCRETE

HVENT 1 2 1 24.4000 10.8000 0.000000 0.000000 0.000000 0.000000

CVENT 1 2 1 1.00000 1.00000 1.00000 1.00000 1.00000 1.00000

1.00000 1.00000 1.00000 1.00000 1.00000 1.00000 1.00000
1.00000 1.00000 1.00000 1.00000 1.00000 1.00000 1.00000
HVENT 1 2 2 24.4000 10.8000 0.000000 0.000000 0.000000 0.000000
CVENT 1 2 2 1.00000 1.00000 1.00000 1.00000 1.00000 1.00000
1.00000 1.00000 1.00000 1.00000 1.00000 1.00000 1.00000
1.00000 1.00000 1.00000 1.00000 1.00000 1.00000 1.00000
HVENT 1 2 3 18.3000 10.8000 0.000000 0.000000 0.000000 0.000000
CVENT 1 2 3 1.00000 1.00000 1.00000 1.00000 1.00000 1.00000
1.00000 1.00000 1.00000 1.00000 1.00000 1.00000 1.00000
1.00000 1.00000 1.00000 1.00000 1.00000 1.00000 1.00000
HVENT 1 2 4 18.3000 10.8000 0.000000 0.000000 0.000000 0.000000
CVENT 1 2 4 1.00000 1.00000 1.00000 1.00000 1.00000 1.00000
1.00000 1.00000 1.00000 1.00000 1.00000 1.00000 1.00000
1.00000 1.00000 1.00000 1.00000 1.00000 1.00000 1.00000
CHEMI 16.0000 50.0000 10.0000 4.30000E+007 302.000 493.150 0.350000
LFBO 1
LFBT 2
CJET CEILING
FPOS -1.00000 -1.00000 0.300000
FTIME 2.00000 4.00000 6.00000 8.00000 10.0000 12.0000
14.0000 16.0000 20.0000 1000.00 1001.00 1002.00 1003.00
1004.00 1005.00 1006.00 1007.00 1008.00 1010.00
FMASS 0.000000 0.00136894 0.00547577 0.0123205 0.0219031 0.0342235
0.0492819 0.0670781 0.0876123 0.157209 0.157209 0.110884
0.0876123 0.0670781 0.0492819 0.0342235 0.0219031 0.0123205
0.00547577 0.000000
FQDOT 0.000000 58864.5 235458. 529780. 941832. 1.47161E+006
2.11912E+006 2.88436E+006 3.76733E+006 6.76000E+006 6.76000E+006
4.76802E+006 3.76733E+006 2.88436E+006 2.11912E+006 1.47161E+006
941832. 529780. 235458. 0.000000
HCR 0.0800000 0.0800000 0.0800000 0.0800000 0.0800000 0.0800000
0.0800000 0.0800000 0.0800000 0.0800000 0.0800000 0.0800000
0.0800000 0.0800000 0.0800000 0.0800000 0.0800000 0.0800000
0.0800000 0.0800000

```
OD      0.0300000   0.0300000   0.0300000   0.0300000   0.0300000   0.0300000
        0.0300000   0.0300000   0.0300000   0.0300000   0.0300000   0.0300000
        0.0300000   0.0300000   0.0300000   0.0300000   0.0300000   0.0300000
        0.0300000   0.0300000
CO      0.0300000   0.0300000   0.0300000   0.0300000   0.0300000   0.0300000
        0.0300000   0.0300000   0.0300000   0.0300000   0.0300000   0.0300000
        0.0300000   0.0300000   0.0300000   0.0300000   0.0300000   0.0300000
        0.0300000   0.0300000
SELECT 1 0 0
#GRAPHICS ON
DEVICE 1
WINDOW   0.   0. -100. 1280. 1024. 1100.
LABEL  1  970.  960.   0. 1231. 1005.   10. 15 00:00:00 0.00  0.00
GRAPH  1  100.   50.   0.  600.  475.   10. 3 TIME HEIGHT
GRAPH  2  100.  550.   0.  600.  940.   10. 3 TIME CELSIUS
GRAPH  3  720.   50.   0. 1250.  475.   10. 3 TIME FIRE_SIZE(kW)
GRAPH  4  720.  550.   0. 1250.  940.   10. 3 TIME O|D2|O()
```

Appendix C: Additional Results

Appendix C contains all the results that were extracted from the modelling comparisons and used for analysis but were not shown in the results section. Comparisons of all the thermocouples are not given because these were not used in the analysis and conclusions in this report.

C.1 McLeans Island Results

55kW Test:

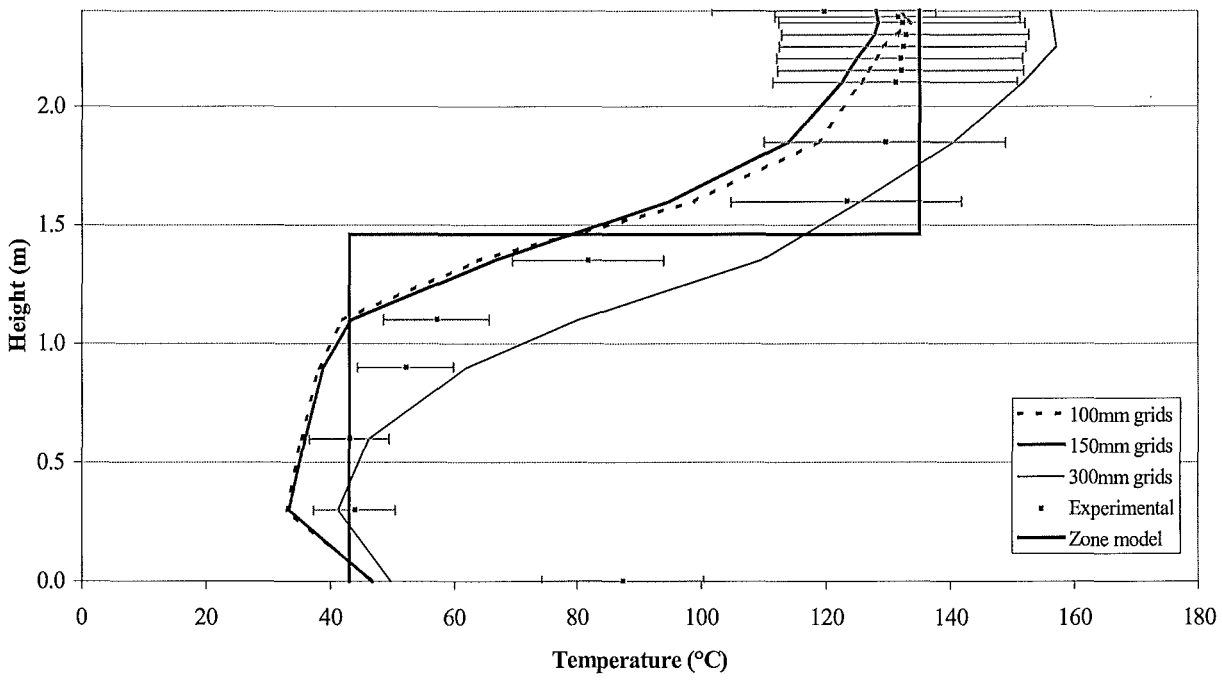

Figure C.1: Temperature profiles for Tree 2 for the 55kW fire.

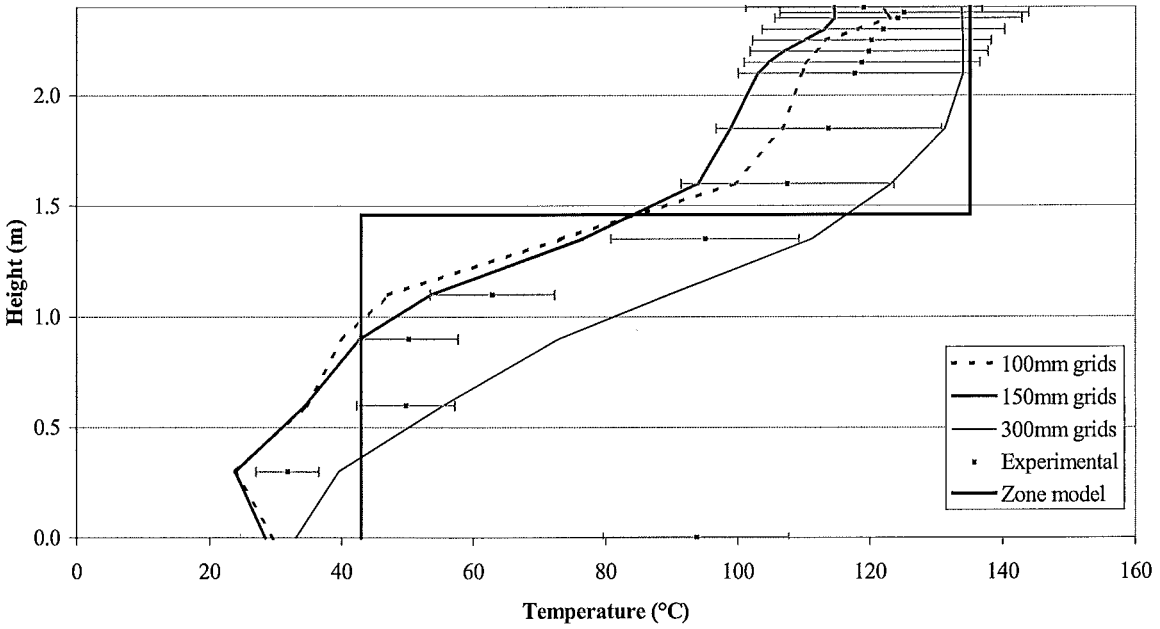

Figure C.2: Temperature profiles for Tree 4 for the 55kW fire.

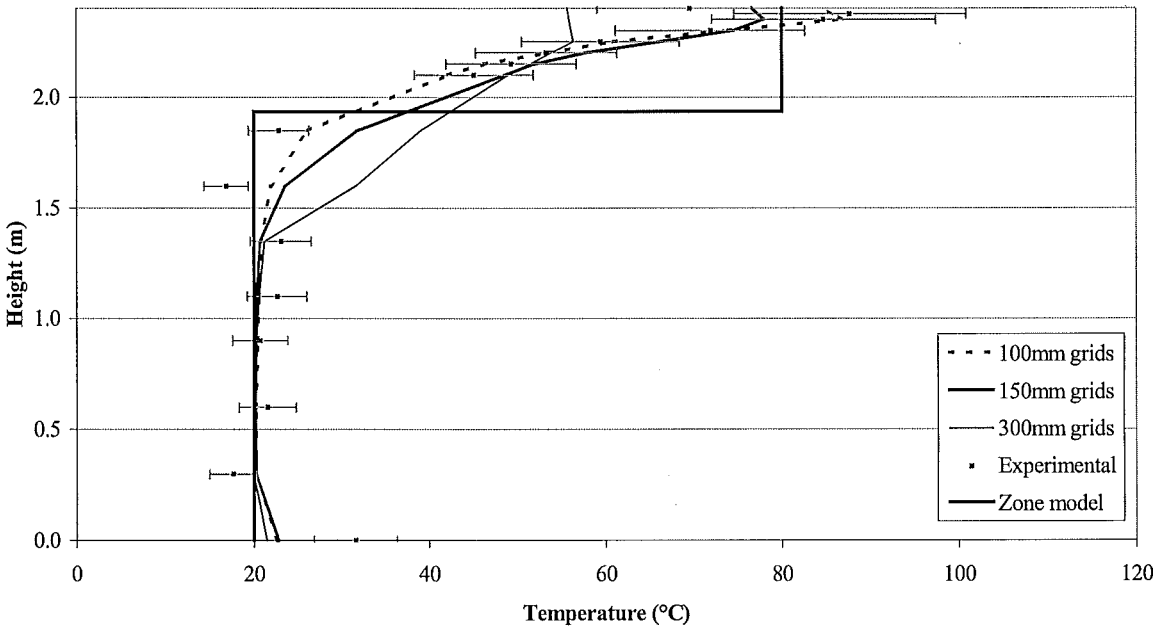

Figure C.3: Temperature profiles for Tree 6 for the 55kW fire.

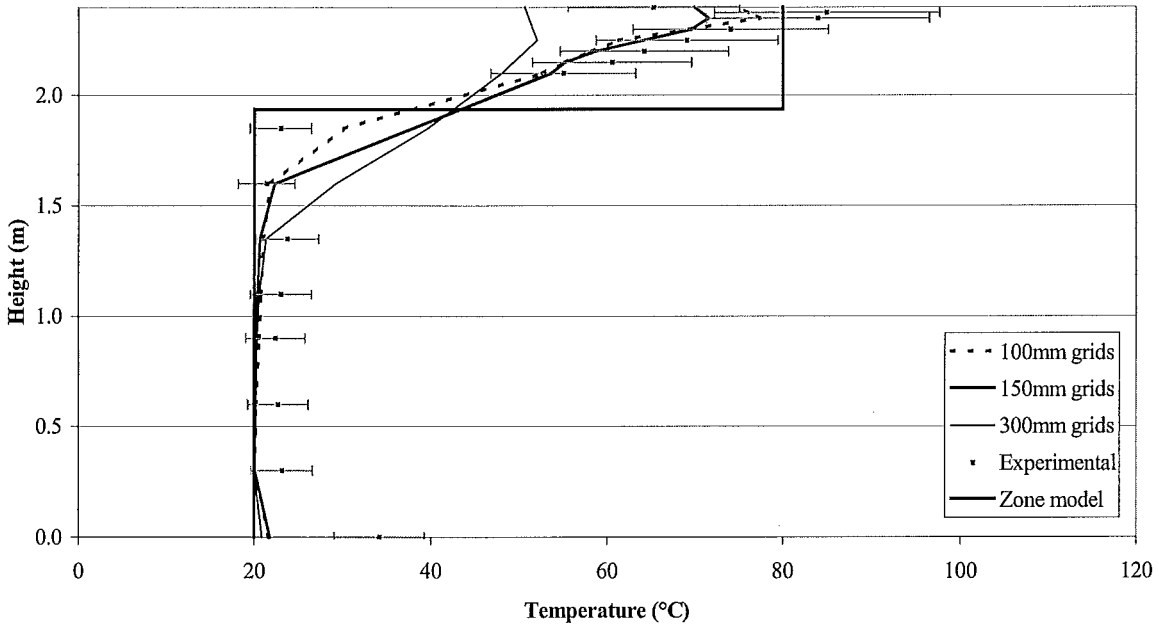

Figure C.4: Temperature profiles for Tree 7 for the 55kW fire.

110kW test:

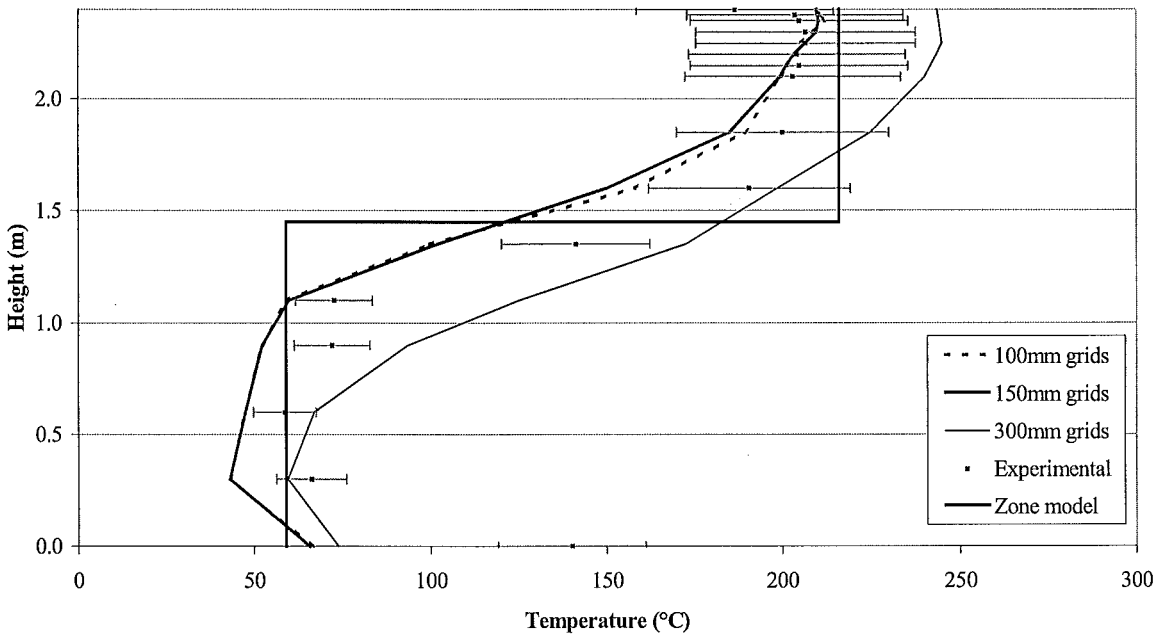

Figure C.5: Temperature profiles for Tree 2 for the 110kW fire.

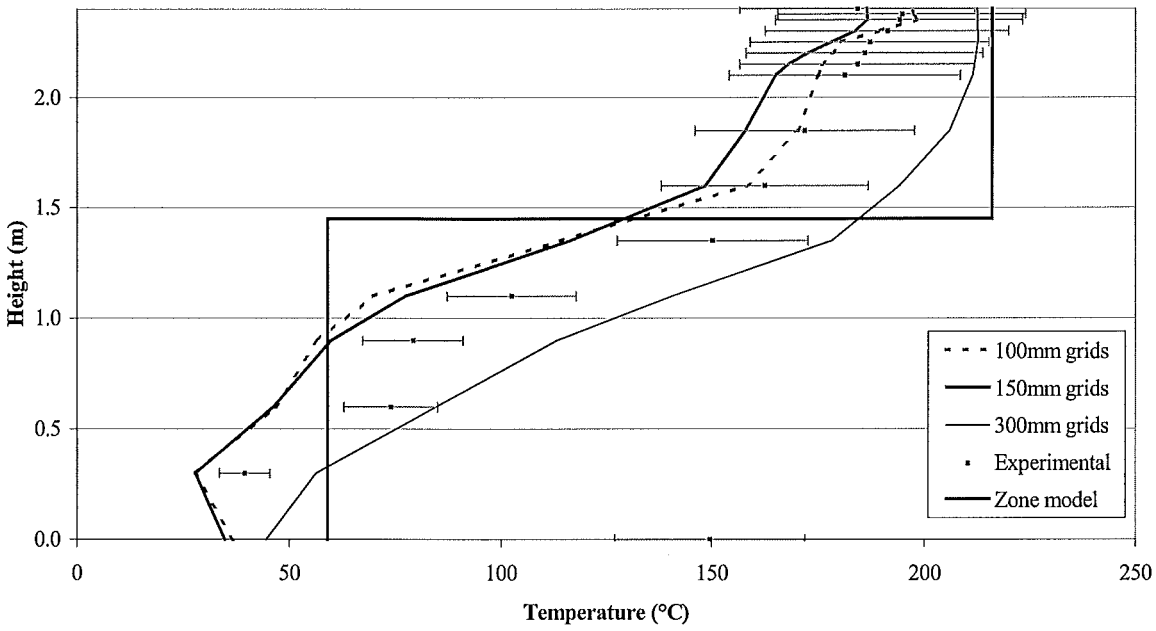

Figure C.6: Temperature profiles for Tree 4 for the 110kW fire.

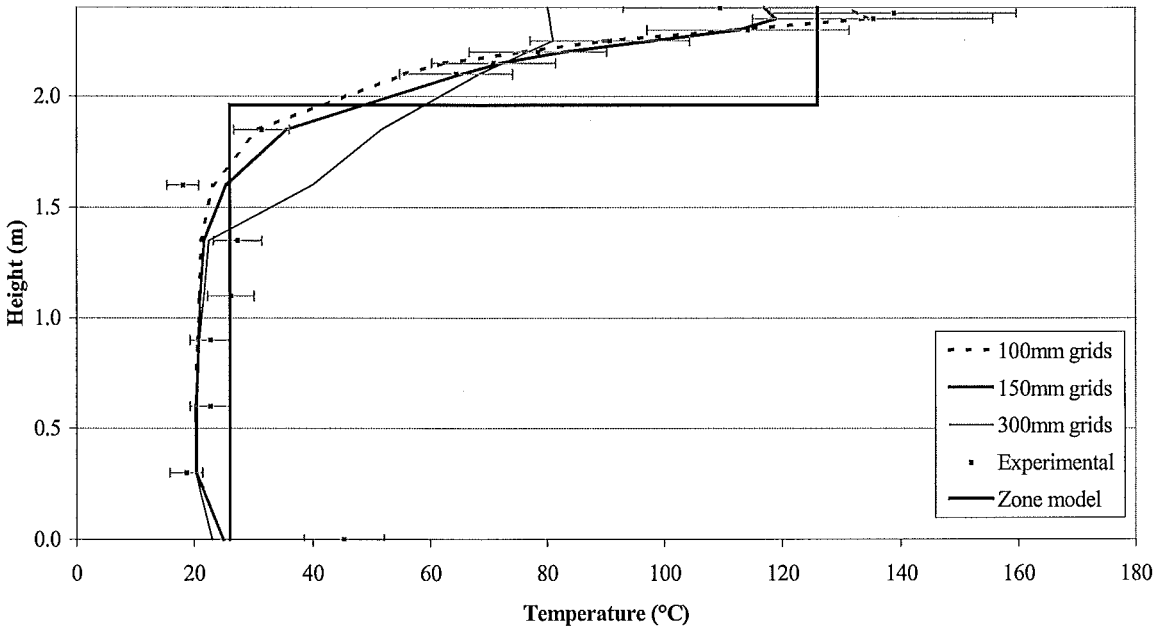

Figure C. 7: Temperature profiles for Tree 6 for the 110kW fire.

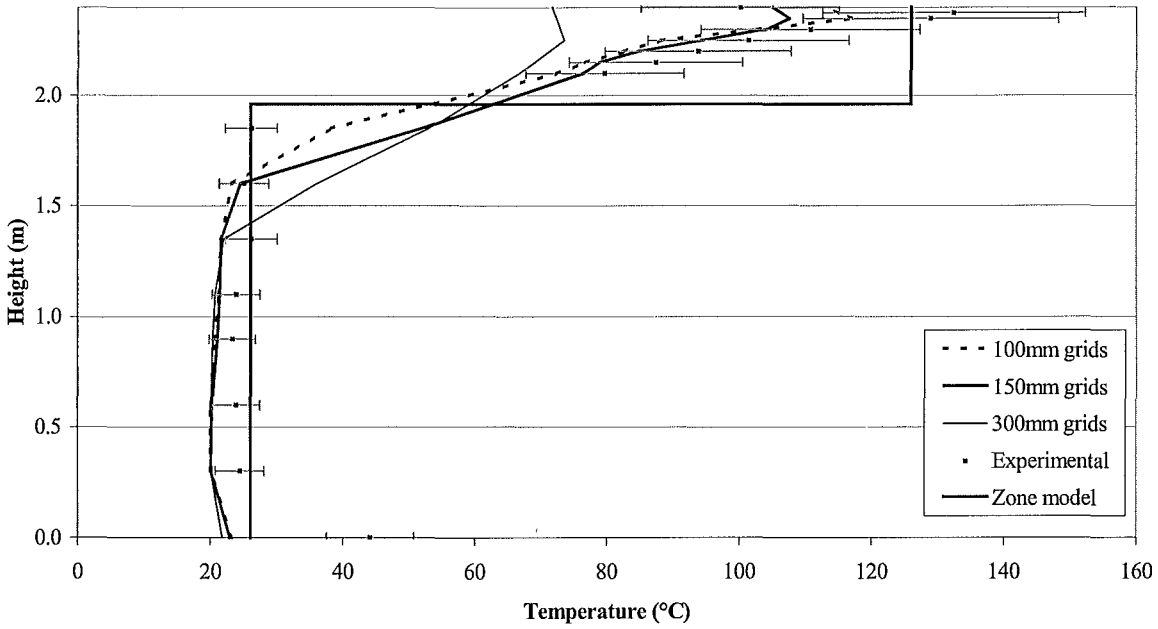

Figure C. 8: Temperature profiles for Tree 7 for the 110kW fire.

C.2 US Navy Hanger Results

Test 7, entire hanger:

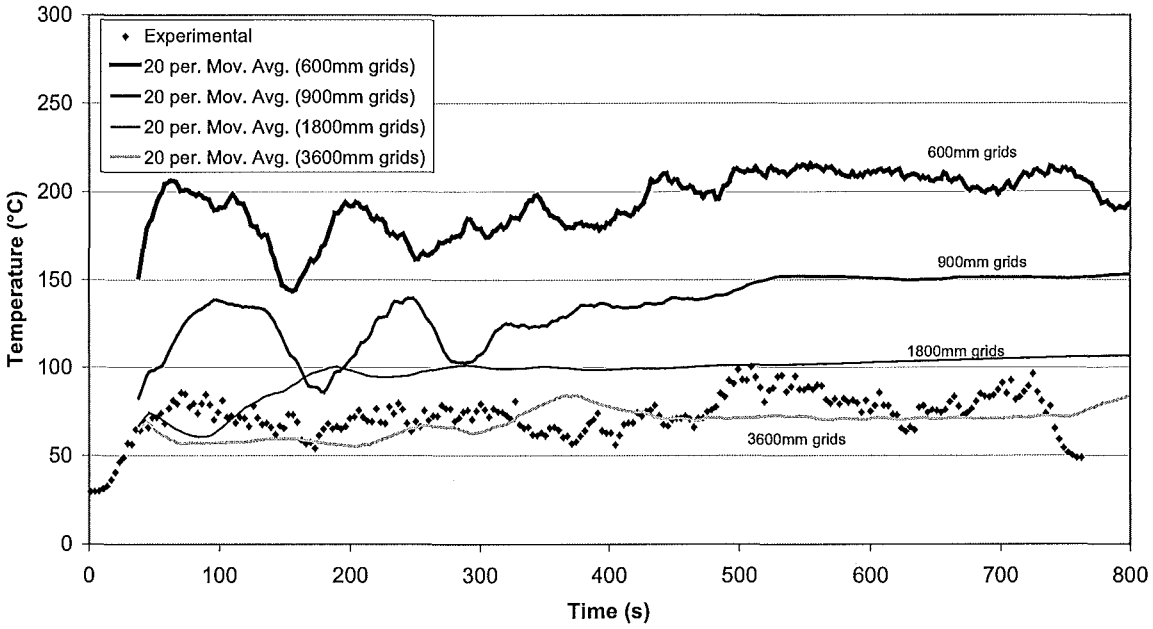

Figure C.9: Test 7, entire hanger; predicted time-temperature profiles for thermocouple C2, directly above the fire, 1.5 metres below the ceiling.

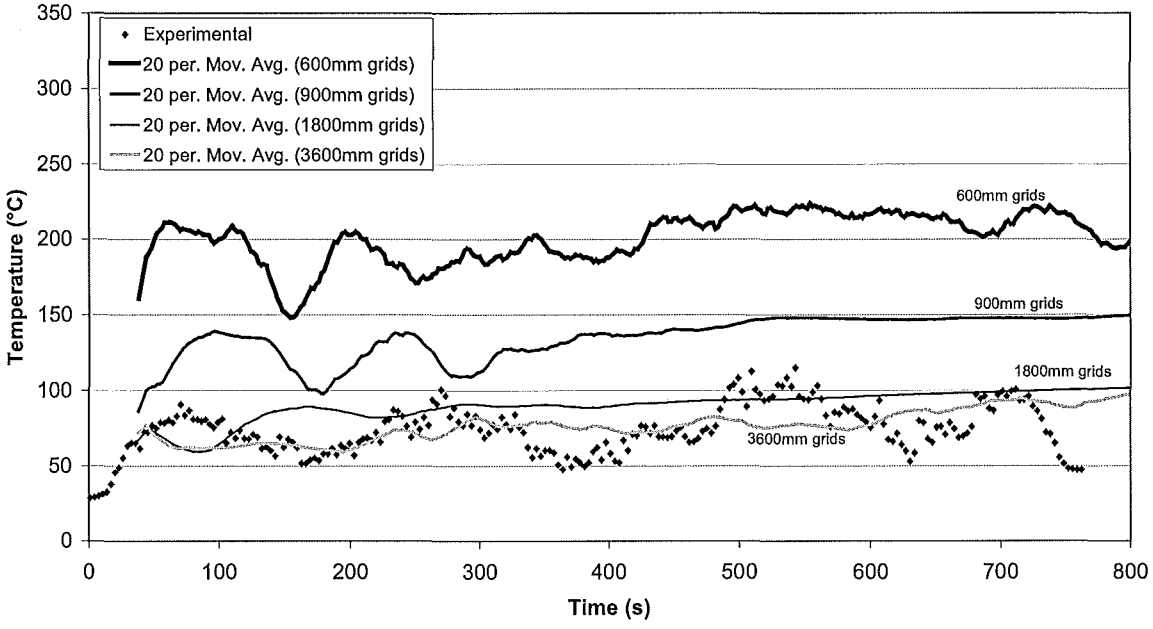

Figure C. 10: Test 7, entire hanger; predicted time-temperature profiles for thermocouple C3, directly above the fire, 1.5 metres below the ceiling.

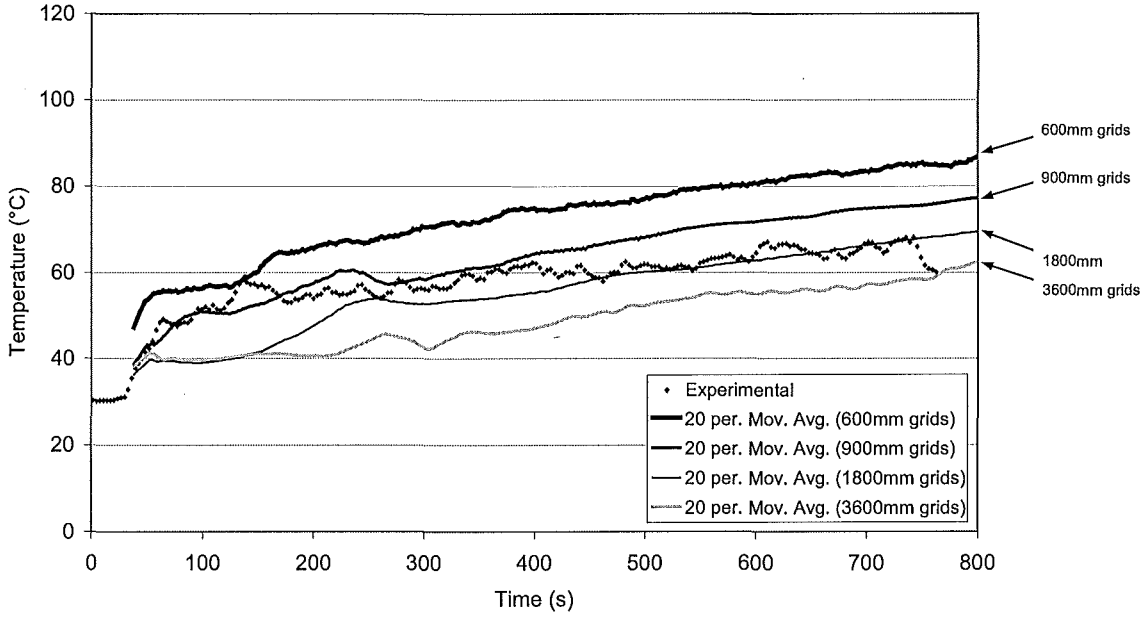

Figure C. 11: Test 7, entire hanger; predicted time-temperature profiles for thermocouple E4, 9.1 metres East of the fire, 0.15 metres below the ceiling.

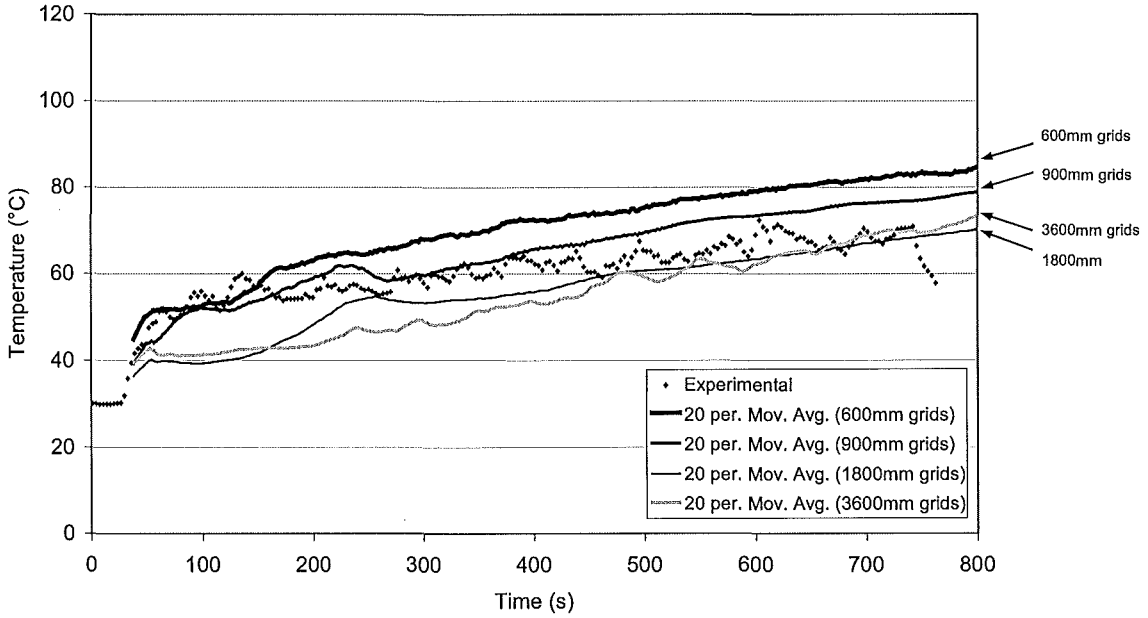

Figure C. 12: Test 7, entire hanger; predicted time-temperature profiles for thermocouple E6, 9.1 metres East of the fire, 0.46 metres below the ceiling.

Test 5, entire hanger:

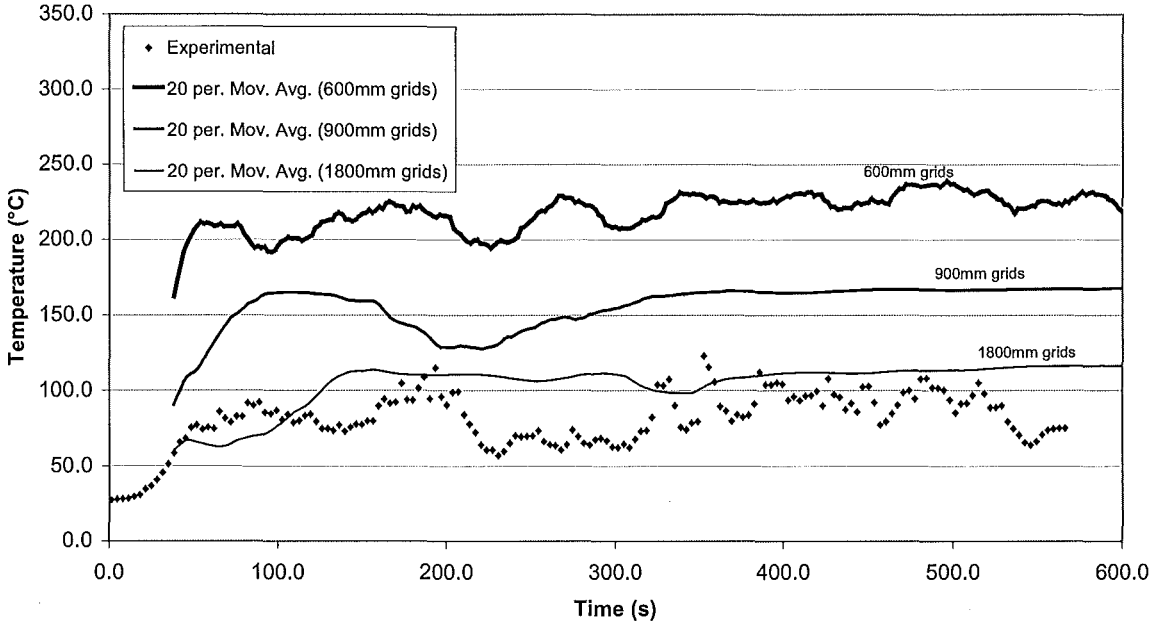

Figure C.13: Test 5, entire hanger; predicted time-temperature profiles for thermocouple C2, directly above the fire, 1.5 metres below the ceiling.

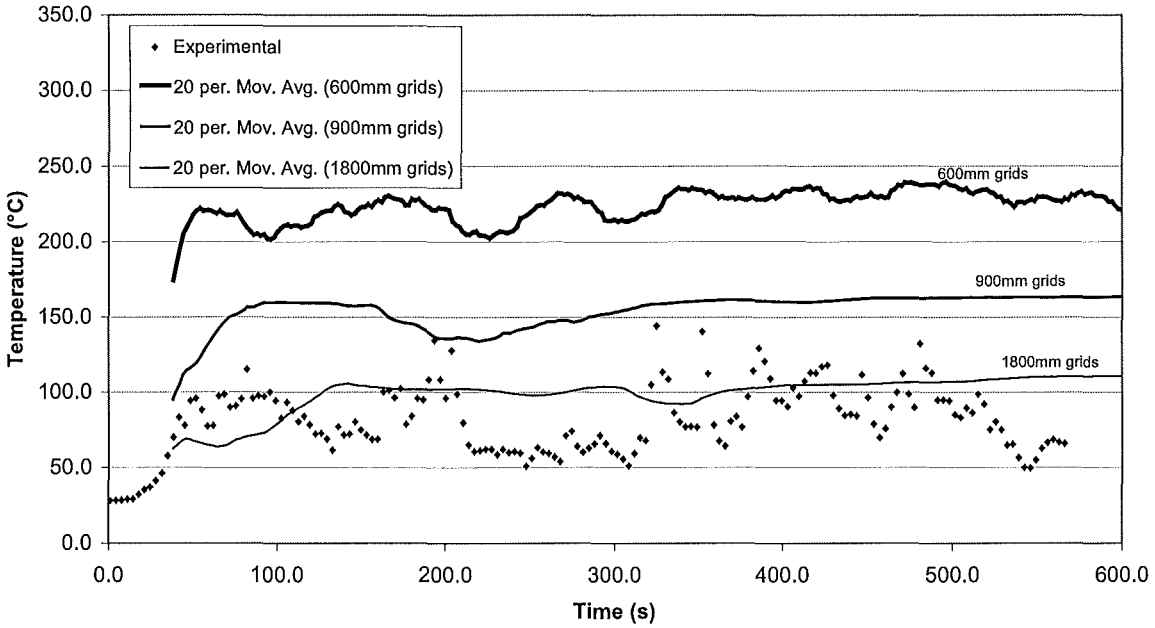

Figure C.14: Test 5, entire hanger; predicted time-temperature profiles for thermocouple C3, directly above the fire, 3 metres below the ceiling.

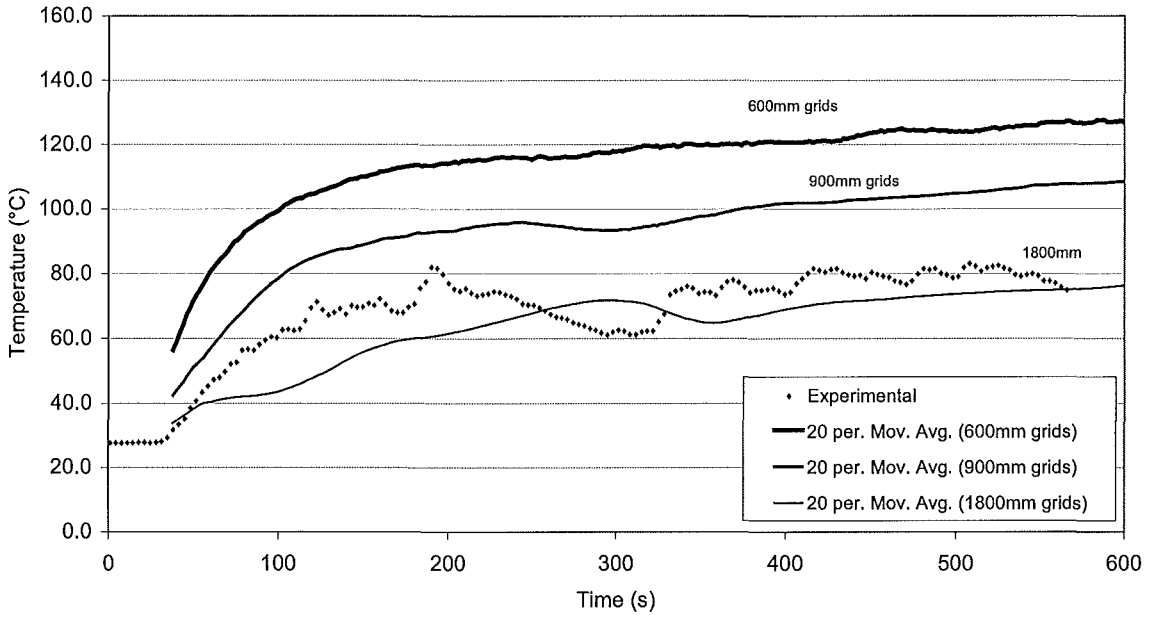

Figure C.15: Test 5, entire hanger; predicted time-temperature profiles for thermocouple E4, 9.1 metres East of the fire, 0.15 metres below the ceiling.

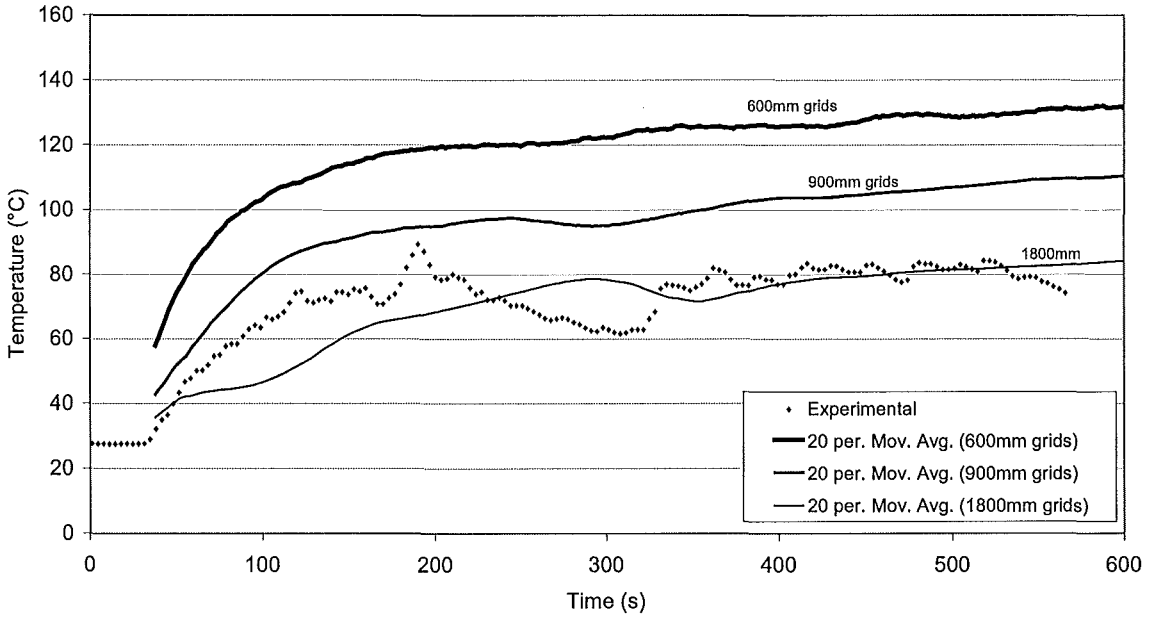

Figure C.16: Test 5, entire hanger; predicted time-temperature profiles for thermocouple E6, 9.1 metres East of the fire, 0.46 metres below the ceiling.

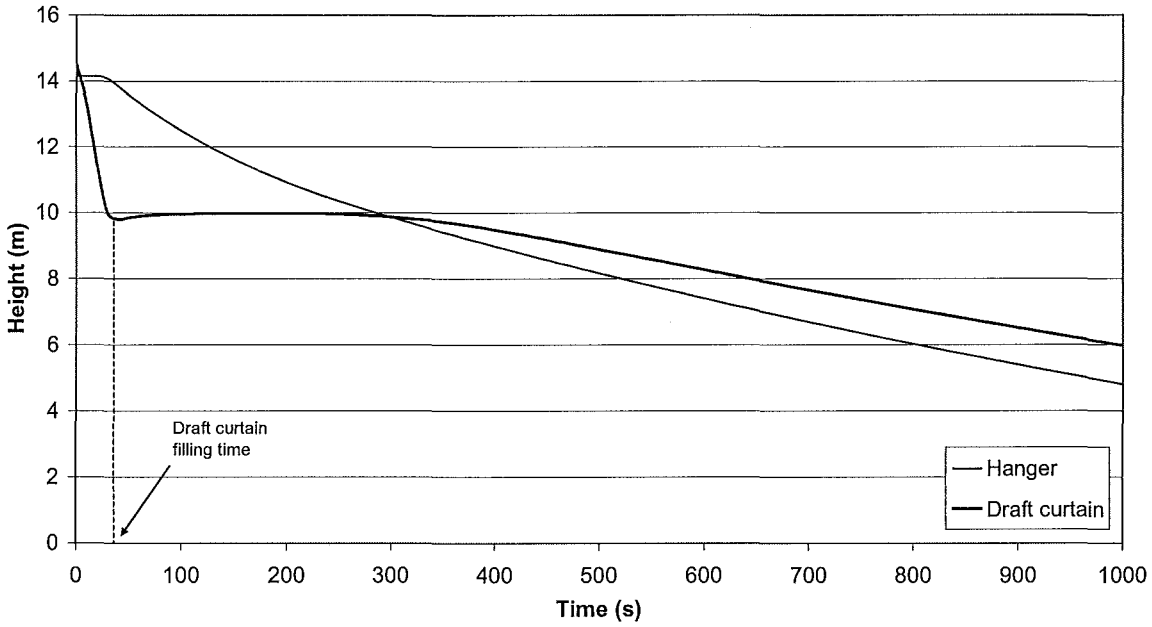

Figure C.17: Zone model predictions of the layer heights in the draft curtain "compartment" and main hanger area.

Test 5, draft curtain only:

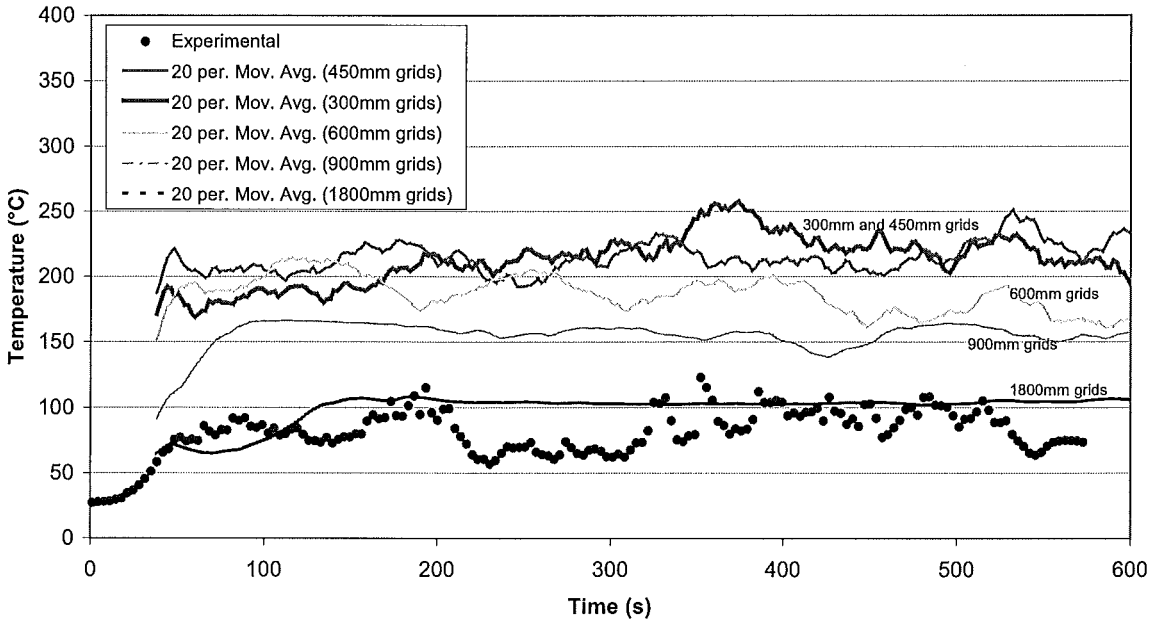

Figure C.18: Test 5, draft curtain; predicted time-temperature profiles for thermocouple C2, directly above the fire, 1.5 metres below the ceiling.

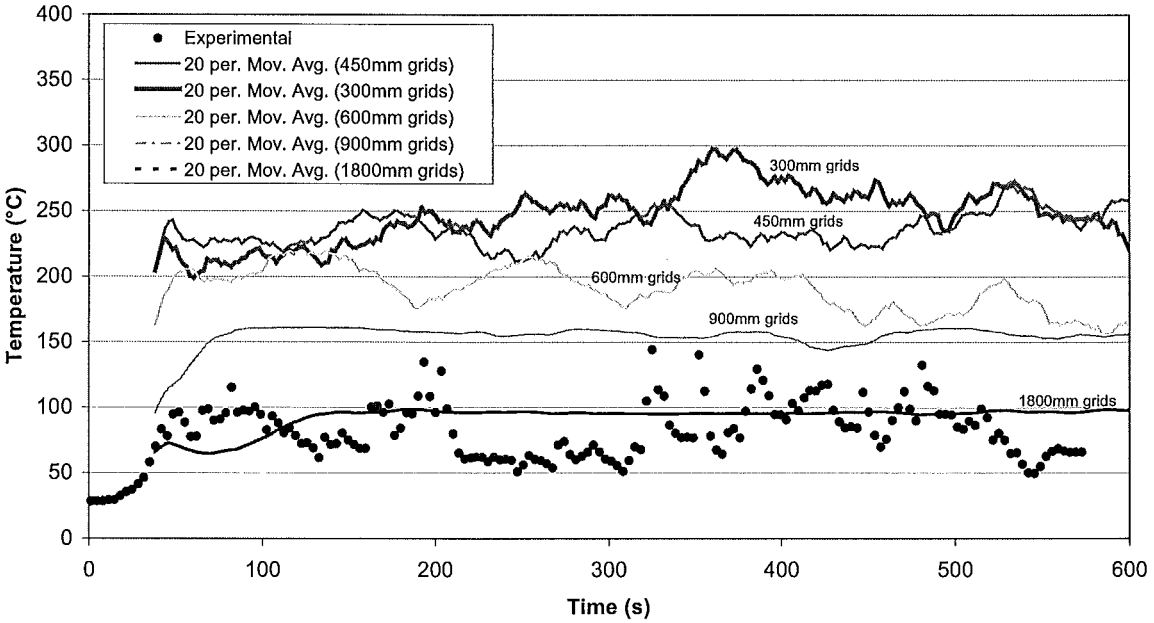

Figure C.19: Test 5, draft curtain; predicted time-temperature profiles for thermocouple C3, directly above the fire, 3 metres below the ceiling.

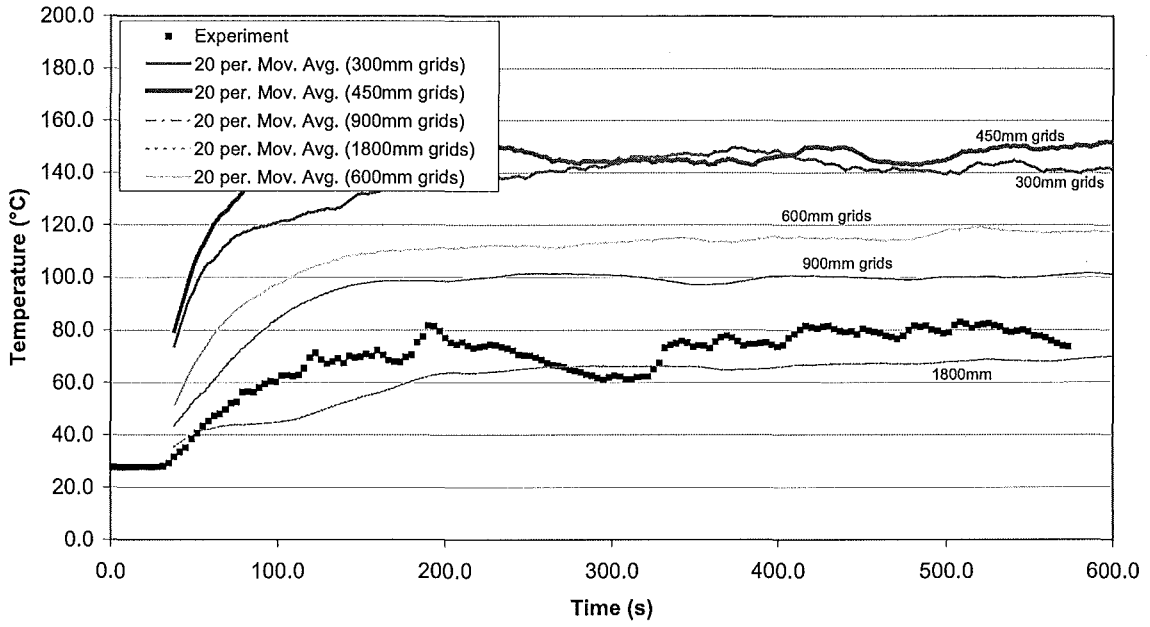

Figure C.20: Test 5, draft curtain; predicted time-temperature profiles for thermocouple E4, 9.1 metres East of the fire, 0.15 metres below the ceiling.

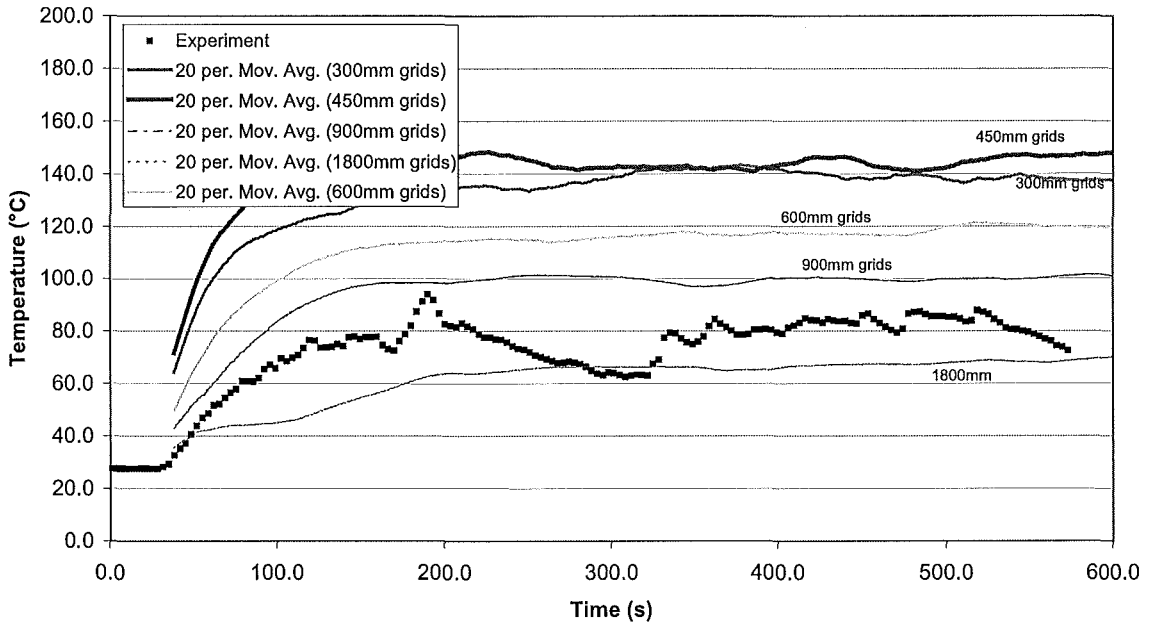

Figure C.21: Test 5, draft curtain; predicted time-temperature profiles for thermocouple E6, 9.1 metres East of the fire, 0.46 metres below the ceiling.

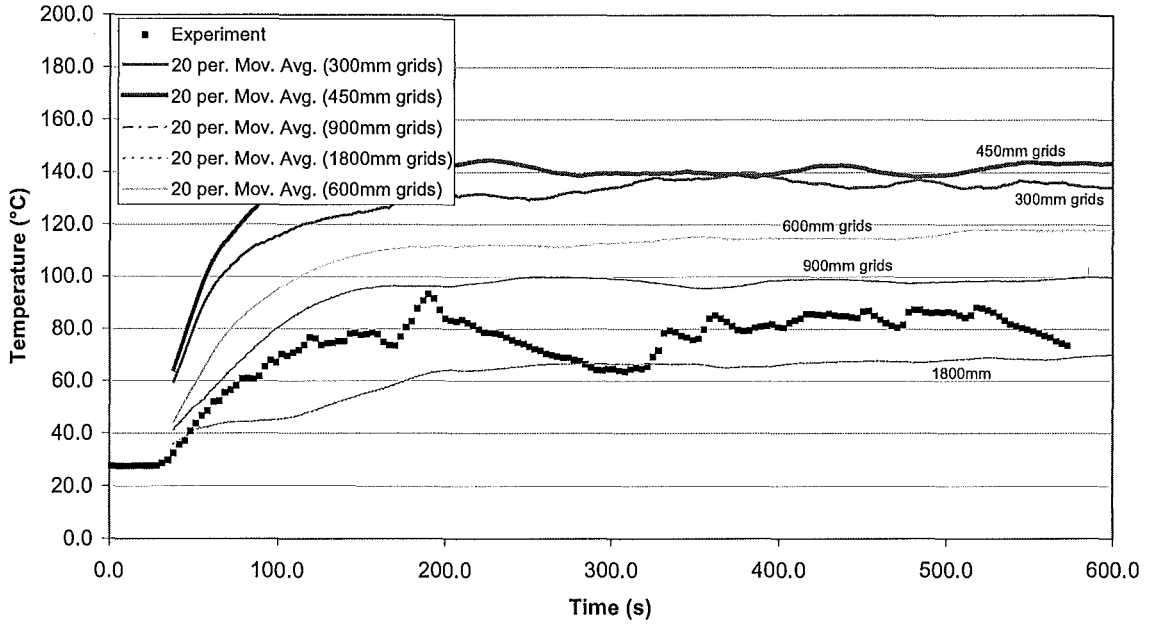

Figure C.22: Test 5, draft curtain; predicted time-temperature profiles for thermocouple E7, 9.1 metres East of the fire, 0.76 metres below the ceiling.

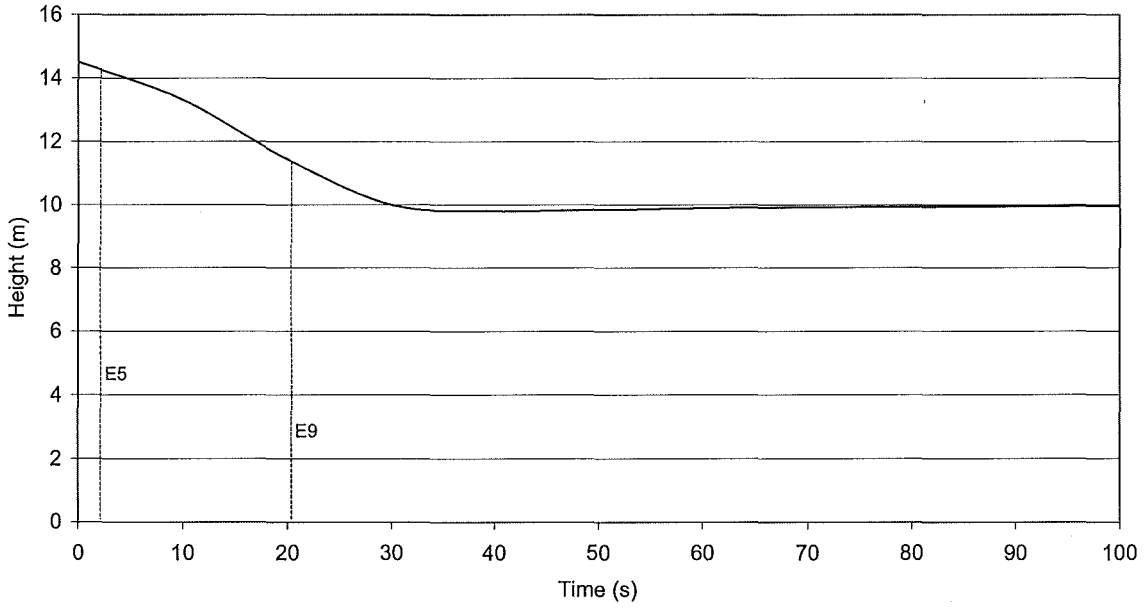

Figure C.23: Test 5, draft curtain; zone model prediction of the layer height in the draft curtain "compartment" showing the times that the layer reaches thermocouples E5 and E9.

Stretched grid FDS model

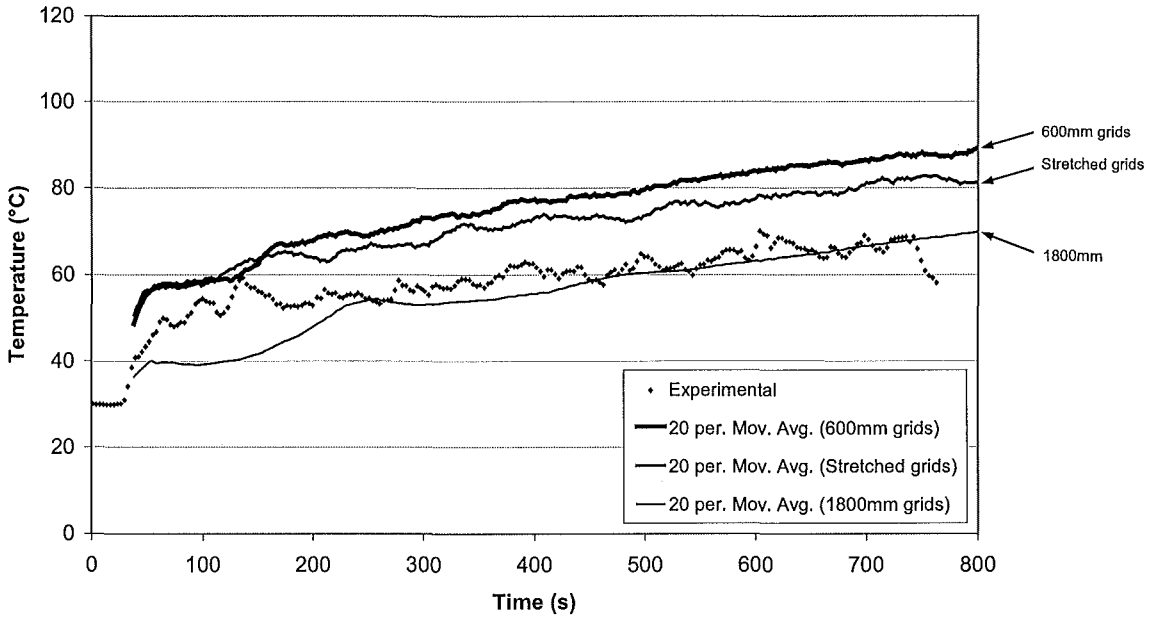

Figure C.24: Stretched grid model; predicted time-temperature profiles for thermocouple E5, 9.1 metres East of the fire, 0.3 metres below the ceiling.

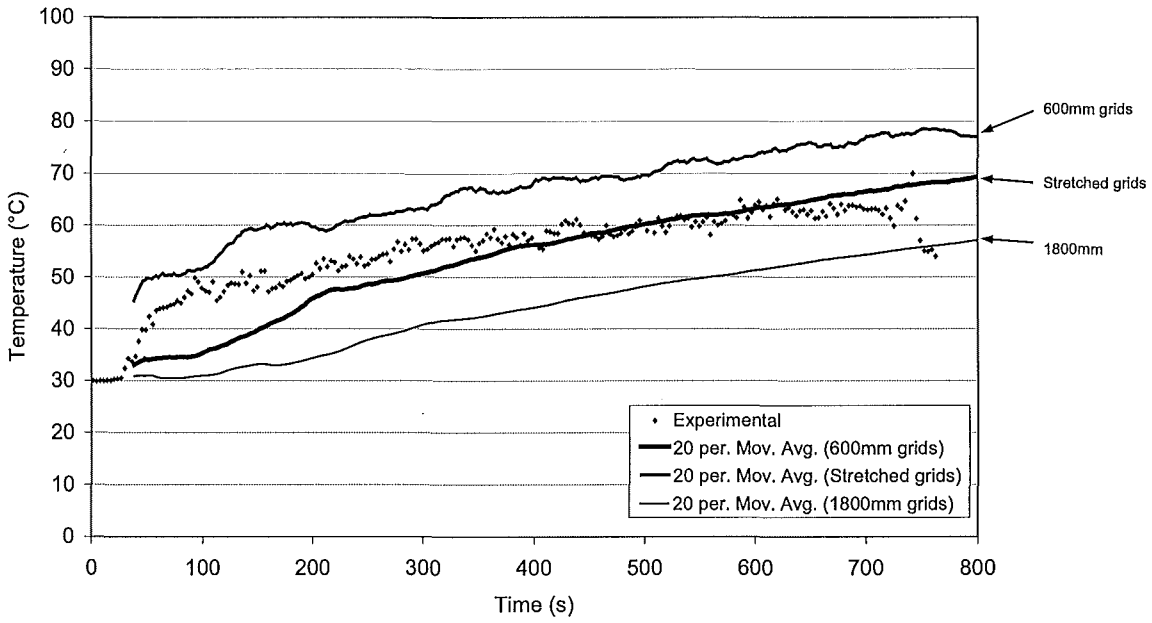

Figure C.25: Stretched grid model; predicted time-temperature profiles for thermocouple E8, 9.1 metres East of the fire, 1.22 metres below the ceiling.

Appendix D: Model Input Parameters

This Appendix provides the model input parameters used. These are given in the text but are tabulated here so they can be referred to more easily.

Table D.1: Properties used in the FDS models of the McLeans Island tests.

	Alpha m^2/s	**k** W/m.K	**Thickness** m
Isoroom lining	8.6E-8	0.036	0.025

Table D.2: Properties used in the CFAST model of the McLeans Island tests.

	Ks W/m.K	**Cp** J/kg.K	**ρ** kg/m3	**ε**	**Thickness** m
Isoroom lining	0.036	2000	300	0.9	0.025

Table D.3: Properties used in the FDS models of the Hawaii hanger tests

	Alpha M^2/s	**k** W/m.K	**C_RHO_DELTA** $KJ/K.m^2$	**Thickness** m
Roof	3.60E-07	0.7	-	0.01
Concrete	5.70E-07	1	-	0.3
Steel	-	-	5.1	0.0015
Curtain	-	-	0.5	0.003

Table D.4: Properties used in the CFAST models of the Hawaii hanger tests

	Ks W/m.K	**Cp** J/kg.K	**ρ** kg/m3	**ε**	**Thickness** m
Roof	0.7	800	2100	0.9	0.01
Curtain	0.078	800	200	0.9	0.003
Concrete floor	CFAST default values for CONCRETE				
Steel doors	CFAST default values for STEEL1/8 (1/8" thick steel)				

The data for the materials given in Tables D.1 to D.4 was extracted from the following sources: DiNenno (Ed.) (1995), Incropera & DeWitt (1996) and Quintiere (1998).

FIRE ENGINEERING RESEARCH REPORTS

95/1	Full Residential Scale Backdraft	I B Bolliger
95/2	A Study of Full Scale Room Fire Experiments	P A Enright
95/3	Design of Load-bearing Light Steel Frame Walls for Fire Resistance	J T Gerlich
95/4	Full Scale Limited Ventilation Fire Experiments	D J Millar
95/5	An Analysis of Domestic Sprinkler Systems for Use in New Zealand	F Rahmanian
96/1	The Influence of Non-Uniform Electric Fields on Combustion Processes	M A Belsham
96/2	Mixing in Fire Induced Doorway Flows	J M Clements
96/3	Fire Design of Single Storey Industrial Buildings	B W Cosgrove
96/4	Modelling Smoke Flow Using Computational Fluid Dynamics	T N Kardos
96/5	Under-Ventilated Compartment Fires - A Precursor to Smoke Explosions	A R Parkes
96/6	An Investigation of the Effects of Sprinklers on Compartment Fires	M W Radford
97/1	Sprinkler Trade Off Clauses in the Approved Documents	G J Barnes
97/2	Risk Ranking of Buildings for Life Safety	J W Boyes
97/3	Improving the Waking Effectiveness of Fire Alarms in Residential Areas	T Grace
97/4	Study of Evacuation Movement through Different Building Components	P Holmberg
97/5	Domestic Fire Hazard in New Zealand	KDJ Irwin
97/6	An Appraisal of Existing Room-Corner Fire Models	D C Robertson
97/7	Fire Resistance of Light Timber Framed Walls and Floors	G C Thomas
97/8	Uncertainty Analysis of Zone Fire Models	A M Walker
97/9	New Zealand Building Regulations Five Years Later	T M Pastore
98/1	The Impact of Post-Earthquake Fire on the Built Urban Environment	R Botting
98/2	Full Scale Testing of Fire Suppression Agents on Unshielded Fires	M J Dunn
98/3	Full Scale Testing of Fire Suppression Agents on Shielded Fires	N Gravestock
98/4	Predicting Ignition Time Under Transient Heat Flux Using Results from Constant Flux Experiments	A Henderson
98/5	Comparison Studies of Zone and CFD Fire Simulations	A Lovatt
98/6	Bench Scale Testing of Light Timber Frame Walls	P Olsson
98/7	Exploratory Salt Water Experiments of Balcony Spill Plume Using Laser Induced Fluorescence Technique	E Y Yii
99/1	Fire Safety and Security in Schools	R A Carter

99/2	A Review of the Building Separation Requirements of the New Zealand Building Code Acceptable Solutions	J M Clarke
99/3	Effect of Safety Factors in Timed Human Egress Simulations	K M Crawford
99/4	Fire Response of HVAC Systems in Multistorey Buildings: An Examination of the NZBC Acceptable Solutions	M Dixon
99/5	The Effectiveness of the Domestic Smoke Alarm Signal	C Duncan
99/6	Post-flashover Design Fires	R Feasey
99/7	An Analysis of Furniture Heat Release Rates by the Nordtest	J Firestone
99/8	Design for Escape from Fire	I J Garrett
99/9	Class A Foam Water Sprinkler Systems	D B Hipkins
99/10	Review of the New Zealand Standard for Concrete Structures (NZS 3101) for High Strength and Lightweight Concrete Exposed to Fire	M J Inwood
99/12	An Analytical Model for Vertical Flame Spread on Solids: An Initial Investigation	G A North
99/13	Should Bedroom Doors be Open or Closed While People are Sleeping? - A Probabilistic Risk Assessment	D L Palmer
99/14	Peoples Awareness of Fire	S J Rusbridge
99/15	Smoke Explosions	B J Sutherland
99/16	Reliability of Structural Fire Design	JKS Wong
99/17	Heat Release from New Zealand Upholstered Furniture	T Enright
00/1	Fire Spread on Exterior Walls	FNP Bong
00/2	Fire Resistance of Lightweight Framed Construction	PCR Collier
00/3	Fire Fighting Water: A Review of Fire Fighting Water Requirements (A New Zealand Perspective)	S Davis
00/4	The Combustion Behaviour of Upholstered Furniture Materials in New Zealand	H Denize
00/5	Full-Scale Compartment Fire Experiments on Upholstered Furniture	N Girgis
00/6	Fire Rated Seismic Joints	M James
00/7	Fire Design of Steel Members	K R Lewis
00/8	Stability of Precast Concrete Tilt Panels in Fire	L Lim
00/9	Heat Transfer Program for the Design of Structures Exposed to Fire	J Mason
00/10	An Analysis of Pre-Flashover Fire Experiments with Field Modelling Comparisons	C Nielsen
00/11	Fire Engineering Design Problems at Building Consent Stage	P Teo
00/12	A Comparison of Data Reduction Techniques for Zone Model Validation	S Weaver
00/13	Effect of Surface Area and Thickness on Fire Loads	H W Yii
00/14	Home Fire Safety Strategies	P Byrne
00/15	Accounting for Sprinkler Effectiveness in Performance Based Design of Steel Buildings in Fire	M Feeney

00/16	A Guideline for the Fire Design of Shopping Centres	J M McMillan
01/1	Flammability of Upholstered Furniture Using the Cone Calorimeter	A Coles
01/2	Radiant Ignition of New Zealand Upholstered Furniture Composites	F Chen
01/3	Statistical Analysis of Hospitality Industry Fire Experience	T Y A Chen
01/4	Performance of Gypsum Plasterboard Assemblies Exposed to Real Building Fires	B H Jones
01/5	Ignition Properties of New Zealand Timber	C K Ngu
01/6	Effect of Support Conditions on Steel Beams Exposed of Fire	J Seputro
01/7	Validation of an Evacuation Model Currently Under Development	A Teo
01/8	2-D Analysis of Composite Steel - Concrete Beams in Fire	R Welsh
01/9	Contribution of Upholstered Furniture to Residential Fire Fatalities in New Zealand	C R Wong
01/10	The Fire Safety Design of Apartment Buildings	S Wu
01/11	Smoke Alarm Ownership in Relation to Socio-Economic Factors in Christchurch	N Buchanan
01/12	Accounting for Sprinkler Effectiveness in Performance Based Design of Steel Buildings for Fire	M Feeney
01/13	Equivalent Fire Resistance Ratings of Construction Elements Exposed to Realistic Fires	J Nyman
02/1	Performance of Expanded Polystyrene Insulated Panel Exposed to Radiant Heat	G Baker
02/2	A Comparison Between Predicted and Actual Behaviour of Domestic Smoke Detectors in a Realistic House Fire	D Brammer
02/3	Development of Bench-Scale Testing of Sprinkler and Smoke Detector Activation/Response Time	K S Chin
02/4	The Effect of Door Angle on Fire Induced Flow Through a Doorway	L R Clark
02/5	Implementation of a Glass Fracture Module for the BRANZ Fire Compartment Fire Zone Modelling Software	R Parry
02/6	Assessing the Feasibility of Reducing the Grid Resolution in FDS Field Modelling	N Patterson
02/7	Fire Safety Design of Ferrymead Heritage Park	M Rangi
02/8	Experimental Results for Pre-Flashover Fire Experiments in Two Adjacent ISO Compartments	L Rutherford
02/9	Measurement of Magnitude and Direction of Hot Gas Flow in a Fire Compartment with a Fire-hole Probe	J Schulz
02/10	Assessment of the Current False Alarm Situation from Fire Detection Systems in New Zealand and the Development of an Expert System for Their Identifications	Y F Tu
02/11	Performance of Unprotected Steel and Composite Steel Frames Exposed to Fire	C Wastney

School of Engineering
University of Canterbury
Private Bag 4800, Christchurch, New Zealand

Phone 643 364-2250
Fax 643 364-2758